

VILNIUS UNIVERSITY

Vaida LINKUVIENĖ

**Observed and intrinsic thermodynamic and  
kinetic parameters of sulfonamide derivative  
binding to carbonic anhydrases**

Doctoral thesis

Biomedical Sciences, biophysics (02 B)

Vilnius, 2017

This doctoral thesis work was performed from October 2013 to September 2017 at the Life Sciences Center, Vilnius University, Lithuania.

Supervisor:

**Prof. Daumantas MATULIS** (Vilnius University, Biomedical Sciences, biophysics – 02 B)

I would like to express a grateful thanks to my supervisor prof. D. Matulis for the opportunity to gain my knowledge and possibility to work in his laboratory.

My sincere gratitude also goes to the group members at the Department of Biothermodynamics and Drug Design for their friendly atmosphere and beneficial advices during this year.

I thank the molecular biology group and chemists for the recombinant proteins and synthetic compounds. My heartfelt appreciation goes to Asta, Lina, and Egidijus for their help when I was lost in the molecular world and biophysical instruments. I personally thank Vytautas for the L<sup>A</sup>T<sub>E</sub>X, rational mind, and the ability to “kill the bad ideas”. I of course would like to thank Agnė and Justina for coffee breaks and hearing out.

For the financial support I thank to Lithuanian Research Council.

For the hospitality, helpful attitude, and preparation of joint articles I am thankful to collaborators in Sweden, Vladimir O. Talibov and prof. U. Helena Danielson.

I feel indebted to my family, my husband Vytautas, for the warmth and support, and friends, especially Edita Vernickaitė and Justina Šarkanė – for the belief and considering me better than I really am, and especially to my brother Marius for being my authority.



# Contents

<b>List of publications</b>	<b>1</b>
Publications included in this thesis . . . . .	1
Publications not included in this thesis . . . . .	2
<b>List of conferences</b>	<b>5</b>
Oral presentations . . . . .	5
Poster presentations . . . . .	5
<b>Abbreviations</b>	<b>7</b>
<b>Introduction</b>	<b>9</b>
<b>Literature overview</b>	<b>13</b>
1 Thermodynamics and kinetics in drug design . . . . .	13
1.1 Thermodynamics in drug design . . . . .	13
1.2 Kinetics in drug design . . . . .	16
1.3 Biophysical methods to study protein-ligand binding . . . . .	17
2 Compound optimization . . . . .	20
3 Carbonic anhydrase as a drug target . . . . .	22
3.1 Catalytic mechanism of CA . . . . .	23
3.2 Diseases related to CAs . . . . .	23
3.3 CA inhibition by sulfonamide compounds . . . . .	26
4 Protonation of interacting components . . . . .	27
5 Intrinsic parameters of protein-ligand binding . . . . .	29
5.1 Intrinsic thermodynamic parameters of binding . . . . .	29
5.2 Intrinsic kinetic parameters of binding . . . . .	31
<b>Materials and methods</b>	<b>33</b>
6 Materials . . . . .	33
6.1 CA inhibitors . . . . .	33
6.2 Proteins . . . . .	33
6.3 Chemicals . . . . .	33
6.4 Buffers . . . . .	34
7 Methods . . . . .	34
7.1 Fluorescent thermal shift assay (FTSA) . . . . .	34
7.2 Isothermal titration calorimetry (ITC) . . . . .	37
7.3 Surface plasmon resonance (SPR) . . . . .	38
7.4 Spectrophotometric measurements . . . . .	39
7.5 Calculation of intrinsic parameters . . . . .	39

---

<b>Results</b>	<b>41</b>
8 Characterization of human carbonic anhydrases I, IX, and XII protonation reaction . . . . .	41
9 Observed and intrinsic thermodynamics of <i>meta</i> - and <i>para</i> -substituted benzenesulfonamide binding to CA . . . . .	45
10 Introduction of intrinsic kinetics of protein-ligand interactions and their implications for drug design . . . . .	68
<b>Discussion</b>	<b>87</b>
<b>Conclusions</b>	<b>91</b>
<b>Bibliography</b>	<b>93</b>
<b>Additional information</b>	<b>107</b>
11 Manuscripts . . . . .	107
12 Permissions . . . . .	144
13 Curriculum Vitae . . . . .	150

# List of publications

## Publications included in this thesis

1. Jogaitė, V., Zubrienė, A., Michailovienė, V., Gylytė, J., **Morkūnaitė, V.**, Matulis, D. Characterization of human carbonic anhydrases XII stability and inhibitor binding. *Bioorg. Med. Chem.* 21(6) (**2013**) 1431-1436.

I have performed the biophysical CA-EZA binding experiments. The protein-ligand interaction dependence on pH was performed by ITC in two different buffers.

2. **Morkūnaitė, V.**, Gylytė, J., Zubrienė, A., Baranauskienė, L., Kišonaitė, M., Michailovienė, V., Juozapaitienė, V., Todd, M. J., Matulis, D. Intrinsic thermodynamics of sulfonamide inhibitor binding to human carbonic anhydrases I and II. *J. Enzyme Inhib. Med. Chem.* 30(2) (**2015**) 204-211.

I have performed biophysical ITC and FTSA experiments of EZA binding to CA I at a series of different pHs. ITC experiments were performed in two buffers: sodium phosphate and TRIS chloride. I have participated in article writing.

3. **Linkuvienė, V.**, Matulienė, J., Juozapaitienė, V., Michailovienė, V., Jachno, J., Matulis, D. Intrinsic thermodynamics of inhibitor binding to human carbonic anhydrase IX. *Biochim.Biophys.Acta, Gen.Subj.* 1860 (**2016**) 708-718.

I have performed all biophysical experiments and data analysis and wrote the manuscript.

4. Talibov, V. O., **Linkuvienė, V.**, Matulis, D., Danielson U. H. Kinetically Selective Inhibitors of Human Carbonic Anhydrase Isozymes I, II, VII, IX, XII, and XIII. *J.Med.Chem.* 59 (**2016**) 2083-2093.

I have performed and analyzed FTSA experiments, edited the manuscript.

5. **Linkuvienė, V.**, Talibov., V. O., Danielson, U. H., Matulis, D. Introduction of intrinsic kinetics of protein-ligand interactions and their implications for drug design. *Submitted.*

I have performed compound binding measurements, analyzed data, and contributed to the manuscript writing.

## Publications not included in this thesis

1. Pirrie, L., McCarthy, A. R., Major, L. L., **Morkūnaitė, V.**, Zubrienė, A., Matulis, D., Lain, S., Lebl, T., Westwood, N. Discovery and Validation of SIRT2 Inhibitors Based on Tenovin-6: Use of a <sup>1</sup>H-NMR Method to Assess Deacetylase Activity. *Molecules* 17 (2012) 12206-12224.

I have measured interaction of inhibitors synthesized in UK by biophysical FTSA assay and edited the manuscript.

2. **Morkūnaitė, V.**, Baranauskienė, L., Kairys, V., Ivanova, J., Trapencieris, P., Matulis, D. Saccharin sulfonamides as inhibitors of carbonic anhydrases I, II, VII, XII, and XIII. *Biomed. Res. Int.* (2014) doi: 10.1155/2014/638902.

I have performed all biophysical measurements of compound binding to proteins by FTSA and ITC methods and prepared the manuscript.

3. Rutkauskas, K., Zubrienė, A., Tumosiėnė, I., Kantminienė, K., Kažemėkaitė, M., Smirnov, A., Kazokaitė, J., **Morkūnaitė, V.**, Čapkauskaitė, E., Manakova, E., Gražulis, S., Beresnevičius, Z. J., Matulis, D. 4-amino-substituted benzenesulfonamides as inhibitors of human carbonic anhydrases. *Molecules*, 19(11) (2014) 17356-17380.

I have performed the FTSA measurements of **26-34** compound binding to CA VII and CA XII.

4. Dudutienė, V., Matulienė, J., Smirnov, A., Timm, D. D., Zubrienė, A., Baranauskienė, L., **Morkūnaitė, V.**, Smirnovienė, J., Michailovienė, V., Juozapaitienė, V., Mickevičiūtė, A., Kazokaitė, J., Bakšytė, S., Kasiliauskaitė, A., Jachno, J., Revuckienė, J., Kišonaitė, M., Pilipuitytė, V., Ivanauskaitė, E., Milinavičiūtė, G., Smirnovas, V., Petrikaitė, V., Kairys, V., Petrauskas, V., Norvaišas, P., Lingė, D., Gibieža, P., Čapkauskaitė, E., Zakšauskas, A., Kazlauskas, E., Manakova, E., Gražulis, S., Ladbury, J. E., Matulis, D. Discovery and characterization of novel selective inhibitors of carbonic anhydrase IX. *J. Med. Chem.* 57(22) (2014) 9435-9446.

I have participated in the carbonic anhydrase inhibitor design project and discussions that led to the publication of our lead compound description.

5. Redhead, M., Satchell, R., **Morkūnaitė, V.**, Swift, D., Petrauskas, V., Golding, E., Onions, S., Matulis, D., Unitt, J. A combinatorial biophysical



---

approach; FTSA and SPR for identifying small molecule ligands and PAINS. *Anal. Biochem.* 479 (2015) 63-73.

I have analyzed the biophysical FTSA data sent by our UK partners and participated in the writing of the manuscript.

- Zubrienė, A., Smirnovienė, J., Smirnov, A., **Morkūnaitė, V.**, Michailovienė, V., Jachno, J., Juozapaitienė, V., Norvaišas, P., Manakova, E., Gražulis, S., Matulis, D. Intrinsic thermodynamics of 4-substituted-2,3,5,6-tetrafluoro benzenesulfonamide binding to carbonic anhydrases by isothermal titration calorimetry. *Biophys. Chem.* 205 (2015) 51-65.

I have performed biophysical ITC experiments of several compound binding to CA VII and CA XII.

- Linkuvienė, V.**, Krainer, G., Chen, W.-Y., Matulis, D. Isothermal titration calorimetry for drug design: Precision of the enthalpy and binding constant measurements and comparison of the instruments. *Anal. Biochemistry.* 515 (2016) 61-64.

I have obtained all described isothermal titration calorimetry data that was important for the benchmarking study of ITC method precision.

- Čapkauskaitė, E., **Linkuvienė, V.**, Smirnov, A., Milinavičiūtė, G., Timm, D., Kasiliauskaitė, A., Manakova, E., Gražulis, S., Matulis, D. Combinatorial design of isoform-selective *N*-alkylated benzimidazole-based inhibitors of carbonic anhydrases. *ChemistrySelect* 2 (2017) 5360-5371.

I have performed all compound binding measurements with a part of CA isoforms (CA III, CA IV, CA IX, and CA XIV), analyzed data, and wrote part of the manuscript.



# List of conferences

## Oral presentations

1. **Linkuvienė, V.**, Talibov, V. O., Danielson, H., Matulis, D. Intrinsic vs. observed thermodynamic and kinetic parameters of carbonic anhydrase-ligand interaction. 19<sup>th</sup> IUPAB/11<sup>th</sup> EBSA/BBS/IoP Congress, Edinburgh, Scotland, 2017.
2. **Linkuvienė, V.**, Matulis, D. Intrinsic thermodynamic parameters of *o*, *m*-substituted benzenesulfonamide inhibitors binding to carbonic anhydrase. XIV International Conference of the Lithuanian Biochemical Society, Druskininkai, Lithuania, 2016.
3. **Linkuvienė, V.**, Matulis, D. Thermodynamics of carbonic anhydrase - inhibitor binding for drug design. XIX ISBC Conference, Basel, Switzerland, 2016.

## Flash presentation of poster

4. **Linkuvienė, V.**, Matulis, D. Comparison of titration calorimeters: High affinity and enthalpy precision. 2<sup>nd</sup> Annual European MicroCal Meeting, Paris, France, 2016.

## Poster presentations

1. **Linkuvienė, V.**, Zubrienė, A., Paketurytė, V., Smirnov, A., Petrauskas, V., Matulis, D. Database of CA Protein-Ligand Binding Gibbs Energies, Enthalpies, Entropies, Volumes, and Crystal Structures. Biophysical Society 61<sup>st</sup> Annual Meeting, New Orleans, Louisiana, USA, 2017.
2. **Linkuvienė, V.**, Matulis, D. Comparison of titration calorimeters: High affinity and enthalpy precision. 2<sup>nd</sup> Annual European MicroCal Meeting, Paris, France, 2016.

3. **Morkūnaitė, V.**, Čapkauskaitė, E., Matulis, D. Intrinsic thermodynamics-structure correlations of sulfonamides binding to carbonic anhydrase IX. 10<sup>th</sup> EBSA European Biophysics Congress, Dresden, Germany, 2015.
4. **Morkūnaitė, V.**, Matulienė, J., Zubrienė, A., Kišonaitė, M., Baranauskienė, L., Jachno, J., Michailovienė, V., Matulis, D. Recombinant production and calorimetric characterization of human carbonic anhydrase IX. XVIII ISBC International Society for Biological Calorimetry Conference, Lund, Sweden, 2014.

# Abbreviations

FTSA	fluorescence thermal shift assay
$T_m$	protein melting temperature
ANS	8-anilino-1-naphthalenesulfonic acid
ITC	isothermal titration calorimetry
SPR	surface plasmon resonance
CA	carbonic anhydrase
CAZnH <sub>2</sub> O	water molecule bound to the Zn(II) cation in the active site of CA
RSO <sub>2</sub> NH <sub>2</sub>	sulfonamide group of a compound
b	binding
p	protonation
buf	buffer
obs	observed
intr	intrinsic
<b>EZA</b>	ethoxzolamide
<b>AZM</b>	acetazolamide
NMR	nuclear magnetic resonance
IR	infrared
MS	mass spectrometry
DMSO	dimethylsulfoxide
NHS	<i>N</i> -hydroxysuccinimide
EDC	1-ethyl-3-(3-(dimethylamino)propyl)carbodiimide-hydrochloride
TRIS	tris(hydroxymethyl)aminomethane
<b><i>p</i>-MBS</b>	<i>para</i> -methyl benzenesulfonamide



# Introduction

The majority of approved drugs bind to and affect the catalytic activity of enzymes. It is difficult to identify how many druggable proteins are in human body, but according to human genome, there could be 600-1500 target proteins that are related to diseases [1]. The understanding of the origin, pathology, and underlying mechanism of human disorder helps to identify the responsible entity that causes such condition. Understanding the relationship between biological effect and three dimensional structure enables to design ligands with activation or inhibition properties and favorable pharmacological characteristics.

One of such targets is the enzyme carbonic anhydrase (CA). It is a highly abundant protein found in all living systems because it is catalyzing a vital enzymatic reaction. The twelve catalytically active human CA isoforms have pharmacological applications in the field of antiepilepsy, antiglaucoma, anticancer agents, etc. The change of CA expression was associated with a disease in 1936 [2], when inhibitor properties of sulfides were noticed (in 1933 [3]) and later the sulfonamide derivatives became the most investigated and important class of CA inhibitors [4–6]. The inhibitors bind in the active site of the protein and suppress the catalytic reaction of over-expressed isoform thus contributing to the treatment of certain disease. Unfortunately, most often the compounds bind not only to the target isoform, but to other isozymes as well. For this reason, design of selective CA inhibitors is a primary goal. Therefore, structure-thermodynamics and structure-kinetics relationship has to be understood.

Thermodynamics of protein-ligand binding provides valuable information about the energies of protein-ligand-water network formation. The binding constant is the first determined parameter that researcher wants to know about the compound. The enthalpy and entropy are the “components” of the Gibbs energy and modifications of a ligand can change their gain to binding potency.

Kinetics of the compound and the target protein interaction, simplified to association and dissociation rate constants, are useful for ranking and optimization of ligands. The assumption that similar compounds have similar association rates still exists. However, small differences in compound structure can have a large effect to interaction kinetics.

Small structural changes of functional groups and determination of the binding

affinity of such small variations provide important information about molecule behavior and properties. However, these differences could be unnoticed if additional reactions are not taken into account during complex formation. Protonation is the most important reaction that should be dissected from the observed thermodynamic and kinetic parameters of molecular interaction. Due to the ionization constants of protein and ligand and the pH of the buffer, the fractions of binding components differ. Therefore, thermodynamic parameters of the same reaction, performed at various buffers and pHs, and association rate constants, performed at different pHs, differ as well. Values, obtained at different conditions, cannot be compared if protonation influence is not subtracted (intrinsic parameters calculated), otherwise wrong conclusions can be made for further drug design.

Development of isoform-selective ligands requires use of biophysical methods that reveal the details of the molecular recognition. The interaction kinetics reveal the dynamics, while binding thermodynamics – energetics of the interaction. A combination of surface plasmon resonance-based analysis with thermodynamic methods, such as the fluorescent thermal shift assay and isothermal titration calorimetry, is therefore necessary for the design and development of efficient drug candidates. Enzymes of the CA family are important not only as targets for many diseases, but also as good models for ligand selectivity studies. Similar logic can be applied to other protein families that are important as drug targets or functionally significant for fundamental research.

### **The goal of the study**

To determine the influence of linked protonation effects to the thermodynamic and kinetic parameters of ligand binding to several recombinant human carbonic anhydrases and to explore the compound structure-thermodynamics and compound structure-kinetics relationship for sulfonamide inhibitor binding to CA isoforms.

### **Objectives**

- To determine ionization constants and enthalpies of Zn(II)-bound hydroxide/water molecule in the active site of CA I, CA IX, and CA XII using thermodynamic methods.
- To obtain the  $pK_a$ s and enthalpies of sulfonamide group of the analyzed compounds.
- To determine the observed thermodynamic and kinetic parameters of sulfonamide compound binding to CA isoforms.
- To calculate the intrinsic thermodynamic and kinetic parameters of CA - sulfonamide binding.



- 
- To establish correlations between the compound structure and thermodynamics and kinetics of binding to CAs.

### **Scientific novelty**

In this work, the thermodynamic parameters of several new compound interaction with CAs were measured and the intrinsic parameters were calculated. Here I determined that the compounds exhibited an exceptionally strong binding affinity (picomolar) and selectivity towards some target CA isoforms.

Detailed characterization of observed compound structure-thermodynamics and compound structure-kinetics relationship was made. Furthermore, for the first time, the surface plasmon resonance method was used to determine the protonation effect of binding kinetics. The ionization constants of several CA isoforms were determined using the isothermal titration calorimetry and fluorescence thermal shift assays and compared with the results obtained by SPR. After the determination of the protein and compound  $pK_a$ s, the protonation influence was dissected and the intrinsic thermodynamic and kinetic parameters of protein-ligand interplay were calculated.

In this work, I developed a novel model that explained the kinetics of sulfonamide inhibitor binding to CAs and dissected the intrinsic kinetic parameters and solved previous inconsistency of binding that was too slow for the simple one-step binding reaction. After the correction of the active fractions, We showed that the compounds behave as common ligands with diffusion-limited association-dissociation kinetics.

### **Defending statements**

- Sulfonamide compounds belonging to the EA class developed in our laboratory exhibit high affinity and selectivity towards target CA isoforms and could be continued to be developed as drugs.
- Determination of the intrinsic thermodynamic parameters is an important step that should be used in the structure-thermodynamics analysis of newly synthesized compound interaction with target proteins.
- The sulfonamide compounds in their binding to CAs behave as common ligands with diffusion-limited kinetics as demonstrated by the novel model that dissected the intrinsic kinetic parameters from the observed parameters.



# Literature overview

## 1 Thermodynamics and kinetics in drug design

### 1.1 Thermodynamics in drug design

In the rational drug design it is important to determine the affinities and other thermodynamic parameters of designed compounds towards the protein target that needs to be inhibited or activated. The binding affinity is the first parameter that is determined after compound synthesis or optimization. Most often, the binding or dissociation constant may be recalculated to the Gibbs energy, which has arising from enthalpic and entropic contributions. These thermodynamic parameters show a more detailed energetic picture of the complex formation and indicate how small changes in compound structure can be correlated with thermodynamic parameters.

#### Principles of thermodynamics in protein-ligand binding

Protein [P] and ligand [L] may form a complex [PL] in aqueous environment and this process should be reversible:



The equilibrium constant of binding  $K_b$  is given by the equation:

$$K_b = \frac{[PL]}{[P][L]} \quad (2)$$

$K_b$  is is the inverse of the dissociation constant,  $K_d$ :

$$K_d = \frac{[P][L]}{[PL]} = \frac{1}{K_b} \quad (3)$$

and  $K_b$  is associated with the change in standard Gibbs energy for the binding reaction,  $\Delta_b G^\circ$ ,

$$\Delta_b G^\circ = -RT \ln K_b \quad (4)$$

where  $R$  is ideal gas constant equal to  $8.314 \text{ J mol}^{-1} \text{ K}^{-1}$  and  $T$  is the absolute temperature (K).

It should be explained that due to this relation, the  $K_b$  should be a unitless number. The lefthand side of the equation (4), the  $\Delta_b G^o$  term, has units of energy ( $\text{J mol}^{-1}$ ). On the righthand side, the  $RT$  term also has units of ( $\text{J mol}^{-1}$ ). Thus,  $K_b$  must be dimensionless and, besides, natural logarithm makes it necessary to convert  $K_b$  to a unitless value [7, 8]. Although the binding constant is a dimensionless number, it is usually presented as if it has  $\text{M}^{-1}$  units, and thus the dissociation constant  $K_d$  has molar units of concentration. Furthermore, the interactions are described as millimolar for weak binding, nanomolar or picomolar for tight complex formation.

The  $\Delta_b G^o$  comprises the change in enthalpy  $\Delta_b H$ , and the change in entropy,  $T\Delta_b S$ :

$$\Delta_b G^o = \Delta_b H^o - T\Delta_b S^o \quad (5)$$

The  $\Delta_b H^o$  term represents the change in the heat that is released or absorbed by breaking or forming the bonds between all components during complex formation (e.g. protein, ligand, water, buffer components, etc.). The heat is equal to the enthalpy only if the pressure is constant and the system does not perform any work. The enthalpy (heat) can be observed directly by calorimetry or indirectly where equilibrium constants at different temperatures and the van't Hoff relationship is used to calculate the binding enthalpy ( $\Delta_b H_{VH}$ ):

$$\Delta_b H_{VH} = -R \frac{\partial \ln K_b}{\partial (1/T)} \quad (6)$$

The discrepancies exist between the calorimetric and the van't Hoff enthalpy values, and the calorimetric data is usually considered as more reliable [9, 10].

In the gas phase, the  $T\Delta S^o$  contribution to the Gibbs energy of binding comes from the loss of translational, rotational, and internal degrees of freedom of the bound molecules, because they no longer move independently. However, in aqueous solution, water reorganization upon binding also contributes to the total entropy of binding, thus complicating the general picture of the energetics. The  $T\Delta S^o$  can differ significantly even between closely related ligands [11] and may be both positive or negative.

It should be mentioned that Gibbs energy, enthalpy, and entropy are state functions and their values do not depend on the route by which the thermodynamic equilibrium states are accessed. Only the *changes* in  $\Delta_b G^o$ ,  $\Delta_b H^o$  and  $T\Delta_b S^o$  are determined, not the absolute values.

The superscript 'o' indicates that the values are obtained for the standard state. At this state, thermodynamic parameters are described for the conversion of 1 M

of protein and 1 M of ligand to 1M of protein-ligand complex at a constant pressure  $p^o = 10^5$  Pa in a hypothetical ideal solution, i.e. in a solution which is so dilute that solute molecules do not interact with each other. Most reactions occur in the aqueous solution, where concentration of water is 55 M. Thus, the concentrations of proteins or small molecules are very low compared to the concentration of water. Despite this, the energy of interaction between solute molecule and the solvent molecules does not change when solute concentration changes.

The standard state is important for the comparability between measurements, because depending on the concentration scale we calculate (M, mM,  $\mu$ M, nM) the value changes [8]. The temperature has to be specified, because it is not a part of the standard state.

The superscript is frequently omitted for brevity and will not be used in this text bellow either, but it should be understood that all listed values are presented for the standard state.

### **Enthalpy-entropy compensation**

The  $\Delta_b G$  drives the protein-ligand binding process, which may be driven by enthalpy and entropy (eq. (5)). The  $\Delta_b H$  and  $T\Delta_b S$  cannot be observed by the independent experiments, thus, these two parameters automatically compensate each other and it is difficult to improve the measured value of the Gibbs energy. Nevertheless, ligand optimization that causes even small changes in enthalpy or entropy can influence the target inhibition.

Enthalpically driven interaction is associated with broken or formed bonds during the complex formation and due to those contacts the ligand is tightly fixed. Compound flexibility in the complex with a protein contributes to entropically driven binding. Water molecules play the major role in enthalpy-entropy compensation as well, because compound can make hydrogen bonds and this interaction will likely be enthalpically favored. In the other case, water may be released or reorganized due to the desolvation upon binding and interaction will be enthalpically driven.

The goal is to optimize the compound and to change the enthalpy and entropy of binding in such a way, that the Gibbs energy would be improved as much as possible.

### **Additional reactions**

When a ligand binds to a protein, many other additional reactions take place: protonation/deprotonation of the protein and/or ligand, solvation of ligand and the protein's binding site, ion binding, etc [12]. All these reactions contribute to the thermodynamic parameters of protein-ligand-solvent system. The most impor-

tant one is proton transfer between the protein-ligand complex and surrounding buffer. Depending on the experimental conditions (such as buffer protonation enthalpy and pH,  $pK_a$  of a compound's sulfonamide group and protein binding site) the resultant thermodynamic values differ. To determine only the energies of bonds and intermolecular contact formation ('intrinsic' parameters), buffer contribution must be subtracted and only interaction between protein-ligand-water molecules have to be calculated [8, 12–18]. It is necessary for the understanding of the thermodynamic profile, to optimize the enthalpic and/or entropic contributions, improving binding affinity and to compare experiments made at different conditions. Furthermore, experimental results should not be compared if they were made at different temperatures. Application of the van't Hoff equation may help to recalculate the values to other temperatures.

## 1.2 Kinetics in drug design

The association rate of the protein-ligand interaction is determined by  $k_a$  and  $k_d$ , the on- and off- rates of the ligand binding and dissociation. Inhibitory effect is extended by a rapid rate of drug binding and/or a slow rate of complex dissociation. These parameters are related with the  $K_d$  value and at the same time strongly complement it.

### Principles of kinetics in protein-ligand binding

The binding process is often represented as a single step model as shown in eq. (1). Despite the fact that real binding process has a complex mechanism, this equation is sufficient for the understanding of the kinetics of interaction. The speed at which the complex forms depends on the rate of complex association ( $k_a$ ) and dissociation ( $k_d$ ):

$$\frac{d[PL]}{dt} = k_a[P][L] - k_d[PL] \quad (7)$$

Thus, equation (1) can be complemented:



The association rate constant  $k_a$  is limited by the diffusion rate of  $\sim 10^8 - 10^9 \text{ M}^{-1} \text{ s}^{-1}$  and it is impossible to make reactions occur faster than the diffusion rate [19].

The kinetics of binding may be related to the thermodynamics by the equilibrium equation:

$$K_d = \frac{k_d}{k_a} \quad (9)$$

This relation can be illustrated by the graph, where the affinity is shown as the difference in heights between the initial and end points (Fig. 1). Affinity does not tell us whether the reaction is fast or slow. Instead,  $k_a$  and  $k_d$  provide this information and thus determine the shape and the energy profile of the binding reaction.

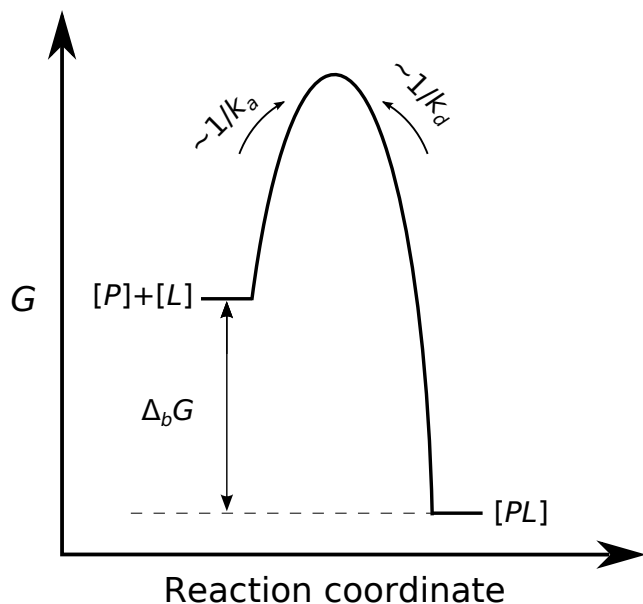


**Figure 1** Free energy profile of protein **P** and ligand **L** binding reaction. The curve shows a one-step mechanism. The heights shown as  $k_a$  and  $k_d$ , the association and dissociation rate constants, respectively. The association  $\Delta_b G$  is proportional to the logarithm of  $k_d$  and  $k_a$  ratio.

Very often  $k_d$  is changed by the term “a residence time” ( $\tau$ ), which is defined as the period of time the target is occupied by the ligand:

$$\tau = \frac{1}{k_d} \quad (10)$$

*In vitro* measurement of the residence time is a better indicator of *in vivo* duration of efficacy than the equilibrium dissociation constant. This is because the concentration of the ligand to which a target receptor is exposed in the open system of *in vivo* experiments is no longer constant as in the closed system of *in vitro* experiment, but varies with time and is influenced by many factors [19]. Therefore, kinetic parameters have significant contribution in the process of compound optimization for drug design.

### 1.3 Biophysical methods to study protein-ligand binding

Monitoring and detection of molecular interactions significantly increases our understanding about protein-ligand binding mechanism. Affinity based technologies

can provide unique data that helps us to evaluate the formation of a complex from multiple viewpoints and identify optimized ligands, which can inhibit or modulate the biological activity of targets of interest [20].

Various techniques provide different information, thus it is important to choose a correct method. The choice depends on solubility of the components, size of the molecules and their affinity. Thermodynamic and kinetic methods help analyze the protein-ligand interactions [20,21].

### **Fluorescent thermal shift assay (FTSA)**

FTSA (also called Thermofluor<sup>®</sup>, differential scanning fluorimetry, DSF) is a high-throughput method that allows to detect the protein-ligand binding constants in a wide range. This assay is based on ligand-induced protein thermal stabilization which is related to the binding constant and ligand concentration [22].

It is well understood that the protein becomes more stable during thermal denaturation when a compound binds to its native form. Unfolding process can be detected when fluorescence of tryptophan of the protein or solvatochromic dye is monitored. Often experiments are performed in real time PCR machines, thus solvatochromic dye such as 8-anilino-1-naphthalenesulfonic acid (ANS) or Sypro orange is used. This dye is quenched in aqueous environment but highly fluoresces when bound to the hydrophobic parts of the protein [23]. Dye-containing protein solution (with or without ligand) is heated, dye binds to hydrophobic sites that are exposed to solvent during protein melting and fluorescence increases. Fluorescence intensity increases when more hydrophobic sites are exposed and reaches a maximum when the protein is fully unfolded. The midpoint of this fluorescence curve is a melting temperature ( $T_m$ ), which shows the temperature where the free energy of the native and non-native forms are equal. The  $T_m$  increases in proportion to ligand concentration [22–24]. By comparing  $T_m$  value of a complex with  $T_m$  value of a protein without a bound ligand, it is possible to calculate the binding affinity [22,24,25]. The higher the difference between these two  $T_m$  values ( $\Delta T_m$ ), the stronger the binding (for the same protein).

FTSA is a good primary method for hit searching and there is no upper limit of the affinity that can be measured - tighter binding gives a greater  $\Delta T_m$ . The only limitation for accurate affinity determination is that some information about studying protein has to be known, e.g. unfolding enthalpy [22].

### **Isothermal titration calorimetry (ITC)**

ITC is one of the main techniques for obtaining the thermodynamic parameters of binding between two molecules interacting in aqueous solution. It is the only method that allows to observe the enthalpy directly and is a standard technique



for direct binding measurements in drug design industry. ITC technique does not require immobilization of interacting components or modification of the molecules. One component (in the syringe) is titrated to another (in the cell) in a series of injections at constant temperature. After each injection the binding occurs and the heat is absorbed or released. In the middle of experiment all molecules are bound and only dilution takes place. ITC determines the binding constant ( $K_b$ ), enthalpy ( $\Delta_b H$ ) and stoichiometry ( $n$ ) in one experiment. The middle point of the titration isotherm shows the quantity of active macromolecules, slope of the curve gives the information about the binding affinity and the height – about binding enthalpy [8, 26, 27]. Equilibrium  $K_b$  is related to the Gibbs energy as shown in equation (4) and  $T\Delta_b S$  can be calculated modifying the equation (5):

$$T\Delta_b S = \Delta_b H - \Delta_b G \quad (11)$$

It is important to note that ITC records not only the energies of two binding components, but the entire binding event and detects heat signals of additional reactions that occur during the formation of the final complex [8]. Therefore, the combination of experimental results, obtained at different conditions, allows characterization of simple processes such as proton- or ligand-linked interactions as well as the binding energetics of complex systems [14, 28, 29].

There are several limitations of this technique. First, it is relatively expensive method that requires milligrams of protein. Second, it is sensitive for changes in solution composition, thus dialysis of protein against the experimental buffer should be performed. The same percentage of DMSO in the cell and syringe must also be kept. Third, it is time consuming method and only one complex formation can be determined at once. And final, limitation is a narrow window of  $K_b$  which is established by Wiseman’s factor (c factor):

$$c = K_b \times P_t \quad (12)$$

$P_t$  is a total concentration of protein.

Sigmoidal curve is too steep when c factor is too high and too flat when c factor is too low, thus  $K_b$  cannot be determined. Various ranges of optimal c-value can be found in the literature: 1-1000 [30], 10-500 [8] or 5-500 [27, 31]. However, when the binding is too tight and cannot be determined, c factor is too large,  $\Delta_b H$  may still be determined accurately. Enthalpies cannot be determined with greater precision than 1 kcal mol<sup>-1</sup> ( $\sim$  4 kJ mol<sup>-1</sup>) [31]. Despite the limitations, calorimetry brings valuable information. Comparing it with primary screening methods such as FTSA, ITC highly improves the understanding about compound optimization at a later stage.

## Surface plasmon resonance (SPR)

SPR is the most often used method for a kinetic characterization of protein-ligand binding [21]. It is used to determine complex formation in real time and without labeling, but with immobilization of one component. Experiments can give information about the ligand affinity, mechanism of binding, and kinetics of interaction.

Method is based on refractive index changes at the interface of two interacting components near the surface [32, 33]. Protein has to be immobilized on a thin metal surface by maintaining native conformation and binding activity during the experiment. Polarized light wave is directed to this surface, induces oscillations of plasmons on it and is reflected. The angle between directed and reflected light wave is called SPR angle. This angle changes after compound binding to a protein. Solution with dissolved interacting molecule passes over the chip, interacts with immobilized protein and thus refractive index changes. SPR angle is plotted as a function of time [34].

By using such microfluidic systems with continuous signal recording, it is possible to observe not only kinetic, but thermodynamic parameters as well. These parameters are calculated from experimental data by using van't Hoff equation, but it requires additional assumptions and is not widely used in SPR. Thermodynamic parameters can also be estimated by doing experiments at different temperatures or  $K_d$  value can be calculated as a  $k_d$  and  $k_a$  ratio (eq. (9)) [21].

The most important advantage is that affinity and kinetic parameters can be determined by using very small amount of protein and there is no need of chemical or radio-labeling. Furthermore, this method can determine association rates in the range from  $10^3$  to  $10^8$   $M^{-1} s^{-1}$ , dissociation rates from  $10^{-6}$  to  $1 s^{-1}$  [34,35] and affinity from 500  $\mu M$  to 1 nM [21]. The ability to accurately determine kinetic rate constants and thermodynamic parameters for protein-ligand interactions provides the possibility of new approaches in drug design.

## 2 Compound optimization

There are many ways to develop novel pharmaceutically active compounds, for example, by fragment screening or by lead compound optimization, which is used in our laboratory.

The history of drug research is based on lucky accidents, but to cite Nobel laureate James Black, "The most fruitful basis of the discovery of a new drug is to start with an old drug" or a lead structure, where term "lead" means that a compound with the inhibition properties to a target molecule can be improved by chemical variations which makes analogue better than the previous structure in,

for instance, its potency or selectivity [36]. Such “old” lead compound should be relatively simple, but in a favorable patent situation. It should have good absorption, distribution, metabolism, and excretion characteristics and well-established structure-activity relationship [37]. The goal is to optimize structure to make the final compound ready for therapeutic use [36].

Unidirectional systematic changes in three-dimensional structure and/or the physicochemical characteristics are very important in compound optimization. Lipophilicity plays a role in absorption, membrane and central nervous system penetration, plasma protein binding, distribution and partitioning into other tissues or organs and can be improved through the introduction or removal of hydrophobic or hydrophilic groups. Aqueous solubility is important to achieve a desired concentration of drug in systemic circulation for the pharmacological response. For this reason, ionizable or polar groups can be added, typically, a basic amine or a carboxylic acid. It is necessary to develop structurally simpler compounds while retaining their bioactivity. This can be achieved by eliminating chiral centers, but otherwise, addition of chiral centers can increase the selectivity. Moreover, compound should be chemically stable, thus elimination, replacement or modification of unstable groups should be done. Variations of substituents at aromatic or heteroaromatic rings and size changes, introduction or elimination of heteroatoms, compound stabilization, flexibility or rigidifying also contribute to drug optimization [36, 38, 39].

Polar groups added to a ligand are able to establish hydrogen bonds with a protein. Such bonds can enhance interaction and contribute favorable enthalpies to the binding energetics by as much as -4 kcal/mol to -5 kcal/mol [14, 39]. However, hydrogen bonds do not necessarily improve binding affinity, because the enthalpy gains can be reduced by opposing entropy changes [39]. Bond, that is formed by a functional group of a ligand, will contribute to affinity if it is stronger than the hydrogen bond that is formed by the group in aqueous solution before complex formation [14]. On the other hand, if a strong hydrogen bond, and thereby strong enthalpic interaction does not contribute to affinity, it might contribute significantly to selectivity [39].

One of the ways to improve binding affinity during late-stage optimization is to introduce nonpolar groups. Such groups increasingly fill the hydrophobic protein pockets and displace water molecules that were found in well-ordered positions before the binding of the ligand. Therefore, increased compound lipophilicity enhances the binding affinity mainly for entropic reasons [14, 40]. By contrast, displacement of water molecules from poorly hydrated hydrophobic pocket, that show high residual mobility before ligand binding, results in an enthalpic gain, i.e. growing hydrophobicity of a compound also can lead into an enthalpy-driven signal [39, 41–43]. Furthermore, the hydrophobic effect can contribute favorably to

both enthalpy and entropy [44]. It shows that hydrophobic interactions are much more complex than generally believed.

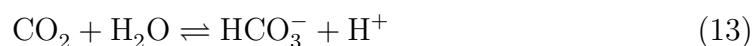
The other late-stage optimization process is to rigidify the ligand to fix it into receptor-bound conformation. Such optimization reduces the conformational degrees of freedom of the bound ligand and reduces entropic contribution, thereby the affinity increases. A conformationally “locked” compound will have a better binding affinity and also better selectivity than its flexible analogs [14].

Compound optimization is often based on the thermodynamic parameters of interaction with the target protein, because modification of the kinetics is difficult to achieve. The factors underlying binding rates are poorly understood, and thus it is not easy to attain promising structure-kinetics relationship. Despite this, there are several examples where association and dissociation rates of interactions are understood and can be applied to ligand design. For example, the length of aliphatic alkyl substituent of a compound can influence the  $k_d$  rate in the case of thrombin inhibitor [45]. For diphenyl ether binding to *Staphylococcus aureus* enoyl-ACP reductase, tighter interaction corresponds to longer residence times [46]. Miller et al. made a study where he analyzed a database of binding kinetic data across multiple targets and found that molecular weight influences the dissociation kinetics more than other molecular properties such as lipophilicity and flexibility [47].

Crystal structures of protein-ligand complex give more information for compound optimization, but it takes a lot of time to obtain them, not all proteins can be crystalized, etc. Thus, it is useful to understand what happens in complex formation by using thermodynamic and kinetic parameters.

### 3 Carbonic anhydrase as a drug target

The carbonic anhydrase (CA, carbonate dehydratase, carbonate hydrolyase ) (EC 4.2.1.1), a superfamily of metalloenzyme, was discovered in bovine erythrocytes in 1932 [3]. It catalyzes the reversible conversion of carbon dioxide to bicarbonate



This reaction can occur without a catalyst, but it is too slow and cannot provide required products for an organism and meet the metabolic needs. The idea that there must be a catalyst for this reaction, was first raised in 1928 and demonstrated [3].

Currently, CAs are divided into  $\alpha$ -,  $\beta$ -,  $\gamma$ -,  $\delta$ -,  $\zeta$ -,  $\eta$ - and  $\theta$ -CA families. Enzymes are distributed in all living world, but only  $\alpha$ -CAs are found in mammals and, herewith, in humans. This is the reason why  $\alpha$  class posses the greatest

interest for scientists. Moreover, CA expression disorders cause many diseases, thus it is “attractive” target for drug design. Therefore, the thesis is focused on the human CAs.

## 3.1 Catalytic mechanism of CA

Most of human CA isoforms are monomers [48–51], but CA VI, IX and XII are dimers [52–55]. The active site of  $\alpha$ -CAs is situated deeply in the center of the molecule at the end of the cone shaped cavity, which begins on the surface. One side of the active site is hydrophobic and the other one is hydrophilic. In the end of the cavity is a zinc ion, coordinated by three imidazoles of histidine residues His94, His96, His119 and a hydroxide ion (catalytically active form) or water molecule (not active form) as a fourth ligand [55–57].

When the protein is in the catalytically active form, hydroxide ion nucleophilically attacks  $\text{CO}_2$  molecule, which is bound in the hydrophobic part [58]. Formed bicarbonate  $\text{HCO}_3^-$ , coordinated by zinc, is exchanged with water molecule and dissociates. The state with Zn(II)-bound water molecule is not active. Proton from the water is transferred to the imidazole ring of His64, and afterwards, imidazole ring transfers  $\text{H}^+$  to buffer solution [57].

Note that amino acid sequences in the active sites slightly differ and His64 residue exists in CA isoforms I, II, IV, VI, VII and XII, while in other isozymes it is changed. For example, isoform CA III possesses a lysine residue at this position and therefore has approximately 0.3 % activity compared to CA II. Furthermore, CA III has replaced His64, His67, and His131 by Lys64, Arg67, and Phe131, and these aminoacids are found to be the key residues for proton transfer during catalysis [56]. CA VA has Tyr64 as proton shuttle, instead of His64 [56].

The catalytic rates of different CA isoforms are ranging between  $10^4$  and  $10^6$  reactions per second. Catalytic activity is modulated by the arrangement of water molecules in the active site [59] while the spontaneous reaction occurs at a rate of  $0.037\text{s}^{-1}$  [60].

## 3.2 Diseases related to CAs

As mentioned above, substrates and products of CA catalyzed reaction are very simple molecules, but vital for homeostasis and pH regulation. Thus, even small changes in protein expression are associated with many diseases. Sulfonamide inhibitors of CAs are used for the treatment of glaucoma, epilepsy, obesity, some neurological conditions, and other. Sulfonamides are also used as diuretics. CA IX and CA XII are highly over-expressed in cancer cells, thus, inhibitors of these isoforms are in clinical development as anticancer agents/diagnostic tools for hypoxic, metastatic tumors [6].

## Cardiovascular diseases

Inhibition of CA II and CA IV are involved in the diuretic effects in humans. These CAs are highly abundant in several specific nephron segments in the kidney and maintain acid-base balance, reabsorb bicarbonate and produce  $\text{NH}_4^+$  [61].

By inhibiting overexpressed CA isoforms, sulfonamides, as diuretics, can alkalize and increase the production of urine [62, 63]. The inhibition of CA II reduces chloride/bicarbonate exchange activity [61, 64], while inhibition of CA IV diminishes renal acid secretion [61, 65, 66]. This leads to accumulation of carbonic acid and reduction in blood pH accompanied with inhibition of reabsorption of bicarbonate and sodium ions from proximal tubule of kidney. Thus, elimination of these ions into urine increases, leading to diuresis, which in turn leads to a reduction in blood volume and pressure.

## Eye disorders

CA II, IV, and XII are responsible for the bicarbonate secretion in the anterior uvea of the eye [67–69]. Bicarbonate is the main constituent of aqueous humor, which causes high intraocular pressure (IOP). Inhibition of these CA isoforms shows the IOP reducing effect by decreasing aqueous humor secretion [70, 71]. It was found, that CA inhibition is more effective when systemic inhibitors are used as compared with topical, but oral consumption causes many side effects [72, 73].

IOP was formerly synonymous with glaucoma, but about 20 % of patients have a normal IOP. Thus, glaucoma can be defined as an optic neuropathy. Despite this, intraocular pressure remains the major and only treatable risk factor [73].

Furthermore, CA IV inhibition contributes to treatment of macular edema [74], which is associated with a variety of ocular conditions, including postoperative inflammation, retinal vein occlusions, uveitis, and diabetic retinopathy [75]. Inhibition of CA IV results in subretinal space acidification and increased chloride ion transport [76].

Study made with topical dorzolamide and oral acetazolamide showed 40 % and 28 % improvement in macular edema, respectively [77]. As in glaucoma treatment, oral CA inhibitors have more side effects than topical ones [76]. There is still a continued effort to improve therapeutic agents for the treatment of eye disorders.

## Obesity

Recent statistics indicate that obesity is an increasingly serious clinical and socio-economic problem, one of the greatest public health challenges, which negatively affects the quality of life and reduces average life expectancy worldwide. To avoid more disorders that arise from overweight, physical activity, maintenance of lower

body weight and behavioral therapy to reinforce weight reduction have to be induced to optimize weight loss. When it does not help to normalize body weight, it may be necessary to involve a pharmacological agent for the treatment in addition with lifestyle intervention [78].

Current potential to treat obesity with drugs is very limited [78]. There have been many weight loss drugs that have been developed to affect the obesity, but all of these drugs have risks of serious side effects [79].

It was shown that weight loss is a side effect in a treatment of epilepsy by CA inhibitors [80]. Three CA isoforms participate in biosynthesis of fatty acids: CA II, CA VA and CA VB [80]. Inhibition of these isozymes decrease lipogenesis in the mitochondria and cell cytosol [78].

#### **Neurological disorders**

High altitude illness is an inadequate acclimatization. It begins with acute mountain sickness and may progress to high-altitude cerebral edema, which is marked by brain swelling and increased intracranial pressure leading to other disorders and ultimately death if not treated quickly [81].

By inhibiting the CA, sulfonamides such as acetazolamide and benzolamide, reduce renal bicarbonate reabsorption, causing a bicarbonate diuresis and metabolic acidosis that increase respiratory rate and speed up acclimatization. CA II is not inhibited at low doses of acetazolamide, so it is still fully functional in the vasculature. However, CA IV is completely inhibited by even very low doses of acetazolamide, leading to CO<sub>2</sub> retention in cerebral tissue and increased CO<sub>2</sub> pressure of cerebrospinal fluid. CO<sub>2</sub> changes in the cerebrospinal fluid is sufficient to drive up alveolar ventilation [82].

Carbonic anhydrase I expression was increased in the spinal cord of patients with amyotrophic lateral sclerosis. This suggests that this isoform may have an important function in motor neuron degeneration [83].

CAs are also associated with obstructive sleep apnea [82], cerebral ischemia [84], Alzheimer's disease [85], epilepsy [86] and others, but the mechanism how CA inhibition contributes to treatment is not clear. Therefore, carbonic anhydrases are very interesting research objects and alternative CA inhibitors could give additional information.

#### **Cancer**

The reversible hydration of carbon dioxide to carbonic acid executed by CA is relevant for metabolism and pH regulation of tumor cells [87, 88]. Expression of two CA isoforms IX and XII is significantly increased under tumor hypoxic conditions, thus these isozymes are characterized as tumor markers in human

cancers [88, 89]. CA XII is expressed in many healthy tissues [89], but CA IX is only detected in the gastrointestinal tract. However, CA IX becomes highly expressed and serves as a hypoxic biomarker in the majority of solid tumors [87, 90, 91]. CA XII, also regulated by hypoxia, has received less attention than CA IX, but is usually expressed in the same cancerous cells as CA IX [89].

Cancer cells differ from normal cells. One of the differences is an abnormal growth of cancerous cells due to an erratic vasculature [92–94]. Strong hypoxic condition is created due to a large diffusion distance between nutritive blood vessels and the lack of oxygenated blood supply [92, 94]. CAs help tumors to adapt to hypoxic stress by neutralizing the acidic conditions of the tumor microenvironment [94, 95]. Other differences of tumor cells comparing to normal ones are prolonged extracellular acidification ( $\text{pH}_e$ ), which contributes to a number of aspects including metastasis, and increased intracellular pH ( $\text{pH}_i$ ), which favors cell proliferation [90, 96].

Inhibition of CA IX affects the  $\text{pH}_e$  and  $\text{pH}_i$  of the cancer cells [97, 98] and stops their growth and migration [99], thus confirming CA IX importance for tumor progress. Selective and potent CA IX and CA XII inhibitors are valuable in cancer treatment.

### 3.3 CA inhibition by sulfonamide compounds

CA inhibitors can be divided into two groups: those that coordinate the zinc in the active site and those that do not [6]. Here we are focus only on primary sulfonamide bearing inhibitors that bind directly to the zinc cation, thus, other inhibition mechanisms will not be described.

Sulfonamides are the most important class of CA inhibitors, with 9 compounds in clinical use today [100] and their inhibition mechanism is well understood. Sulfonamide bind to the active site in deprotonated form. CA must be protonated, thus binding occurs when hydroxy group is replaced by  $\text{H}_2\text{O}$  molecule (CA is not catalytically active). Deprotonated sulfonamide replace Zn(II)-bound solvent molecule. Sulfonamide N atom is involved in a coordinating bond with the zinc and hydrogen atoms act as a H-bond donor to Thr199 and to Glu106 [101].



Even if strong electrostatic interaction occurs between the negatively charged sulfonamide and the positively charged zinc cation, association of these two molecules is described as a slow process. Therefore, many hypothesis about multistep mechanisms appeared [102–104].

The existing drugs [100] suggest that the most successful and mostly used inhibitor design is “the tail approach”, when appending “tails” to the scaffolds of



aromatic-heterocyclic sulfonamides possessing different derivatives, in such way that an elongated molecule is obtained with its tail being able to interact with amino acid residues from the middle of the active site cavity, where they could interact with either the hydrophobic, the hydrophilic (or both) edge, which is the most variable region of the various CA isoforms [6].

Due to active site conservation among CA isoforms, cross-reactivity of CA inhibitors occurs and causes side effects. It necessitates the development of isoform-specific binders. Therefore, membrane impermeant inhibitors, which would specifically inhibit membrane-associated CAs without interacting with the cytosolic or mitochondrial isoforms, were designed.

## 4 Protonation of interacting components

As mentioned above, deprotonated sulfonamide can bind to protonated active site of CA and inhibit it. When protonation influence to binding affinity was noticed, inhibition activity of sulfonamides towards CA was related to ionization constants and indicated that the more potent inhibitor has lower  $pK_a$  [105].

CA interaction with thiocyanate at different pHs shows that the highest inhibition constant is at low pH [106]. Thiocyanic acid has a very low  $pK_a$  and in pH range between 5 and 11 exists in deprotonated form, while CA has  $pK_a$  about 7 and most of protein is protonated at low pH and becomes deprotonated when  $pH > pK_a$ . So, at pH 5 no protonation reactions have to occur, thus inhibition constant is highest. At basic pHs protonated fraction of CA becomes lower, less molecules can interact with thiocyanic acid, therefore the affinity becomes less potent.

In the case of sulfonamidic compounds, sulfonamide group has  $pK_a$  in the range between 8 and 11. Thus, at physiological pH half of CA and almost all compound is protonated. It means that at every pH only a small part of CA and sulfonamide can interact and the observed constant will never reach the highest (intrinsic) value.

The enthalpy of protein-ligand binding depends on protonation enthalpies of protein ( $\Delta_p H_{CA}$ ) and ligand ( $\Delta_p H_{\text{RSO}_2\text{NH}_2}$ ). Protons are picked up from the buffer or released to it, thus pH and protonation enthalpy of buffer ( $\Delta_p H_{\text{buf}}$ ) also influences the observed thermodynamic and kinetic values [14]. Buffer does not have influence on binding, inhibition or association constants of interaction, i.e. constants should be similar in every buffer. However, for enthalpy measurements, deprotonation of sulfonamide group, protonation of zinc-bound hydroxide, absorption or donation of buffer protons needed for interacting components are important. All these reactions are reflected in the measured ITC heat signals and due to different protonation enthalpies of various buffers, the observed enthalpies

of binding vary and may even change the sign in the presence of binding-linked protonation reactions.

Human CA isoforms have slightly different amino acid residues in the active sites and this is the reason why catalytic activity and ionization constants of Zn(II)-bound  $\text{H}_2\text{O}/\text{OH}^-$  are not similar [107–109]. All  $\text{p}K_a$  and  $\Delta_p H_{\text{CA}}$  values, are listed in Table 1. Since the interest of CA as a target protein has risen, ionization constants were observed by different catalytic methods, such as stopped-flow, Wilburn-Anderson or by using  $\text{O}^{18}$  exchange method. Taking into account that some discrepancies can appear in comparison of kinetic and thermodynamic assays,  $\text{p}K_a$  values were determined by FTSA and ITC methods. Protonation enthalpies of CA-Zn(II)- $\text{H}_2\text{O}$  can be determined only by ITC measuring  $\Delta_b H$  of CA-ligand interaction at different pHs. Note, that the values presented in Results section are listed in Table 1 too.

The  $\text{p}K_a$  of sulfonamide group of a compound can be determined spectrophotometrically, collecting spectra of equal concentrations of compound at different pHs [43] or by potentiometric titration using a pH-meter [110]. In some cases, compound can have limited solubility or two protonation groups that cannot be separated, then  $\text{p}K_a$  of structurally similar compound, which is more soluble or has only  $\text{SO}_2\text{NH}_2$  as protonated group, is used. The other way to determine ionization constant of such compounds is the linear correlation of NMR chemical shifts of sulfonamide group protons and experimentally determined  $\text{p}K_a$ . The  $\text{p}K_a$  of the sulfonamide group often correlates with the thermodynamic parameters of binding to CA [109]. The  $\Delta_p H_{\text{RSO}_2\text{NH}_2}$  of sulfonamide group can be easily obtained by ITC [110].

To summarize, the  $K_b$  or association constants of interaction cannot be compared if measured at different pHs,  $\Delta_b H$  cannot be compared if observed at different buffers, unless protonation influence is subtracted.

**Table 1** Thermodynamics of CA protonation were obtained at 25°C and 37°C. The  $\text{p}K_a$ s are compared with the values found in literature.

CA isoform	$\text{p}K_a$ (lit.)	$\text{p}K_a$		$\Delta_p G$		$\Delta_p H$		$-T\Delta_p S$	
		25°C	37°C	25°C	37°C	25°C	37°C	25°C	37°C
CA I	8.1 [111]								
	6.9 [112]	8.4	8.1	-47.9	-48.2	-41.0	-38.5	6.9	9.7
	7.1 [113]								
	7.3 [114–116]								
CA II	6.9 [117, 118]								
	7.1 [112]	7.1	6.9	-40.5	-41.1	-26.0	-23.5	14.5	17.6
	6.8 [119]								
CA III	$\sim 5.0$ [119–121]	6.6	6.5	-44.0	n/d	n/d	n/d	n/d	n/d
	<6 [122]								
CA IV e.coli	6.2 [123]	6.8	6.6	-38.8	-39.0	-33.0	-30.5	5.8	8.5
CA IV murine	6.6 [124]								
CA VA		7.3	7.3	n/d	n/d	n/d	n/d	n/d	n/d

*Continued on next page*

## 5. Intrinsic parameters of protein-ligand binding

Table 1 – Continued from previous page

CA isoform	$pK_a$ (lit.)	$pK_a$		$\Delta_p G$		$\Delta_p H$		$-T\Delta_p S$	
		25°C	37°C	25°C	37°C	25°C	37°C	25°C	37°C
CA VB		7.2	7.0	-41.1	-41.5	-30.0	n/d	11.1	n/d
CA VI e.coli		6.2	6.0	-35.4	-35.6	-32.0	-29.0	3.4	6.6
CA VI saliva		5.5	n/d	-31.4	n/d	n/d	n/d	n/d	n/d
CA VI mammalian		5.5	n/d	-31.4	n/d	n/d	n/d	n/d	n/d
CA VII									
CA VII murine	6.2 [125]	7.0	6.8	-40.0	-40.2	-33.0	-30.5	7.0	9.7
CA IX	6.3 [126]								
CA <sup>cd</sup> IX <sup>a</sup>	7.0 [112]	6.8	6.6	-38.8	-39.4	-24.0	-21.5	14.8	17.9
CA <sup>fl</sup> IX <sup>b</sup>	6.5 [112]								
CA XII	7.1 [127]	7.0	6.8	-40.0	-40.4	-28.0	-25.5	12.0	14.9
CA XII	6.9 [112]								
CA XIII		8.3	8.0	-47.4	-47.5	-44.0	-41.5	3.4	6.0
CA XIV	6.9 [112]	6.3	6.1	-36.0	-36.2	n/d	n/d	n/d	n/d

Unpublished data is listed in italic; n/d - no data;  $\Delta_p G$ ,  $\Delta_p H$ , and  $-T\Delta_p S$  units are  $\text{kJ mol}^{-1}$

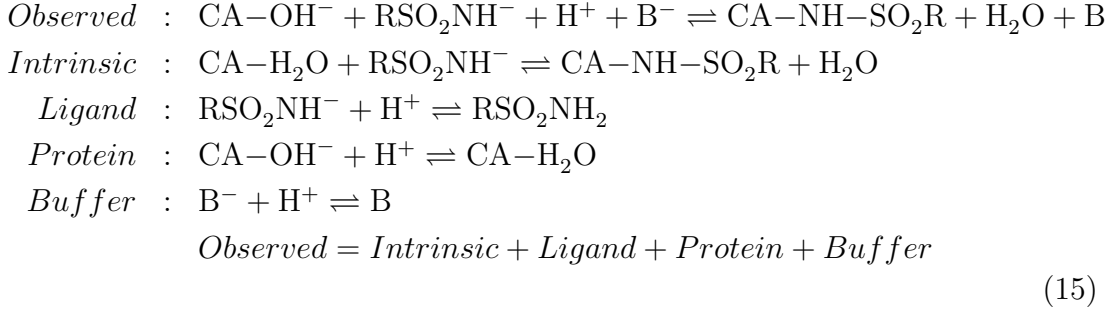
## 5 Intrinsic parameters of protein-ligand binding

Proton linkage can dramatically influence observed thermodynamic and kinetic values. This was determined with different protein systems [128–130]. In case of carbonic anhydrase binding, the observation that the inhibition constants vary due to protonation changes was made in 1963 [131]. Thus, the pH at which protein-ligand interaction occurs, plays a critical role in defining the binding affinity. The protonation enthalpy of buffer plays a critical role in defining the binding enthalpy too. As entropy cannot be determined experimentally, but is calculated from the difference between  $\Delta_b G$  and  $\Delta_b H$ , this will result in a false partitioning of enthalpy and entropy. An investigation of the binding energetics requires the dissection of the buffer-related contributions. Unfortunately, the observed parameters could mislead us when comparing compounds with significantly different  $pK_a$ s. In such cases, the structure — thermodynamics and structure — kinetics correlations may lead to incorrectly understood physical reasons for an increased or decreased affinity.

### 5.1 Intrinsic thermodynamic parameters of binding

First time the term “intrinsic” was mentioned in 1997 by Javier Gomez and Ernesto Freire [132]. They described all reactions that take place during protein ligand binding and derived the equations.

For the carbonic anhydrases, the observed thermodynamic parameters represent the sum of linked events: protein-ligand binding and at least three protonation–deprotonation reactions:



Fraction of deprotonated sulfonamide can be calculated when the protonation  $\text{p}K_a$  is known:

$$f_{\text{RSO}_2\text{NH}^-} = \frac{10^{\text{pH}-\text{p}K_{a-\text{RSO}_2\text{NH}^-}}}{1 + 10^{\text{pH}-\text{p}K_{a-\text{RSO}_2\text{NH}^-}}} \tag{16}$$

Similarly, the fraction of enzyme molecules with protonated water molecules bound to the active site Zn atom can be calculated if respective protonation  $\text{p}K_a$  is known:

$$f_{\text{CAZnH}_2\text{O}} = \frac{10^{\text{p}K_{a-\text{CAZnH}_2\text{O}}-\text{pH}}}{1 + 10^{\text{p}K_{a-\text{CAZnH}_2\text{O}}-\text{pH}}} \tag{17}$$

The intrinsic binding constant  $K_{b\_intr}$  is equal to the observed binding constant  $K_{b\_obs}$  divided by the available fractions of protonated Zn(II) hydroxy anion and deprotonated inhibitor:

$$K_{b\_intr} = \frac{K_{b\_obs}}{f_{\text{CAZnH}_2\text{O}}f_{\text{RSO}_2\text{NH}^-}} \tag{18}$$

The intrinsic Gibbs energy can be calculated according to equation (4):

$$\Delta_b G_{intr} = -RT \ln K_{b\_intr} \tag{19}$$

The intrinsic enthalpy of binding has contributions from the observed binding enthalpy ( $\Delta_b H_{obs}$ ), protonation enthalpies of inhibitor ( $\Delta_p H_{\text{RSO}_2\text{NH}_2}$ ), CA ( $\Delta_p H_{\text{CA}}$ ) and the buffer ( $\Delta_p H_{\text{buf}}$ ):

$$\Delta_b H_{intr} = \Delta_b H_{obs} - n_{\text{RSO}_2\text{NH}_2} \Delta_p H_{\text{RSO}_2\text{NH}_2} - n_{\text{CA}} \Delta_p H_{\text{CA}} + n_{\text{buf}} \Delta_p H_{\text{buf}} \tag{20}$$

where  $n_{\text{RSO}_2\text{NH}_2} = f_{\text{RSO}_2\text{NH}^-} - 1$  is the number of protons binding to the inhibitor,  $n_{\text{CA}} = 1 - f_{\text{CAZnH}_2\text{O}}$  is the number of protons bound to Zn(II)-hydroxide, and  $n = -(n_{\text{CA}} + n_{\text{RSO}_2\text{NH}_2})$  is the sum of uptaken or released protons.

However, it is enough to perform this analysis only once for each CA isoform by using one model inhibitor. Intrinsic parameters of binding of other inhibitors

can be calculated.

## 5.2 Intrinsic kinetic parameters of binding

The association and dissociation rate of sulfonamide-CA interaction depend on pH. It was shown by Taylor, King, and Burgen in 1970 [133]. They showed that  $k_a$  as a function of pH is related to the ionization constants of the protein and ligand and can be calculated. However,  $k_d$  of binding was insensitive to pH changes.

Fractions of ligand and protein, interacting at certain pH, can be calculated using equations (16) and (17). Intrinsic association constant  $k_{a\_intr}$  is:

$$k_{a\_intr} = \frac{k_{a\_obs}}{f_{CAZnH_2O}f_{RSO_2NH^-}} \quad (21)$$

Despite this finding in 1970s, there are no more studies, where protonation effect would be dissected from the kinetic data.



# Materials and methods

## 6 Materials

### 6.1 CA inhibitors

Commercial ligands were purchased from “Sigma Chemical Co” (**EZA**, **AZM**, *para*-methyl benzenesulfonamide (***p*-MBS**)). These compounds were used without further purification.

All other CA inhibitors used in this study were synthesized in the Department of Biothermodynamics and Drug Design, Institute of Biotechnology, Vilnius university. Structures and purity of these compounds were confirmed by NMR, IR spectroscopy and MS methods.

### 6.2 Proteins

All recombinant human CA isoforms used in this study - CA I (3-261 amino acids), CA II (1-260 amino acids), CA III (4-260 amino acids), CA IV (19-284 amino acids), CA VA (35-305 amino acids), CA VB (40-317 amino acids), CA VI (21-290 amino acids), CA VII (1-264 amino acids), CA IX (138-390 amino acids), CA XII (30-291), CA XIII (1-262 amino acids) and CA XIV (16-280 amino acids) - were expressed and purified in Department of Biothermodynamics and Drug Design, Institute of Biotechnology, Vilnius university. CAs were expressed in *Escherichia coli*, except CA IX, which was expressed in mammalian cells, and purified using chromatography. Their purity, as determined by electrophoretic analysis SDS-PAGE, was  $\sim 90\%$ . Protein concentration before experiments were measured spectrophotometrically.

### 6.3 Chemicals

ANS (Aldrich Chemicals,  $\geq 97\%$ ),  $\text{CH}_3\text{COONa}$  (Fluka Chemie,  $\geq 99\%$ ), DMSO (Roth,  $\geq 99.5\%$ ),  $\text{H}_3\text{PO}_4$  (Sigma Aldrich, 85 % solution), HCl (Alfa Aesar, 36.5–38 %),  $\text{Na}_2\text{B}_4\text{O}_7 \cdot 10\text{H}_2\text{O}$  (Spectrum Chemical MFG corp.,  $\geq 99.5\%$ ),  $\text{Na}_2\text{HPO}_4$  (Fluka Chemie,  $\geq 99\%$ ),  $\text{Na}_3\text{PO}_4 \cdot 12\text{H}_2\text{O}$  (Roth,  $\geq 98\%$ ), NaCl (Roth,  $\geq 99.5\%$ )

%),  $\text{NaH}_2\text{PO}_4 \cdot \text{H}_2\text{O}$  (Fisher Scientific, 99.4 %),  $\text{NaOH}$  (Alfa Aesar,  $\geq 98$  %),  $\text{Tris-OH}$  (Sigma,  $\geq 99.9$  %),  $\text{Tris-HCl}$  (Sigma,  $\geq 99$  %),  $\text{NHS}$  (N-hydroxysuccinimide) (Sigma Aldrich, 98 %),  $\text{EDC}$  (1-ethyl-3-(3-(dimethylamino)propyl) carbodiimide-hydrochloride) (Sigma Aldrich, 98 %), ethanolamine hydrochloride (Sigma Aldrich,  $\geq 99$  %).

## 6.4 Buffers

**Phosphate buffer:** solutions of 50 or 100 mM  $\text{Na}_2\text{HPO}_4$ , containing 100 mM  $\text{NaCl}$  and 50 or 100 mM  $\text{NaH}_2\text{PO}_4$ , containing 100 mM  $\text{NaCl}$  were mixed at appropriate ratios to reach desired pH value.

**TRIS buffer:** solutions of 50 mM  $\text{Tris-OH}$ , containing 100 mM  $\text{NaCl}$  and 50 mM  $\text{Tris-HCl}$ , containing 100 mM  $\text{NaCl}$  were mixed at appropriate ratios to reach desired pH value.

**Universal buffer:** Four solutions of

- 50 mM  $\text{CH}_3\text{COONa}$ , 25 mM  $\text{Na}_2\text{B}_4\text{O}_7$ , 100 mM  $\text{NaCl}$  and  $\text{Na}_3\text{PO}_4$
- 50 mM  $\text{CH}_3\text{COONa}$ , 25 mM  $\text{Na}_2\text{B}_4\text{O}_7$ , 100 mM  $\text{NaCl}$  and  $\text{Na}_2\text{HPO}_4$
- 50 mM  $\text{CH}_3\text{COONa}$ , 25 mM  $\text{Na}_2\text{B}_4\text{O}_7$ , 100 mM  $\text{NaCl}$  and  $\text{NaH}_2\text{PO}_4$
- 50 mM  $\text{CH}_3\text{COONa}$ , 25 mM  $\text{H}_3\text{BO}_3$ , 100 mM  $\text{NaCl}$  and  $\text{H}_3\text{PO}_4$

were mixed to reach desired pH value that was verified by pH-meter.

## 7 Methods

### 7.1 Fluorescent thermal shift assay (FTSA)

#### Experimental procedure

Fluorescent thermal shift assay experiments were performed in a Corbett Rotor-Gene 6000 (Qiagen Rotor-Gene Q) instrument using the blue channel (excitation  $\lambda=365\pm 20$  nm, detection  $\lambda=460\pm 15$  nm). Protein samples containing various concentrations of inhibitor were heated from  $25^\circ\text{C}$  to  $99^\circ\text{C}$  while recording extrinsic fluorescence and determining the protein melting temperatures at each inhibitor concentration. Samples contained 10  $\mu\text{M}$  protein, 0–200  $\mu\text{M}$  ligand, 50  $\mu\text{M}$  solvatochromic dye ANS and 50 mM sodium phosphate buffer containing 100 mM  $\text{NaCl}$  at pH 7.0, with a final DMSO concentration of 2 %. The applied heating rate was  $1^\circ\text{C min}^{-1}$ .



### Determination of protein melting temperature

Protein melting temperatures ( $T_m$ s) were determined by fitting the experimental protein melting curve according to equation, which describes fluorescence of protein-dye complex:

$$y(T) = y_N + \frac{y_U - y_N}{1 + e^{\Delta_U G/RT}} = y_U + \frac{y_N - y_U}{1 + e^{-\Delta_U G/RT}} \quad (22)$$

where  $\Delta_U G$  is the Gibbs energy of unfolding, and  $y_N$  and  $y_U$  are the fluorescence intensity of native and unfolded proteins, respectively.

The  $\Delta_U G$  can be described as a difference of unfolding enthalpy  $\Delta_U H$  and unfolding entropy  $\Delta_U S$  of protein:

$$\Delta_U G = \Delta_U H - T\Delta_U S, \quad (23)$$

The  $y_N$  and  $y_U$  depend on temperature:

$$y_N(T) = y_{N,T_m} + m_N(T - T_m), \quad (24)$$

$$y_U(T) = y_{U,T_m} + m_U(T - T_m), \quad (25)$$

where  $m_N$  and  $m_U$  are the slopes of the fluorescence dependencies on temperature of native and unfolded protein, respectively (Fig. 2).

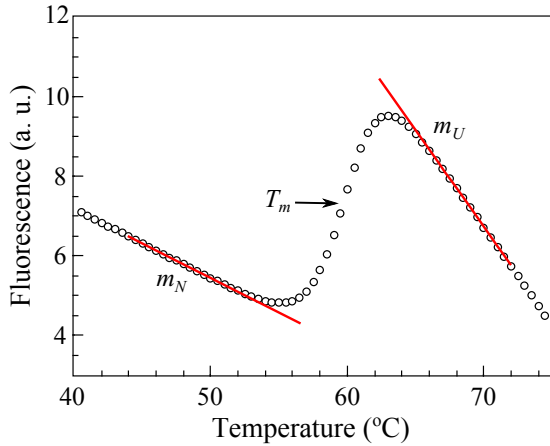
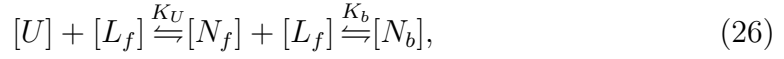


**Figure 2** Fluorescence intensity changes dependence on protein stability. Red lines show the slopes of the fluorescence intensity of the native ( $m_N$ ) and unfolded ( $m_U$ ) protein. The  $T_m$  is a melting point where half of the protein molecules are native and half of them are unfolded.

### Determination of the binding constant

The temperature-induced protein transition from native (N) to unfolded (U) state can be affected by a ligand (L) which stabilizes or destabilizes the protein upon binding:



where  $[L_f]$  is concentration of a free ligand,  $[N_b]$  is concentration of bound native protein and ligand. The  $K_U$  and  $K_b$  are constants of protein unfolding and binding, respectively, and they can be described:

$$K_U = \frac{[U]}{[N_f]} = e^{-(\Delta G_U/RT)}, \quad (27)$$

$$K_b = \frac{[N_b]}{[N_f][L_f]} = e^{-(\Delta G_b/RT)}, \quad (28)$$

where  $\Delta G_U$  and  $\Delta G_b$  are the Gibbs energies of unfolding and binding, respectively.  $[L_f]$  can be expressed from equation 28:

$$[L_f] = \frac{[N_b]}{K_b[N_f]}. \quad (29)$$

Total ligand concentration  $L_t$  is equal to the sum of  $[L_f]$  and bound ligand  $[N_b]$ :

$$L_t = [L_f] + [N_b]. \quad (30)$$

Combining equation 29 and 30 one obtains:

$$L_t = \frac{[N_b]}{K_b[N_f]} + [N_b] = [N_b] \left( \frac{1}{K_b[N_f]} + 1 \right). \quad (31)$$

From the equation 27,  $[N_f]$  is equal to:

$$[N_f] = \frac{[U]}{K_U}. \quad (32)$$

$P_t$  is total concentration of protein and, thus, a sum of concentrations of unfolded  $[U]$ , native free  $[N_f]$  and native bound  $[N_b]$  protein:

$$P_t = [U] + [N_f] + [N_b]. \quad (33)$$

Using equations 32 and 33 one obtains:

$$[N_b] = P_t - \frac{[U]}{K_U} - [U]. \quad (34)$$

This expression together with equation 31 leads to:

$$L_t = \left( P_t - \frac{[U]}{K_U} - [U] \right) \left( \frac{1}{K_b \frac{[U]}{K_U}} + 1 \right). \quad (35)$$

At a melting temperature,  $T_m$ ,  $[U] = \frac{P_t}{2}$  and thus the determination of binding constant, using  $T_m$ s of various ligand concentrations, are described using the equation:

$$\begin{aligned} L_t &= (P_t - \frac{P_t}{2K_U} - \frac{P_t}{2})(\frac{2K_U}{K_b P_t} + 1) = (\frac{P_t}{2} - \frac{P_t}{2K_U})(\frac{2K_U}{K_b P_t} + 1) = \\ &= \frac{P_t}{2K_U}(K_U - 1)(\frac{2}{P_t} \frac{K_U}{K_b} + 1) = (K_U - 1)(\frac{1}{K_b} + \frac{P_t}{2K_U}). \end{aligned} \quad (36)$$

## 7.2 Isothermal titration calorimetry (ITC)

### Protein-ligand binding

ITC experiments were performed by using VP-ITC instrument (Microcal, Inc., part of Malvern, Northampton, MA, USA). For the binding reactions the calorimeter cell contained 4-10  $\mu$ M protein, 2 % DMSO, 50-100 mM sodium phosphate buffer (pH 7.0) and 100 mM sodium chloride. Syringe contained 40-100  $\mu$ M ligand, 2% DMSO, 50-100 mM phosphate buffer (pH 7.0) and 100 mM sodium chloride. Experiments consisted of 25 injections, volume of the first injection was 1-5  $\mu$ L, while others were 10  $\mu$ L, added at 200 s intervals, at 25 or 37  $^{\circ}$ C.

The experiments of EZA binding at various pHs were performed using 4-6  $\mu$ M of protein, 2% DMSO, 50-100 mM sodium phosphate or TRIS buffer containing 100 mM sodium chloride in the cell and 40-60  $\mu$ M of EZA, 2% DMSO and 50-100  $\mu$ M phosphate or TRIS buffer containing 100 mM sodium chloride in the syringe. Buffer solution was the same in the syringe and in the cell and pH values were checked before and after the experiment. Experiments consisted of 25 injections, volume of the first injection was 5  $\mu$ L, while others were 10  $\mu$ L, added at 3-4 min intervals, at 25  $^{\circ}$ C.

ITC data were analyzed using MicroCal Origin software. The first point in the integrated data graph was omitted. The binding constants, enthalpies, and entropies of binding were estimated after fitting the data with the single binding site model.

### Protonation enthalpy of the compound

The enthalpy of inhibitor protonation was measured by titrating with 5 mM  $\text{HNO}_3$  the cell solution containing the inhibitor (0.25 mM) and 1.5 equivalent (0.375 mM) of NaOH. The experiment consisted of 56 injections. The volume of each injection was 5  $\mu$ L, added at 200 s intervals. DMSO concentrations in the syringe and the sample cell were equal (2.5%). Experiments were performed at 37  $^{\circ}$ C.

### 7.3 Surface plasmon resonance (SPR)

Interaction kinetic assays were performed with Biacore S51, Biacore T200 surface plasmon resonance biosensor instruments (GE Healthcare, Uppsala, Sweden). Vladimir O. Talibov at Uppsala University (Sweden) performed experiments using Biacore 2000 instrument (GE Healthcare, Uppsala, Sweden) as well. All experiments were performed at 25 °C.

#### Sensor surface preparation

Proteins were buffer-exchanged against the buffers without primary amines and immobilized on a research-grade CM5 and Series S CM5 Sensor Chip (GE Healthcare, Uppsala, Sweden) using a standard amine coupling procedure. Carboxymethyl-dextran matrix of the sensorchip was activated with 0.1 M NHS and 0.4 M EDC at a flow rate of 10-20  $\mu\text{L min}^{-1}$  for 7 min.

For immobilization, 75  $\mu\text{g mL}^{-1}$  of CA I, 100  $\mu\text{g mL}^{-1}$  of CA II, 25  $\mu\text{g mL}^{-1}$  of CA VII, 100-200  $\mu\text{g mL}^{-1}$  of CA IX, 25  $\mu\text{g mL}^{-1}$  of CA XII, and 75-200  $\mu\text{g mL}^{-1}$  of CA XIII were used. The coupling buffer (10 mM sodium acetate buffer) pH 5.0 was used for CA I, CA II, CA VII, CA XII, and CA XIII and pH 4.5 for CA IX. Unreacted activated groups of the dextran matrix were deactivated by injection of 1 M ethanolamine hydrochloride (pH 8.5) for 10 min. Immobilization was performed using 10 mM phosphate buffer containing 150 mM NaCl, pH 7.4 as a running buffer.

#### Interaction kinetic analysis

Interaction assays were performed using 50 mM sodium phosphate (in the pH range from 6 to 8), TRIS (at pHs 8.5 and 9) or sodium acetate (at pH 5.5) buffers supplemented with 100 mM NaCl and 2% (v/v) DMSO as a running buffer. Compounds were prepared from 10 mM DMSO stock solutions, diluted in the running buffer. At a flow rate of 30 or 90  $\mu\text{L min}^{-1}$  association was monitored for 30-60 s, dissociation time was varied upon the interaction stability. For ligands with a slow dissociation rate, a regeneration step was included in the assay cycle. Regeneration was performed by a 60 s injection of 200  $\mu\text{M}$  sulphanilamide dissolved in the running buffer. At the end of each cycle, the flow system except for the flow cell itself was washed with 25% DMSO to avoid carry-over effects.

Theoretical binding constants at every pH were calculated using equation 18. Concentration ten times higher than expected  $K_D$  value was used as the highest concentration in 2-fold dilution series for each pair of protein-ligand at each pH value. Each concentration series consisted of 6 analytical injections and 2 blank injections of a running buffer.

### **SPR data analysis**

Acquired sensorgrams were double-referenced against an empty surface and an average of blank injections, solvent corrected and analysed using BIAcore T100 v.2.0, BIAcore T200 v.1.0 and BIAevaluation v.3.0 software (GE Healthcare, Uppsala, Sweden). Global curve analysis was performed according to the standard 1:1 interaction model.

### **7.4 Spectrophotometric measurements**

To determine the  $pK_a$  of the ligands, the spectrophotometer model “Agilent 89090A” was used. Ligand solution (final concentration 30–50  $\mu\text{M}$ , containing 1% DMSO) was added to a buffer solution (100 mM, ranging from pH 5.5 to 12.5 at every half pH unit) and a UV–VIS spectra were recorded at 37°C. The ratio of absorbances (typically 10 nm above and below the isosbestic point) was plotted as a function of pH.

### **7.5 Calculation of intrinsic parameters**

The equations which were used to calculate intrinsic parameters are described in Literature overview section 5.



# Results

## 8 Characterization of human carbonic anhydrases I, IX, and XII protonation reaction

All catalytically active CA isoforms have zinc ion, coordinated by three histidine residues and hydroxy ion/water molecule, in the active site. Surrounding amino acids slightly differ in isoforms, thus catalytic activity and  $pK_a$  values of Zn(II)-bound  $\text{OH}^-/\text{H}_2\text{O}$  varies among the CAs. Due to these variations, the influence of protonation to binding energetics of every isozyme is different and must be defined.

The  $pK_a$  values of CA I, IX and XII were determined by FTSA<sup>1</sup> and ITC methods at 25°C temperature. Ethoxzolamide (**EZA**), well known CA inhibitor, was chosen for the experiments. Figure 3 panel A shows FTSA results of ligand binding to CA IX at two different pHs. The stronger binding at pH 6.0 than at pH 5.0 can be seen from the greater upshift. Addition of the compound to the solution of CA IX shifts the protein melting temperature upwards. The inset shows  $T_m$ s as a function of added ligand and melting curves exhibit a continuously increasing behavior.

Figure 3 panel B demonstrates the ITC data in buffers with different protonation enthalpies at various pHs, indicating that the pH influences not only the binding constants but also the enthalpies. However, the Gibbs energies do not depend on buffer at the same pH (Table 2).

**Table 2** Observed thermodynamic parameters of **EZA** binding to CA I, CA IX, and CA XII in phosphate and TRIS buffers, determined by FTSA and ITC at 25°C. The data of  $\Delta_b G_{obs}^{ITC}$  is the average of the Gibbs energies observed in phosphate and TRIS buffers.

CA	pH	$\Delta_b G_{obs}^{FTSA}$	$\Delta_b G_{obs}^{ITC}$	$\Delta_b H_{obs}^{Pi}$	$\Delta_b H_{obs}^{Tris}$
	5.0	-33.4	-	-	-
CA I	6.5	-43.1	-41.7	-24.7	-66.6
	7	-46.3	-44.0	-28.4	-63.4

*Continued on next page*

<sup>1</sup>FTSA experiments of EZA binding to CA I at various pHs were performed by Vaida Linkuvienė, Miglė Kišonaitė, dr. Asta Zubrienė, and dr. Lina Baranauskienė. FTSA experiments of EZA binding to CA XII at various pHs were performed by dr. Asta Zubrienė.

Table 2 – Continued from previous page

CA	pH	$\Delta_b G_{obs}^{FTSA}$	$\Delta_b^{ITC} G_{obs}$	$\Delta_b H_{obs}^{Pi}$	$\Delta_b H_{obs}^{Tris}$
CA	7.5	-46.5	-42.4	-34.4	-63.4
CA I	9	-44.9	-41.0	-38.0	-47.5
	7	-49.9	-50.2	-42.6	-58.2
CA IX	7.5	-50.1	-49.1	-50.2	-49.0
	8	-49.1	-49.3	-55.9	-38.0
	8.5	-48.4	-48.2	-65.9	-38.7
	6	-44.5	-41.4	-30.4	-64.2
CA XII	7.5	-45.7	-45.2	-39.5	-55.7
	8	-43.5	-45.2	-57.1	-45.6
	8.5	-39.4	-42.3	-67.4	-38.2

The ligand binding affinity as a function of pH is shown in Figure 4. The Gibbs energy has a U-shape dependence on pH (Fig. 4 Panels A, C, and E). The solid U-shape line is a fit of experimental data to a model and the intrinsic Gibbs energies of isozymes binding to **EZA** (solid straight line) were determined ( $\Delta_b G_{intr} = -51.4 \text{ kJ mol}^{-1}$  for CA I,  $\Delta_b G_{intr} = -59.6 \text{ kJ mol}^{-1}$  for CA IX, and  $\Delta_b G_{intr} = -53.5 \text{ kJ mol}^{-1}$  for CA XII). The intrinsic affinity is always greater compared with observed. The  $pK_a$  values of CA I, IX, and XII were also determined from these data and are equal to 8.4, 6.8, and 7.0, respectively (Table 1).

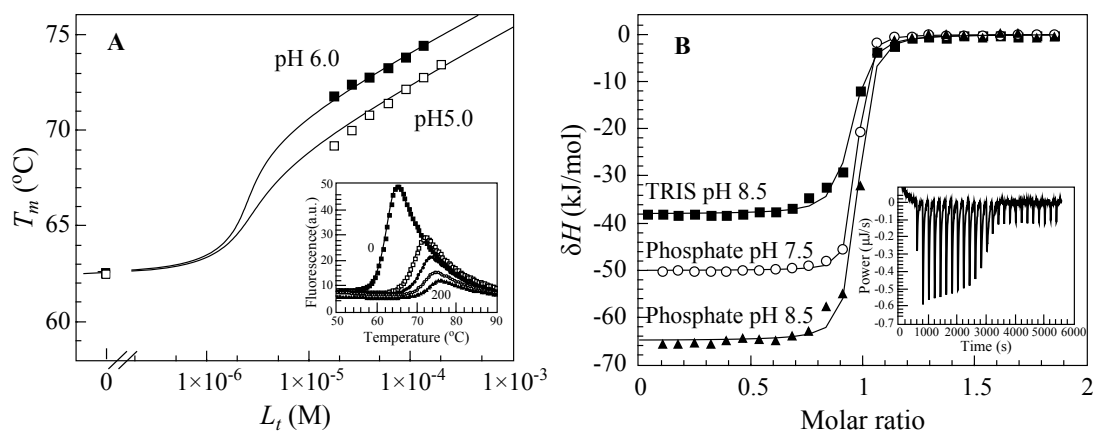


**Figure 3** The observed FTSA and ITC data of **EZA** binding to CA IX at different pHs. Panel A shows the protein melting temperature dependence on ligand concentration at pH 5.0 (open squares) and 6.0 (filled squares). The inset shows the raw curves of CA IX unfolding as a function of temperature in universal buffer at pH 5.0. Panel B shows ITC titrations of **EZA** binding to CA IX in phosphate and TRIS buffers, and different pHs. The inset shows the raw data of binding in phosphate buffer at pH 7.5. The filled squares represent the ITC data in TRIS buffer at pH 8.5, filled triangles - in phosphate at pH 8.5 and open squares - in phosphate at pH 7.5. The experiments were performed at 25°C.

To determine the protonation enthalpies of the Zn(II)-bound hydroxide anion in the active sites of studied CAs and the intrinsic enthalpy of **EZA** binding, ITC titrations in buffers with highly different protonation enthalpies (TRIS and



## 8. Characterization of human carbonic anhydrases I, IX, and XII protonation reaction

---

sodium phosphate) were performed in a series of pHs (Figure 4, panels B, D, and F). The pH dependence of the observed enthalpy ( $\Delta_b H_{obs}$ ) of **EZA** binding to CAs exhibited an X-shape. The solid sigmoidal line shows the observed enthalpy that would be determined if the buffers had zero enthalpy of protonation. It means that only the protonation contributions from the ligand and protein would be observed. The horizontal solid line shows the intrinsic enthalpy ( $\Delta_b H_{intr}$ ) that was obtained from this analysis of the ITC data. The dashed and dotted lines represent the fits of experimental data in phosphate and TRIS buffers, respectively. These fits show that the intrinsic enthalpy of **EZA** binding to studied isozymes is  $\Delta_b H_{intr} = -50.0 \text{ kJ mol}^{-1}$  for CA I,  $\Delta_b H_{intr} = -53.0 \text{ kJ mol}^{-1}$  for CA IX,  $\Delta_b H_{intr} = -50.6 \text{ kJ mol}^{-1}$  for CA XII. Thus, the  $\Delta_b H_{intr}$  was slightly less exothermic for CA I than for CA IX and CA XII due to more exothermic protonation enthalpy of CA I. The intrinsic enthalpies contribute the dominant fraction to the Gibbs energy of binding of EZA to CAI, CA IX and CA XII. The entropy contribution to binding affinities is negligible. Fit of ITC data also confirmed  $pK_a$  values determined by FTSA method.

In conclusion, the protonation  $pK_a$  of the Zn(II)-bound hydroxide anion in the catalytic domain of human recombinant CA isoforms I, IX, and XII is equal to 8.4, 6.8, and 7.0, respectively, determined by FTSA and ITC methods at 25°C. The enthalpies of protonation of the hydroxide bound to the Zn atom in the active center of CAI, CA IX and CAXII are equal to  $-41.0 \text{ kJ mol}^{-1}$ ,  $-24.0 \text{ kJ mol}^{-1}$ , and  $-28.0 \text{ kJ mol}^{-1}$ , respectively. Subtraction of the pH and buffer effects by using the model of linked protonation reactions yielded the intrinsic binding enthalpies and Gibbs energies of **EZA** binding to three isoforms of human CAs. The obtained enthalpies of protonation of these three CA isoforms can be used to calculate the intrinsic Gibbs energy and enthalpy of binding of any compound of interest without the need to perform these large series of titrations at various conditions.

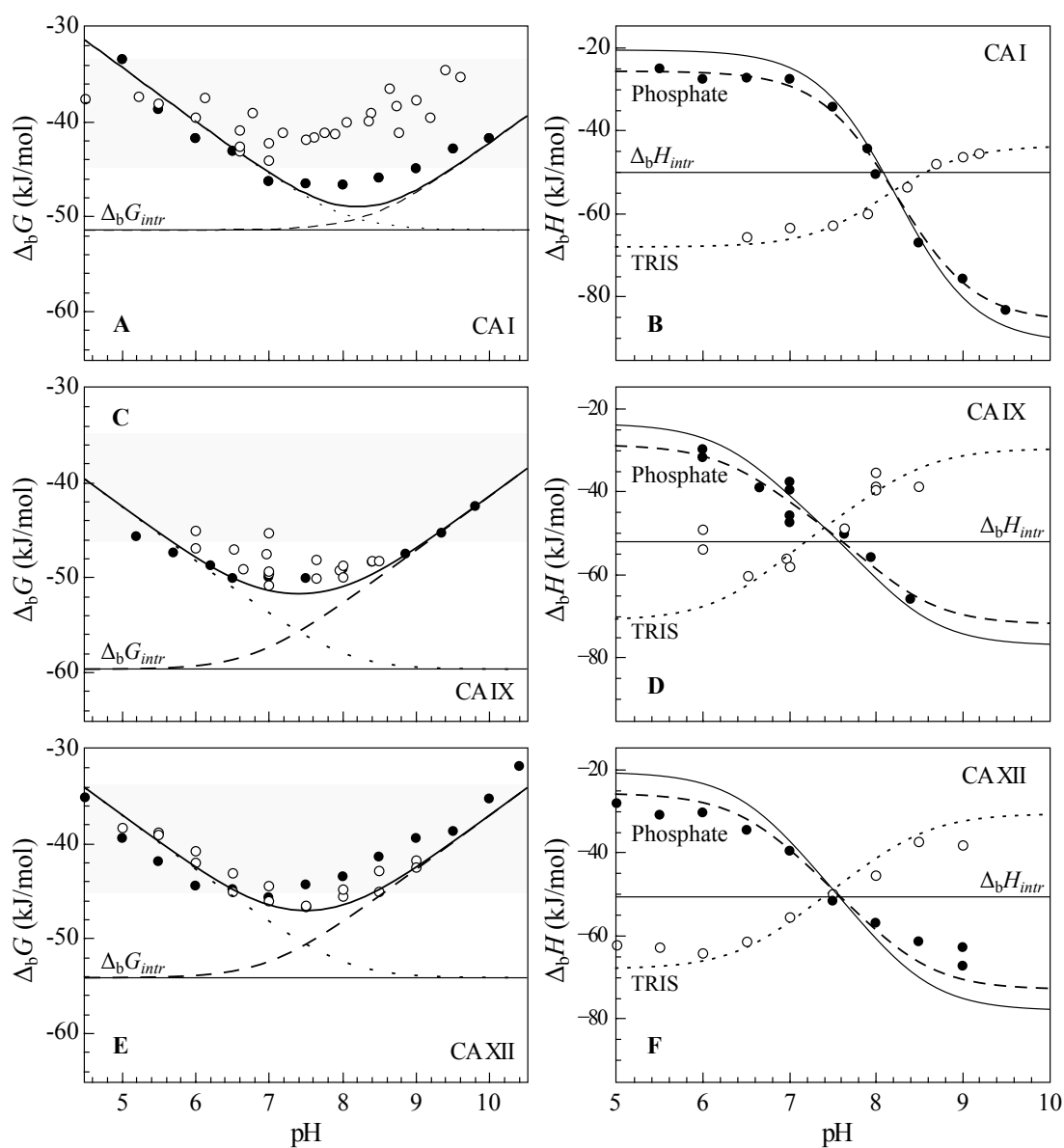


**Figure 4** EZA binding to CA I, IX, and XII dependence on pH. Panels A, C, and E show the Gibbs energy as a function of pH. Filled circles are the datapoints observed by FTSA, open circles - obtained by ITC method. Solid curve is a theoretical model of binding according to equation 19, dotted and dashed lines show a contribution of a fraction of deprotonated EZA and protonated CA. The straight line is the intrinsic Gibbs energy of binding. Panels B, D, and F show binding enthalpy dependence on pH obtained by ITC. Filled and open circles show the data observed in sodium phosphate and TRIS buffer, respectively. Dashed and dotted curves correspond theoretical models, solid curve is a theoretical model of  $\Delta_b H_{obs}$  when buffer does not have protonation enthalpy. Solid straight line is the intrinsic enthalpy of binding.

## 9 Observed and intrinsic thermodynamics of *meta*- and *para*-substituted benzenesulfonamide binding to CA

Modifications of benzenesulfonamide compounds influence their binding to carbonic anhydrases. Rational changes in tail moiety can modulate interactions with the enzyme and increase or decrease binding affinity. It is known that active site of several CA isoforms is composed of a hydrophobic and a hydrophilic side. For this reason compounds bearing two tails, one more hydrophobic than the other one, were synthesized and thermodynamic properties of complex formation were investigated. The binding thermodynamics of the two-tailed compounds was compared to the single-tailed compounds.

The dissociation constants (or Gibbs energies) of 25 structurally related benzenesulfonamides binding to 12 CA isoforms were experimentally determined by FTSA. Figures 5 and 6 show the structures of studied compounds and Gibbs energies of binding, where numbers on the arrows show the differences between  $\Delta_b G_{obs}$ s of two structurally similar compounds. Observed dissociation constants are listed in Table 3. Comparison of  $K_d$  values observed by FTSA and ITC methods are shown in Fig. 7. Although both FTSA and ITC methods are in a good agreement, binding constants determined calorimetrically were not used in this analysis, because several compounds bound CAs with  $K_{d\_obs} < 10$  nM and Wiseman  $c$  factor was too high for accurate  $K_b$  determination. To avoid discrepancies only FTSA data were used. However, compound **EA4-7** interaction to CA XIII could not be observed by FTSA due to high fluorescence (Fig. 8) and  $K_b$  obtained by ITC were used in analysis.

**Table 3** Experimentally measured observed dissociation constants ( $K_{d\_obs}$  (nM), determined by FTSA) of the compound binding to CA isoforms. Experiments were performed in sodium phosphate buffer at pH 7.0, data shown for 37°C.

Cpd	Observed dissociation constants $K_{d\_obs}$ (nM) for CA isoforms											
	I	II	III	IV	VA	VB	VI	VII	IX	XII	XIII	XIV
<b>EA8-1</b>	50000	63	12000	10	3400	250	590	11	71	200	710	40
<b>EA4-1-2</b>	100000	63	50000	50	17000	670	1200	17	130	330	830	100
<b>EA11-1</b>	100000	50	50000	110	1200	67	1000	20	140	130	500	59
<b>EA3-1</b>	100000	83	83000	400	5000	400	620	10	170	130	560	67
<b>EA4-1</b>	200000	10	25000	7.1	8300	770	1000	10	50	170	620	63
<b>EA5-1</b>	33000	20	7100	83	5000	83	170	5.0	50	50	400	50
<b>EA12-1</b>	200000	140	45000	n/d	2000	2300	1400	67	290	40	670	87
<b>EA10-1</b>	25000	20	2000	22	670	7.7	140	5.0	91	130	330	13
<b>EA9-1</b>	71000	170	200000	170	2500	77	1400	29	250	1700	180	67
<b>EA7-1</b>	200000	200	100000	330	200000	4000	1400	33	150	400	1200	170
<b>EA3-7</b>	14000	420	500000	n/d	50000	50000	33000	3300	20	4.0	670	n/d
<b>EA3-8</b>	1100	77	20000	n/d	20000	14000	1200	360	1.4	130	180	20
<b>EA4-7</b>	33000	170	160000	n/d	160000	25000	25000	1400	8.3	21	526	77
<b>EA4-8</b>	25000	20	50000	n/d	48000	7700	13000	67	n/d	130	1100	48

*Continued on next page*

Table 3 – Continued from previous page

Cpd	I	II	III	IV	VA	VB	VI	VII	IX	XII	XIII	XIV
<b>EA3-3o</b>	1400	3.3	25000	33	330	10	1200	4.0	3.1	20	25	1.8
<b>EA3-3</b>	1000	10	13000	10	590	77	1200	2.5	1.2	2.0	29	n/d
<b>EA4-3</b>	1200	3.7	25000	33	430	29	1700	0.67	0.71	1.0	67	2.0
<b>EA4-3o</b>	1000	1.1	33000	n/d	1400	11	1200	1.4	0.67	8.3	50	1.4
<b>EA3-2o</b>	2000	5.0	8300	n/d	1000	17	910	1.2	3.0	5.6	17	2.5
<b>EA3-2</b>	10000	31	15000	1.4	5600	330	1400	11	4.0	6.2	100	n/d
<b>EA4-2</b>	6700	5.0	33000	1.7	4500	130	830	1.2	2.0	0.83	180	5.6
<b>EA4-2o</b>	1400	3.3	17000	n/d	5600	19	1400	0.33	1.5	3.1	67	4.0
<b>EA3-4o</b>	6300	36	14000	250	710	77	2400	9.1	45	83	130	20
<b>EA3-4</b>	2100	13	5000	33	500	150	1600	3.3	15	10	91	13
<b>EA4-2c</b>	10000	25	77000	2.9	2200	100	1400	7.7	5.0	10	330	6.2

Italic value is for ITC data; the standard error of  $K_d$  measurements is  $\pm 2$  times [31, 134]; n/d – no data; the weakest binders are determined with the limit of 200000 nM.

The enthalpies of compound binding to 4 isoforms (CA II, CA VII, CA XII, and CA XIII) were also determined by ITC and the entropies were calculated using eq. 5 (Table 4). Several ITC experiments were repeated in the sodium phosphate and TRIS chloride buffers, because peaks of raw curves were too small in phosphate and accurate thermodynamic parameters could not be observed (Fig. 9, Panels A and B) or raw curves were too noisy and baselines were not flat (Fig. 9, Panels C and D). Several experiments were repeated in TRIS buffer solution even if the results obtained in phosphate buffer were suitable, to compare thermodynamic parameters of binding (Fig. 9, Panels E and F).

**Table 4** Experimentally determined compound  $pK_a$  and protonation enthalpy  $\Delta_p H$  (listed in the first column below compound name), measured the observed Gibbs energies (determined by FTSA), enthalpies (determined by ITC), and entropies (calculated from the difference between  $\Delta_b H$  and  $\Delta_b G$ ) of the compound binding to four isoforms of recombinant human CAs. Binding experiments were performed in sodium phosphate (Pi) and TRIS chloride (TRIS) buffers at pH 7.0. All values were determined at 37°C.

Compound		Observed thermodynamic parameters				
		CA II	CA VII	CA XII	CA XIII	
<b>EA3-1</b>	$\Delta_b G$ , kJ mol <sup>-1</sup>	-42.0	-47.5	-40.9	-37.1	
	$\Delta_b H^{Pi}$ , kJ mol <sup>-1</sup>	-17.8	-21.9	-35.4	-22.4	
	$\Delta_b H^{TRIS}$ , kJ mol <sup>-1</sup>	n/d	-44.4	n/d	n/d	
	$pK_a=8.8$	$-T\Delta_b S^{Pi}$ , kJ mol <sup>-1</sup>	-24.2	-25.6	-5.5	-14.7
	$\Delta_p H=-29.7$ kJ mol <sup>-1</sup>	$-T\Delta_b S^{TRIS}$ , kJ mol <sup>-1</sup>	n/d	-3.1	n/d	n/d
<b>EA4-1</b>	$\Delta_b G$ , kJ mol <sup>-1</sup>	-47.5	-47.5	-40.2	-36.9	
	$\Delta_b H^{Pi}$ , kJ mol <sup>-1</sup>	-17.0	-15.4	-27.6	-20.5	
	$\Delta_b H^{TRIS}$ , kJ mol <sup>-1</sup>	-38.7	-28.9	n/d	n/d	
	$pK_a=8.8$	$-T\Delta_b S^{Pi}$ , kJ mol <sup>-1</sup>	-30.5	-32.1	-12.6	-16.4
	$\Delta_p H=-29.3$ kJ mol <sup>-1</sup>	$-T\Delta_b S^{TRIS}$ , kJ mol <sup>-1</sup>	-8.8	-18.6	n/d	n/d
<b>EA4-1-2</b>	$\Delta_b G$ , kJ mol <sup>-1</sup>	-42.8	-46.1	-38.5	-36.1	
	$\Delta_b H^{Pi}$ , kJ mol <sup>-1</sup>	-15.0	-19.5	-14.1	-16.4	
	$\Delta_b H^{TRIS}$ , kJ mol <sup>-1</sup>	n/d	-22.0	n/d	n/d	
	$pK_a=8.7$	$-T\Delta_b S^{Pi}$ , kJ mol <sup>-1</sup>	-27.8	-26.6	-24.4	-19.7
	$\Delta_p H=-27.6$ kJ mol <sup>-1</sup>	$-T\Delta_b S^{TRIS}$ , kJ mol <sup>-1</sup>	n/d	-24.1	n/d	n/d
<b>EA5-1</b>	$\Delta_b G$ , kJ mol <sup>-1</sup>	-45.7	-49.3	-43.4	-38.0	
	$pK_a=8.8$	$\Delta_b H^{Pi}$ , kJ mol <sup>-1</sup>	-18.7	-10.3	-19.0	-8.0
	$\Delta_p H=-31.4$ kJ mol <sup>-1</sup>	$\Delta_b H^{TRIS}$ , kJ mol <sup>-1</sup>	n/d	-27.8	n/d	n/d

Continued on next page

9. Observed and intrinsic thermodynamics of meta- and para-substituted benzenesulfonamide binding to CA

Table 4 – Continued from previous page

Compound		CA II	CA VII	CA XII	CA XIII
<b>EA5-1</b>	$-T\Delta_b S^{Pi}$ , kJ mol <sup>-1</sup>	-27.0	-39.0	-24.4	-30.0
	$-T\Delta_b S^{TRIS}$ , kJ mol <sup>-1</sup>	n/d	-21.5	n/d	n/d
<b>EA7-1</b> p <i>K</i> <sub>a</sub> =8.8 $\Delta_p H = -31.0$ kJ mol <sup>-1</sup>	$\Delta_b G$ , kJ mol <sup>-1</sup>	-39.8	-44.4	-38.0	-35.2
	$\Delta_b H^{Pi}$ , kJ mol <sup>-1</sup>	-8.9	-11.8	-20.5	-19.8
	$\Delta_b H^{TRIS}$ , kJ mol <sup>-1</sup>	-20.6	-30.5	n/d	n/d
	$-T\Delta_b S^{Pi}$ , kJ mol <sup>-1</sup>	-30.9	-32.6	-17.5	-15.4
	$-T\Delta_b S^{TRIS}$ , kJ mol <sup>-1</sup>	-19.2	-13.9	n/d	n/d
<b>EA8-1</b> p <i>K</i> <sub>a</sub> =8.8 $\Delta_p H = -29.7$ kJ mol <sup>-1</sup>	$\Delta_b G$ , kJ mol <sup>-1</sup>	-42.8	-47.3	-39.8	-36.5
	$\Delta_b H^{Pi}$ , kJ mol <sup>-1</sup>	-18.5	n/d	-27.3	-16.0
	$\Delta_b H^{TRIS}$ , kJ mol <sup>-1</sup>	n/d	-41.1	n/d	n/d
	$-T\Delta_b S^{Pi}$ , kJ mol <sup>-1</sup>	-24.3	n/d	-12.5	-20.5
	$-T\Delta_b S^{TRIS}$ , kJ mol <sup>-1</sup>	n/d	-6.2	n/d	n/d
<b>EA9-1</b> p <i>K</i> <sub>a</sub> =8.8 $\Delta_p H = -29.7$ kJ mol <sup>-1</sup>	$\Delta_b G$ , kJ mol <sup>-1</sup>	-40.0	-44.8	-34.3	-36.5
	$\Delta_b H^{Pi}$ , kJ mol <sup>-1</sup>	-9.9	n/d	-14.6	-25.8
	$\Delta_b H^{TRIS}$ , kJ mol <sup>-1</sup>	-35.64	-14.21	n/d	n/d
	$-T\Delta_b S^{Pi}$ , kJ mol <sup>-1</sup>	-30.1	n/d	-19.74	-10.7
	$-T\Delta_b S^{TRIS}$ , kJ mol <sup>-1</sup>	-4.4	-30.6	n/d	n/d
<b>EA10-1</b> p <i>K</i> <sub>a</sub> =8.8 $\Delta_p H = -27.6$ kJ mol <sup>-1</sup>	$\Delta_b G$ , kJ mol <sup>-1</sup>	-45.7	-49.3	-40.9	-38.5
	$\Delta_b H^{Pi}$ , kJ mol <sup>-1</sup>	-13.0	-17.4	-29.0	-22.0
	$\Delta_b H^{TRIS}$ , kJ mol <sup>-1</sup>	-34.8	-36.2	n/d	n/d
	$-T\Delta_b S^{Pi}$ , kJ mol <sup>-1</sup>	-32.7	-31.9	-11.9	-16.5
	$-T\Delta_b S^{TRIS}$ , kJ mol <sup>-1</sup>	-10.9	-13.1	n/d	n/d
<b>EA11-1</b> p <i>K</i> <sub>a</sub> =8.8 $\Delta_p H = -31.4$ kJ mol <sup>-1</sup>	$\Delta_b G$ , kJ mol <sup>-1</sup>	-43.4	-45.7	-40.9	-37.4
	$\Delta_b H^{Pi}$ , kJ mol <sup>-1</sup>	-13.5	n/d	-26.6	-28.1
	$\Delta_b H^{TRIS}$ , kJ mol <sup>-1</sup>	n/d	-31.4	n/d	n/d
	$-T\Delta_b S^{Pi}$ , kJ mol <sup>-1</sup>	-29.9	n/d	-14.3	-9.3
	$-T\Delta_b S^{TRIS}$ , kJ mol <sup>-1</sup>	n/d	-14.3	n/d	n/d
<b>EA12-1</b> p <i>K</i> <sub>a</sub> =8.9 $\Delta_p H = -29.3$ kJ mol <sup>-1</sup>	$\Delta_b G$ , kJ mol <sup>-1</sup>	-40.7	-42.6	-43.9	-36.7
	$\Delta_b H^{Pi}$ , kJ mol <sup>-1</sup>	-22.9	n/d	-36.0	-36.5
	$\Delta_b H^{TRIS}$ , kJ mol <sup>-1</sup>	n/d	-32.3	n/d	n/d
	$-T\Delta_b S^{Pi}$ , kJ mol <sup>-1</sup>	-17.8	n/d	-7.9	-0.2
	$-T\Delta_b S^{TRIS}$ , kJ mol <sup>-1</sup>	n/d	-10.3	n/d	n/d
<b>EA3-2</b> p <i>K</i> <sub>a</sub> =9.0 $\Delta_p H = -31.8$ kJ mol <sup>-1</sup>	$\Delta_b G$ , kJ mol <sup>-1</sup>	-44.6	-47.3	-48.7	-41.6
	$\Delta_b H^{Pi}$ , kJ mol <sup>-1</sup>	-21.5	n/d	n/d	-15.6
	$\Delta_b H^{TRIS}$ , kJ mol <sup>-1</sup>	n/d	-33.4	-64.1	n/d
	$-T\Delta_b S^{Pi}$ , kJ mol <sup>-1</sup>	-23.1	n/d	n/d	-26.0
	$-T\Delta_b S^{TRIS}$ , kJ mol <sup>-1</sup>	n/d	-13.9	15.4	n/d
<b>EA3-2o</b> p <i>K</i> <sub>a</sub> =8.3 $\Delta_p H = -26.8$ kJ mol <sup>-1</sup>	$\Delta_b G$ , kJ mol <sup>-1</sup>	-49.3	-53.0	-49.0	-46.1
	$\Delta_b H^{Pi}$ , kJ mol <sup>-1</sup>	-19.1	n/d	n/d	-19.4
	$\Delta_b H^{TRIS}$ , kJ mol <sup>-1</sup>	n/d	-40.0	-57.9	n/d
	$-T\Delta_b S^{Pi}$ , kJ mol <sup>-1</sup>	-30.2	n/d	n/d	-26.7
	$-T\Delta_b S^{TRIS}$ , kJ mol <sup>-1</sup>	n/d	-13.0	8.9	n/d
<b>EA3-3</b> p <i>K</i> <sub>a</sub> =9.0 $\Delta_p H = -32.6$ kJ mol <sup>-1</sup>	$\Delta_b G$ , kJ mol <sup>-1</sup>	-47.5	-51.1	-51.7	-44.8
	$\Delta_b H^{Pi}$ , kJ mol <sup>-1</sup>	-14.9	n/d	n/d	-14.2
	$\Delta_b H^{TRIS}$ , kJ mol <sup>-1</sup>	n/d	-29.5	-53.4	n/d
	$-T\Delta_b S^{Pi}$ , kJ mol <sup>-1</sup>	-32.6	n/d	n/d	-30.6
	$-T\Delta_b S^{TRIS}$ , kJ mol <sup>-1</sup>	n/d	-21.6	1.7	n/d
<b>EA3-3o</b> p <i>K</i> <sub>a</sub> =8.2 $\Delta_p H = -26.4$ kJ mol <sup>-1</sup>	$\Delta_b G$ , kJ mol <sup>-1</sup>	-50.4	-49.9	-45.7	-45.1
	$\Delta_b H^{Pi}$ , kJ mol <sup>-1</sup>	n/d	n/d	n/d	-19.0
	$\Delta_b H^{TRIS}$ , kJ mol <sup>-1</sup>	-31.3	-47.3	-48.0	n/d
	$-T\Delta_b S^{Pi}$ , kJ mol <sup>-1</sup>	n/d	n/d	n/d	-26.1
	$-T\Delta_b S^{TRIS}$ , kJ mol <sup>-1</sup>	-19.1	-2.6	2.3	n/d

Continued on next page

Table 4 – Continued from previous page

Compound		CA II	CA VII	CA XII	CA XIII
<b>EA3-4</b>	$\Delta_b G$ , kJ mol <sup>-1</sup>	-46.8	-50.4	-47.5	-41.8
	$\Delta_b H^{Pi}$ , kJ mol <sup>-1</sup>	n/d	n/d	n/d	-16.8
	$\Delta_b H^{TRIS}$ , kJ mol <sup>-1</sup>	-43.2	-42.7	-62.5	n/d
	$pK_a=9.2$ $-T\Delta_b S^{Pi}$ , kJ mol <sup>-1</sup>	n/d	n/d	n/d	-25.0
	$\Delta_p H=-31.4$ kJ mol <sup>-1</sup> $-T\Delta_b S^{TRIS}$ , kJ mol <sup>-1</sup>	-3.6	-7.7	15	n/d
<b>EA3-4o</b>	$\Delta_b G$ , kJ mol <sup>-1</sup>	-44.2	-47.7	-42.0	-40.9
	$\Delta_b H^{Pi}$ , kJ mol <sup>-1</sup>	n/d	n/d	n/d	-17.0
	$\Delta_b H^{TRIS}$ , kJ mol <sup>-1</sup>	-37.8	-33.8	-37.7	n/d
	$pK_a=8.2$ $-T\Delta_b S^{Pi}$ , kJ mol <sup>-1</sup>	n/d	n/d	n/d	-23.9
	$\Delta_p H=-25.9$ kJ mol <sup>-1</sup> $-T\Delta_b S^{TRIS}$ , kJ mol <sup>-1</sup>	n/d	-6.4	-13.9	-4.3
<b>EA3-7</b>	$\Delta_b G$ , kJ mol <sup>-1</sup>	-37.9	-32.5	-49.9	-36.7
	$\Delta_b H^{Pi}$ , kJ mol <sup>-1</sup>	n/d	n/d	-30.6	-12.1
	$\Delta_b H^{TRIS}$ , kJ mol <sup>-1</sup>	-16.7	-16.8	n/d	n/d
	$pK_a=9.7$ $-T\Delta_b S^{Pi}$ , kJ mol <sup>-1</sup>	n/d	n/d	-19.3	-24.6
	$\Delta_p H=-39.3$ kJ mol <sup>-1</sup> $-T\Delta_b S^{TRIS}$ , kJ mol <sup>-1</sup>	-21.2	-15.7	n/d	n/d
<b>EA3-8</b>	$\Delta_b G$ , kJ mol <sup>-1</sup>	-42.2	-38.3	-40.8	-40.0
	$pK_a=10.2$ $\Delta_b H^{TRIS}$ , kJ mol <sup>-1</sup>	-31.2	-33.7	-49.0	-57.7
	$\Delta_p H=-38.1$ kJ mol <sup>-1</sup> $-T\Delta_b S^{TRIS}$ , kJ mol <sup>-1</sup>	-16.8	n/d	-2.7	-13.3
<b>EA4-2</b>	$\Delta_b G$ , kJ mol <sup>-1</sup>	-49.3	-53.0	-53.9	-40.0
	$\Delta_b H^{Pi}$ , kJ mol <sup>-1</sup>	-23.5	-23.3	-39.8	-21.1
	$\Delta_b H^{TRIS}$ , kJ mol <sup>-1</sup>	-38.8	n/d	n/d	-62.6
	$pK_a=9.0$ $-T\Delta_b S^{Pi}$ , kJ mol <sup>-1</sup>	-25.8	-29.7	-14.1	-18.9
	$\Delta_p H=-29.3$ kJ mol <sup>-1</sup> $-T\Delta_b S^{TRIS}$ , kJ mol <sup>-1</sup>	-10.5	n/d	n/d	-22.6
<b>EA4-2o</b>	$\Delta_b G$ , kJ mol <sup>-1</sup>	-50.4	-56.3	-50.5	-42.6
	$pK_a=8.3$ $\Delta_b H^{Pi}$ , kJ mol <sup>-1</sup>	-19.4	-19.6	-19.4	-22.0
	$\Delta_p H=-24.3$ kJ mol <sup>-1</sup> $-T\Delta_b S^{Pi}$ , kJ mol <sup>-1</sup>	-31.0	-36.7	-31.1	-20.6
<b>EA4-3</b>	$\Delta_b G$ , kJ mol <sup>-1</sup>	-50.1	-54.5	-53.4	-42.6
	$\Delta_b H^{Pi}$ , kJ mol <sup>-1</sup>	-18.9	-13.7	-37.8	n/d
	$\Delta_b H^{TRIS}$ , kJ mol <sup>-1</sup>	-31.3	n/d	n/d	-59.4
	$pK_a=8.9$ $-T\Delta_b S^{Pi}$ , kJ mol <sup>-1</sup>	-31.2	-40.8	-15.6	n/d
	$\Delta_p H=-31.8$ kJ mol <sup>-1</sup> $-T\Delta_b S^{TRIS}$ , kJ mol <sup>-1</sup>	-18.8	n/d	n/d	16.8
<b>EA4-3o</b>	$\Delta_b G$ , kJ mol <sup>-1</sup>	-53.2	-52.6	-48.0	-43.4
	$\Delta_b H^{Pi}$ , kJ mol <sup>-1</sup>	n/d	-12.0	-23.1	n/d
	$\Delta_b H^{TRIS}$ , kJ mol <sup>-1</sup>	-34.7	n/d	n/d	-53.6
	$pK_a=8.3$ $-T\Delta_b S^{Pi}$ , kJ mol <sup>-1</sup>	n/d	-40.6	-24.9	n/d
	$\Delta_p H=-24.3$ kJ mol <sup>-1</sup> $-T\Delta_b S^{TRIS}$ , kJ mol <sup>-1</sup>	-18.5	n/d	n/d	10.2
<b>EA4-7</b>	$\Delta_b G$ , kJ mol <sup>-1</sup>	-40.2	-34.8	-45.6	-37.3
	$\Delta_b H^{Pi}$ , kJ mol <sup>-1</sup>	n/d	n/d	n/d	-15.1
	$\Delta_b H^{TRIS}$ , kJ mol <sup>-1</sup>	-23.0	-13.8	-27.6	n/d
	$pK_a=9.8$ $-T\Delta_b S^{Pi}$ , kJ mol <sup>-1</sup>	n/d	n/d	n/d	-22.2
	$\Delta_p H=-39.7$ kJ mol <sup>-1</sup> $-T\Delta_b S^{TRIS}$ , kJ mol <sup>-1</sup>	-17.2	-21.0	-18.0	n/d
<b>EA4-8</b>	$\Delta_b G$ , kJ mol <sup>-1</sup>	-45.7	-42.6	-40.9	-35.4
	$\Delta_b H^{Pi}$ , kJ mol <sup>-1</sup>	-16.9	-11.6	-27.1	-16.1
	$\Delta_b H^{TRIS}$ , kJ mol <sup>-1</sup>	n/d	-27.4	n/d	-47.7
	$pK_a=9.7$ $-T\Delta_b S^{Pi}$ , kJ mol <sup>-1</sup>	-28.8	-31.0	-13.8	-19.3
	$\Delta_p H=-36.8$ kJ mol <sup>-1</sup> $-T\Delta_b S^{TRIS}$ , kJ mol <sup>-1</sup>	n/d	-15.2	n/d	12.3
<b>EA4-2c</b>	$\Delta_b G$ , kJ mol <sup>-1</sup>	-45.1	-48.2	-47.5	-38.5
	$\Delta_b H^{Pi}$ , kJ mol <sup>-1</sup>	-11.2	n/d	-27.0	-13.1
	$\Delta_b H^{TRIS}$ , kJ mol <sup>-1</sup>	n/d	-25.8	n/d	-53.6
	$pK_a=9.0$ $-T\Delta_b S^{Pi}$ , kJ mol <sup>-1</sup>	-33.9	n/d	-20.5	-25.4
	$\Delta_p H=-28.5$ kJ mol <sup>-1</sup> $-T\Delta_b S^{TRIS}$ , kJ mol <sup>-1</sup>	n/d	-22.4	n/d	15.1

9. Observed and intrinsic thermodynamics of meta- and para-substituted benzenesulfonamide binding to CA

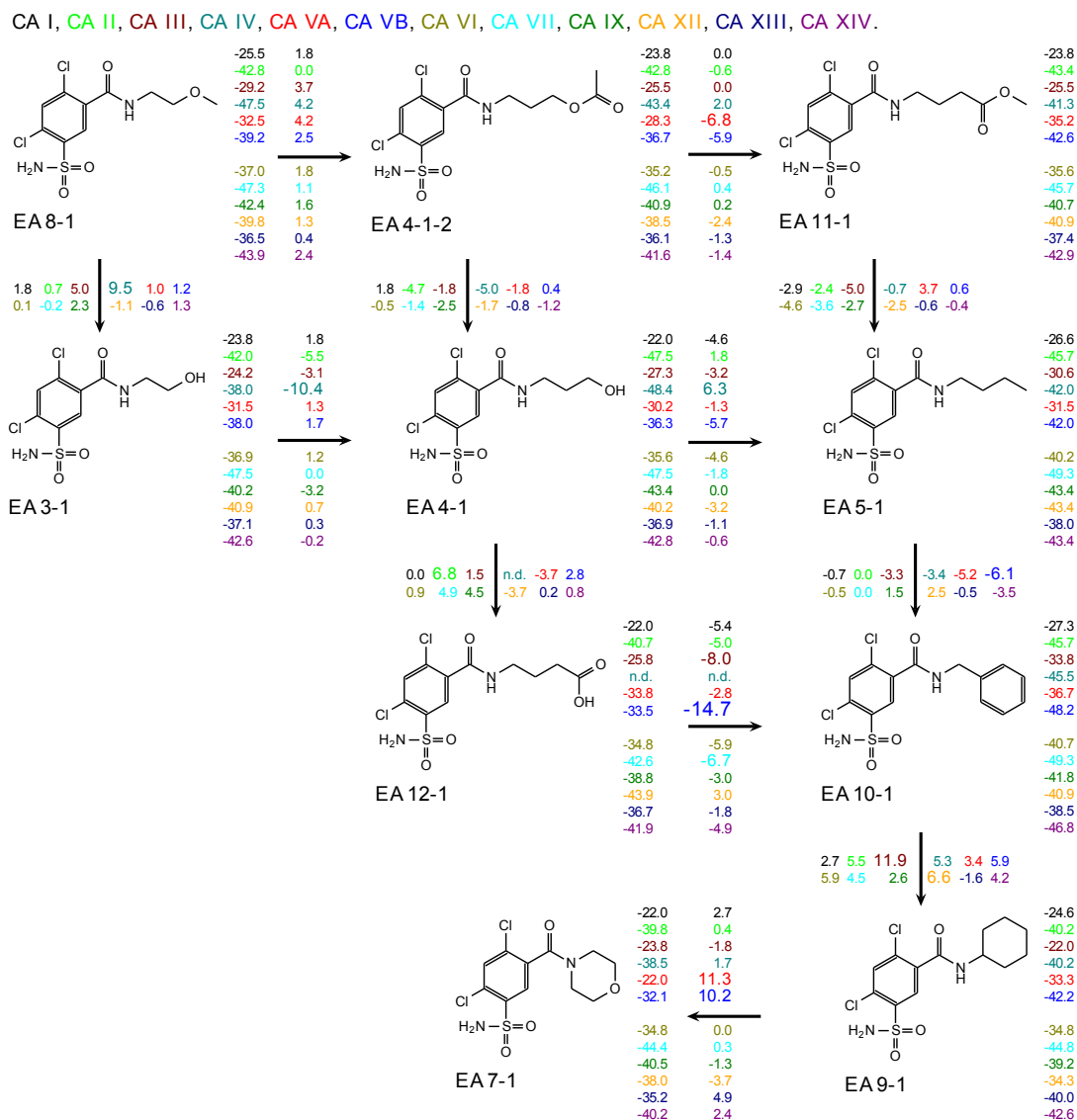


**Figure 5** Correlation map of the inhibitor chemical structures with the observed Gibbs energies. Observed  $\Delta_b G_{obs}$  values are shown next to the chemical structures. Differences in the binding affinity between compounds are listed on the connecting arrows. Colors show different CA isoforms.

CA I, CA II, CA III, CA IV, CA VA, CA VB, CA VI, CA VII, CA IX, CA XII, CA XIII, CA XIV.

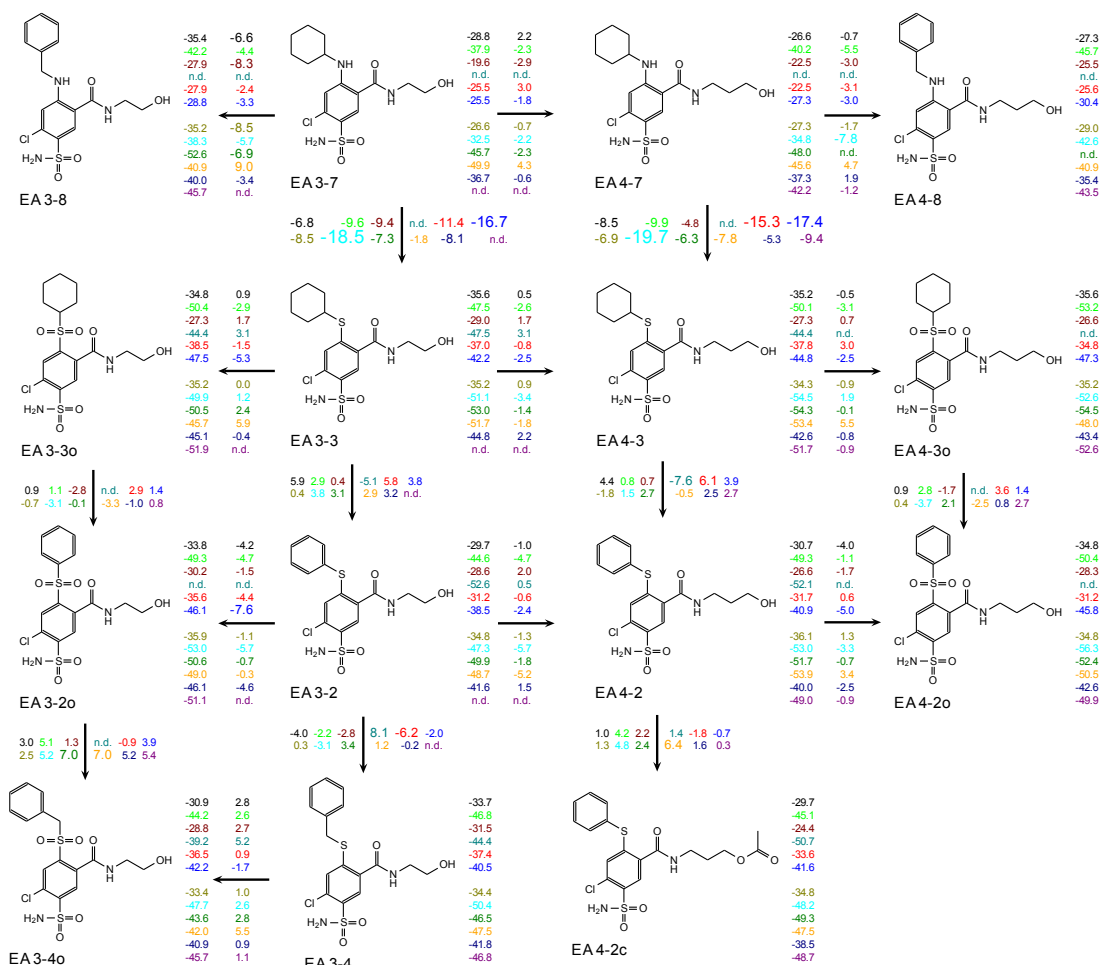


**Figure 6** Correlation map of the inhibitor chemical structures with the observed Gibbs energies. Observed  $\Delta_b G_{obs}$  values are shown next to the chemical structures. Differences in the binding affinity between compounds are listed on the connecting arrows. Colors show different CA isoforms.

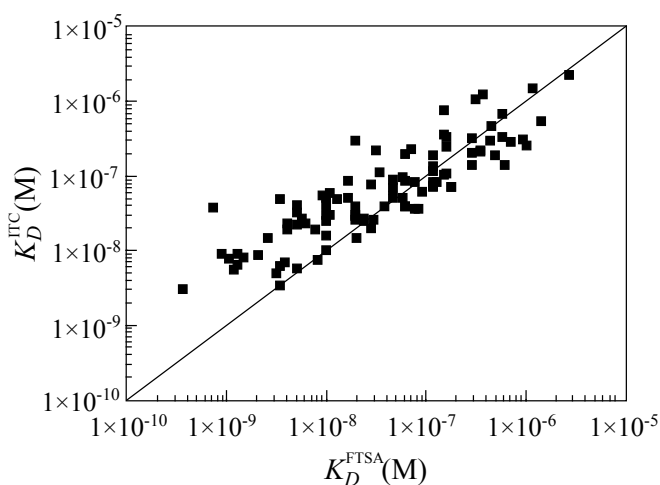


**Figure 7** Relationship between dissociation constants determined by FTSA and ITC. Data taken from Table 4.



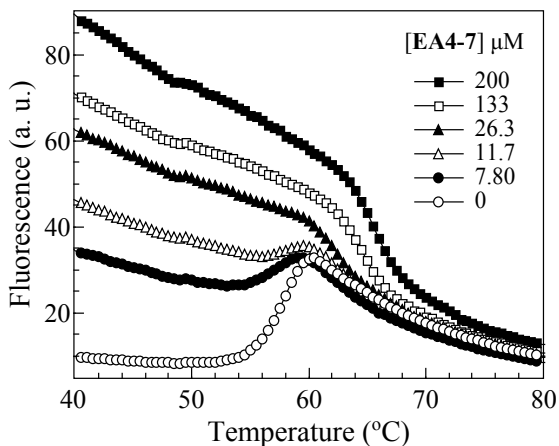


**Figure 8** Raw FTSA curves of compound **EA4-7** binding to CA XIII at pH 7.0, 37°C. The  $T_m$  values cannot be determined due to the high fluorescence.

### Analysis of observed thermodynamic parameters

As discussed above, the observed binding data should not be correlated with compound structures. However, many researchers do not calculate intrinsic values and compare observed parameters. Observed values can be compared only when experiments are performed at identical conditions and at these cases it is useful to take a look at the tendencies in the observed data too. However, we decided to include both the observed and intrinsic values to help the reader to follow the path how the intrinsic values could be obtained when there are additional developments in the model and the calculation procedure changes.

The analysis of compound affinities to 12 CA isoforms is shown in Fig. 5 and 6. Values next to structures show the Gibbs energies of binding and values next to arrows show the differences between the compounds linked by the arrow. The error margin of the determinations is approximately  $2 \text{ kJ mol}^{-1}$ . The  $K_d$  value of  $1 \text{ nM}$  corresponds to Gibbs energy of binding of  $-53.4 \text{ kJ mol}^{-1}$ . The 10 times increase of binding affinity corresponds to the difference in Gibbs energies  $\Delta\Delta_b G = -5.93 \text{ kJ mol}^{-1}$ . Therefore, only the differences above this value are of interest.

In some cases even apparently small structural changes caused the affinities to change significantly. For example, comparing compound **EA3-1** with **EA4-1** we see that they differed by only one methylene group in the *meta* tail. This difference had greatest influence for the compound binding to CA IV. The addition of the methylene group increased the affinity towards CA IV by nearly 100 fold, making the compound **EA4-1** slightly selective for this isoform. Such significant increase cannot be explained by simple hydrophobic effect and most likely involves a hydrogen bond that can be formed for compound **EA4-1** but most likely cannot be formed for **EA3-1**. This is also confirmed by the fact that the removal of oxygen

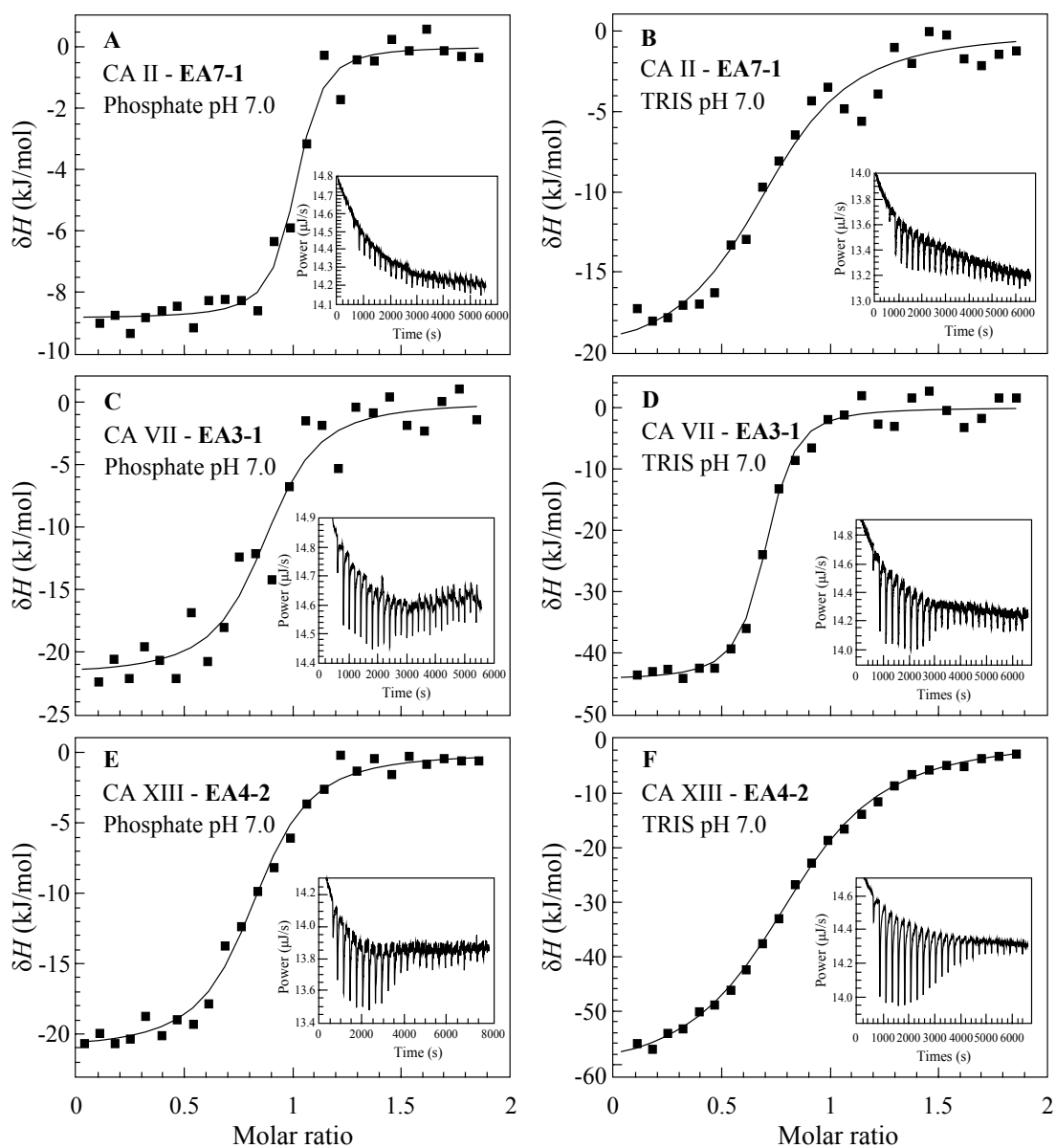


**Figure 9** representative ITC data of the compound binding to CA. Panels A, C, and E show isotherms of experiments performed in sodium phosphate buffer, panels B, D, and F show the same experiments performed in TRIS chloride buffer. Raw curves are presented in insets. Experiments were performed at 37°C.

in compound **EA5-1** the affinity towards CA IV dropped back by over 10 fold.

Overall, single-tailed compounds were more effective CA VII inhibitors, as compared with other 12 CA isoforms. Compounds **EA5-1** and **EA10-1** were selective CA VII inhibitors showing nanomolar binding affinity ( $K_{d\_obs}=5$  nM,  $\Delta_b G_{obs}=-49.3$  kJ mol<sup>-1</sup>).

Comparing the influence of tail modification in *para* position of benzenesulfonamide it is interesting to see the differences between binding affinity of N- and S-substituted compounds. In case of comparing **EA3-7** vs **EA3-3** and **EA4-7** vs **EA4-3** all CA isoforms were bound stronger by S-substituted compounds, except for CA IX binding with **EA3-8** and **EA3-4**. In this case N-substituted benzenesulfonamide bound stronger to this isoform than S-substituted. This can be due to the longer tail in *para* position. Therefore, **EA3-2o** vs **EA3-4o** and **EA3-2** vs **EA3-4** were compared. Note that first pair of compounds has SO<sub>2</sub>- and the second has S-substituted tails in *para* position. In first ligand pair, compound with shorter tail **EA3-2o** showed stronger binding to all CA isoforms (except to CA VA,  $\Delta\Delta_b G_{obs}$  is 0.9 kJ mol<sup>-1</sup>) than compound with longer tail moiety. However, **EA3-2** bound stronger to CA IV (8.1 kJ mol<sup>-1</sup>) and CA IX (3.4 kJ mol<sup>-1</sup>) than **EA3-4**.

Five pairs of S- and SO<sub>2</sub>-substituted compounds bearing two tails were compared as well. At first compounds bearing phenyl and benzyl groups as a tail moiety were compared. Pair of **EA3-4** and **EA3-4o** shows that S-substituted compound bound with similar or higher affinity to all CA isoforms and pair of **EA3-2** vs **EA3-2o** shows that SO<sub>2</sub>-substituted compound was stronger binder of all CA isoforms ( $\Delta\Delta_b G_{obs}$  varies from 0.3 to 7.6 kJ mol<sup>-1</sup>). However, **EA4-2** bound with higher affinity to CA XII, **EA4-2o** bound stronger to CA I, CA VB, CA VII, and CA XIII. To other CA isoforms both these compounds bound equally.

Comparing the pairs of SO<sub>2</sub>- and S-substituted compounds bearing cyclohexyl group (**EA3-3** vs **EA3-3o** and **EA4-3** vs **EA4-3o**) there was no clear tendency. Comparing binding affinities of compounds shown in Fig. 6 with different length of the tails in *meta* position and compounds bearing phenyl group as a tail moiety were compared with analogs bearing cyclohexyl group in the same position and no tendency was found as well.

Two-tailed compounds are stronger binders of all CAs than single-tailed compounds. The most effective CA VII inhibitor **EA4-2o** bound with  $K_d = 0.33$  nM ( $\Delta_b G_{obs}=-56.3$  kJ mol<sup>-1</sup>). Compounds **EA4-3** and **EA4-3o** showed low nanomolar binding affinities towards CA IX ( $K_{d\_obs} \sim 0.7$  nM,  $\Delta_b G_{obs} \sim -54.5$  kJ mol<sup>-1</sup>).

Differently from the Gibbs energies, the enthalpies and entropies of binding (Table 4) highly depend on buffer. Therefore, the observed enthalpy and entropy values have even less meaning than the Gibbs energies. There should be

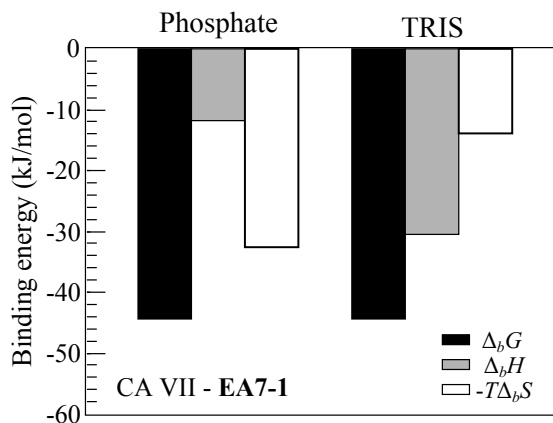


**Figure 10** Observed thermodynamic parameters of compound **EA7-1** binding to CA VII in two different buffers. The graph shows the difference of enthalpy and entropy values observed in sodium phosphate and TRIS chloride buffer at pH 7.0, 37°C. Black bar is the Gibbs energy of binding observed by FTSA, grey bar - binding enthalpy observed by ITC, and white bar is the calculated entropy.

no far reaching conclusions made on observations as e.g. CA VII interaction with compound **EA7-1** observed in sodium phosphate buffer is entropy driven, while observed in TRIS buffer is enthalpy driven (Fig. 10).

### Protonation of interacting components

To calculate the intrinsic binding parameters ( $K_{d\_intr}$  and  $\Delta_b G_{intr}$ ) for all compound interaction with CA isoforms the  $pK_a$ s of interacting components have to be known. The ionization constants of sulfonamide group deprotonation were determined spectrophotometrically as described in Methods part and are listed in Table 4. Single-tail benzenesulfonamides had similar  $pK_a$  values. The  $pK_a$ s of two-tailed benzenesulfonamides differed due to the substituents in *para* position:  $SO_2$ -substituted compounds had the lowest  $pK_a$  (8.2 - 8.3), values for S-substituted compounds were in range from 8.9 to 9.2, and N-substituted had the highest  $pK_a$  values (9.7 - 10.2). The example of  $pK_a$  determination by spectrophotometric method is shown in Fig. 11, Panel A. Experimentally determined  $pK_a$ s show linear correlation with the NMR chemical shifts of protons of sulfonamide group (Fig. 11, Panel B).

The enthalpies of protonation were observed for all compounds by ITC titration of alkaline inhibitor solution with  $HNO_3$  (Fig. 12, Table 4). The most exothermic protonation enthalpies were determined for N-substituted compounds (from  $-36.8 \text{ kJ mol}^{-1}$  to  $-39.7 \text{ kJ mol}^{-1}$ ). The least exothermic protonation enthalpies were measured for  $SO_2$ -substituted compounds and values vary from  $-24.3 \text{ kJ mol}^{-1}$  to  $-26.8 \text{ kJ mol}^{-1}$ .

Thermodynamic parameters of protonation of the hydroxide bound to the zinc in the active site of CAs were described in part 8 and listed in Table 1.

9. Observed and intrinsic thermodynamics of *meta*- and *para*-substituted benzenesulfonamide binding to CA

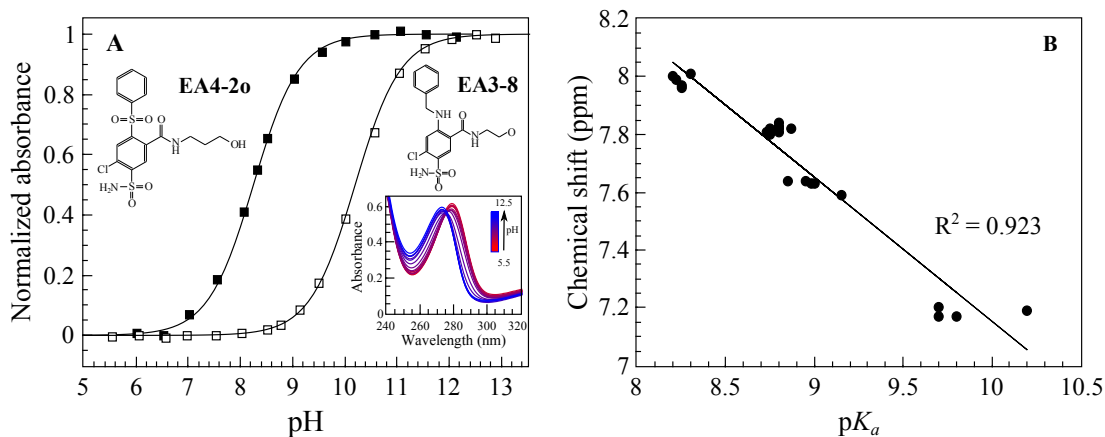


**Figure 11** Determination of the compound sulfonamide group protonation  $pK_a$ . Panel A shows spectrophotometric determination yielded the  $pK_a$  values of 8.3 for **EA4-2o** (black squares) and 10.2 for **EA3-8** (open squares), at 37°C. The inset shows the absorbance spectra of 30 μM **EA3-8** at pH range from 5.5 (red) to 12.5 (blue). Panel B shows approximately linear correlation between spectrophotometrically determined  $pK_a$  and the NMR chemical shift of the  $\text{NH}_2$  group proton on the sulfonamide group.

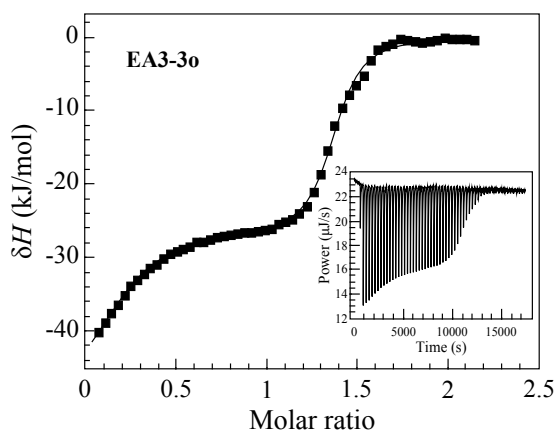


**Figure 12** Direct ITC measurement of the compound's **EA3-3o** sulfonamide protonation enthalpy at 37°C. The inset shows the raw ITC data. The enthalpy of the first stage of the titration curve represents the enthalpy of the reaction between  $\text{H}^+$  and excess  $\text{OH}^-$ , while the enthalpy of the second stage represents the enthalpy of sulfonamide protonation.

## Analysis of intrinsic thermodynamic parameters

The intrinsic binding parameters provides valuable information about energies of complex formation, therefore detailed investigation of the ligand structure-activity relationship is required for rational design of new compounds with desired properties. Studied compounds were mapped in the direction of incrementally changing functional groups. Correlation of compound structures with the intrinsic thermodynamic parameters provides the ability to assess the important contributions to affinity and further compound modification.

The intrinsic dissociation constants  $K_{d\_intr}$  of compounds binding to CAs are listed in Table 5. All  $K_{d\_intr}$ s are lower (higher affinities) comparing with the observed and it can be seen in Figure 13 where the intrinsic  $K_{d\_intr}$ s for compounds binding to CA II are arranged from the lowest to the greatest value. The observed  $K_{d\_obs}$ s do not fully match the increasing order, because interacting fractions of compounds differ due to different  $pK_a$ s. For example, as shown in inset of the figure, the intrinsic  $K_{d\_intr}$  values for two compounds **EA3-2o** and **EA4-7** were equal ( $K_{d\_intr} = 0.12$  nM), however the observed values differed 34 times ( $K_{d\_obs} = 5$  nM for **EA3-2o** and  $K_{d\_obs} = 170$  nM for **EA4-7**). The fraction of deprotonated **EA3-2o** was 0.05 and fraction of deprotonated **EA4-7** was 0.002 at pH 7.0. The fraction of CA II in the active protonated Zn-bound water form was 0.4.

**Table 5** Intrinsic dissociation constants ( $K_{d\_intr}$  (nM)) of the compound binding to CA isoforms. Values were calculated from FTSA data, listed in Table 3.

Cpd	Intrinsic dissociation constants $K_{d\_intr}$ (nM) for CA isoforms												
	I	II	III	IV	VA	VB	VI	VII	IX	XII	XIII	XIV	
<b>EA8-1</b>	810	0.48	81	0.05	54	2.2	0.93	0.075	0.36	1.4	11	0.27	
<b>EA4-1-2</b>	1700	0.51	354	0.26	283	6.1	2.0	0.12	0.65	2.4	14	0.71	
<b>EA11-1</b>	1600	0.39	338	0.55	19	0.58	1.6	0.14	0.69	0.84	7.9	0.4	
<b>EA3-1</b>	1400	0.58	501	1.8	71	3.1	0.89	0.06	0.74	0.75	7.9	0.4	
<b>EA4-1</b>	2900	0.069	150	0.032	120	6.0	1.4	0.06	0.22	1.0	8.9	0.38	
<b>EA5-1</b>	540	0.15	48	0.41	79	0.73	0.26	0.034	0.25	0.34	6.3	0.34	
<b>EA12-1</b>	2500	0.84	230	n/d	24	15	1.7	0.34	1.1	0.21	8.1	0.45	
<b>EA10-1</b>	360	0.14	12	0.099	9.5	0.06	0.2	0.03	0.4	0.75	4.7	0.078	
<b>EA9-1</b>	1000	1.2	1200	0.74	35	0.6	2	0.17	1.1	10	2.6	0.4	
<b>EA7-1</b>	3200	1.5	680	1.7	3200	35	2.3	0.23	0.77	2.7	19	1.1	
<b>EA3-7</b>	26	0.37	390	n/d	91	50	6.0	2.6	0.011	0.0031	1.2	n/d	
<b>EA3-8</b>	0.64	0.022	4.9	n/d	11	4.5	0.072	0.088	0.00026	0.032	0.1	0.0049	
<b>EA4-7</b>	49	0.12	98	n/d	230	20	3.6	0.87	0.0038	n/d	n/d	0.047	
<b>EA4-8</b>	46	0.018	39	n/d	87	7.7	2.3	0.051	n/d	0.096	2.0	0.037	
<b>EA3-3o</b>	75	0.084	550	0.54	17	0.28	6.5	0.088	0.051	0.44	1.3	0.04	
<b>EA3-3</b>	9.2	0.044	50	0.028	5.3	0.38	1.1	0.0096	0.0035	0.0077	0.26	n/d	
<b>EA4-3</b>	16	0.023	130	0.13	5.4	0.2	2.1	0.0036	0.0028	0.0054	0.84	0.011	
<b>EA4-3o</b>	44	0.022	610	n/d	61	0.27	5.4	0.026	0.0091	0.15	2.2	0.026	
<b>EA3-2o</b>	99	0.12	170	n/d	48	0.44	4.4	0.026	0.046	0.11	0.81	0.051	
<b>EA3-2</b>	96	0.14	60	0.0042	53	1.7	1.3	0.045	0.012	0.025	0.94	n/d	
<b>EA4-2</b>	69	0.025	140	0.0053	45	0.69	0.84	0.0054	0.0063	0.0036	1.8	0.024	
<b>EA4-2o</b>	70	0.079	350	n/d	270	0.5	6.9	0.0069	0.023	0.064	3.2	0.082	
<b>EA3-4o</b>	340	0.94	320	4.2	38	2.3	13	0.21	0.77	1.9	6.7	0.46	
<b>EA3-4</b>	14	0.04	14	0.067	3.2	0.54	1.0	0.0091	0.029	0.027	0.58	0.035	
<b>EA4-2c</b>	86	0.1	280	0.0076	18	0.46	1.2	0.028	0.013	0.036	2.8	0.022	

9. Observed and intrinsic thermodynamics of *meta*- and *para*-substituted benzenesulfonamide binding to CA

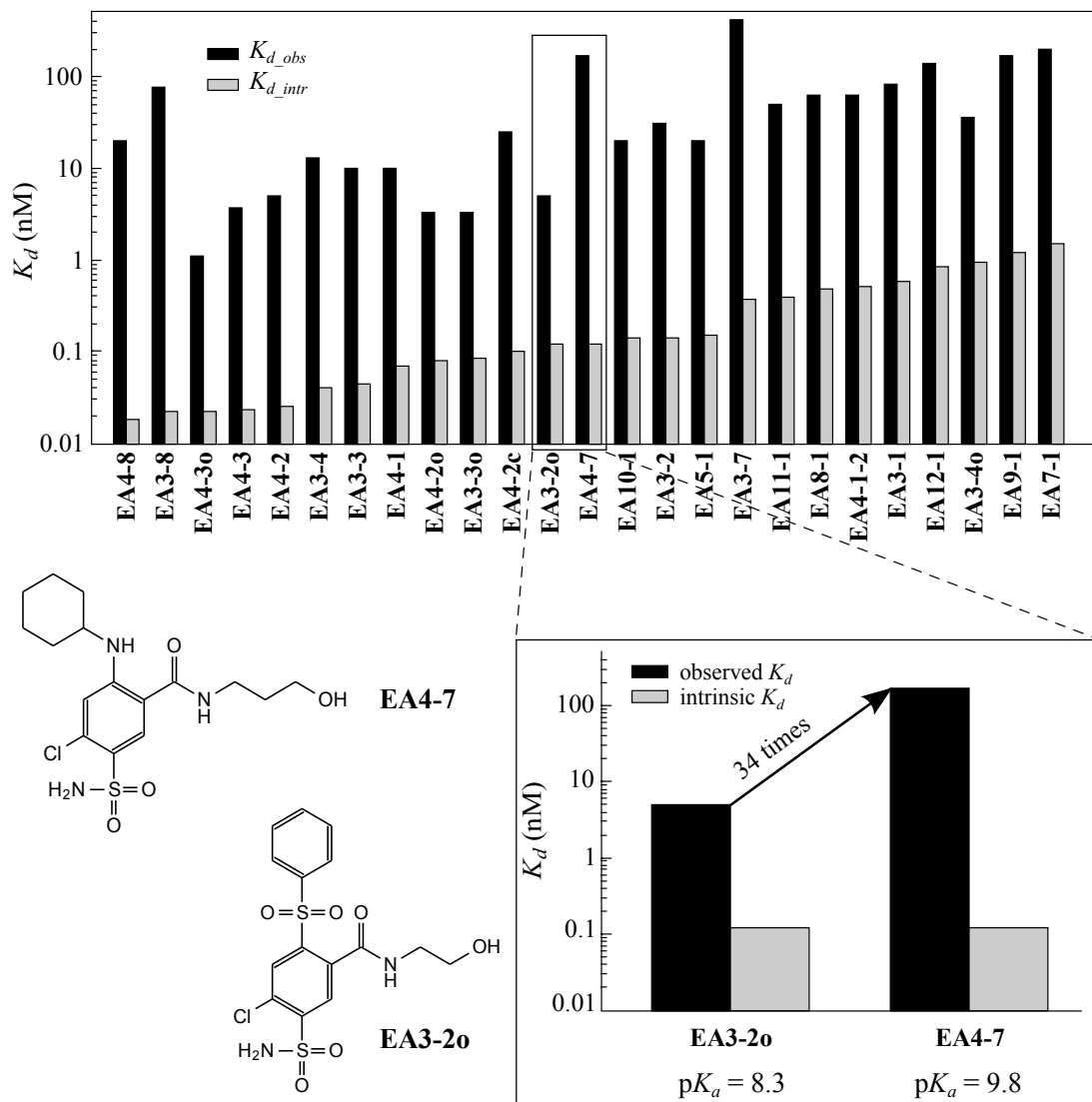


**Figure 13** Comparison of experimentally measured  $K_{d\_obs}$  (black bars) and calculated intrinsic  $K_{d\_intr}$  (grey bars) of CA II interaction with tested compounds. The  $K_{d\_obs}$  values were determined by FTSA in sodium phosphate buffer pH 7.0 at 37°C. The additional graph compares  $K_d$  values of compounds **EA4-7** and **EA3-2o** (structures are shown) with equal  $K_{d\_intr}$  values, but different  $pK_a$ s and different observed affinities.

All studied two-tailed compounds showed picomolar binding affinity to CA II, CA IV, CA VII, CA IX, CA XII, and CA XIV. These compounds are low nanomolar binders of CA VA, CA VB, CA VI, and CA XIII. The binding to CA I and CA III was weakest as compared with other CA isoforms.

For easier comparison, the intrinsic affinities are shown in Figures 14 and 15 prepared with  $\Delta_b G_{intr}$  listed near the structures of compounds and difference of values on the arrows. The starting single-tailed **EA3-1** and dual-tailed **EA3-3** benzenesulfonamides are shown in shaded areas.

The single-tailed starting compound **EA3-1** was modified to understand how structural changes in *meta* position influence binding energies and the results

showed that binding affinity depended on the length and hydrophobicity of the tail. The elongation of the tail (compounds **EA3-1** vs **EA4-1**) was the most favorable for CA IV ( $\Delta\Delta_b G_{intr} = -10.4 \text{ kJ mol}^{-1}$ ), however, the substitution of hydroxy group (**EA4-1**) with methyl group (**EA5-1**) decreased the binding to CA IV ( $\Delta\Delta_b G_{intr} = 6.6 \text{ kJ mol}^{-1}$ ). All other modifications of tail group did not improve the binding affinity to CA IV. Compound **EA4-1** was the strongest binder of CA IV in the series of single-tailed compounds. The nature of *meta* substituent influenced the binding affinity for CA VA and CA VB, but had negligible effect to the binding to other CA isoforms ( $\Delta\Delta_b G_{intr} \leq 5.5 \text{ kJ mol}^{-1}$ ).

The dual-tailed starting compound **EA3-3** was made by adding S-substituted cyclohexyl group in *para* position of **EA3-1**. This modification increased binding affinity to all CAs, only the Gibbs energy of interaction with CA VI remained the same.

The change of S-substituted cyclohexyl group to N-substituted group (**EA3-7**) decreased the binding affinity to all CAs or had minor effect to the binding to CA XII. The S-substituted cyclohexyl group was changed to S-substituted phenyl group (compounds **EA3-3** and **EA3-2**, respectively) and this change increased binding affinity to CA IV by  $-5.0 \text{ kJ mol}^{-1}$ , however decreased binding affinity to all other isoforms.

The elongation of the *meta* tail (compounds **EA3-3** vs **EA4-3** and **EA3-2** vs **EA4-2**) had negligible effect to the binding of all CAs.

Change of S-substituted cyclohexyl group to  $\text{SO}_2$ -substituted moiety (**EA3-3**  $\rightarrow$  **EA3-3o** and **EA4-3**  $\rightarrow$  **EA4-3o**) decreased binding affinity to all CAs. The same change was made for analog of compound **EA3-3** bearing longer tail in *meta* position (**EA4-3**). Compound **EA4-3o** was weaker binder comparing with **EA4-3**. Compounds bearing phenyl moieties were compared as well. Comparing pair of **EA3-2** vs **EA3-2o**  $\text{SO}_2$ -substituted compound showed stronger affinity only to CA VB ( $\Delta\Delta_b G_{obs} = -3.4 \text{ kJ mol}^{-1}$ ). To other CA isoforms compound **EA3-2o** bound weaker or with equal affinity than **EA3-2**. Comparing **EA4-2** with **EA4-2o**, S-substituted benzenesulfonamide showed higher affinity to all CAs.

Phenyl group of compounds **EA3-2** and **EA3-2o** was changed to benzyl yielding **EA3-4** and **EA3-4o**. Compound **EA3-4** bearing longer and more flexible S-substituted tail in *para* position was better binder of CAs (except CA IV and CA IX) than **EA3-2** bearing shorter phenyl group. However, the comparison of  $\text{SO}_2$ -substituted analogs shows that compound bearing shorter tail in *para* position was stronger binder to all CAs except CA III and CA VA (to these two isoforms compounds **EA3-2o** and **EA3-4o** bound equally).

The most interesting finding was made after the comparison of weak binder **EA3-7** and its analog **EA3-8** bearing N-substituted benzyl group. This compound showed the greatest binding affinity to CA I, CA III, CA VI, CA IX, CA



## 9. Observed and intrinsic thermodynamics of *meta*- and *para*-substituted benzenesulfonamide binding to CA

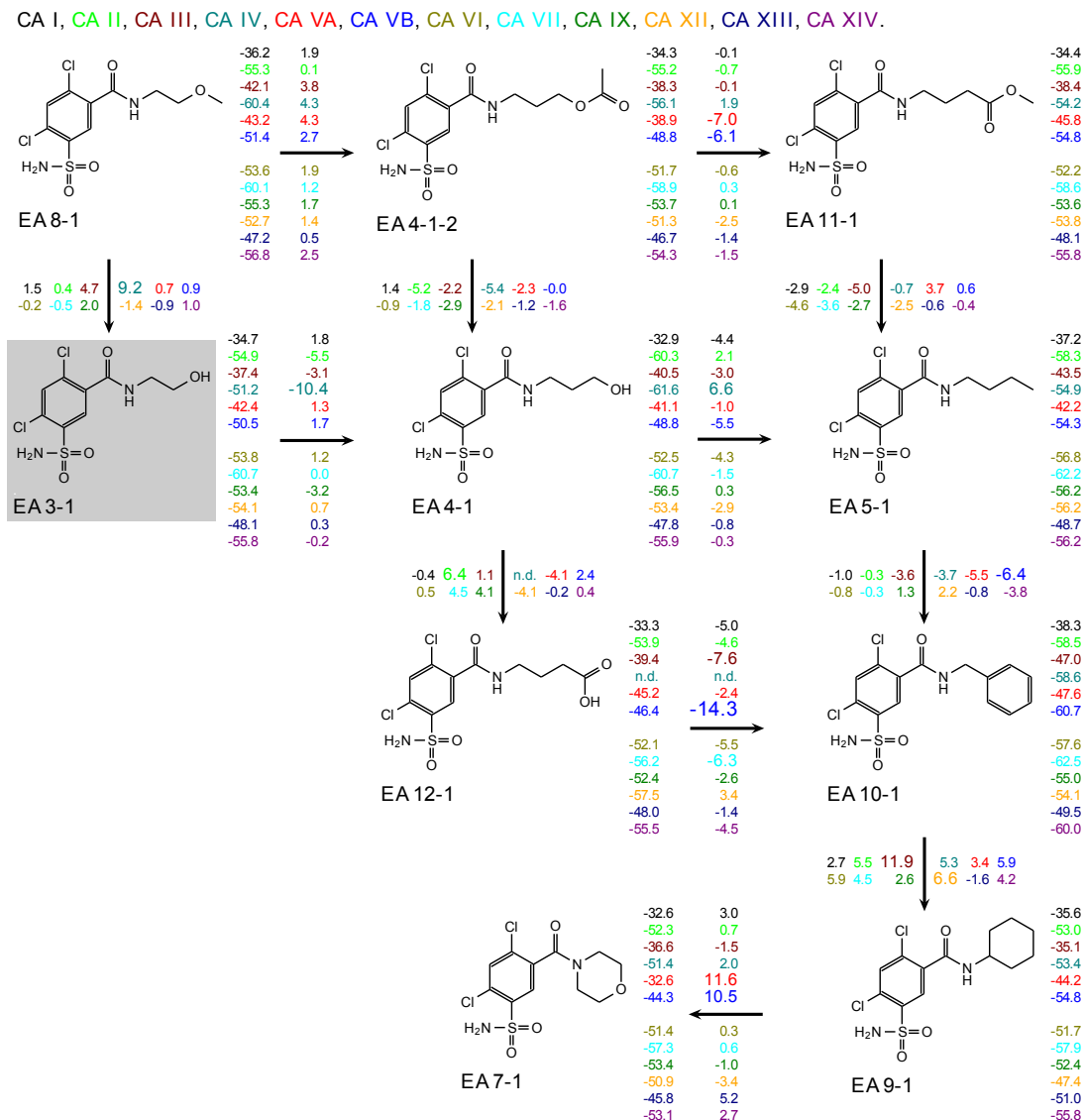


**Figure 14** Correlation map of the inhibitor chemical structures with the intrinsic Gibbs energies. Intrinsic  $\Delta_b G_{intr}$  values are shown next to the chemical structures. Differences in the binding affinity between compounds are listed on the connecting arrows. Colors show different CA isoforms.

XIII, and CA XIV comparing with all tested dual-tailed benzenesulfonamides. N-substituted cyclohexyl group (compound **EA3-7**) and S-substituted benzyl group (compound **EA3-4**) diminished binding affinity comparing with starting **EA3-3**, but N-substituted benzyl group highly increased. However, longer *meta* tail (**EA4-8**) diminished binding affinity to all CAs, except CA II and CA VII where binding affinity remained the same comparing with **EA3-8**.

To better understand such affinities of protein-ligand interaction, contribution arising from enthalpic and entropic reasons were analyzed. The  $\Delta_b G_{intr}$  (bold),  $\Delta_b H_{intr}$  (normal) and  $-T\Delta_b S_{intr}$  (italic) values are shown in Figures 16 and 17 near the structures and differences of these values – on the arrows. Figure 18

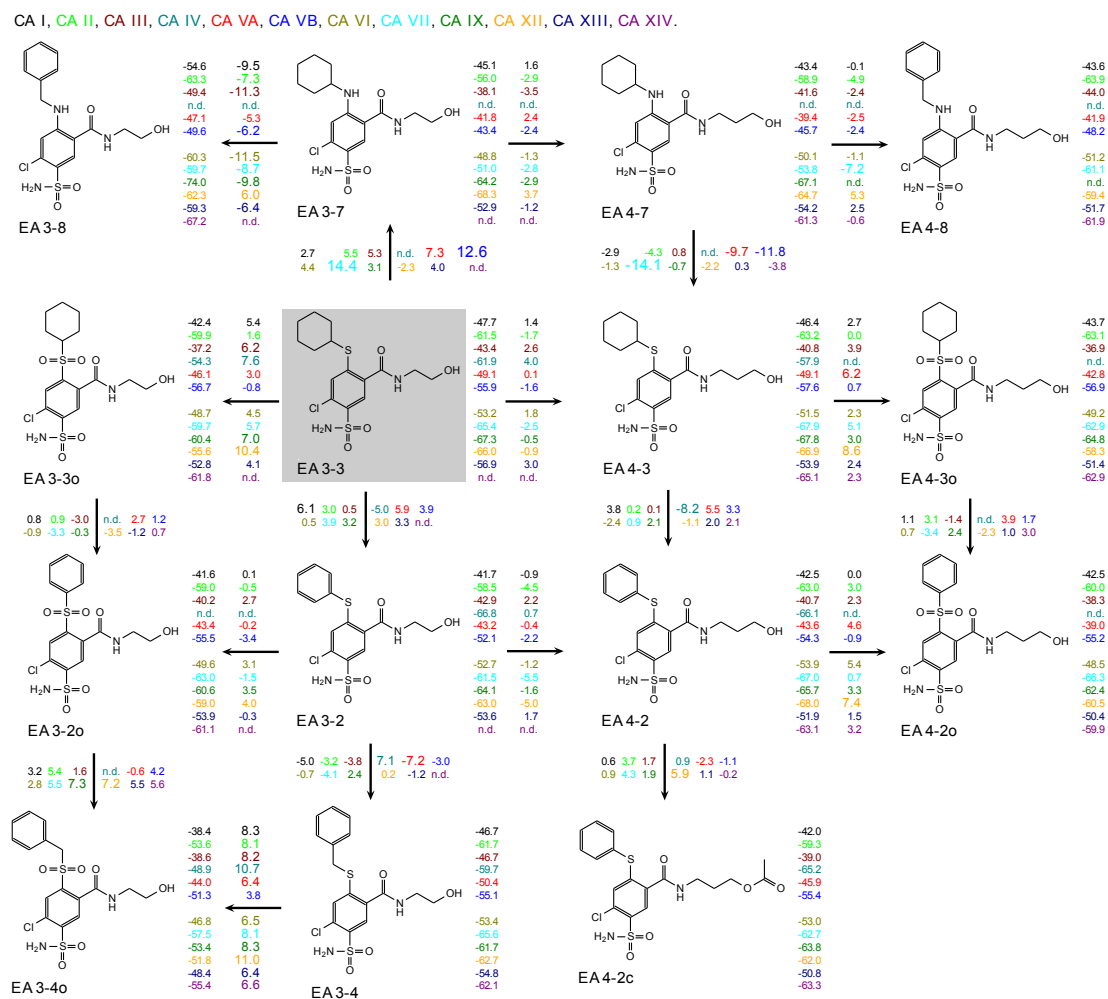


**Figure 15** Correlation map of the inhibitor chemical structures with the intrinsic Gibbs energies. Intrinsic  $\Delta_b G_{intr}$  values are shown next to the chemical structures. Differences in the binding affinity between compounds are listed on the connecting arrows. Colors show different CA isoforms.

## 9. Observed and intrinsic thermodynamics of *meta*- and *para*-substituted benzenesulfonamide binding to CA

---

shows the intrinsic thermodynamic parameters as bars, lined from the strongest to the weakest binding. These graphs show that compounds exhibit strongly enthalpy-driven binding to CA XII (with the partial exception) and CA XIII, while contribution arising from both enthalpic and entropic reasons are for CA II and CA VII. There was no clear trend in the order of the compound structure-binding affinity relationship, but some tendencies could be determined.

Carbonic anhydrase II interaction with analyzed compounds showed large contributions of both enthalpy and entropy. The comparison of starting compound **EA3-1** with structurally similar **EA4-1** showed that  $\Delta_b H_{intr}$ s were very similar and equal to  $-32.7 \text{ kJ mol}^{-1}$  and  $-30.4 \text{ kJ mol}^{-1}$ , respectively. However,  $-T\Delta_b S$  of compound bearing longer and more flexible tail in *meta* position **EA4-1** was  $-29.9 \text{ kJ mol}^{-1}$ , while  $-T\Delta_b S$  of **EA3-1** was  $-22.2 \text{ kJ mol}^{-1}$  and due to this greater entropic contribution **EA4-1** bound to CA II with higher affinity.

Modifications of *meta* tails gave more favorable enthalpy contribution to the binding affinity, except **EA4-1-2**, where values of enthalpy and entropy were equal. Compounds **EA7-1**, **EA9-1**, and **EA10-1** have cyclic tails and **EA9-1** is more enthalpically driven than **EA7-1** and **EA10-1**.

It was interesting to compare how enthalpic and entropic contribution to the Gibbs energy changes by adding and modifying tails in *para* position. The addition and modification of a tail to a compound **EA3-1** showed that only two compounds had the greater entropic than enthalpic influence to  $\Delta_b G_{intr}$ : **3-3o** and **3-7**, bearing  $\text{SO}_2$ - and N-substituted cyclohexyl groups, respectively. S-substituted phenyl group in *para* position (**EA3-2**) made binding more enthalpically driven comparing with **EA3-3**.

Change of S-substituted to  $\text{SO}_2$ -substituted group diminished enthalpic contribution to binding affinity.

The influence of entropy to the Gibbs energy became greater when one methylene group was added to tail in *meta* position, except for compound **EA4-8**.

Replacing the cyclohexyl group to phenyl moiety increased the enthalpic and decreased entropic contribution to binding affinity. The same tendency was found by changing phenyl group to benzyl.

Binding of all studied single-tailed Cl-substituted benzenesulfonamides to CA VII was entropy driven, except **EA8-1**, where the contribution arising from enthalpic and entropic reasons was equal, and **EA3-1**, where enthalpic contribution was greater than entropic. But enthalpic influence became lower when the second tail in *para* position was added. The only exception was compound **EA3-3o**.

Modification of S-substituted compound **EA3-3** by changing cyclohexyl group to phenyl and benzyl groups increased enthalpic contribution to the binding affinity of all tested CAs.

It seems that tails in *meta* position makes the greatest influence for enthalpic

CA II, CA VII, CA XII, CA XIII.

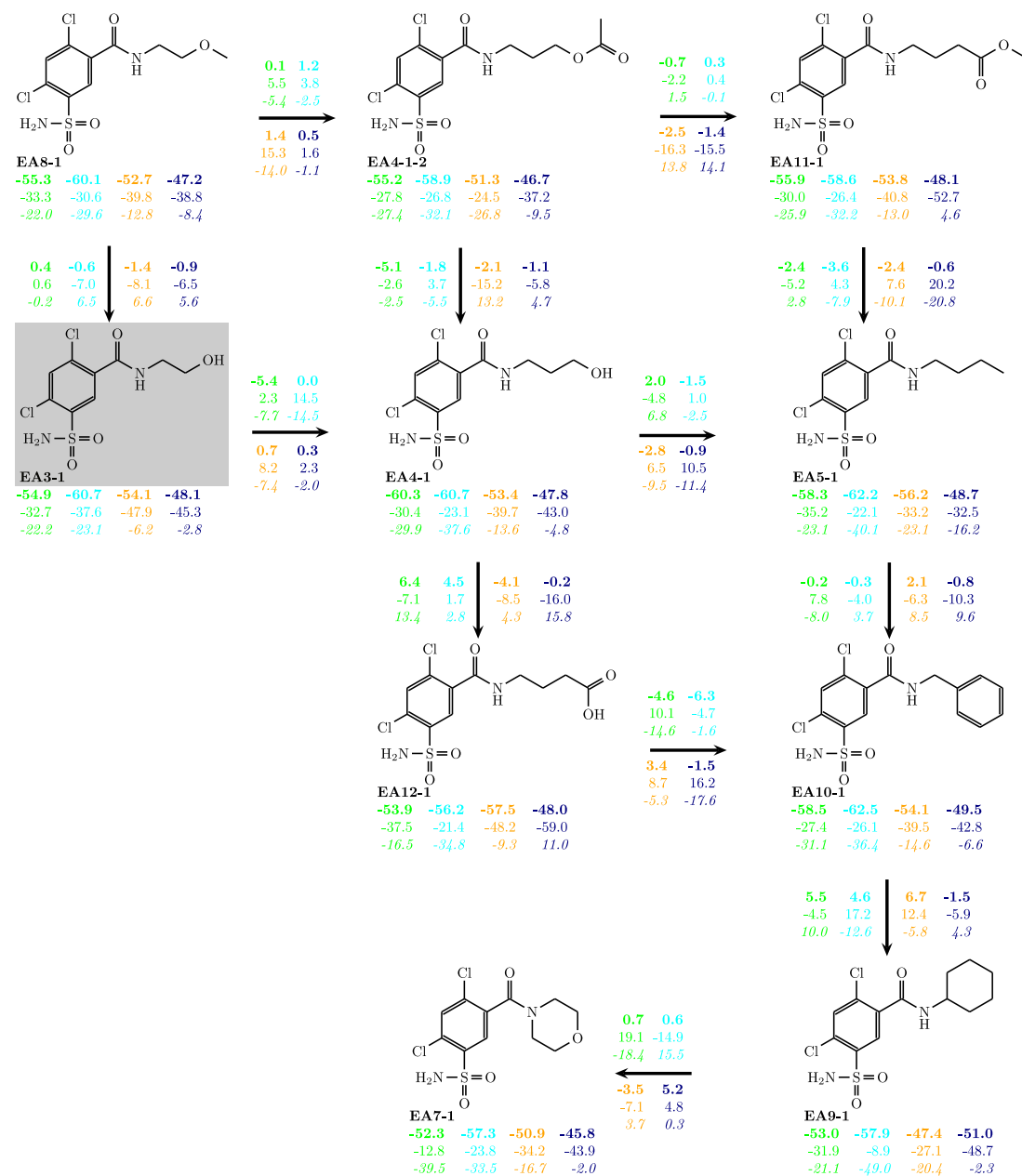


**Figure 16** Correlation map of the inhibitor chemical structures with the intrinsic thermodynamic parameters (37°C). The  $\Delta_b G_{intr}$  (bold),  $\Delta_b H_{intr}$  (normal), and  $-T\Delta_b S_{intr}$  (italic) values are shown next to the chemical structures. Differences in the binding affinity between compounds are listed on the connecting arrows. Colors show different CA isoforms: green color represents CA II, aqua - CA VII, orange - CA XII, and navy - CA XIII.

## 9. Observed and intrinsic thermodynamics of meta- and para-substituted benzenesulfonamide binding to CA

CA II, CA VII, CA XII, CA XIII.

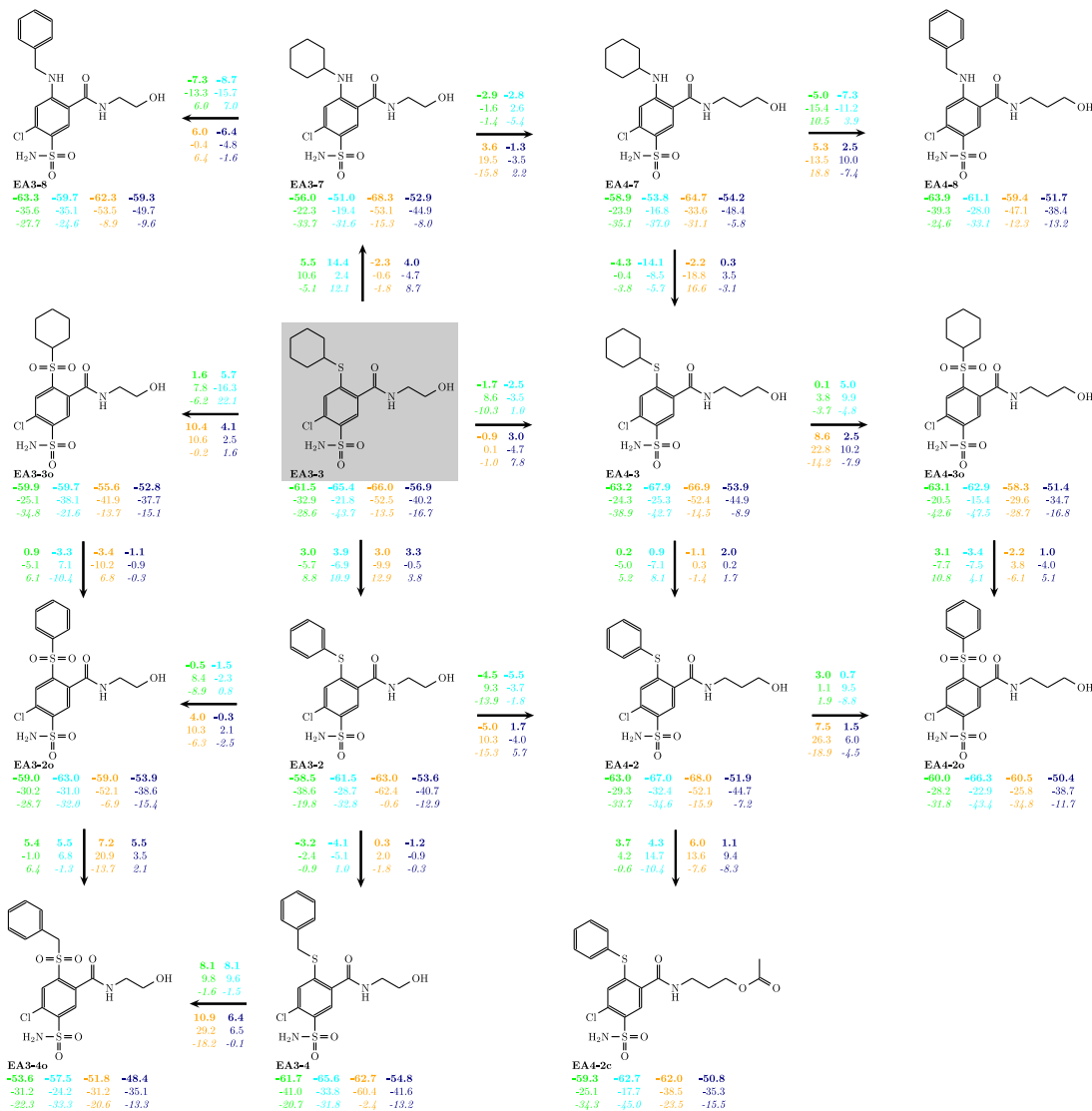


**Figure 17** Correlation map of the inhibitor chemical structures with the intrinsic thermodynamic parameters (37°C). The  $\Delta_b G_{intr}$  (bold),  $\Delta_b H_{intr}$  (normal), and  $-T\Delta_b S_{intr}$  (italic) values are shown next to the chemical structures. Differences in the binding affinity between compounds are listed on the connecting arrows. Colors show different CA isoforms: black color represents CA II, aqua - CA VII, orange - CA XII, and navy - CA XIII.

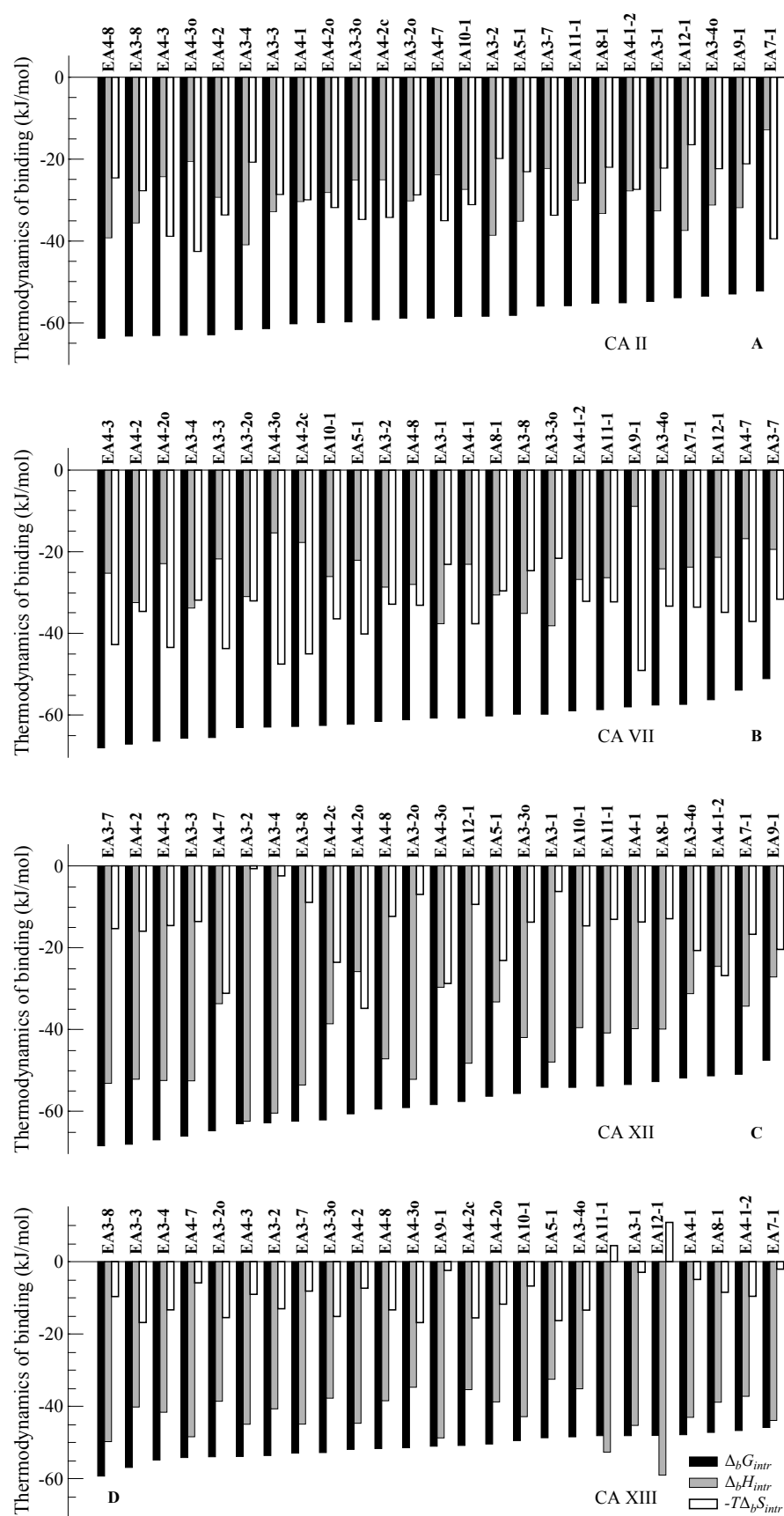


**Figure 18** Intrinsic thermodynamics of compound binding to four CA isoforms: CA II (A), CA VII (B), CA XII (C) and CA XIII (D). Compounds are arranged in the order of increasing intrinsic affinities ( $\Delta_b G_{intr}$ , black bars). Enthalpies are colored grey, while the entropies - white.

9. Observed and intrinsic thermodynamics of *meta*- and *para*-substituted benzenesulfonamide binding to CA

---

and entropic contribution to the affinity of CA VII binding with tested benzenesulfonamides. Comparing compounds **EA3-8** vs **EA4-8**, **EA3-3o** vs **EA4-3o**, and **EA3-2o** vs **EA4-2o** it is clear that longer *meta* tail by one carbon atom makes protein-ligand interaction entropically driven. However, entropic contribution to binding affinity of **EA3-3** vs **EA4-3** and **EA3-2** vs **EA4-2** to CA VII was equal.

Binding of CA XII to all *meta*-substituted dichlorobenzenesulfonamides were enthalpy driven, except **EA4-1-2**, where the contribution arising from enthalpic and entropic reasons was almost equal. Compounds **EA11-1** and **EA12-1**, bearing quite similar tails, had dominant enthalpic contribution to the binding affinity. Binding of these compounds and **EA3-1** to CA XII was the most enthalpy driven comparing with other studied single-tailed benzenesulfonamides. The addition of second tail to *para* position of the compound **EA3-1** increased the binding affinity to all CAs (except **EA3-4o**). The entropic contribution to binding affinity became smaller for compounds **EA3-8** → **EA3-2o** → **EA3-4** → **EA3-2**, the entropic contribution for the latter compound was equal to  $-0.6 \text{ kJ mol}^{-1}$ . However, this compound is not the best CA XII binder. The best binder **EA3-7** ( $\Delta_b G_{intr} = -68.3 \text{ kJ mol}^{-1}$ ) had dominant enthalpic ( $\Delta_b H_{intr} = -53.1 \text{ kJ mol}^{-1}$ ) contribution.

Two-tailed compound **EA3-3** binding to CA XII was enthalpy driven. The change of S-substituted cyclohexyl group of this compound to  $\text{SO}_2$ - or N-substituted derivatives, or lengthening the tail in *meta* position by one methylene group did not change entropic contribution. However, S-substituted phenyl (**EA3-2**) and benzyl (**EA3-4**) groups highly diminished it.  $\text{SO}_2$ -substituted compounds bearing longer tails in *meta* position (**EA4-3o** and **EA4-2o**) increased entropic and decreased enthalpic contribution to binding affinity, the same as N-substituted compound **EA4-7**.

The interaction of CA XIII with single-tailed chlorinated compounds was enthalpy driven. Binding of **EA11-1** and **EA12-1** to CA XIII had the unfavorable entropic contribution.

After the addition of a tail in *para* position binding to CA XIII became stronger and entropic contribution slightly increased. The change of cyclohexyl group to S-substituted phenyl and benzyl groups did not change enthalpic contribution. N-substituted cyclohexyl group instead of S-alkylated analog showed increased enthalpic contribution.

Compound **EA3-8** was the strongest binder of CA XIII comparing with all studied benzenesulfonamides and had the greater enthalpic contribution than other dual-tailed compounds. It would be interesting to determine enthalpic and entropic influence of modified **EA11-1** and **EA12-1** compounds bearing N-substituted benzyl groups. Tail in *para* position increased entropic contribution,

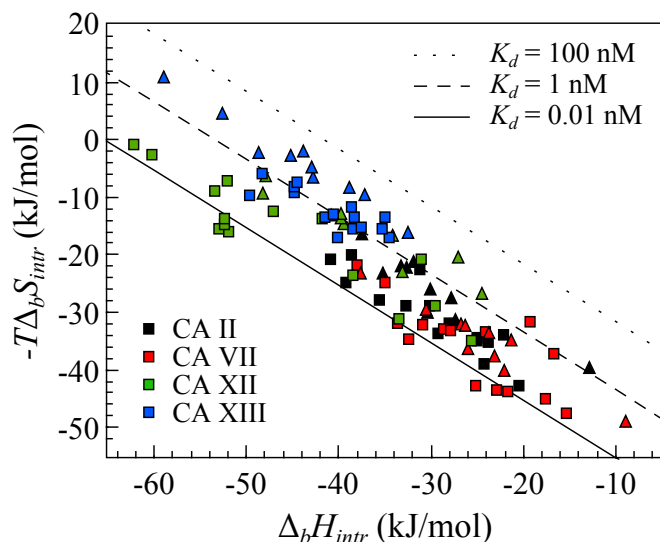


**Figure 19** The intrinsic enthalpy-entropy compensation graph. Colors represent CA isozymes (black - CA II, red - CA VII, green - CA XII, and blue - CA XIII). Squares correspond to the dual-tailed benzenesulfonamides, while triangles – benzenesulfonamides bearing a tail in *meta* position. Diagonal lines represent the  $K_{ds}$  (solid line - 0.01 nM, dashed is 1 nM, and dotted is 100 nM).

thus this thermodynamic parameter might become favorable after such modification.

The longer tail in *meta* position of dual-tailed compounds increased enthalpic contribution to binding affinity. It can be seen comparing **EA3-7** vs **EA4-7**, **EA3-3** vs **EA4-3**, and **EA3-2** vs **EA4-2**. However,  $\text{SO}_2$ -substituted group in *para* position diminished enthalpic contribution of benzenesulfonamides comparing with S-substituted derivatives.

Figure 19 shows the enthalpy-entropy compensation graph for the studied compounds binding to four CAs. Squares represent the dual-tailed benzenesulfonamides and triangles represent the benzenesulfonamides bearing a single tail in *meta* position. Different colors show different CA isozymes. Binding affinities span in a relatively narrow range, while the range of enthalpies and entropies are very large. Thermodynamic properties of CA II and CA VII binding are very similar - enthalpies and entropies span equally and thus black and red squares overlap in the figure. Equal contribution arising from enthalpic and entropic reasons to CA XII binding affinity also overlaps red and black datapoints, however part of CA XII datapoints are shifted due to enthalpically driven interaction. Blue datapoints are the most separated, because CA XIII binding with these compounds is exclusively enthalpy driven with two compounds exhibiting an unfavorable binding entropy.



9. *Observed and intrinsic thermodynamics of meta- and para-substituted benzenesulfonamide binding to CA*

---

In conclusion, the binding of chlorinated benzenesulfonamides to CA II, CA VII, CA XII, and CA XIII is both enthalpy and entropy driven. There are only two cases when singly-tailed compounds bound CA XIII with slightly unfavorable entropy. Dual-tailed benzenesulfonamides are stronger binders of CA XII and CA XIII and to a lesser extent CA II and CA VII than single-tailed derivatives. Small structural changes in compound structure highly affect the thermodynamic binding parameters.

## 10 Introduction of intrinsic kinetics of protein-ligand interactions and their implications for drug design

The design of efficient and specific drugs requires a thorough understanding of how lead compounds interact with their protein targets and interfere with their function over time. The molecular details can be revealed by analysis of the interaction mechanism and kinetics, where the intrinsic rate constants have to be resolved in addition to the more easily accessible observed kinetics. Surface plasmon resonance biosensor technology (SPR) is suitable for kinetic studies of ligand-protein interactions, but is typically only used for estimation of observed rate constants. However, we used SPR to determine the intrinsic rate constants for sulfonamide inhibitors and pharmacologically relevant isoforms of carbonic anhydrase. This enabled a structure-intrinsic kinetic relationship analysis.

### Observed binding kinetics dependence on pH

The determined association and dissociation rates of protein-ligand complex formation provide important information about interaction mechanisms and inhibitor properties, allowing the rational modification of compounds and optimization of their binding characteristics. After published doubts of CA-sulfonamide interaction mechanism [104], to better understand it and its pH dependency, we have considered that it is possible to determine the intrinsic rate constants for CA inhibitors by analyzing the pH-dependency of the interactions using surface plasmon resonance (SPR) biosensor technology<sup>2</sup>.

The protonation effect on the kinetics of protein-ligand interactions was demonstrated by analysing the interaction between the selected ligands (Fig. 20) and CA II, CA IX, and CA XIII as a function of pH (Table 6). Representative sensorgrams are shown in Fig. 21 for the interactions between **VD10-39b** and CA II. Figure 22 demonstrates the dependency of observed kinetic parameters for the interaction between **AZM** and three different CA enzymes. The top panels illustrate that the observed association rate constants  $k_a$  are clearly pH-dependent, with an optimum around 7. However, the intrinsic  $k_a$  does not depend on pH and it is shown as a straight solid line. In contrast, the observed dissociation rate  $k_d$  for CAs were essentially pH independent (middle panels). Consequently, the equilibrium dissociation constants were pH-dependent, with a minimum around 7 for CA II and CA XIII (bottom panels). The  $K_D$  for CA IX was low for pH up to around 7, above which it increased linearly. As a reference, the corresponding equilibrium data determined by FTSA is included for CA II, confirming that the

<sup>2</sup>Vladimir O. Talibov contributed equally to this work.

10. Introduction of intrinsic kinetics of protein-ligand interactions and their implications for drug design

two techniques give equivalent results. Figure 22 shows the same pH dependence as Figure 4, except that the  $K_D$  values are not calculated to the Gibbs energies in Fig. 22.

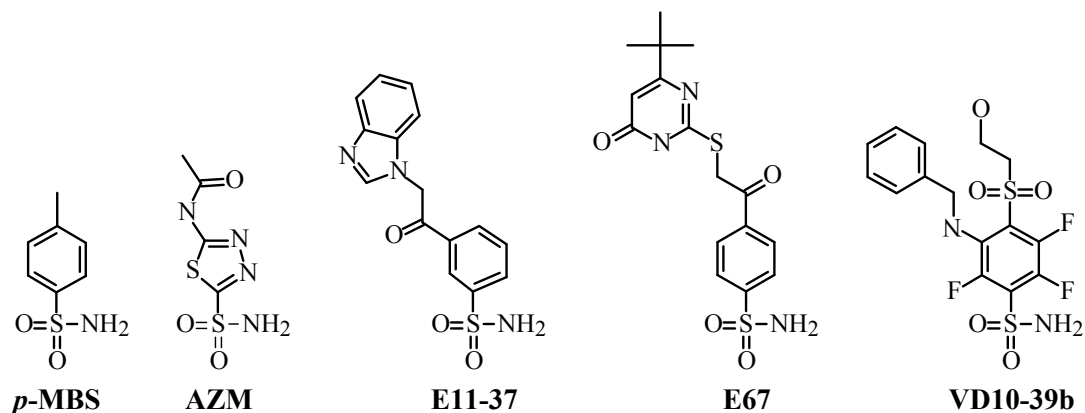


**Figure 20** Compound structures used in the SPR kinetic determination of CA-sulfonamide binding dependence on pH.

**Table 6** Observed kinetic and thermodynamic parameters were determined at different pHs by SPR (25°C). The  $pK_a$  of each compound is written near it.

Compound	Target	pH	$k_a$	$k_d$	$K_D$
<b>E67</b> $pK_a=9.2$	CA II	5.5	$2.07 \times 10^4$	$3.79 \times 10^{-2}$	$1.83 \times 10^{-6}$
		6.0	$9.05 \times 10^4$	$3.82 \times 10^{-2}$	$4.23 \times 10^{-7}$
		6.5	$3.45 \times 10^5$	$4.42 \times 10^{-2}$	$1.28 \times 10^{-7}$
		7.0	$7.75 \times 10^5$	$3.69 \times 10^{-2}$	$4.77 \times 10^{-8}$
		7.5	$1.10 \times 10^6$	$3.16 \times 10^{-2}$	$2.88 \times 10^{-8}$
		8.0	$1.63 \times 10^6$	$3.44 \times 10^{-2}$	$2.12 \times 10^{-8}$
		8.5	$1.48 \times 10^6$	$3.21 \times 10^{-2}$	$2.16 \times 10^{-8}$
		9.0	$1.11 \times 10^6$	$2.78 \times 10^{-2}$	$2.50 \times 10^{-8}$
<b>VD10-39b</b> $pK_a=8.0$	CA II	5.5	$3.48 \times 10^4$	$5.52 \times 10^{-2}$	$1.59 \times 10^{-6}$
		6.0	$1.50 \times 10^5$	$5.60 \times 10^{-2}$	$3.74 \times 10^{-7}$
		6.5	$3.67 \times 10^5$	$4.59 \times 10^{-2}$	$1.25 \times 10^{-7}$
		7.0	$1.03 \times 10^6$	$5.88 \times 10^{-2}$	$5.73 \times 10^{-8}$
		7.5	$1.42 \times 10^6$	$4.95 \times 10^{-2}$	$3.49 \times 10^{-8}$
		8.0	$1.37 \times 10^6$	$4.69 \times 10^{-2}$	$3.43 \times 10^{-8}$
		8.5	$7.50 \times 10^5$	$4.33 \times 10^{-2}$	$5.77 \times 10^{-8}$
		9.0	$2.71 \times 10^5$	$3.22 \times 10^{-2}$	$1.19 \times 10^{-7}$
<b>AZM</b> $pK_a=7.3$	CA II	5.5	$3.04 \times 10^5$	$5.31 \times 10^{-2}$	$1.75 \times 10^{-7}$
		6.0	$1.18 \times 10^6$	$6.04 \times 10^{-2}$	$5.11 \times 10^{-8}$
		6.5	$3.51 \times 10^6$	$8.19 \times 10^{-2}$	$2.34 \times 10^{-8}$
		7.0	$3.70 \times 10^6$	$5.32 \times 10^{-2}$	$1.44 \times 10^{-8}$
		7.5	$2.63 \times 10^6$	$4.59 \times 10^{-2}$	$1.75 \times 10^{-8}$
		8.0	$2.18 \times 10^6$	$7.17 \times 10^{-2}$	$3.29 \times 10^{-8}$
		8.5	$5.19 \times 10^5$	$3.65 \times 10^{-2}$	$7.03 \times 10^{-8}$
		9.0	$1.97 \times 10^5$	$5.64 \times 10^{-2}$	$2.87 \times 10^{-7}$
<b>p-MBS</b> $pK_a=10.2$	CA II	5.5	$1.04 \times 10^4$	$7.83 \times 10^{-2}$	$7.55 \times 10^{-6}$
		6.0	$3.77 \times 10^4$	$7.69 \times 10^{-2}$	$2.04 \times 10^{-6}$
		6.5	$7.96 \times 10^4$	$6.59 \times 10^{-2}$	$8.29 \times 10^{-7}$
		7.0	$1.39 \times 10^5$	$6.02 \times 10^{-2}$	$4.32 \times 10^{-7}$
		7.5	$1.88 \times 10^5$	$4.60 \times 10^{-2}$	$2.44 \times 10^{-7}$
		8.0	$2.38 \times 10^5$	$5.23 \times 10^{-2}$	$2.19 \times 10^{-7}$
		8.5	$2.37 \times 10^5$	$5.16 \times 10^{-2}$	$2.18 \times 10^{-7}$
		9.0	$3.03 \times 10^5$	$5.97 \times 10^{-2}$	$1.97 \times 10^{-7}$

Continued on next page

Table 6 – Continued from previous page

Compound	Target	pH	$k_a$	$k_d$	$K_D$
<b>E67</b> $pK_a=9.2$	CA IX	6.0	$4.19 \times 10^5$	$1.42 \times 10^{-1}$	$3.40 \times 10^{-7}$
		6.5	$7.05 \times 10^5$	$9.36 \times 10^{-2}$	$8.65 \times 10^{-8}$
		7.0	$1.65 \times 10^6$	$6.80 \times 10^{-2}$	$4.13 \times 10^{-8}$
		7.5	$1.95 \times 10^6$	$3.04 \times 10^{-2}$	$1.56 \times 10^{-8}$
		8.0	$1.17 \times 10^7$	$1.75 \times 10^{-1}$	$1.49 \times 10^{-8}$
		8.5	$4.46 \times 10^6$	$6.40 \times 10^{-2}$	$1.44 \times 10^{-8}$
		9.0	$2.49 \times 10^7$	$3.19 \times 10^{-1}$	$1.28 \times 10^{-8}$
<b>E11-37</b> $pK_a=9.7$	CA IX	6.0	$1.33 \times 10^5$	$4.71 \times 10^{-1}$	$3.54 \times 10^{-6}$
		6.5	$4.29 \times 10^5$	$6.42 \times 10^{-1}$	$1.50 \times 10^{-6}$
		7.0	$5.34 \times 10^5$	$3.53 \times 10^{-1}$	$6.60 \times 10^{-7}$
		7.5	$5.41 \times 10^5$	$2.74 \times 10^{-1}$	$5.07 \times 10^{-7}$
		8.0	$7.07 \times 10^5$	$2.83 \times 10^{-1}$	$4.00 \times 10^{-7}$
		8.5	$7.65 \times 10^5$	$3.26 \times 10^{-1}$	$4.26 \times 10^{-7}$
		9.0	$6.50 \times 10^5$	$3.37 \times 10^{-1}$	$5.17 \times 10^{-7}$
<b>AZM</b> $pK_a=7.3$	CA IX	6.0	$1.55 \times 10^6$	$1.62 \times 10^{-2}$	$1.05 \times 10^{-8}$
		6.5	$2.25 \times 10^6$	$2.37 \times 10^{-2}$	$1.06 \times 10^{-8}$
		7.0	$2.52 \times 10^6$	$2.52 \times 10^{-2}$	$1.00 \times 10^{-8}$
		7.5	$1.43 \times 10^6$	$1.68 \times 10^{-2}$	$1.18 \times 10^{-8}$
		8.0	$1.12 \times 10^6$	$3.39 \times 10^{-2}$	$3.02 \times 10^{-8}$
		8.5	$5.74 \times 10^5$	$4.00 \times 10^{-2}$	$6.98 \times 10^{-8}$
		9.0	$2.59 \times 10^5$	$5.22 \times 10^{-2}$	$2.02 \times 10^{-7}$
<b>VD10-39b</b> $pK_a=8.0$	CA XIII	6.0	$6.30 \times 10^4$	$8.93 \times 10^{-3}$	$1.42 \times 10^{-7}$
		6.5	$3.31 \times 10^5$	$1.48 \times 10^{-2}$	$4.46 \times 10^{-8}$
		7.0	$9.71 \times 10^5$	$1.16 \times 10^{-2}$	$1.19 \times 10^{-8}$
		7.5	$2.80 \times 10^6$	$1.38 \times 10^{-2}$	$4.93 \times 10^{-9}$
		8.0	$7.49 \times 10^6$	$1.14 \times 10^{-2}$	$1.53 \times 10^{-9}$
		8.5	$5.18 \times 10^6$	$9.57 \times 10^{-3}$	$1.85 \times 10^{-9}$
		9.0	$3.36 \times 10^6$	$1.25 \times 10^{-2}$	$3.72 \times 10^{-9}$
<b>E11-37</b> $pK_a=9.7$	CA XIII	6.5	$2.56 \times 10^4$	$1.16 \times 10^{-1}$	$4.55 \times 10^{-6}$
		7.0	$7.28 \times 10^4$	$8.56 \times 10^{-2}$	$1.18 \times 10^{-6}$
		7.5	$1.90 \times 10^5$	$7.80 \times 10^{-2}$	$4.11 \times 10^{-7}$
		8.0	$3.68 \times 10^5$	$7.20 \times 10^{-2}$	$1.96 \times 10^{-7}$
		8.5	$8.16 \times 10^5$	$8.59 \times 10^{-2}$	$1.05 \times 10^{-7}$
		9.0	$8.48 \times 10^5$	$5.83 \times 10^{-2}$	$6.87 \times 10^{-8}$
<b>AZM</b> $pK_a=7.3$	CA XIII	6.0	$1.04 \times 10^5$	$1.45 \times 10^{-2}$	$1.40 \times 10^{-7}$
		6.5	$1.78 \times 10^5$	$1.34 \times 10^{-2}$	$7.52 \times 10^{-8}$
		7.0	$4.90 \times 10^5$	$1.56 \times 10^{-2}$	$3.18 \times 10^{-8}$
		7.5	$7.97 \times 10^5$	$1.28 \times 10^{-2}$	$1.61 \times 10^{-8}$
		8.0	$6.80 \times 10^5$	$1.49 \times 10^{-2}$	$2.20 \times 10^{-8}$
		8.5	$2.64 \times 10^5$	$8.31 \times 10^{-3}$	$3.15 \times 10^{-8}$
9.0	$1.29 \times 10^5$	$1.72 \times 10^{-2}$	$1.33 \times 10^{-7}$		

The standard deviation did not exceed 1.4 fold of the value.

To rationalize the difference between the observed and intrinsic rate constants and the pH dependence of the kinetic parameters for sulfonamides interacting with carbonic anhydrase, a mechanistic model was developed (Fig. 23). The molecular species that occur and account for the observed interaction are indicated in the Fig. 23 top scheme (A), while those involved in the intrinsic interaction, and their inter-conversions, are specified below (Fig. 23, scheme B). This model assumes that sulfonamides are in the deprotonated, anionic form when they interact with the Zn cation in the active site of the CA, and that the water molecule occupying the fourth coordination space of the metal ion has to be in a protonated, electrostatically neutral form in order to be substituted by the deprotonated sulfonamide.

10. Introduction of intrinsic kinetics of protein-ligand interactions and their implications for drug design

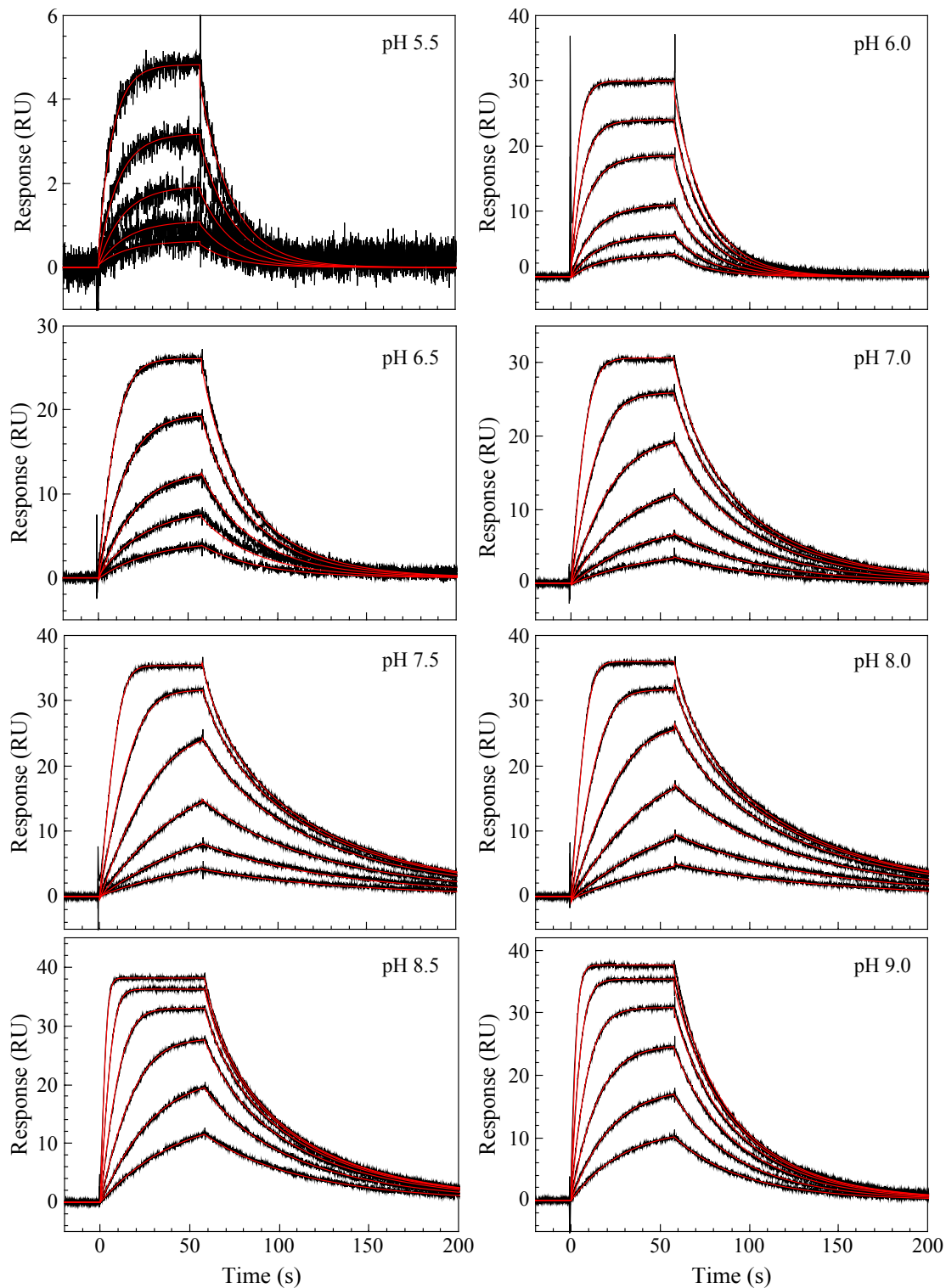


**Figure 21** Sensorgrams for interactions between **VD10-39b** and immobilised CA II. The compound was injected in a 2-fold dilution series, starting at a concentration estimated to be 10 times the expected  $K_D$ . Running buffers were adjusted to the indicated pH. Red lines represent best fit curves from non-linear regression analysis, using a reversible 1:1 interaction model.

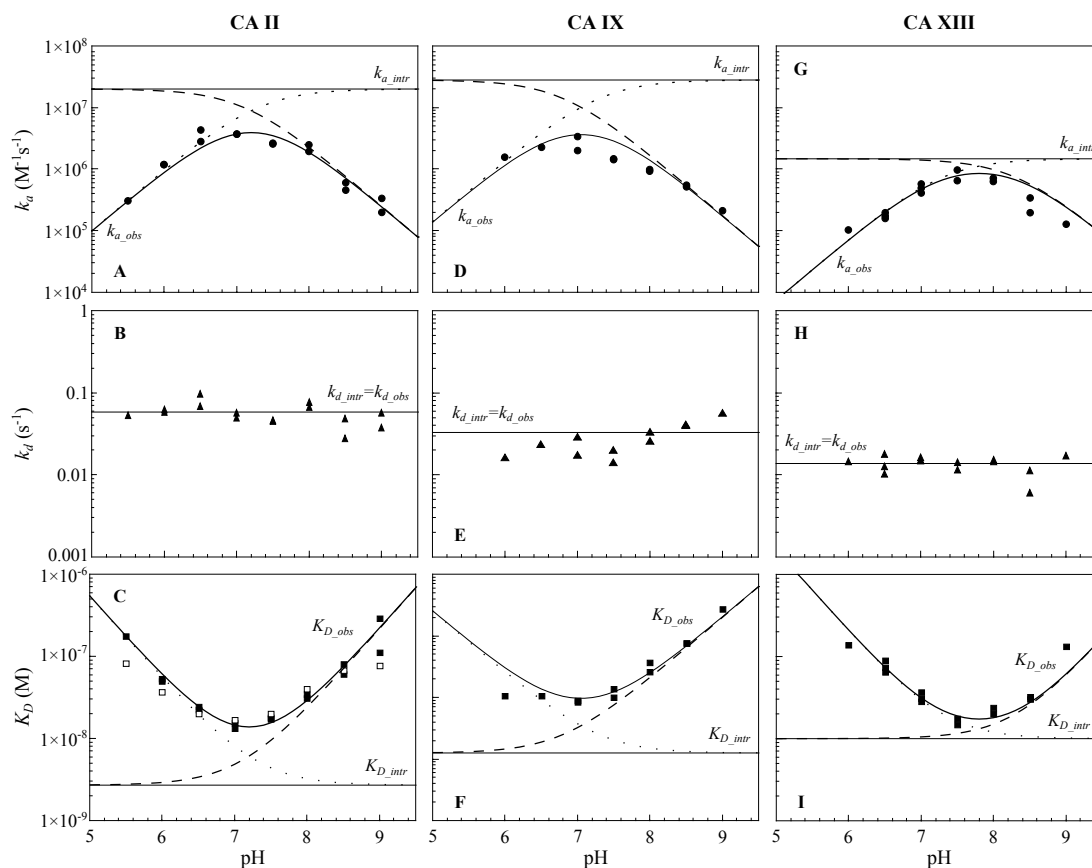


**Figure 22** Observed kinetic and equilibrium data as a function of pH and the intrinsic values that are independent of pH. The kinetic parameters of **AZM** interaction with CA II, CA IX, and CA XIII were determined by SPR (solid symbols).  $K_D$  values, obtained by FTSA for the CA II–**AZM** interaction at various pH are included as open squares in the left bottom panel. Solid curve is a theoretical model of binding according to equation 21, dotted and dashed lines show a contribution of a fraction of deprotonated **AZM** and protonated CA. Protein  $pK_a$ s were taken from Table 1.

Depending on the pH, two reactions may consequently have to occur before the ligand can interact with the active site Zn(II): 1) protonation of the Zn(II)-bound hydroxide (top, black), and 2) deprotonation of the sulfonamide (bottom, red).

The fraction of inhibitor in the deprotonated form ( $f_{\text{RSO}_2\text{NH}^-}$ ) and the fraction of CA bearing a protonated water molecule in its active site ( $f_{\text{CAZnH}_2\text{O}}$ ) were described by equations 16 and 17, previously.

These equations were used to visualize how the fraction of the reactants vary with pH (Fig. 23, C). The graph illustrates that the fraction of binding competent CA is lower above the  $pK_a$ , which for most CA isoforms is in the near-neutral pH range. The opposite relationship applies to the sulfonamides, which have a higher fraction of the binding competent form at pH values above their near neutral  $pK_a$ . The binding of sulfonamides to CA is thus expected to be optimal at near-neutral pH, as the charges on the interacting groups are unfavourable in both acidic and alkaline environments. To translate this structural information into

10. Introduction of intrinsic kinetics of protein-ligand interactions and their implications for drug design

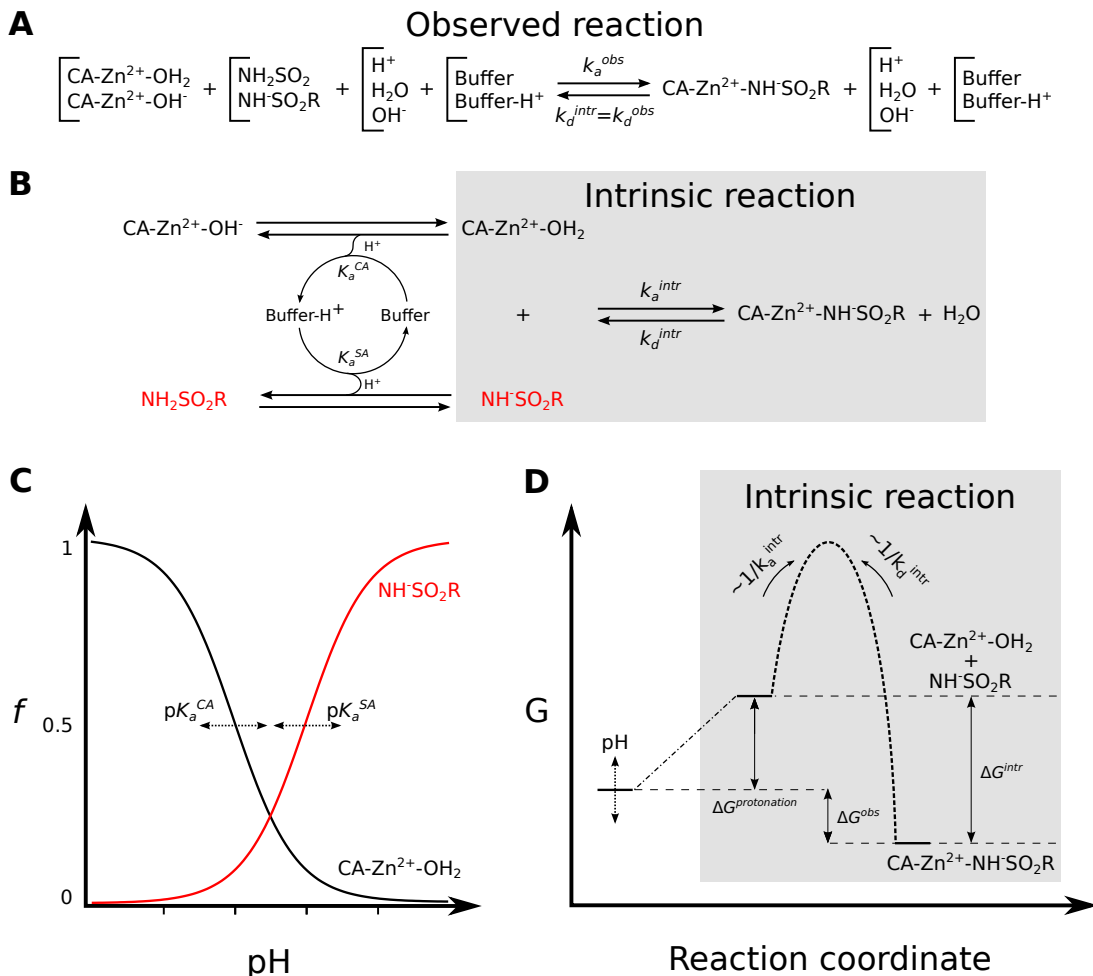


**Figure 23** Mechanistic principles for an interaction between a sulfonamide inhibitor and a carbonic anhydrase. A) Scheme for the observed reaction and the molecular species involved. B) Scheme for the intrinsic reaction (shaded in gray) and the molecular species involved. C) pH-dependencies of the concentrations of protonated CA active site (black) and deprotonated sulfonamide (red); mathematical expressions are given in Eq.s 17 and 16, respectively. D) Free energy (G) profile for the observed and the intrinsic reactions.

terms of kinetics and affinity, we modified the standard reversible second-order rate equation.

The observed association rate is a function of the intrinsic association rate and the available fractional concentrations of the interacting species:

$$k_{a\_obs} = k_{a\_intr} f_{\text{CAZnH}_2\text{O}} f_{\text{RSO}_2\text{NH}^-} \quad (37)$$

The intrinsic association constant  $k_{a\_intr}$  can thus be expressed as a function of the observed association constant and the fraction of binding-competent forms:

$$k_{a\_intr} = \frac{k_{a\_obs}}{f_{\text{CAZnH}_2\text{O}} f_{\text{RSO}_2\text{NH}^-}} \quad (38)$$

The fractional concentration of the associating species is pH-dependent but opposite (Fig. 23, C). As the exact lateral position of two curves depend on the  $pK_a$ s of the sulfonamide and the Zn(II)-bound water molecule, the exact pH for the optimum is a characteristic for both the specific inhibitor and the CA isoform.

Furthermore, the model assumes that the observed and intrinsic dissociation rates are equal and essentially pH independent as they both involve a simple dissociation of the ligand-target complex:

$$k_{d\_obs} = k_{d\_intr} \quad (39)$$

Taken together, these equations can be used to define affinities and their pH dependencies, as the intrinsic equilibrium dissociation constant ( $K_{D\_intr}$ ) is equal to the ratio of association and dissociation rates:

$$K_{D\_intr} = \frac{k_{d\_intr}}{k_{a\_intr}} \quad (40)$$

This is illustrated in the free energy diagram (Fig. 23, D), that also shows the kinetic barrier of association and dissociation and why the observed rate of association and affinities vary with pH, while the rate of dissociation is pH insensitive.

### Observed vs. intrinsic kinetic parameters

To determine intrinsic parameters,  $k_a$  rates of protein ligand binding were observed<sup>3</sup>. For this study 18 benzenesulfonamide-based inhibitors (Fig. 24) and 6 CA isoforms (CA I, II, VII, IX, XII, and XIII) were chosen. The affinities for the interactions determined by SPR ( $K_D^{SPR}$ ) were similar to the affinities obtained using FTSA ( $K_D^{FTSA}$ ), as shown in Table 7 and Figure 25. The largest mismatches were observed for the interactions with slow dissociation rates. However, essentially irreversible interactions identified by SPR analysis had subnanomolar  $K_D^{FTSA}$  values.

**Table 7** Kinetic parameters and equilibrium dissociation constants for the interactions between benzenesulfonamides and recombinant human CA isoforms I, II, VII, IX, XII, and XIII. The SPR-estimated dissociation constants ( $K_D^{SPR}$ ) were determined from the kinetic parameters according to Equation 9 and compared with dissociation constants determined by FTSA ( $K_D^{FTSA}$ ). Blue numbers represent approximate association constants obtained for the tightest interactions that exhibited too slow dissociation rates that could not be determined. SPR experiments were performed at pH 7.4, while FTSA – at pH 7.0. Spectrophotometrically obtained  $pK_a$ s of compounds are listed in the first column near the compound name. All data is shown for 25 °C

Observed kinetic and thermodynamic parameters of binding							
Compound		CA I	CA II	CA VII	CA IX	CA XII	CA XIII
<b>E79</b>	$k_{a\_obs}, M^{-1}s^{-1}$	$2.0 \times 10^5$	n/d	$8.1 \times 10^5$	$1.6 \times 10^6$	$2.8 \times 10^5$	$2.3 \times 10^5$
<b>(1)</b>	$k_d, s^{-1}$	$7.9 \times 10^{-3}$	n/d	$5.5 \times 10^{-3}$	$5.9 \times 10^{-2}$	$5.1 \times 10^{-2}$	$5.7 \times 10^{-3}$

*Continued on next page*



10. Introduction of intrinsic kinetics of protein-ligand interactions and their implications for drug design

Table 7 – Continued from previous page

Compound	CA I	CA II	CA VII	CA IX	CA XII	CA XIII	
pK <sub>a</sub> =9.1	K <sub>D</sub> <sup>SPR</sup> , M	3.7 × 10 <sup>-8</sup>	n/d	6.8 × 10 <sup>-9</sup>	3.7 × 10 <sup>-8</sup>	1.9 × 10 <sup>-7</sup>	2.4 × 10 <sup>-8</sup>
	K <sub>D</sub> <sup>FTSA</sup> , M	1.4 × 10 <sup>-8</sup>	1.5 × 10 <sup>-9</sup>	8.3 × 10 <sup>-9</sup>	1.8 × 10 <sup>-8</sup>	3.2 × 10 <sup>-7</sup>	3.3 × 10 <sup>-8</sup>
<b>E11-36</b> (2)	k <sub>a_obs</sub> , M <sup>-1</sup> s <sup>-1</sup>	3.3 × 10 <sup>5</sup>	7.7 × 10 <sup>5</sup>	9.8 × 10 <sup>5</sup>	3.1 × 10 <sup>6</sup>	3.8 × 10 <sup>5</sup>	6.3 × 10 <sup>5</sup>
	k <sub>d</sub> , s <sup>-1</sup>	7.5 × 10 <sup>-3</sup>	4.6 × 10 <sup>-3</sup>	1.7 × 10 <sup>-2</sup>	1.4 × 10 <sup>-1</sup>	1.7 × 10 <sup>-1</sup>	2.0 × 10 <sup>-3</sup>
pK <sub>a</sub> =8.6	K <sub>D</sub> <sup>SPR</sup> , M	2.2 × 10 <sup>-8</sup>	6.0 × 10 <sup>-9</sup>	1.7 × 10 <sup>-8</sup>	4.7 × 10 <sup>-8</sup>	4.5 × 10 <sup>-7</sup>	3.2 × 10 <sup>-9</sup>
	K <sub>D</sub> <sup>FTSA</sup> , M	5.0 × 10 <sup>-9</sup>	3.3 × 10 <sup>-9</sup>	1.5 × 10 <sup>-9</sup>	2.0 × 10 <sup>-8</sup>	3.3 × 10 <sup>-7</sup>	8.0 × 10 <sup>-9</sup>
<b>E11-37</b> (3)	k <sub>a_obs</sub> , M <sup>-1</sup> s <sup>-1</sup>	1.8 × 10 <sup>4</sup>	8.2 × 10 <sup>5</sup>	4.4 × 10 <sup>5</sup>	1.3 × 10 <sup>6</sup>	7.2 × 10 <sup>4</sup>	9.3 × 10 <sup>4</sup>
	k <sub>d</sub> , s <sup>-1</sup>	7.9 × 10 <sup>-1</sup>	6.2 × 10 <sup>-1</sup>	6.5 × 10 <sup>-1</sup>	3.1 × 10 <sup>-1</sup>	5.1 × 10 <sup>-1</sup>	4.9 × 10 <sup>-2</sup>
pK <sub>a</sub> =9.7	K <sub>D</sub> <sup>SPR</sup> , M	4.4 × 10 <sup>-5</sup>	7.6 × 10 <sup>-7</sup>	1.5 × 10 <sup>-6</sup>	2.4 × 10 <sup>-7</sup>	7.1 × 10 <sup>-6</sup>	5.2 × 10 <sup>-7</sup>
	K <sub>D</sub> <sup>FTSA</sup> , M	1.7 × 10 <sup>-6</sup>	1.7 × 10 <sup>-6</sup>	2.9 × 10 <sup>-6</sup>	2.0 × 10 <sup>-7</sup>	4.3 × 10 <sup>-6</sup>	9.1 × 10 <sup>-7</sup>
<b>E2</b> (4)	k <sub>a_obs</sub> , M <sup>-1</sup> s <sup>-1</sup>	n/d	2.8 × 10 <sup>5</sup>	1.6 × 10 <sup>5</sup>	1.8 × 10 <sup>6</sup>	1.6 × 10 <sup>5</sup>	n/d
	k <sub>d</sub> , s <sup>-1</sup>	n/d	1.5 × 10 <sup>-1</sup>	2.7 × 10 <sup>-1</sup>	8.4 × 10 <sup>-1</sup>	1.4 × 10 <sup>-1</sup>	n/d
pK <sub>a</sub> =9.0	K <sub>D</sub> <sup>SPR</sup> , M	n/d	5.3 × 10 <sup>-7</sup>	1.7 × 10 <sup>-6</sup>	4.6 × 10 <sup>-7</sup>	9.0 × 10 <sup>-7</sup>	n/d
	K <sub>D</sub> <sup>FTSA</sup> , M	4.8 × 10 <sup>-6</sup>	5.9 × 10 <sup>-7</sup>	3.3 × 10 <sup>-7</sup>	3.0 × 10 <sup>-7</sup>	7.7 × 10 <sup>-7</sup>	1.1 × 10 <sup>-7</sup>
<b>E7</b> (5)	k <sub>a_obs</sub> , M <sup>-1</sup> s <sup>-1</sup>	n/d	3.8 × 10 <sup>5</sup>	2.0 × 10 <sup>5</sup>	n/d	1.0 × 10 <sup>5</sup>	8.3 × 10 <sup>4</sup>
	k <sub>d</sub> , s <sup>-1</sup>	n/d	1.3 × 10 <sup>-1</sup>	6.1 × 10 <sup>-2</sup>	n/d	2.0 × 10 <sup>-2</sup>	4.3 × 10 <sup>-2</sup>
pK <sub>a</sub> =9.0	K <sub>D</sub> <sup>SPR</sup> , M	n/d	3.3 × 10 <sup>-7</sup>	3.1 × 10 <sup>-7</sup>	n/d	2.0 × 10 <sup>-7</sup>	5.1 × 10 <sup>-7</sup>
	K <sub>D</sub> <sup>FTSA</sup> , M	2.2 × 10 <sup>-6</sup>	6.7 × 10 <sup>-7</sup>	9.1 × 10 <sup>-7</sup>	4.0 × 10 <sup>-7</sup>	3.7 × 10 <sup>-7</sup>	1.8 × 10 <sup>-7</sup>
<b>E90</b> (6)	k <sub>a_obs</sub> , M <sup>-1</sup> s <sup>-1</sup>	2.0 × 10 <sup>5</sup>	1.6 × 10 <sup>6</sup>	2.9 × 10 <sup>6</sup>	3.2 × 10 <sup>6</sup>	2.0 × 10 <sup>7</sup>	2.8 × 10 <sup>5</sup>
	k <sub>d</sub> , s <sup>-1</sup>	1.2 × 10 <sup>-2</sup>	8.0 × 10 <sup>-3</sup>	2.2 × 10 <sup>-2</sup>	2.1 × 10 <sup>-1</sup>	2.7	1.7 × 10 <sup>-2</sup>
pK <sub>a</sub> =9.4	K <sub>D</sub> <sup>SPR</sup> , M	6.3 × 10 <sup>-8</sup>	5.2 × 10 <sup>-9</sup>	7.7 × 10 <sup>-9</sup>	6.6 × 10 <sup>-8</sup>	1.4 × 10 <sup>-7</sup>	6.1 × 10 <sup>-8</sup>
	K <sub>D</sub> <sup>FTSA</sup> , M	2.5 × 10 <sup>-8</sup>	7.1 × 10 <sup>-9</sup>	2.0 × 10 <sup>-8</sup>	8.3 × 10 <sup>-8</sup>	2.2 × 10 <sup>-7</sup>	5.0 × 10 <sup>-8</sup>
<b>E11-8</b> (7)	k <sub>a_obs</sub> , M <sup>-1</sup> s <sup>-1</sup>	3.1 × 10 <sup>5</sup>	3.9 × 10 <sup>5</sup>	3.7 × 10 <sup>6</sup>	1.8 × 10 <sup>6</sup>	1.6 × 10 <sup>6</sup>	7.2 × 10 <sup>5</sup>
	k <sub>d</sub> , s <sup>-1</sup>	8.4 × 10 <sup>-3</sup>	4.2 × 10 <sup>-3</sup>	4.4 × 10 <sup>-2</sup>	2.6 × 10 <sup>-1</sup>	3.2 × 10 <sup>-1</sup>	4.6 × 10 <sup>-3</sup>
pK <sub>a</sub> =8.9	K <sub>D</sub> <sup>SPR</sup> , M	2.7 × 10 <sup>-8</sup>	1.1 × 10 <sup>-8</sup>	1.2 × 10 <sup>-8</sup>	1.5 × 10 <sup>-7</sup>	2.0 × 10 <sup>-7</sup>	6.4 × 10 <sup>-9</sup>
	K <sub>D</sub> <sup>FTSA</sup> , M	3.3 × 10 <sup>-9</sup>	3.3 × 10 <sup>-9</sup>	2.0 × 10 <sup>-9</sup>	1.1 × 10 <sup>-7</sup>	3.3 × 10 <sup>-7</sup>	5.6 × 10 <sup>-9</sup>
<b>E67</b> (8)	k <sub>a_obs</sub> , M <sup>-1</sup> s <sup>-1</sup>	6.3 × 10 <sup>5</sup>	6.4 × 10 <sup>5</sup>	4.9 × 10 <sup>5</sup>	2.5 × 10 <sup>6</sup>	4.0 × 10 <sup>5</sup>	2.4 × 10 <sup>6</sup>
	k <sub>d</sub> , s <sup>-1</sup>	1.7 × 10 <sup>-3</sup>	3.0 × 10 <sup>-2</sup>	2.5 × 10 <sup>-2</sup>	8.4 × 10 <sup>-2</sup>	2.5 × 10 <sup>-2</sup>	1.0 × 10 <sup>-2</sup>
pK <sub>a</sub> =9.2	K <sub>D</sub> <sup>SPR</sup> , M	2.6 × 10 <sup>-9</sup>	4.7 × 10 <sup>-8</sup>	5.1 × 10 <sup>-8</sup>	3.3 × 10 <sup>-8</sup>	6.3 × 10 <sup>-8</sup>	4.2 × 10 <sup>-9</sup>
	K <sub>D</sub> <sup>FTSA</sup> , M	4.8 × 10 <sup>-10</sup>	1.7 × 10 <sup>-8</sup>	1.3 × 10 <sup>-8</sup>	1.1 × 10 <sup>-8</sup>	7.1 × 10 <sup>-8</sup>	1.4 × 10 <sup>-9</sup>
<b>E11-9</b> (9)	k <sub>a_obs</sub> , M <sup>-1</sup> s <sup>-1</sup>	1.8 × 10 <sup>5</sup>	3.4 × 10 <sup>5</sup>	6.4 × 10 <sup>5</sup>	1.2 × 10 <sup>6</sup>	n/d	7.1 × 10 <sup>4</sup>
	k <sub>d</sub> , s <sup>-1</sup>	2.1 × 10 <sup>-1</sup>	1.8 × 10 <sup>-1</sup>	1.4	3.1 × 10 <sup>-1</sup>	n/d	5.1 × 10 <sup>-2</sup>
pK <sub>a</sub> =9.6	K <sub>D</sub> <sup>SPR</sup> , M	1.2 × 10 <sup>-6</sup>	5.2 × 10 <sup>-7</sup>	2.2 × 10 <sup>-6</sup>	2.6 × 10 <sup>-7</sup>	n/d	7.1 × 10 <sup>-7</sup>
	K <sub>D</sub> <sup>FTSA</sup> , M	3.3 × 10 <sup>-7</sup>	4.3 × 10 <sup>-7</sup>	2.0 × 10 <sup>-6</sup>	3.3 × 10 <sup>-7</sup>	1.3 × 10 <sup>-6</sup>	5.0 × 10 <sup>-7</sup>
<b>E89</b> (10)	k <sub>a_obs</sub> , M <sup>-1</sup> s <sup>-1</sup>	1.2 × 10 <sup>5</sup>	5.5 × 10 <sup>5</sup>	4.1 × 10 <sup>5</sup>	2.0 × 10 <sup>6</sup>	8.8 × 10 <sup>5</sup>	1.2 × 10 <sup>5</sup>
	k <sub>d</sub> , s <sup>-1</sup>	4.3 × 10 <sup>-1</sup>	7.3 × 10 <sup>-2</sup>	1.5 × 10 <sup>-1</sup>	4.0 × 10 <sup>-1</sup>	1.6 × 10 <sup>-1</sup>	2.2 × 10 <sup>-2</sup>
pK <sub>a</sub> =8.9	K <sub>D</sub> <sup>SPR</sup> , M	3.5 × 10 <sup>-6</sup>	1.3 × 10 <sup>-7</sup>	3.7 × 10 <sup>-7</sup>	2.0 × 10 <sup>-7</sup>	1.8 × 10 <sup>-7</sup>	1.8 × 10 <sup>-7</sup>
	K <sub>D</sub> <sup>FTSA</sup> , M	1.8 × 10 <sup>-6</sup>	1.4 × 10 <sup>-7</sup>	3.1 × 10 <sup>-7</sup>	3.6 × 10 <sup>-7</sup>	5.0 × 10 <sup>-7</sup>	1.4 × 10 <sup>-7</sup>
<b>VD12-05</b> (11)	k <sub>a_obs</sub> , M <sup>-1</sup> s <sup>-1</sup>	8.1 × 10 <sup>5</sup>	s/d	5.2 × 10 <sup>6</sup>	9.2 × 10 <sup>6</sup>	1.3 × 10 <sup>6</sup>	1.4 × 10 <sup>6</sup>
	k <sub>d</sub> , s <sup>-1</sup>	s/d	s/d	3.3 × 10 <sup>-2</sup>	1.1 × 10 <sup>-1</sup>	2.5 × 10 <sup>-2</sup>	s/d
pK <sub>a</sub> =8.3	K <sub>D</sub> <sup>SPR</sup> , M	s/d	s/d	6.5 × 10 <sup>-9</sup>	1.1 × 10 <sup>-8</sup>	1.9 × 10 <sup>-8</sup>	s/d
	K <sub>D</sub> <sup>FTSA</sup> , M	3.3 × 10 <sup>-11</sup>	9.1 × 10 <sup>-10</sup>	3.3 × 10 <sup>-10</sup>	1.7 × 10 <sup>-9</sup>	1.4 × 10 <sup>-8</sup>	5.3 × 10 <sup>-10</sup>
<b>VD12-09</b> (12)	k <sub>a_obs</sub> , M <sup>-1</sup> s <sup>-1</sup>	n/d	n/d	2.0 × 10 <sup>4</sup>	2.9 × 10 <sup>5</sup>	1.3 × 10 <sup>5</sup>	1.0 × 10 <sup>4</sup>
	k <sub>d</sub> , s <sup>-1</sup>	n/d	n/d	1.0 × 10 <sup>-2</sup>	7.7 × 10 <sup>-3</sup>	5.0 × 10 <sup>-2</sup>	s/d
pK <sub>a</sub> =8.9	K <sub>D</sub> <sup>SPR</sup> , M	n/d	n/d	5.1 × 10 <sup>-7</sup>	2.7 × 10 <sup>-8</sup>	4.0 × 10 <sup>-7</sup>	s/d
	K <sub>D</sub> <sup>FTSA</sup> , M	9.1 × 10 <sup>-6</sup>	4.5 × 10 <sup>-7</sup>	7.4 × 10 <sup>-8</sup>	1.7 × 10 <sup>-10</sup>	1.0 × 10 <sup>-7</sup>	3.3 × 10 <sup>-8</sup>
<b>VD11-4-2</b> (13)	k <sub>a_obs</sub> , M <sup>-1</sup> s <sup>-1</sup>	n/d	8.6 × 10 <sup>4</sup>	4.9 × 10 <sup>4</sup>	1.9 × 10 <sup>6</sup>	4.8 × 10 <sup>5</sup>	5.1 × 10 <sup>5</sup>
	k <sub>d</sub> , s <sup>-1</sup>	n/d	8.7 × 10 <sup>-3</sup>	2.0 × 10 <sup>-3</sup>	s/d	s/d	7.9 × 10 <sup>-3</sup>
pK <sub>a</sub> =8.2	K <sub>D</sub> <sup>SPR</sup> , M	n/d	1.0 × 10 <sup>-7</sup>	4.0 × 10 <sup>-8</sup>	s/d	s/d	1.5 × 10 <sup>-8</sup>
	K <sub>D</sub> <sup>FTSA</sup> , M	3.3 × 10 <sup>-7</sup>	2.0 × 10 <sup>-8</sup>	3.2 × 10 <sup>-9</sup>	6.7 × 10 <sup>-12</sup>	1.1 × 10 <sup>-9</sup>	2.2 × 10 <sup>-9</sup>
<b>VD11-26</b> (14)	k <sub>a_obs</sub> , M <sup>-1</sup> s <sup>-1</sup>	3.9 × 10 <sup>5</sup>	1.3 × 10 <sup>6</sup>	2.9 × 10 <sup>5</sup>	6.5 × 10 <sup>6</sup>	1.5 × 10 <sup>6</sup>	2.5 × 10 <sup>5</sup>
	k <sub>d</sub> , s <sup>-1</sup>	1.0 × 10 <sup>-2</sup>	8.2 × 10 <sup>-3</sup>	1.3 × 10 <sup>-2</sup>	1.0 × 10 <sup>-1</sup>	1.4 × 10 <sup>-1</sup>	s/d
pK <sub>a</sub> =8.0	K <sub>D</sub> <sup>SPR</sup> , M	2.5 × 10 <sup>-8</sup>	6.4 × 10 <sup>-9</sup>	4.5 × 10 <sup>-8</sup>	1.6 × 10 <sup>-8</sup>	9.5 × 10 <sup>-8</sup>	s/d
	K <sub>D</sub> <sup>FTSA</sup> , M	2.5 × 10 <sup>-8</sup>	2.4 × 10 <sup>-9</sup>	3.1 × 10 <sup>-9</sup>	2.0 × 10 <sup>-9</sup>	1.0 × 10 <sup>-7</sup>	4.2 × 10 <sup>-10</sup>
<b>VD11-25</b> (15)	k <sub>a_obs</sub> , M <sup>-1</sup> s <sup>-1</sup>	n/d	s/d	2.4 × 10 <sup>5</sup>	7.0 × 10 <sup>5</sup>	1.8 × 10 <sup>5</sup>	7.7 × 10 <sup>4</sup>
	k <sub>d</sub> , s <sup>-1</sup>	n/d	s/d	s/d	6.4 × 10 <sup>-3</sup>	1.1 × 10 <sup>-2</sup>	s/d
pK <sub>a</sub> =8.0	K <sub>D</sub> <sup>SPR</sup> , M	n/d	s/d	s/d	9.2 × 10 <sup>-9</sup>	5.9 × 10 <sup>-8</sup>	s/d

Continued on next page

Table 7 – Continued from previous page

Compound	CA I	CA II	CA VII	CA IX	CA XII	CA XIII
$K_D^{FTSA}$ , M	$2.2 \times 10^{-7}$	$5.9 \times 10^{-10}$	$7.7 \times 10^{-11}$	$2.0 \times 10^{-10}$	$1.7 \times 10^{-8}$	$1.5 \times 10^{-9}$
<b>VD12-63</b> (16) $k_{a\_obs}$ , $M^{-1}s^{-1}$	s/d	$1.4 \times 10^6$	$2.6 \times 10^6$	$1.5 \times 10^7$	$8.8 \times 10^5$	$9.2 \times 10^5$
$k_d$ , $s^{-1}$	s/d	$9.3 \times 10^{-3}$	$7.1 \times 10^{-2}$	$1.5 \times 10^{-1}$	$4.1 \times 10^{-2}$	$1.1 \times 10^{-2}$
$K_D^{SPR}$ , M	s/d	$6.8 \times 10^{-9}$	$2.7 \times 10^{-8}$	$1.0 \times 10^{-8}$	$4.6 \times 10^{-8}$	$1.1 \times 10^{-8}$
$pK_a=8.4$ $K_D^{FTSA}$ , M	$2.9 \times 10^{-11}$	$4.5 \times 10^{-9}$	$56 \times 10^{-9}$	$2.0 \times 10^{-8}$	$3.3 \times 10^{-8}$	$4.0 \times 10^{-9}$
<b>VD12-69-1</b> (17) $k_{a\_obs}$ , $M^{-1}s^{-1}$	$1.1 \times 10^5$	$3.9 \times 10^5$	$3.0 \times 10^4$	$1.8 \times 10^6$	n/d	$1.0 \times 10^5$
$k_d$ , $s^{-1}$	$6.6 \times 10^{-3}$	$2.6 \times 10^{-2}$	$1.4 \times 10^{-1}$	$2.6 \times 10^{-1}$	n/d	$2.2 \times 10^{-2}$
$K_D^{SPR}$ , M	$6.1 \times 10^{-8}$	$6.6 \times 10^{-8}$	$4.8 \times 10^{-6}$	$1.5 \times 10^{-7}$	n/d	$2.1 \times 10^{-7}$
$pK_a=8.7$ $K_D^{FTSA}$ , M	$2.5 \times 10^{-8}$	$7.7 \times 10^{-8}$	$2.5 \times 10^{-7}$	$2.2 \times 10^{-8}$	$3.3 \times 10^{-7}$	$5.0 \times 10^{-8}$
<b>VD10-39b</b> (18) $k_{a\_obs}$ , $M^{-1}s^{-1}$	n/d	$1.5 \times 10^6$	n/d	n/d	n/d	$1.7 \times 10^5$
$k_d$ , $s^{-1}$	n/d	$5.1 \times 10^{-2}$	n/d	n/d	n/d	$7.7 \times 10^{-2}$
$K_D^{SPR}$ , M	n/d	$3.3 \times 10^{-8}$	n/d	n/d	n/d	$4.5 \times 10^{-7}$
$pK_a=8.0$ $K_D^{FTSA}$ , M	$6.7 \times 10^{-8}$	$7.7 \times 10^{-8}$	$4.2 \times 10^{-8}$	$2.0 \times 10^{-10}$	$1.0 \times 10^{-8}$	$6.3 \times 10^{-9}$

n/d - no data, s/d - slow dissociation rate. The standard deviation did not exceed 1.4 fold of the value.

Blue numbers represent approximate  $k_{a\_obs}$  determined by SPR. Compounds exhibited too slow  $k_{d\_obs}$ .

In general, *p*-substituted acetylated heterocyclic derivatives of the studied benzenesulfonamides showed higher affinities than *m*-substituted derivatives. With some exceptions, the benzimidazole heterocyclic moiety within the benzenesulfonamide structure was more favorable than the pyrimidine. Within the compound groups of N-substituted benzimidazole derivatives and S-substituted 2-thiopyrimidine derivatives (Figure 24, compounds **1-5** and **6-10**), the introduction of chlorine at *ortho* position reduced the  $K_D$  for the binding to all isozymes except for CA IX. The highest affinities possessed fluorine containing derivatives (Table 7 and Figure 27). Fluorinated compounds bearing bulky hydrophobic functional group such as tert-butyl (**VD11-25**), benzyl (**VD10-39b**) or cyclooctyl (**VD12-09** and **VD11-4-2**), demonstrated the lowest dissociation rate constants for the interaction with CA IX.

As long as association constants are pH dependent, intrinsic kinetic parameters were calculated. Figure 28 compares the intrinsic and observed thermodynamic parameters of the fluorinated compounds interaction with five CA isoforms. The most tightly binding compounds exhibited rates of dissociation that were too slow to be reliably determined by SPR. Therefore, the values for these compounds were estimated by multiplying the approximate association rates determined by SPR by the  $K_D$ s previously determined by the FTSA. They are found in the grey shaded area of the graph with very slow dissociation rates. The intrinsic  $k_a$ s were 1 to 2 orders of magnitude greater than the observed ones, with slight differences depending on the  $pK_a$ s of the compound and the CA isoform and several  $k_a$ s of compounds interaction with CAs reach the diffusion-limited association rates (e.g. **6** with CA XII, **3** with CA IX). However, intrinsic  $k_d$ s were the same as observed ones. It is clear that the rates are highly dependent both on the structure of the compound and on the microenvironment in the active site of the CA isoform.

All intrinsic association rate constants (Figure 28) were between  $3.3 \times 10^5$  and  $8.8 \times 10^8 M^{-1} s^{-1}$ , while the observed rates varied between  $\sim 10^4$  and  $10^7 M^{-1} s^{-1}$ .

10. Introduction of intrinsic kinetics of protein-ligand interactions and their implications for drug design

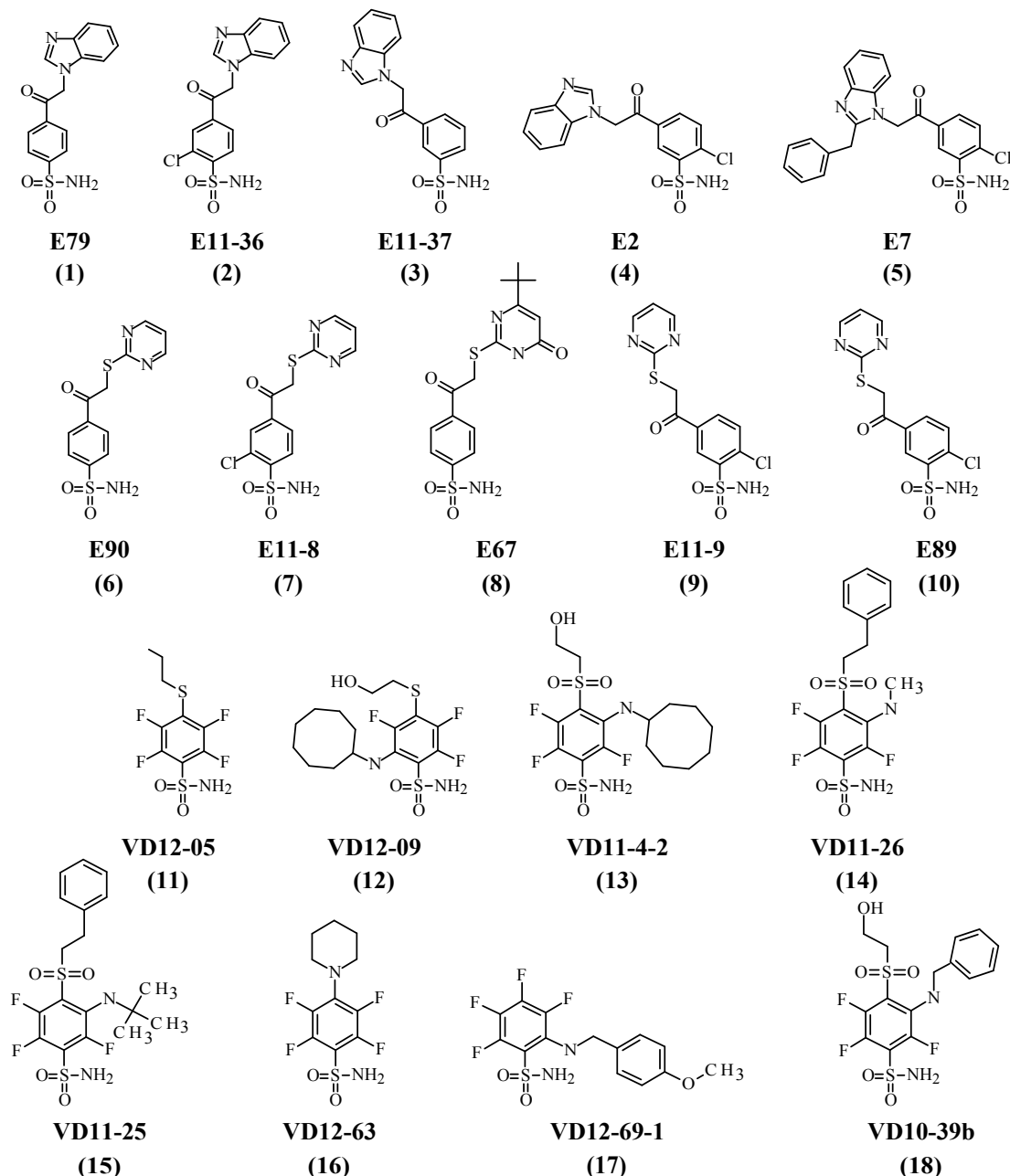


**Figure 24** Structures of the studied benzenesulfonamides: N-substituted benzimidazole derivatives **E79**, **E11-36**, **E11-37** [135], **E2**, and **E7** [136]; S-substituted 2-thiopyrimidine derivatives **E90**, **E67**, **E89** [137], **E11-8**, and **E11-9** [136]; and fluorinated benzenesulfonamides **VD12-05**, **VD12-63** [138], **VD12-09**, **VD11-4-2** [139,140], **VD11-26**, **VD11-25**, **VD12-69-1** [140], and **VD10-39b**.

The intrinsic dissociation rate constants spanned an even greater interval, from  $1.0 \times 10^{-1} \text{ s}^{-1}$  to  $6.6 \times 10^{-5} \text{ s}^{-1}$  (equivalent to residence times from 10 sec to 4.2 hours). The tightest binder of CA IX, compound **13**, whose intrinsic thermodynamic dissociation constant  $K_D$  is equal to approximately 1 pM is such a great binder of CA IX primarily due to its long residence time while the association rate is not exceptional. Similarly, the high affinity of compound **11** to CA I, and **15** to

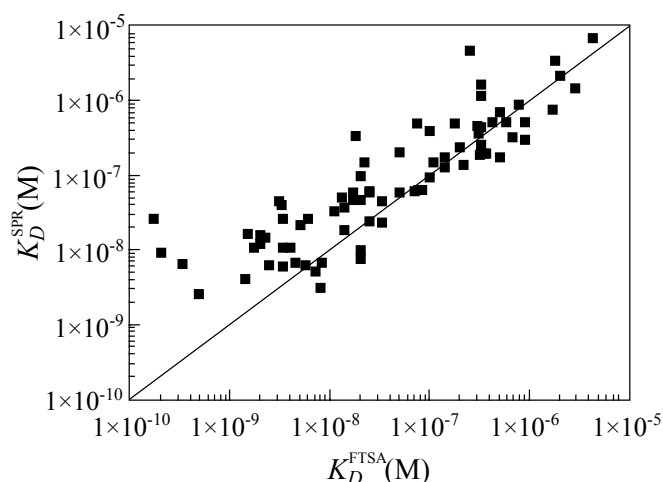


**Figure 25** Relationship between dissociation constants determined by FTSA and SPR. Data taken from Table 7.

CA VII is exceptionally strong, primarily due to extremely long residence times. It should be noted that association and dissociation rate constants and the  $K_d$ s for compounds in the right part of the Figure 28 were determined accurately by SPR. In contrast, the parameters on the left shaded part of the figure are approximate since they were generated indirectly using  $K_d$  values obtained by FTSA. However, the leftmost datapoints are of great interest because these compounds possess an exceptional stability in their interaction with certain CA isoforms.

To better understand the reasons behind the exceptional residence times of selected compounds, the correlations between intrinsic kinetic constants and the chemical structures of compounds were analyzed. The kinetic intrinsic interaction values for CA isoforms and compounds are listed in Table 8. The kinetic parameters of compounds with similar chemical structures are plotted in Figures 29 and 30.

**Table 8** Intrinsic kinetic rate constants of association ( $k_a$ ) and dissociation ( $k_d$ ) and the intrinsic thermodynamic equilibrium constants ( $K_D$ ) for all tested compound interaction with 6 CA isoforms, 25°C. Blue numbers represent values, where  $K_D$ s were taken from FTSA,  $k_a$  from SPR data, and  $k_d$ s were calculated using these observed values. All other intrinsic parameters were calculated from SPR data.

Intrinsic kinetic and thermodynamic parameters of binding							
Compound		CA I	CA II	CA VII	CA IX	CA XII	CA XIII
<b>E79</b> (1)	$k_{a\_intr}$ , $M^{-1}s^{-1}$	$1.1 \times 10^7$	n/d	$1.5 \times 10^8$	$4.1 \times 10^8$	$5.0 \times 10^7$	$1.3 \times 10^7$
	$k_d$ , $s^{-1}$	$7.9 \times 10^{-3}$	n/d	$5.5 \times 10^{-3}$	$5.9 \times 10^{-2}$	$5.1 \times 10^{-2}$	$5.7 \times 10^{-3}$
	$K_D$ , M	$7.0 \times 10^{-10}$	n/d	$3.8 \times 10^{-11}$	$1.5 \times 10^{-10}$	$1.0 \times 10^{-9}$	$4.3 \times 10^{-10}$
<b>E11-36</b> (2)	$k_{a\_intr}$ , $M^{-1}s^{-1}$	$5.5 \times 10^6$	$3.5 \times 10^7$	$5.2 \times 10^7$	$2.3 \times 10^8$	$2.0 \times 10^7$	$1.1 \times 10^7$
	$k_d$ , $s^{-1}$	$7.5 \times 10^{-3}$	$4.6 \times 10^{-3}$	$1.7 \times 10^{-2}$	$1.4 \times 10^{-1}$	$1.7 \times 10^{-1}$	$2.0 \times 10^{-3}$
	$K_D$ , M	$1.4 \times 10^{-9}$	$1.3 \times 10^{-10}$	$3.3 \times 10^{-10}$	$6.0 \times 10^{-10}$	$8.4 \times 10^{-9}$	$1.9 \times 10^{-10}$
<b>E11-37</b> (3)	$k_{a\_intr}$ , $M^{-1}s^{-1}$	$4.0 \times 10^6$	$4.9 \times 10^8$	$3.1 \times 10^8$	$1.3 \times 10^9$	$5.1 \times 10^7$	$2.1 \times 10^7$
	$k_d$ , $s^{-1}$	$7.9 \times 10^{-1}$	$6.2 \times 10^{-1}$	$6.5 \times 10^{-1}$	$3.1 \times 10^{-1}$	$5.1 \times 10^{-1}$	$4.9 \times 10^{-2}$
	$K_D$ , M	$2.0 \times 10^{-7}$	$1.3 \times 10^{-9}$	$2.1 \times 10^{-9}$	$2.4 \times 10^{-10}$	$1.0 \times 10^{-8}$	$2.3 \times 10^{-9}$
<b>E2</b>	$k_{a\_intr}$ , $M^{-1}s^{-1}$	n/d	$3.1 \times 10^7$	$2.1 \times 10^7$	$3.3 \times 10^8$	$2.1 \times 10^7$	n/d

Continued on next page

10. Introduction of intrinsic kinetics of protein-ligand interactions and their implications for drug design

Table 8 – Continued from previous page

Compound		CA I	CA II	CA VII	CA IX	CA XII	CA XIII
<b>E2</b> (4)	$k_d, s^{-1}$	n/d	$1.5 \times 10^{-1}$	$2.7 \times 10^{-1}$	$8.4 \times 10^{-1}$	$1.4 \times 10^{-1}$	n/d
	$K_D, M$	n/d	$4.9 \times 10^{-9}$	$1.3 \times 10^{-8}$	$2.6 \times 10^{-9}$	$6.8 \times 10^{-9}$	n/d
<b>E7</b> (5)	$k_{a\_intr}, M^{-1}s^{-1}$	n/d	$4.2 \times 10^7$	$2.6 \times 10^7$	n/d	$1.3 \times 10^7$	$3.4 \times 10^6$
	$k_d, s^{-1}$	n/d	$1.3 \times 10^{-1}$	$6.1 \times 10^{-2}$	n/d	$2.0 \times 10^{-2}$	$4.3 \times 10^{-2}$
	$K_D, M$	n/d	$3.1 \times 10^{-9}$	$2.4 \times 10^{-9}$	n/d	$1.6 \times 10^{-9}$	$1.3 \times 10^{-8}$
<b>E90</b> (6)	$k_{a\_intr}, M^{-1}s^{-1}$	$2.2 \times 10^7$	$4.8 \times 10^8$	$1.0 \times 10^9$	$1.6 \times 10^9$	$7.1 \times 10^9$	$3.2 \times 10^7$
	$k_d, s^{-1}$	$1.2 \times 10^{-2}$	$8.0 \times 10^{-3}$	$2.2 \times 10^{-2}$	$2.1 \times 10^{-1}$	2.7	$1.7 \times 10^{-2}$
	$K_D, M$	$5.4 \times 10^{-10}$	$1.7 \times 10^{-11}$	$2.1 \times 10^{-11}$	$1.3 \times 10^{-10}$	$3.8 \times 10^{-10}$	$5.3 \times 10^{-10}$
<b>E11-8</b> (7)	$k_{a\_intr}, M^{-1}s^{-1}$	$1.1 \times 10^7$	$3.8 \times 10^7$	$4.2 \times 10^8$	$2.9 \times 10^8$	$1.8 \times 10^8$	$2.6 \times 10^7$
	$k_d, s^{-1}$	$8.4 \times 10^{-3}$	$4.2 \times 10^{-3}$	$4.6 \times 10^{-3}$	$2.6 \times 10^{-1}$	$3.2 \times 10^{-1}$	$1 \times 10^{-8}$
	$K_D, M$	$7.6 \times 10^{-10}$	$1.1 \times 10^{-10}$	$1.0 \times 10^{-10}$	$8.9 \times 10^{-10}$	$1.8 \times 10^{-9}$	$1.7 \times 10^{-10}$
<b>E67</b> (8)	$k_{a\_intr}, M^{-1}s^{-1}$	$4.4 \times 10^7$	$1.2 \times 10^8$	$1.1 \times 10^8$	$8.0 \times 10^8$	$9.0 \times 10^7$	$1.7 \times 10^8$
	$k_d, s^{-1}$	$1.7 \times 10^{-3}$	$3.0 \times 10^{-2}$	$1.0 \times 10^{-2}$	$8.4 \times 10^{-2}$	$2.5 \times 10^{-2}$	$1 \times 10^{-8}$
	$K_D, M$	$3.8 \times 10^{-11}$	$2.4 \times 10^{-10}$	$2.3 \times 10^{-10}$	$1.1 \times 10^{-10}$	$2.8 \times 10^{-10}$	$5.8 \times 10^{-11}$
<b>E11-9</b> (9)	$k_{a\_intr}, M^{-1}s^{-1}$	$3.2 \times 10^7$	$1.6 \times 10^8$	$3.6 \times 10^8$	$9.5 \times 10^8$	n/d	$1.3 \times 10^7$
	$k_d, s^{-1}$	$2.1 \times 10^{-1}$	$1.8 \times 10^{-1}$	1.4	$3.1 \times 10^{-1}$	n/d	$5.1 \times 10^{-2}$
	$K_D, M$	$6.8 \times 10^{-9}$	$1.1 \times 10^{-9}$	$3.9 \times 10^{-9}$	$3.3 \times 10^{-10}$	n/d	$4.0 \times 10^{-9}$
<b>E89</b> (10)	$k_{a\_intr}, M^{-1}s^{-1}$	$3.9 \times 10^6$	$4.8 \times 10^7$	$4.2 \times 10^7$	$2.9 \times 10^8$	$9.0 \times 10^7$	$3.9 \times 10^6$
	$k_d, s^{-1}$	$4.3 \times 10^{-1}$	$7.3 \times 10^{-2}$	$2.2 \times 10^{-2}$	$4.0 \times 10^{-1}$	$1.6 \times 10^{-1}$	$1 \times 10^{-8}$
	$K_D, M$	$1.1 \times 10^{-7}$	$1.5 \times 10^{-9}$	$3.6 \times 10^{-9}$	$1.4 \times 10^{-9}$	$1.8 \times 10^{-9}$	$5.6 \times 10^{-9}$
<b>VD12-05</b> (11)	$k_{a\_intr}, M^{-1}s^{-1}$	$8.5 \times 10^6$	s/d	$1.7 \times 10^8$	$4.4 \times 10^8$	$4.3 \times 10^7$	$1.5 \times 10^7$
	$k_d, s^{-1}$	$2.7 \times 10^{-5}$	s/d	$3.3 \times 10^{-2}$	$1.1 \times 10^{-1}$	$2.5 \times 10^{-2}$	$7.6 \times 10^{-4}$
	$K_D, M$	$3.2 \times 10^{-12}$	s/d	$1.9 \times 10^{-10}$	$2.5 \times 10^{-10}$	$5.8 \times 10^{-10}$	$5.0 \times 10^{-11}$
<b>VD12-09</b> (12)	$k_{a\_intr}, M^{-1}s^{-1}$	n/d	n/d	$2.1 \times 10^6$	$4.2 \times 10^7$	$1.3 \times 10^7$	$3.3 \times 10^5$
	$k_d, s^{-1}$	n/d	n/d	$1.0 \times 10^{-2}$	$7.7 \times 10^{-3}$	$5.0 \times 10^{-2}$	$3.3 \times 10^{-4}$
	$K_D, M$	n/d	n/d	$4.9 \times 10^{-9}$	$1.8 \times 10^{-10}$	$3.8 \times 10^{-9}$	$1.0 \times 10^{-9}$
<b>VD11-4-2</b> (13)	$k_{a\_intr}, M^{-1}s^{-1}$	n/d	$1.8 \times 10^6$	$1.2 \times 10^6$	$6.6 \times 10^7$	$1.2 \times 10^7$	$4.0 \times 10^6$
	$k_d, s^{-1}$	n/d	$8.7 \times 10^{-3}$	$2.0 \times 10^{-3}$	$1.3 \times 10^{-5}$	$5.3 \times 10^{-4}$	$7.9 \times 10^{-3}$
	$K_D, M$	n/d	$4.8 \times 10^{-9}$	$1.7 \times 10^{-9}$	$1.9 \times 10^{-13}$	$4.5 \times 10^{-11}$	$2.0 \times 10^{-9}$
<b>VD11-26</b> (14)	$k_{a\_intr}, M^{-1}s^{-1}$	$2.3 \times 10^6$	$2.1 \times 10^7$	$5.5 \times 10^6$	$1.7 \times 10^8$	$2.8 \times 10^7$	$1.5 \times 10^6$
	$k_d, s^{-1}$	$1.0 \times 10^{-2}$	$8.2 \times 10^{-3}$	$9.0 \times 10^{-4}$	$1.0 \times 10^{-1}$	$1.4 \times 10^{-1}$	$1 \times 10^{-8}$
	$K_D, M$	$4.3 \times 10^{-9}$	$3.9 \times 10^{-10}$	$1.7 \times 10^{-10}$	$5.8 \times 10^{-10}$	$5.0 \times 10^{-9}$	$4.5 \times 10^{-10}$
<b>VD11-25</b> (15)	$k_{a\_intr}, M^{-1}s^{-1}$	n/d	s/d	$4.5 \times 10^6$	$1.9 \times 10^7$	$3.4 \times 10^6$	$4.6 \times 10^5$
	$k_d, s^{-1}$	n/d	s/d	$1.8 \times 10^{-5}$	$6.4 \times 10^{-3}$	$1.1 \times 10^{-2}$	$3.8 \times 10^{-4}$
	$K_D, M$	n/d	s/d	$4.1 \times 10^{-12}$	$3.4 \times 10^{-10}$	$3.2 \times 10^{-9}$	$8.3 \times 10^{-10}$
<b>VD12-63</b> (16)	$k_{a\_intr}, M^{-1}s^{-1}$	s/d	$4.9 \times 10^7$	$1.1 \times 10^8$	$8.8 \times 10^8$	$3.6 \times 10^7$	$1.2 \times 10^7$
	$k_d, s^{-1}$	s/d	$9.3 \times 10^{-3}$	$7.1 \times 10^{-2}$	$1.5 \times 10^{-1}$	$4.1 \times 10^{-2}$	$1.1 \times 10^{-2}$
	$K_D, M$	s/d	$1.9 \times 10^{-10}$	$6.6 \times 10^{-10}$	$1.7 \times 10^{-10}$	$1.1 \times 10^{-9}$	$9.1 \times 10^{-10}$
<b>VD12-69-1</b> (17)	$k_{a\_intr}, M^{-1}s^{-1}$	$2.7 \times 10^6$	$2.6 \times 10^7$	$2.4 \times 10^6$	$2.0 \times 10^8$	n/d	$2.5 \times 10^6$
	$k_d, s^{-1}$	$6.6 \times 10^{-3}$	$2.6 \times 10^{-2}$	$1.4 \times 10^{-1}$	$2.6 \times 10^{-1}$	n/d	$2.2 \times 10^{-2}$
	$K_D, M$	$2.4 \times 10^{-9}$	$10 \times 10^{-10}$	$5.9 \times 10^{-8}$	$1.3 \times 10^{-9}$	n/d	$8.7 \times 10^{-9}$
<b>VD10-39b</b> (18)	$k_{a\_intr}, M^{-1}s^{-1}$	n/d	$2.2 \times 10^7$	n/d	n/d	n/d	$1.4 \times 10^7$
	$k_d, s^{-1}$	n/d	$4.9 \times 10^{-2}$	n/d	n/d	n/d	$1.2 \times 10^{-2}$
	$K_D, M$	n/d	$2.0 \times 10^{-9}$	n/d	n/d	n/d	$1.0 \times 10^{-9}$

n/d - no data, s/d - slow dissociation rate. The standard deviation did not exceed 1.4 fold of the value.

Figure 29 compares the intrinsic kinetic binding parameters of compounds with and without chlorine in *ortho* position of benzenesulfonamides. In Panel A, for compound **1**, the Cl *ortho*-substitution reduced the affinity towards most tested isoforms primarily due to slowing the association rate (CA VII, CA IX, and CA XII) but also for one isoform due to slower dissociation rate. Similar observations are shown in Panels B-D, for *ortho* Cl addition to compounds **3**, **6**, and **9**.

Compounds **3**, **4**, and **5** had higher  $k_d$  values compared to compounds **1** and **2**. The fastest interaction occurred for compound **3** and CA IX. This compound as-

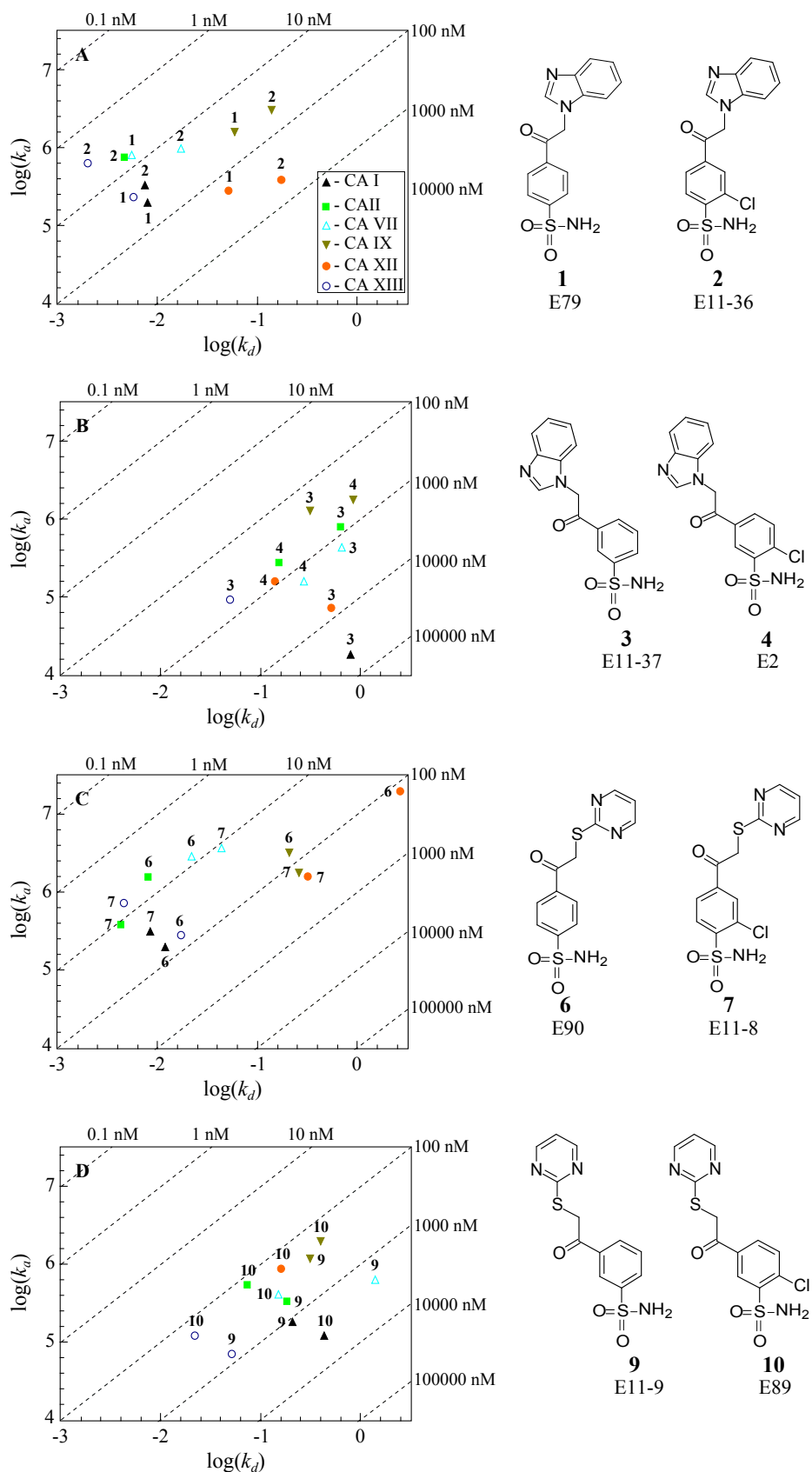
sociated rapidly with CA II and CA VII and dissociated fast from all studied CAs except CA XIII. Dissociation from CA XIII was the slowest of all 10 compounds, shown in Fig. 29, with several exceptions, *e.g.* compound **5** dissociation from CA XII. The fastest association ( $k_a$ ) and dissociation ( $k_d$ ) rates were determined for the interaction between compound **6** and CA XII. Its analogue bearing chlorine **7** had lower affinity. Compounds with (**10**) and without (**9**) *ortho*-chlorine are compared in Panel D, Figure 29. Compound **9** associated faster and dissociated slower from to CA IX compared to compound **10**. This tendency is illustrated in Panels A, B and C, Figure 29.

Figure 30 shows the intrinsic kinetic parameters of the fluorinated compounds. Compounds **11** and **16** are *para*-substituted benzenesulfonamides while the remaining compounds bear additional substitutions at *ortho* or *meta* positions that cause selectivities towards particular CA isoforms. Compound **17** does not possess any *para*-substitution and only an *ortho*-substitution. Figure 30 shows only the data where both the association and dissociation rates were accurately determined. The strongest binders with slow dissociation rates could not be determined and thus only some of them are shown in the shaded area of Figure 28, as explained above.

Addition of the octylamine *ortho*-substitution to compound **11** diminished both the association and dissociation rates thus not affecting the affinity towards CA IX. However, FTSA data indicated that **12** bound stronger than **11**. This slight inconsistency is likely due to different measurement approaches, SPR requiring immobilization while FTSA involves heating. Still, the overall tendencies are the same in both techniques. Addition of *meta*-substitution of octylamine to compound **11**, resulting in compound **13**, caused significantly slower dissociation from CA IX as shown in the grey area of Figure 28.

In conclusion, lower fractions of ready to interact components slow down the observed association rates. Calculated intrinsic parameters show that carbonic anhydrase – sulfonamide compound association can reach diffusion-limited rate.

10. Introduction of intrinsic kinetics of protein-ligand interactions and their implications for drug design



**Figure 26** Interaction kinetic plots based on observed association and dissociation rate constants for sulfonamides with CA I (black filled triangle), CA II (green filled square), CA VII (aqua open triangle), CA IX (olive filled down-pointing triangle), CA XII (orange filled circle), and CA XIII (navy open circle).

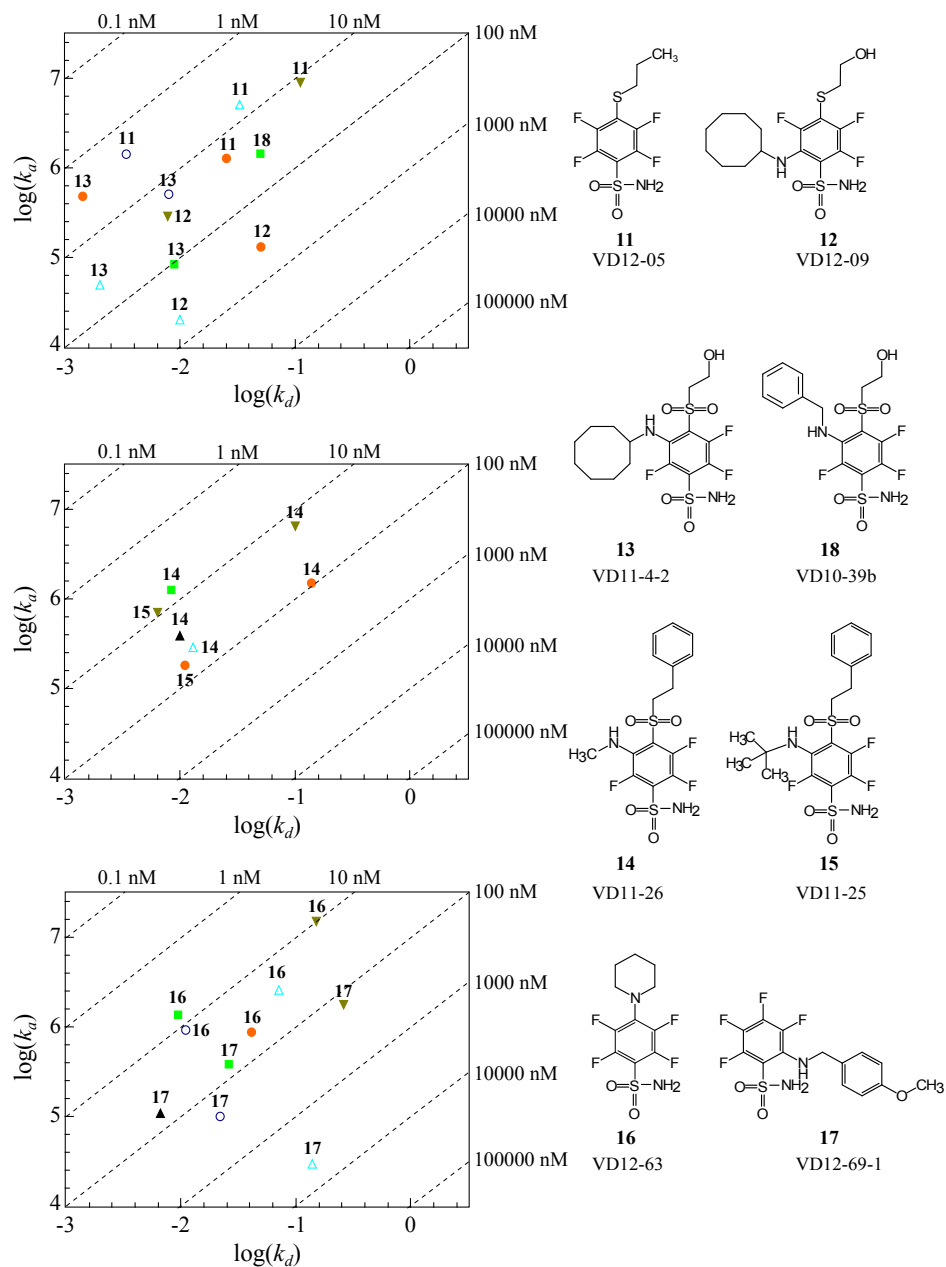


**Figure 27** Interaction kinetic plots based on observed association and dissociation rate constants for fluorinated benzenesulfonamides with CA I (black filled triangle), CA II (green filled square), CA VII (aqua open triangle), CA IX (olive filled down-pointing triangle), CA XII (orange filled circle), and CA XIII (navy open circle).



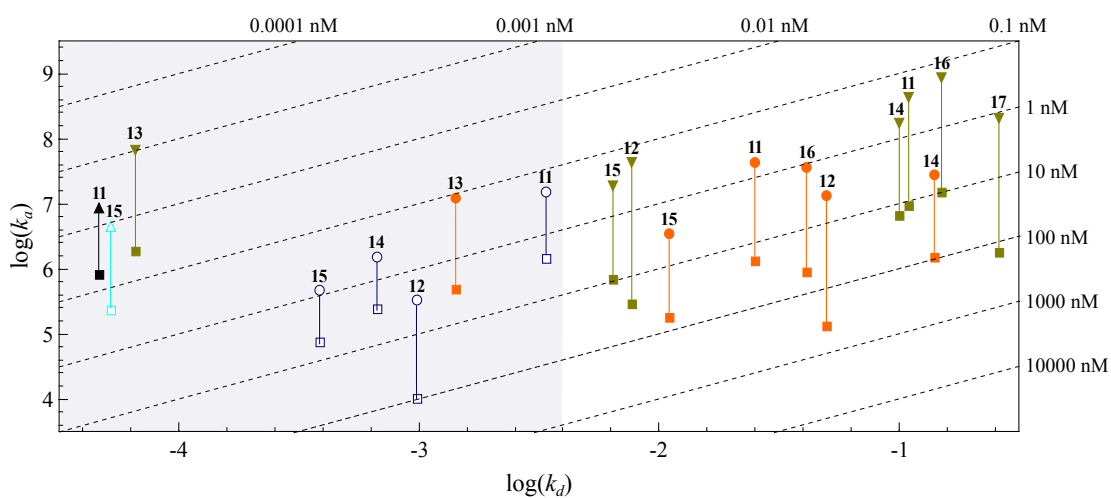


**Figure 28** Comparison of observed (bottom squares) and intrinsic (upper shapes) kinetic parameters for sulfonamides **11-17** interacting with CA IX (olive down-pointing triangle), CA XII (orange filled circles), CA I (black filled triangle), CA VII (aqua open triangle), and CA XIII (navy open circle). Intrinsic and observed values for a certain interaction are connected by vertical lines. Interaction rate constants which could be determined directly by SPR are located on the right hand half of the plot (unshaded), while rate constants determined approximately by SPR ( $k_a$ ) and the corresponding  $k_d$  values estimated by multiplying the  $k_a$ s by  $K_D$  determined by thermal shift are located on the left half of the plot (shaded).

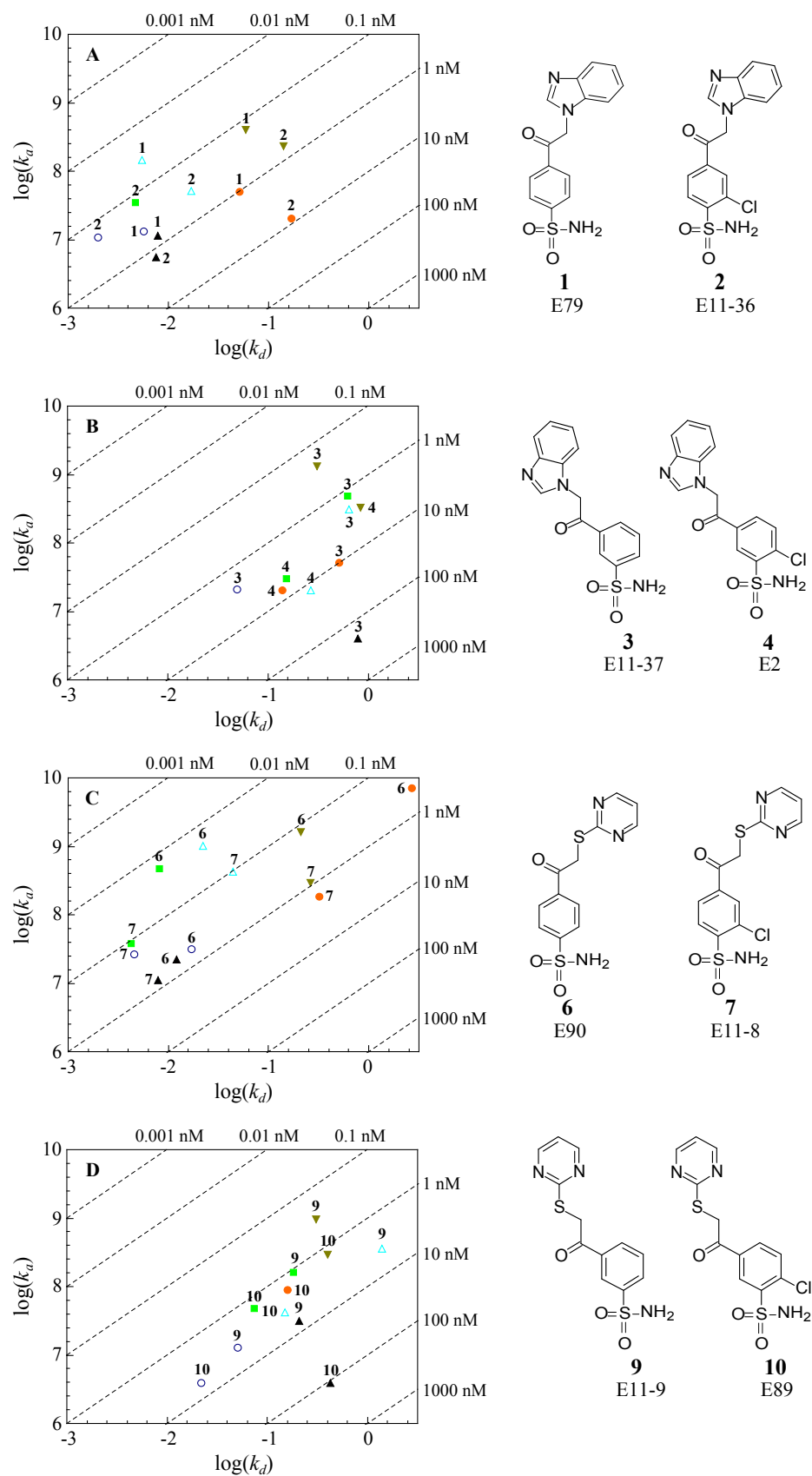


**Figure 29** Interaction kinetic plots based on intrinsic association and dissociation rate constants for *ortho*-substituted sulfonamides with CA I (black filled triangle), CA II (green filled square), CA VII (aqua open triangle), CA IX (olive filled down-pointing triangle), CA XII (orange filled circle), and CA XIII (navy open circle).

10. Introduction of intrinsic kinetics of protein-ligand interactions and their implications for drug design

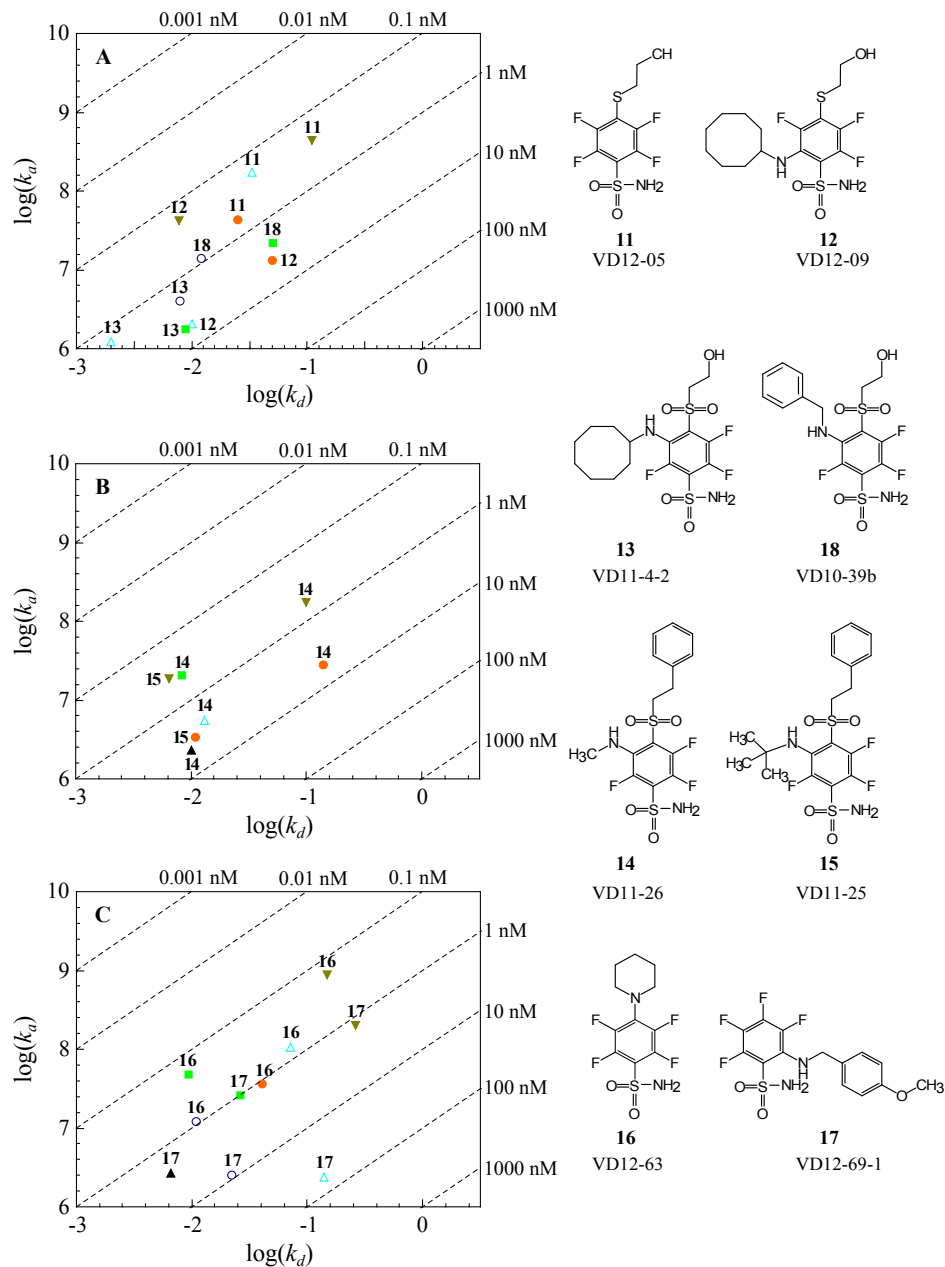


**Figure 30** Interaction kinetic plots based on intrinsic association and dissociation rate constants for fluorinated benzenesulfonamide compounds with CA I (black filled triangle), CA II (green filled square), CA VII (aqua open triangle), CA IX (olive filled down-pointing triangle), CA XII (orange filled circle), and CA XIII (navy open circle).



# Discussion

Structure-thermodynamic and structure-kinetic relationships provide valuable information for structure based drug design. However, the observed experimental parameters should not be directly translated into structure-activity relationship. The observed gain in inhibitor potency after chemical modification can be attributed to a change in  $pK_a$  value for ionizable group and corresponding change in observed affinity instead of an improvement in the interaction network [139].

To obtain the intrinsic parameters of sulfonamide binding to CAs, it is necessary to dissect contributions of three linked protonation reactions - deprotonation of sulfonamide, protonation of the active site zinc hydroxide and protonation-deprotonation of buffer. The calculated intrinsic thermodynamic and kinetic parameters were independent of the fractions of sulfonamide and CA in the active forms. To obtain them, a large series of FTSA, ITC, and SPR experiments were necessary to be performed at various pHs.

Here we determined the  $pK_a$ s of the hydroxide anion bound to the Zn(II) located in the active sites of CA I, CA IX, and CA XII and found it to be equal to 8.4, 6.8, and 7.0, respectively (at 25°C). The  $pK_a$  of zinc hydroxide protonation of CA I was assumed by other researchers to be the same as that of the CA I containing cobalt atom in the active site. The presence of cobalt enabled  $pK_a$  determination by spectral methods [141]. The Co(II) hydroxide protonation  $pK_a$  was equal to  $7.41 \pm 0.04$ . Therefore, an assumption that Co(II) and Zn(II) enzymes will have the same  $pK_a$  is not correct.

The  $pK_a$ s of the full length and the catalytic domain of the CA IX were previously determined to be 6.49 and 7.01, respectively [112]. Wingo et al. determined the  $pK_a$  equal to 6.3 [126]. Our obtained  $pK_a$  confirms previous determinations. The  $pK_a$  of CA XII nicely confirms previous determinations ( $pK_a$ s of 7.1 [127] and 6.9 [112]) as well.

It is clear that  $pK_a$  of CA I is similar to the  $pK_a$  of CA XIII, CA IX is similar to CA IV and CA XII is equal to CA VII (Table 1). However, there is no clear  $pK_a$  correlation with the enthalpy and entropy of Zn(II)-bound hydroxy anion protonation.

Thermodynamic dissection of contributing linked reactions should improve the design of CA inhibitors. This study of the intrinsic thermodynamics of sulfon-

amide inhibitor binding to CA isoforms enabled to determine the intrinsic binding parameters of other compounds. It will be possible to calculate the  $K_{d\_intr}$  and the  $\Delta_b G_{intr}$  of studied compounds binding to CA I, CA IX, and CA XII, only the  $pK_a$  of the newly-synthesized compound had to be determined experimentally. Furthermore, the observed enthalpies of binding ( $\Delta_b H_{obs}$ ) of the studied compounds were determined by ITC, therefore it will be possible to calculate the intrinsic enthalpy and entropy of the compound binding to CAs as well.

Taking this into account, observed and intrinsic thermodynamic parameters of 25 structurally related chlorinated benzenesulfonamides binding to CAs were obtained. Part of these compounds bearing one tail in *meta* position and others were *meta*- and *para*-substituted two-tailed compounds. All of them showed good binding properties to the target protein.

Small structural changes can highly influence thermodynamic parameters. Therefore, it is difficult to make the conclusions about binding properties of CA isozymes, because enthalpic and entropic contribution differ significantly even if binding affinities are similar. However, with some exceptions, two-tailed benzenesulfonamides show greater intrinsic binding to CAs than compounds bearing one tail in *meta* position (in **EA3-1** and **EA4-1** cases). These results oppose the data published by Tanpure et al. [142]. However, compounds used in the mentioned manuscript and in this study are completely different. Synthesis of compounds described in the manuscript are based on compound acetazolamide (**AZM**), while compounds used in this study are benzenesulfonamide derivatives. Moreover, only 9 compounds are described in publication. After comparison of 25 inhibitors in this study it is still difficult to make conclusions about binding based on compound structure. To achieve this goal, big databases of thermodynamic and kinetic binding parameters have to be analyzed.

Quantification of intrinsic interaction parameters, including  $\Delta_b H_{intr}$ ,  $\Delta_b S_{intr}$ ,  $K_{D\_intr}$ ,  $k_{a\_intr}$  and  $k_{d\_intr}$  provide a better link between the ligand structure and its activity towards the target. In addition, knowledge of the intrinsic parameters allows one to predict the desired activity of a compound in a certain environment and how it depends on pH or ionic strength.

It was possible to quantify intrinsic association rate constants using Equation 38. As expected, for a given interaction, the value of  $k_a^{intr}$  is significantly higher than the maximal observed  $k_a^{obs}$ . Comparison of the observed and intrinsic association rates shows that for this series of compounds, the difference may reach 1–4 orders of magnitude. If the structure-activity analysis of the interaction kinetics is performed by using the observed association rates, the error may be more than 1000-fold and the compounds may be ranked in a wrong order, assigning the observed gain of the interaction potency to wrong structural changes. Therefore, it is important to determine the intrinsic rates for any protein-ligand binding sys-

---

tem where binding-linked protonation events occur either for the protein or for the ligand.

Interestingly enough, sulfonamides are generally considered to be “slow” ligands, with second-order rate constants for the association below expected from a small molecule that encounter and interact within relatively huge active site cavity. This observed phenomenon is explained here by inconsistency between the total concentration of various ligand and protein forms and the real concentration of reactive species. Similar conclusions can be drawn for other families of proteins and ligands chemotypes.





# Conclusions

- The protonation  $pK_a$ s of the Zn(II)-bound hydroxide anion in the catalytic domain of human recombinant CA isoforms I, IX, and XII are equal to 8.4, 6.8, and 7.0, respectively, as determined by FTSA and ITC methods (25°C). The enthalpies of protonation of the hydroxide bound to the Zn(II) ion in the active site of CA I, CA IX and CA XII are equal to -41.0 kJ mol<sup>-1</sup>, -24.0 kJ mol<sup>-1</sup>, and -28.0 kJ mol<sup>-1</sup>, respectively.
- After the determination of the observed thermodynamic parameters of ligand binding to CAs, the subtraction of the pH and buffer effects by using the model of linked protonation reactions yielded the intrinsic binding enthalpies and Gibbs energies of sulfonamide binding.
- Application of the novel model that dissected the intrinsic kinetic parameters of sulfonamide inhibitor association-dissociation kinetics showed that the compounds behave as common ligands with diffusion-limited kinetics.



# Bibliography

- [1] Hopkins, A.L., Groom, C.R.: The druggable genome. *Nature Reviews Drug Discovery* **1**(9), 727–730 (2002). doi:10.1038/nrd892
- [2] Hodgson, T.H.: The Carbonic Anhydrase Content of Blood in Pathological States in Man. *British Journal of Experimental Pathology* **17**(1), 75–80 (1936)
- [3] Meldrum, N.U., Roughton, F.J.W.: Carbonic anhydrase. Its preparation and properties. *The Journal of Physiology* **80**(2), 113–142 (1933)
- [4] Alterio, V., Di Fiore, A., D’Ambrosio, K., Supuran, C.T., De Simone, G.: Multiple Binding Modes of Inhibitors to Carbonic Anhydrases: How to Design Specific Drugs Targeting 15 Different Isoforms? *Chemical Reviews* **112**(8), 4421–4468 (2012). doi:10.1021/cr200176r
- [5] Supuran, C.T., Fiore, A.D., Simone, G.D.: Carbonic anhydrase inhibitors as emerging drugs for the treatment of obesity. *Expert Opinion on Emerging Drugs* **13**(2), 383–392 (2008). doi:10.1517/14728214.13.2.383
- [6] Supuran, C.T.: How many carbonic anhydrase inhibition mechanisms exist? *Journal of Enzyme Inhibition and Medicinal Chemistry* **31**(3), 345–360 (2016). doi:10.3109/14756366.2015.1122001
- [7] *The Molecules of Life: Physical and Chemical Principles*. <https://www.crcpress.com/The-Molecules-of-Life-Physical-and-Chemical-Principles/Kuriyan-Konforti-Wemmer/p/book/9780815341888> (2012)
- [8] Krimmer, S.G., Klebe, G.: Thermodynamics of protein–ligand interactions as a reference for computational analysis: How to assess accuracy, reliability and relevance of experimental data. *Journal of Computer-Aided Molecular Design* **29**(9), 867–883 (2015). doi:10.1007/s10822-015-9867-y
- [9] Liu, Y., Sturtevant, J.M.: Significant discrepancies between van’t Hoff and calorimetric enthalpies. II. *Protein Science* **4**(12), 2559–2561 (1995). doi:10.1002/pro.5560041212
- [10] Naghibi, H., Tamura, A., Sturtevant, J.M.: Significant discrepancies between van’t Hoff and calorimetric enthalpies. *Proceedings of the National Academy of Sciences of the United States of America* **92**(12), 5597–5599 (1995)

- [11] Martin, S.F., Clements, J.H.: Correlating Structure and Energetics in Protein-Ligand Interactions: Paradigms and Paradoxes. *Annual Review of Biochemistry* **82**(1), 267–293 (2013). doi:10.1146/annurev-biochem-060410-105819
- [12] Jogaitė, V., Zubrienė, A., Michailovienė, V., Gylytė, J., Morkūnaitė, V., Matulis, D.: Characterization of human carbonic anhydrase XII stability and inhibitor binding. *Bioorganic & Medicinal Chemistry* **21**(6), 1431–1436 (2013). doi:10.1016/j.bmc.2012.10.016
- [13] Perozzo, R., Folkers, G., Scapozza, L.: Thermodynamics of Protein–Ligand Interactions: History, Presence, and Future Aspects. *Journal of Receptors and Signal Transduction* **24**(1-2), 1–52 (2004). doi:10.1081/RRS-120037896
- [14] Klebe, G.: Applying thermodynamic profiling in lead finding and optimization. *Nature Reviews Drug Discovery* **14**(2), 95–110 (2015). doi:10.1038/nrd4486
- [15] Baranauskienė, L., Matulis, D.: Intrinsic thermodynamics of ethoxzolamide inhibitor binding to human carbonic anhydrase XIII. *BMC Biophysics* **5**, 12 (2012). doi:10.1186/2046-1682-5-12
- [16] Kišonaitė, M., Zubrienė, A., Čapkauskaitė, E., Smirnov, A., Smirnovienė, J., Kairys, V., Michailovienė, V., Manakova, E., Gražulis, S., Matulis, D.: Intrinsic Thermodynamics and Structure Correlation of Benzenesulfonamides with a Pyrimidine Moiety Binding to Carbonic Anhydrases I, II, VII, XII, and XIII. *PLoS ONE* **9**(12) (2014). doi:10.1371/journal.pone.0114106
- [17] Pilipuitytė, V., Matulis, D.: Intrinsic thermodynamics of trifluoromethanesulfonamide and ethoxzolamide binding to human carbonic anhydrase VII. *Journal of Molecular Recognition* **28**(3), 166–172 (2015). doi:10.1002/jmr.2404
- [18] Kazokaitė, J., Milinavičiūtė, G., Smirnovienė, J., Matulienė, J., Matulis, D.: Intrinsic binding of 4-substituted-2,3,5,6-tetrafluorobenzenesulfonamides to native and recombinant human carbonic anhydrase VI. *FEBS Journal* **282**(5), 972–983 (2015). doi:10.1111/febs.13196
- [19] Copeland, R.A., Pompliano, D.L., Meek, T.D.: Drug–target residence time and its implications for lead optimization. *Nature Reviews Drug Discovery* **5**(9), 730–739 (2006). doi:10.1038/nrd2082
- [20] Holdgate, G.A., Anderson, M., Edfeldt, F., Geschwindner, S.: Affinity-based, biophysical methods to detect and analyze ligand binding to recombinant proteins: Matching high information content with high throughput. *Journal of Structural Biology* **172**(1), 142–157 (2010). doi:10.1016/j.jsb.2010.06.024
- [21] Renaud, J.-P., Chung, C.-w., Danielson, U.H., Egner, U., Hennig, M., Hubbard, R.E., Nar, H.: Biophysics in drug discovery: Impact, challenges and opportunities. *Nature Reviews Drug Discovery* **15**(10), 679–698 (2016). doi:10.1038/nrd.2016.123

- [22] Matulis, D., Kranz, J.K., Salemme, F.R., Todd, M.J.: Thermodynamic Stability of Carbonic Anhydrase: Measurements of Binding Affinity and Stoichiometry Using ThermoFluor. *Biochemistry* **44**(13), 5258–5266 (2005). doi:10.1021/bi048135v
- [23] Pantoliano, M.W., Petrella, E.C., Kwasnoski, J.D., Lobanov, V.S., Myslik, J., Graf, E., Carver, T., Asel, E., Springer, B.A., Lane, P., Salemme, F.R.: High-Density Miniaturized Thermal Shift Assays as a General Strategy for Drug Discovery. *Journal of Biomolecular Screening* **6**(6), 429–440 (2001). doi:10.1177/108705710100600609
- [24] Kranz, J.K., Schalk-Hihi, C.: Chapter eleven - Protein Thermal Shifts to Identify Low Molecular Weight Fragments. In: Kuo, L.C. (ed.) *Methods in Enzymology. Fragment-Based Drug Design Tools, Practical Approaches, and Examples*, vol. 493, pp. 277–298. Academic Press, ??? (2011). doi:10.1016/B978-0-12-381274-2.00011-X
- [25] Cimperman, P., Baranauskienė, L., Jachimovičiūtė, S., Jachno, J., Torressan, J., Michailovienė, V., Matulienė, J., Sereikaitė, J., Bumelis, V., Matulis, D.: A Quantitative Model of Thermal Stabilization and Destabilization of Proteins by Ligands. *Biophysical Journal* **95**(7), 3222–3231 (2008). doi:10.1529/biophysj.108.134973
- [26] Freyer, M.W., Lewis, E.A.: Isothermal Titration Calorimetry: Experimental Design, Data Analysis, and Probing Macromolecule/Ligand Binding and Kinetic Interactions. *Biophysical Tools for Biologists, Volume One: In Vitro Techniques*, vol. 84, pp. 79–113. Academic Press (2008). doi:10.1016/S0091-679X(07)84004-0
- [27] Damian, L.: Isothermal Titration Calorimetry for Studying Protein–Ligand Interactions. In: Williams, M.A., Daviter, T. (eds.) *Protein-Ligand Interactions. Methods in Molecular Biology*, pp. 103–118. Humana Press, ??? (2013)
- [28] Ladbury, J.E.: Counting the calories to stay in the groove. *Structure* **3**(7), 635–639 (1995). doi:10.1016/S0969-2126(01)00197-6
- [29] Brautigam, C.A., Zhao, H., Vargas, C., Keller, S., Schuck, P.: Integration and global analysis of isothermal titration calorimetry data for studying macromolecular interactions. *Nature Protocols* **11**(5), 882–894 (2016). doi:10.1038/nprot.2016.044
- [30] Tellinghuisen, J.: Isothermal titration calorimetry at very low c. *Analytical Biochemistry* **373**(2), 395–397 (2008). doi:10.1016/j.ab.2007.08.039
- [31] Linkuvienė, V., Krainer, G., Chen, W.-Y., Matulis, D.: Isothermal titration calorimetry for drug design: Precision of the enthalpy and binding constant measurements and comparison of the instruments. *Analytical Biochemistry* **515**, 61–64 (2016). doi:10.1016/j.ab.2016.10.005

- [32] Mueller, W.H., Francis: Biomolecular Interaction Analysis in Drug Discovery Using Surface Plasmon Resonance Technology. <http://www.eurekaselect.com/58060/article>
- [33] Cooper, M.A.: Optical biosensors in drug discovery. *Nature Reviews Drug Discovery* **1**(7), 515–528 (2002). doi:10.1038/nrd838
- [34] Kemp, M.M., Weïwer, M., Koehler, A.N.: Unbiased binding assays for discovering small-molecule probes and drugs. *Bioorganic & Medicinal Chemistry* **20**(6), 1979–1989 (2012). doi:10.1016/j.bmc.2011.11.071
- [35] Myszka, D.G., Rich, R.L.: Implementing surface plasmon resonance biosensors in drug discovery. *Pharmaceutical Science & Technology Today* **3**(9), 310–317 (2000). doi:10.1016/S1461-5347(00)00288-1
- [36] Klebe, G.: *Drug Design: Methodology, Concepts, and Mode-of-Action*. Springer Publishing Company, Incorporated, ??? (2013)
- [37] Oprea, T.I., Davis, A.M., Teague, S.J., Leeson, P.D.: Is There a Difference between Leads and Drugs? A Historical Perspective. *Journal of Chemical Information and Computer Sciences* **41**(5), 1308–1315 (2001). doi:10.1021/ci010366a
- [38] Chung, T.D.Y., Terry, D.B., Smith, L.H.: In Vitro and In Vivo Assessment of ADME and PK Properties During Lead Selection and Lead Optimization – Guidelines, Benchmarks and Rules of Thumb. In: Sittampalam, G.S., Coussens, N.P., Brimacombe, K., Grossman, A., Arkin, M., Auld, D., Austin, C., Baell, J., Bejcek, B., Chung, T.D.Y., Dahlin, J.L., Devanaryan, V., Foley, T.L., Glicksman, M., Hall, M.D., Hass, J.V., Inglese, J., Iversen, P.W., Kahl, S.D., Lal-Nag, M., Li, Z., McGee, J., McManus, O., Riss, T., Trask, O.J., Weidner, J.R., Xia, M., Xu, X. (eds.) *Assay Guidance Manual*. Eli Lilly & Company and the National Center for Advancing Translational Sciences, Bethesda (MD) (2004)
- [39] Kawasaki, Y., Freire, E.: Finding a better path to drug selectivity. *Drug Discovery Today* **16**(21–22), 985–990 (2011). doi:10.1016/j.drudis.2011.07.010
- [40] Biela, A., Sielaff, F., Terwesten, F., Heine, A., Steinmetzer, T., Klebe, G.: Ligand Binding Stepwise Disrupts Water Network in Thrombin: Enthalpic and Entropic Changes Reveal Classical Hydrophobic Effect. *Journal of Medicinal Chemistry* **55**(13), 6094–6110 (2012). doi:10.1021/jm300337q
- [41] Bingham, R.J., Findlay, J.B.C., Hsieh, S.-Y., Kalverda, A.P., Kjellberg, A., Perazzolo, C., Phillips, S.E.V., Seshadri, K., Trinh, C.H., Turnbull, W.B., Bodenhausen, G., Homans, S.W.: Thermodynamics of Binding of 2-Methoxy-3-isopropylpyrazine and 2-Methoxy-3-isobutylpyrazine to the Major Urinary Protein. *Journal of the American Chemical Society* **126**(6), 1675–1681 (2004). doi:10.1021/ja038461i
- [42] Englert, L., Biela, A., Zayed, M., Heine, A., Hangauer, D., Klebe, G.: Displacement of disordered water molecules from hydrophobic pocket creates

- enthalpic signature: Binding of phosphoramidate to the S1'-pocket of thermolysin. *Biochimica et Biophysica Acta (BBA) - General Subjects* **1800**(11), 1192–1202 (2010). doi:10.1016/j.bbagen.2010.06.009
- [43] Snyder, P.W., Mecinović, J., Moustakas, D.T., Thomas, S.W., Harder, M., Mack, E.T., Lockett, M.R., Héroux, A., Sherman, W., Whitesides, G.M.: Mechanism of the hydrophobic effect in the biomolecular recognition of aryl-sulfonamides by carbonic anhydrase. *Proceedings of the National Academy of Sciences* **108**(44), 17889–17894 (2011). doi:10.1073/pnas.1114107108
- [44] Mecinović, J., Snyder, P.W., Mirica, K.A., Bai, S., Mack, E.T., Kwant, R.L., Moustakas, D.T., Héroux, A., Whitesides, G.M.: Fluoroalkyl and Alkyl Chains Have Similar Hydrophobicities in Binding to the “Hydrophobic Wall” of Carbonic Anhydrase. *Journal of the American Chemical Society* **133**(35), 14017–14026 (2011). doi:10.1021/ja2045293
- [45] Winkvist, J., Geschwindner, S., Xue, Y., Gustavsson, L., Musil, D., Deinum, J., Danielson, U.H.: Identification of Structural–Kinetic and Structural–Thermodynamic Relationships for Thrombin Inhibitors. *Biochemistry* **52**(4), 613–626 (2013). doi:10.1021/bi301333z
- [46] Chang, A., Schiebel, J., Yu, W., Bommineni, G.R., Pan, P., Baxter, M.V., Khanna, A., Sotriffer, C.A., Kisker, C., Tonge, P.J.: Rational optimization of drug-target residence time: Insights from inhibitor binding to the *Staphylococcus aureus* FabI enzyme-product complex. *Biochemistry* **52**(24), 4217–4228 (2013). doi:10.1021/bi400413c
- [47] C. Miller, D., Lunn, G., Jones, P., Sabnis, Y., L. Davies, N., Driscoll, P.: Investigation of the effect of molecular properties on the binding kinetics of a ligand to its biological target. *MedChemComm* **3**(4), 449–452 (2012). doi:10.1039/C2MD00270A
- [48] Lehtonen, J., Shen, B., Vihinen, M., Casini, A., Scozzafava, A., Supuran, C.T., Parkkila, A.-K., Saarnio, J., Kivelä, A.J., Waheed, A., Sly, W.S., Parkkila, S.: Characterization of CA XIII, a novel member of the carbonic anhydrase isozyme family. *The Journal of Biological Chemistry* **279**(4), 2719–2727 (2004). doi:10.1074/jbc.M308984200
- [49] Duda, D.M., Yoshioka, C., Govindasamy, L., An, H., Tu, C., Silverman, D.N., McKenna, R.: Crystallization and preliminary X-ray analysis of human carbonic anhydrase III. *Acta Crystallographica. Section D, Biological Crystallography* **58**(Pt 5), 849–852 (2002)
- [50] Di Fiore, A., Monti, S.M., Hilvo, M., Parkkila, S., Romano, V., Scaloni, A., Pedone, C., Scozzafava, A., Supuran, C.T., De Simone, G.: Crystal structure of human carbonic anhydrase XIII and its complex with the inhibitor acetazolamide. *Proteins* **74**(1), 164–175 (2009). doi:10.1002/prot.22144
- [51] Stams, T., Nair, S.K., Okuyama, T., Waheed, A., Sly, W.S., Christianson, D.W.: Crystal structure of the secretory form of membrane-associated human carbonic anhydrase IV at 2.8-Å resolution. *Proceedings of the National*

- Academy of Sciences of the United States of America **93**(24), 13589–13594 (1996)
- [52] Pilka, E.S., Kochan, G., Oppermann, U., Yue, W.W.: Crystal structure of the secretory isozyme of mammalian carbonic anhydrases CA VI: Implications for biological assembly and inhibitor development. *Biochemical and Biophysical Research Communications* **419**(3), 485–489 (2012). doi:10.1016/j.bbrc.2012.02.038
- [53] Alterio, V., Hilvo, M., Di Fiore, A., Supuran, C.T., Pan, P., Parkkila, S., Scaloni, A., Pastorek, J., Pastorekova, S., Pedone, C., Scozzafava, A., Monti, S.M., De Simone, G.: Crystal structure of the catalytic domain of the tumor-associated human carbonic anhydrase IX. *Proceedings of the National Academy of Sciences of the United States of America* **106**(38), 16233–16238 (2009). doi:10.1073/pnas.0908301106
- [54] Whittington, D.A., Waheed, A., Ulmasov, B., Shah, G.N., Grubb, J.H., Sly, W.S., Christianson, D.W.: Crystal structure of the dimeric extracellular domain of human carbonic anhydrase XII, a bitopic membrane protein overexpressed in certain cancer tumor cells. *Proceedings of the National Academy of Sciences of the United States of America* **98**(17), 9545–9550 (2001). doi:10.1073/pnas.161301298
- [55] Aggarwal, M., Boone, C.D., Kondeti, B., McKenna, R.: Structural annotation of human carbonic anhydrases. *Journal of Enzyme Inhibition and Medicinal Chemistry* **28**(2), 267–277 (2013). doi:10.3109/14756366.2012.737323
- [56] Imtaiyaz Hassan, M., Shajee, B., Waheed, A., Ahmad, F., Sly, W.S.: Structure, function and applications of carbonic anhydrase isozymes. *Bioorganic & Medicinal Chemistry* **21**(6), 1570–1582 (2013). doi:10.1016/j.bmc.2012.04.044
- [57] Supuran, C.T.: Structure and function of carbonic anhydrases. *Biochemical Journal* **473**(14), 2023–2032 (2016). doi:10.1042/BCJ20160115
- [58] Domsic, J.F., Avvaru, B.S., Kim, C.U., Gruner, S.M., Agbandje-McKenna, M., Silverman, D.N., McKenna, R.: Entrapment of Carbon Dioxide in the Active Site of Carbonic Anhydrase II. *The Journal of Biological Chemistry* **283**(45), 30766–30771 (2008). doi:10.1074/jbc.M805353200
- [59] Maupin, C.M., Saunders, M.G., Thorpe, I.F., McKenna, R., Silverman, D.N., Voth, G.A.: Origins of Enhanced Proton Transport in the Y7F Mutant of Human Carbonic Anhydrase II. *Journal of the American Chemical Society* **130**(34), 11399–11408 (2008). doi:10.1021/ja802264j
- [60] Khalifah, R.G.: The Carbon Dioxide Hydration Activity of Carbonic Anhydrase I. STOP-FLOW KINETIC STUDIES ON THE NATIVE HUMAN ISOENZYMES B AND C. *Journal of Biological Chemistry* **246**(8), 2561–2573 (1971)



- [61] Purkerson, J.M., Schwartz, G.J.: The role of carbonic anhydrases in renal physiology. *Kidney International* **71**(2), 103–115 (2007). doi:10.1038/sj.ki.5002020
- [62] Zahedi, K., Barone, S., Xu, J., Soleimani, M.: Potentiation of the effect of thiazide derivatives by carbonic anhydrase inhibitors: Molecular mechanisms and potential clinical implications. *PloS One* **8**(11), 79327 (2013). doi:10.1371/journal.pone.0079327
- [63] Husain, A., Madhesia, D., Rashid, M., Ahmad, A., Khan, S.A.: Synthesis and in vivo diuretic activity of some new benzothiazole sulfonamides containing quinoxaline ring system. *Journal of Enzyme Inhibition and Medicinal Chemistry* **31**(6), 1682–1689 (2016). doi:10.3109/14756366.2015.1128425
- [64] Sterling, D., Reithmeier, R.A.F., Casey, J.R.: A transport metabolon: Functional interaction of carbonic anhydrase II and chloride/bicarbonate exchangers. *Journal of Biological Chemistry* (2001). doi:10.1074/jbc.M105959200
- [65] Brechue, W.F., Kinne-Saffran, E., Kinne, R.K., Maren, T.H.: Localization and activity of renal carbonic anhydrase (CA) in CA-II deficient mice. *Biochimica Et Biophysica Acta* **1066**(2), 201–207 (1991)
- [66] Sly, W.S., Whyte, M.P., Krupin, T., Sundaram, V.: Positive Renal Response to Intravenous Acetazolamide in Patients with Carbonic Anhydrase II Deficiency. *Pediatric Research* **19**(10), 1033–1036 (1985). doi:10.1203/00006450-198510000-00017
- [67] Liao, S., Ivanov, S., Ivanova, A., Ghosh, S., Cote, M., Keefe, K., Coca-Prados, M., Stanbridge, E., Lerman, M.: Expression of cell surface transmembrane carbonic anhydrase genes CA9 and CA12 in the human eye: Overexpression of CA12 (CAXII) in glaucoma. *Journal of Medical Genetics* **40**(4), 257–261 (2003). doi:10.1136/jmg.40.4.257
- [68] Malikowski, T.M., Bosch, J.B., Min, S., Duffey, M.E., Patel, S.P.: Carbonic Anhydrase Inhibitors in Corneal Endothelial TransportCAIs in Corneal Endothelial Transport. *Investigative Ophthalmology & Visual Science* **55**(4), 2652–2658 (2014). doi:10.1167/iovs.13-13534
- [69] Yang, Z., Alvarez, B.V., Chakarova, C., Jiang, L., Karan, G., Frederick, J.M., Zhao, Y., Sauvé, Y., Li, X., Zrenner, E., Wissinger, B., Hollander, A.I.D., Katz, B., Baehr, W., Cremers, F.P., Casey, J.R., Bhattacharya, S.S., Zhang, K.: Mutant carbonic anhydrase 4 impairs pH regulation and causes retinal photoreceptor degeneration. *Human Molecular Genetics* **14**(2), 255–265 (2005). doi:10.1093/hmg/ddi023
- [70] Carta, F., Supuran, C.T., Scozzafava, A.: Novel therapies for glaucoma: A patent review 2007 – 2011. *Expert Opinion on Therapeutic Patents* **22**(1), 79–88 (2012). doi:10.1517/13543776.2012.649006

- [71] Masini, E., Carta, F., Scozzafava, A., Supuran, C.T.: Antiglaucoma carbonic anhydrase inhibitors: A patent review. *Expert Opinion on Therapeutic Patents* **23**(6), 705–716 (2013). doi:10.1517/13543776.2013.794788
- [72] Sugrue, M.F.: Pharmacological and ocular hypotensive properties of topical carbonic anhydrase inhibitors. *Progress in Retinal and Eye Research* **19**(1), 87–112 (2000). doi:10.1016/S1350-9462(99)00006-3
- [73] Gupta, S.K., Niranjana D., G., Agrawal, S.S., Srivastava, S., Saxena, R.: Recent advances in pharmacotherapy of glaucoma. *Indian Journal of Pharmacology* **40**(5), 197–208 (2008). doi:10.4103/0253-7613.44151
- [74] Wolfensberger, T.J., Mahieu, I., Jarvis-Evans, J., Boulton, M., Carter, N.D., N6gr6di, A., Hollande, E., Bird, A.C.: Membrane-bound carbonic anhydrase in human retinal pigment epithelium. *Investigative Ophthalmology & Visual Science* **35**(9), 3401–3407 (1994)
- [75] Asahi, M.G., Dogaru, G.L.B., Onishi, S.M., Gallemore, R.P.: Strong Topical Steroid, NSAID, and Carbonic Anhydrase Inhibitor Cocktail for Treatment of Cystoid Macular Edema. <https://www.dovepress.com/strong-topical-steroid-nsaid-and-carbonic-anhydrase-inhibitor-cocktail%0020-peer-reviewed-article-IMCRJ> (2015)
- [76] Strong, S., Liew, G., Michaelides, M.: Retinitis pigmentosa-associated cystoid macular oedema: Pathogenesis and avenues of intervention. *British Journal of Ophthalmology* **101**(1), 31–37 (2017). doi:10.1136/bjophthalmol-2016-309376
- [77] Liew, G., Moore, A.T., Webster, A.R., Michaelides, M.: Efficacy and Prognostic Factors of Response to Carbonic Anhydrase Inhibitors in Management of Cystoid Macular Edema in Retinitis Pigmentosa. *Investigative Ophthalmology & Visual Science* **56**(3), 1531–1536 (2015). doi:10.1167/iovs.14-15995
- [78] Cannon, C.P., Kumar, A.: Treatment of overweight and obesity: Lifestyle, pharmacologic, and surgical options. *Clinical Cornerstone* **9**(4), 55–71 (2009). doi:10.1016/S1098-3597(09)80005-7
- [79] Bray, G.A., Tartaglia, L.A.: Medicinal strategies in the treatment of obesity. *Nature* **404**(6778), 672–677 (2000). doi:10.1038/35007544
- [80] Supuran, C.T.: Carbonic anhydrase inhibitors as emerging drugs for the treatment of obesity. *Expert Opinion on Emerging Drugs* **17**(1), 11–15 (2012). doi:10.1517/14728214.2012.664132
- [81] Swenson, E.R.: Pharmacology of acute mountain sickness: Old drugs and newer thinking. *Journal of Applied Physiology* **120**(2), 204–215 (2016). doi:10.1152/jappphysiol.00443.2015
- [82] Wang, T., Eskandari, D., Zou, D., Grote, L., Hedner, J.: Increased Carbonic Anhydrase Activity is Associated with Sleep Apnea Severity and Related Hypoxemia. *Sleep* **38**(7), 1067–1073 (2015). doi:10.5665/sleep.4814

- [83] Liu, X., Lu, D., Bowser, R., Liu, J.: Expression of Carbonic Anhydrase I in Motor Neurons and Alterations in ALS. *International Journal of Molecular Sciences* **17**(11), 1820 (2016). doi:10.3390/ijms17111820
- [84] Mannelli, L.D.C., Micheli, L., Carta, F., Cozzi, A., Ghelardini, C., Supuran, C.T.: Carbonic anhydrase inhibition for the management of cerebral ischemia: In vivo evaluation of sulfonamide and coumarin inhibitors. *Journal of Enzyme Inhibition and Medicinal Chemistry* **31**(6), 894–899 (2016). doi:10.3109/14756366.2015.1113407
- [85] Jang, B.G., Yun, S.-M., Ahn, K., Song, J.H., Jo, S.A., Kim, Y.-Y., Kim, D.K., Park, M.H., Han, C., Koh, Y.H.: Plasma Carbonic Anhydrase II protein is Elevated in Alzheimer’s Disease. *Journal of Alzheimer’s Disease* **21**(3), 939–945 (2010). doi:10.3233/JAD-2010-100384
- [86] Aggarwal, M., Kondeti, B., McKenna, R.: Anticonvulsant/antiepileptic carbonic anhydrase inhibitors: A patent review. *Expert Opinion on Therapeutic Patents* **23**(6), 717–724 (2013). doi:10.1517/13543776.2013.782394
- [87] Chiche, J., Ilc, K., Brahimi-Horn, M.C., Pouyssegur, J.: Membrane-bound carbonic anhydrases are key pH regulators controlling tumor growth and cell migration. *Advances in Enzyme Regulation* **50**(1), 20–33 (2010). doi:10.1016/j.advenzreg.2009.10.005
- [88] Granja, S., Tavares-Valente, D., Queirós, O., Baltazar, F.: Value of pH regulators in the diagnosis, prognosis and treatment of cancer. *Seminars in Cancer Biology*. doi:10.1016/j.semcancer.2016.12.003
- [89] Waheed, A., Sly, W.S.: Carbonic anhydrase XII functions in health and disease. *Gene* **623**, 33–40 (2017). doi:10.1016/j.gene.2017.04.027
- [90] Parks, S.K., Cormerais, Y., Pouyssegur, J.: Hypoxia and cellular metabolism in tumour pathophysiology. *The Journal of Physiology* **595**(8), 2439–2450 (2017). doi:10.1113/JP273309
- [91] Parks, S.K., Chiche, J., Pouyssegur, J.: Disrupting proton dynamics and energy metabolism for cancer therapy. *Nature Reviews Cancer* **13**(9), 611–623 (2013). doi:10.1038/nrc3579
- [92] Vaupel, P., Harrison, L.: Tumor Hypoxia: Causative Factors, Compensatory Mechanisms, and Cellular Response. *The Oncologist* **9**(Supplement 5), 4–9 (2004). doi:10.1634/theoncologist.9-90005-4
- [93] Swietach, P., Vaughan-Jones, R.D., Harris, A.L., Hulikova, A.: The chemistry, physiology and pathology of pH in cancer. *Phil. Trans. R. Soc. B* **369**(1638), 20130099 (2014). doi:10.1098/rstb.2013.0099
- [94] Mokhtari, R.B., Homayouni, T.S., Baluch, N., Morgatskaya, E., Kumar, S., Das, B., Yeger, H., Mokhtari, R.B., Homayouni, T.S., Baluch, N., Morgatskaya, E., Kumar, S., Das, B., Yeger, H.: Combination therapy in combating cancer. *Oncotarget* **5**(0) (2017). doi:10.18632/oncotarget.16723

- [95] Neri, D., Supuran, C.T.: Interfering with pH regulation in tumours as a therapeutic strategy. *Nature Reviews Drug Discovery* **10**(10), 767–777 (2011). doi:10.1038/nrd3554
- [96] Parks, S.K., Pouysségur, J.: Targeting pH regulating proteins for cancer therapy—Progress and limitations. *Seminars in Cancer Biology*. doi:10.1016/j.semcancer.2017.01.007
- [97] Janoniene, A., Liu, Z., Baranauskiene, L., Mäkilä, E., Ma, M., Salonen, J., Hirvonen, J., Zhang, H., Petrikaite, V., Santos, H.A.: A Versatile Carbonic Anhydrase IX Targeting Ligand-Functionalized Porous Silicon Nanoplat-form for Dual Hypoxia Cancer Therapy and Imaging. *ACS Applied Materials & Interfaces* **9**(16), 13976–13987 (2017). doi:10.1021/acsami.7b04038
- [98] Kazokaitė, J., Ames, S., Becker, H.M., Deitmer, J.W., Matulis, D.: Selective inhibition of human carbonic anhydrase IX in *Xenopus* oocytes and MDA-MB-231 breast cancer cells. *Journal of Enzyme Inhibition and Medicinal Chemistry* **31**(sup4), 38–44 (2016). doi:10.1080/14756366.2016.1217854
- [99] Ward, C., Meehan, J., Mullen, P., Supuran, C., Dixon, J.M., Thomas, J.S., Winum, J.-Y., Lambin, P., Dubois, L., Pavathaneni, N.-K., Jarman, E.J., Renshaw, L., Um, I., Kay, C., Harrison, D.J., Kunkler, I.H., Langdon, S.P., Ward, C., Meehan, J., Mullen, P., Supuran, C., Dixon, J.M., Thomas, J.S., Winum, J.-Y., Lambin, P., Dubois, L., Pavathaneni, N.-K., Jarman, E.J., Renshaw, L., Um, I., Kay, C., Harrison, D.J., Kunkler, I.H., Langdon, S.P.: Evaluation of carbonic anhydrase IX as a therapeutic target for inhibition of breast cancer invasion and metastasis using a series of in vitro breast cancer models. *Oncotarget* **6**(28), 24856–24870 (2015). doi:10.18632/oncotarget.4498
- [100] Supuran, C.T.: Drug interaction considerations in the therapeutic use of carbonic anhydrase inhibitors. *Expert Opinion on Drug Metabolism & Toxicology* **12**(4), 423–431 (2016). doi:10.1517/17425255.2016.1154534
- [101] Fisher, S.Z., Aggarwal, M., Kovalevsky, A.Y., Silverman, D.N., McKenna, R.: Neutron Diffraction of Acetazolamide-Bound Human Carbonic Anhydrase II Reveals Atomic Details of Drug Binding. *Journal of the American Chemical Society* **134**(36), 14726–14729 (2012). doi:10.1021/ja3068098
- [102] King, R.W., Burgen, A.S.V., S, F.R.: Kinetic aspects of structure-activity relations: The binding of sulphonamides by carbonic anhydrase. *Proc. R. Soc. Lond. B* **193**(1111), 107–125 (1976). doi:10.1098/rspb.1976.0034
- [103] Taylor, P.W., King, R.W., Burgen, A.S.V.: Kinetics of complex formation between human carbonic anhydrases and aromatic sulfonamides. *Biochemistry* **9**(13), 2638–2645 (1970). doi:10.1021/bi00815a012
- [104] Gaspari, R., Rechlin, C., Heine, A., Bottegoni, G., Rocchia, W., Schwarz, D., Bomke, J., Gerber, H.-D., Klebe, G., Cavalli, A.: Kinetic and Structural Insights into the Mechanism of Binding of Sulfonamides to Human Carbonic Anhydrase by Computational and Experimental Studies. *Journal of Medicinal Chemistry* **59**(9), 4245–4256 (2016). doi:10.1021/acs.jmedchem.5b01643

- [105] Miller, W.H., Dessert, A.M., Roblin, R.O.: Heterocyclic Sulfonamides as Carbonic Anhydrase Inhibitors. *Journal of the American Chemical Society* **72**(11), 4893–4896 (1950). doi:10.1021/ja01167a012
- [106] Taylor, P.W., Burgen, A.S.V.: Kinetics of carbonic anhydrase-inhibitor complex formation. Comparison of anion- and sulfonamide-binding mechanisms. *Biochemistry* **10**(21), 3859–3866 (1971). doi:10.1021/bi00797a010
- [107] Liang, Z., Xue, Y., Behravan, G., Jonsson, B.-H., Lindskog, S.: Importance of the conserved active-site residues Try7, Glu106 and Thr199 for the catalytic function of human carbonic anhydrase II. *European Journal of Biochemistry* **211**(3), 821–827 (1993). doi:10.1111/j.1432-1033.1993.tb17614.x
- [108] Kiefer, L.L., Fierke, C.A.: Functional Characterization of Human Carbonic Anhydrase II Variants with Altered Zinc Binding Sites. *Biochemistry* **33**(51), 15233–15240 (1994). doi:10.1021/bi00255a003
- [109] Krishnamurthy, V.M., Kaufman, G.K., Urbach, A.R., Gitlin, I., Gudiksen, K.L., Weibel, D.B., Whitesides, G.M.: Carbonic Anhydrase as a Model for Biophysical and Physical-Organic Studies of Proteins and Protein-Ligand Binding. *Chemical Reviews* **108**(3), 946–1051 (2008). doi:10.1021/cr050262p
- [110] Matulis, D., Todd, M.: Thermodynamics–Structure Correlations of Sulfonamide Inhibitor Binding to Carbonic Anhydrase. In: Ladbury, J.E., Doyle, M.L. (eds.) *Biocalorimetry 2*, pp. 107–132. John Wiley & Sons, Ltd, ??? (2004). doi:10.1002/0470011122.ch6
- [111] Coleman, J.E.: Mechanism of Action of Carbonic Anhydrase SUBSTRATE, SULFONAMIDE, AND ANION BINDING. *Journal of Biological Chemistry* **242**(22), 5212–5219 (1967)
- [112] Innocenti, A., Pastorekova, S., Pastorek, J., Scozzafava, A., Simone, G.D., Supuran, C.T.: The proteoglycan region of the tumor-associated carbonic anhydrase isoform IX acts as an intrinsic buffer optimizing CO<sub>2</sub> hydration at acidic pH values characteristic of solid tumors. *Bioorganic & Medicinal Chemistry Letters* **19**(20), 5825–5828 (2009). doi:10.1016/j.bmcl.2009.08.088
- [113] Engstrand, C., Jonsson, B.-H., Lindskog, S.: Catalytic and Inhibitor-Binding Properties of Some Active-Site Mutants of Human Carbonic Anhydrase I. *European Journal of Biochemistry* **229**(3), 696–702 (1995). doi:10.1111/j.1432-1033.1995.0696j.x
- [114] Whitney, P.L., Brandt, H.: Effects of two ionizing groups on the active site of human carbonic anhydrase B. *Journal of Biological Chemistry* **251**(13), 3862–3867 (1976)
- [115] Khalifah, R.G.: Histidine-200 alters inhibitor binding in human carbonic anhydrase B. A carbon-13 nuclear magnetic resonance identification. *Biochemistry* **16**(10), 2236–2240 (1977). doi:10.1021/bi00629a030

- [116] Khalifah, R.G., Strader, D.J., Bryant, S.H., Gibson, S.M.: Carbon-13 nuclear magnetic resonance probe of active-site ionizations in human carbonic anhydrase B. *Biochemistry* **16**(10), 2241–2247 (1977). doi:10.1021/bi00629a031
- [117] Duda, D., Tu, C., Qian, M., Laipis, P., Agbandje-McKenna, M., Silverman, D.N., McKenna, R.: Structural and Kinetic Analysis of the Chemical Rescue of the Proton Transfer Function of Carbonic Anhydrase II. *Biochemistry* **40**(6), 1741–1748 (2001). doi:10.1021/bi002295z
- [118] Mikulski, R., Domsic, J.F., Ling, G., Tu, C., Robbins, A.H., Silverman, D.N., McKenna, R.: Structure and catalysis by carbonic anhydrase II: Role of active-site tryptophan 5. *Archives of Biochemistry and Biophysics* **516**(2), 97–102 (2011). doi:10.1016/j.abb.2011.09.011
- [119] Tu, C., Qian, M., An, H., Wadhwa, N.R., Duda, D., Yoshioka, C., Pathak, Y., McKenna, R., Laipis, P.J., Silverman, D.N.: Kinetic Analysis of Multiple Proton Shuttles in the Active Site of Human Carbonic Anhydrase. *Journal of Biological Chemistry* **277**(41), 38870–38876 (2002). doi:10.1074/jbc.M205791200
- [120] Jewell, D.A., Tu, C., Paranawithana, S.R., Tanhauser, S.M., LoGrasso, P.V., Laipis, P.J., Silverman, D.N.: Enhancement of the catalytic properties of human carbonic anhydrase III by site-directed mutagenesis. *Biochemistry* **30**(6), 1484–1490 (1991). doi:10.1021/bi00220a006
- [121] Qian, M., Tu, C., Earnhardt, J.N., Laipis, P.J., Silverman, D.N.: Glutamate and Aspartate as Proton Shuttles in Mutants of Carbonic Anhydrase. *Biochemistry* **36**(50), 15758–15764 (1997). doi:10.1021/bi972081q
- [122] Elder, I., Fisher, Z., Laipis, P.J., Tu, C., McKenna, R., Silverman, D.N.: Structural and kinetic analysis of proton shuttle residues in the active site of human carbonic anhydrase III. *Proteins: Structure, Function, and Bioinformatics* **68**(1), 337–343 (2007). doi:10.1002/prot.21403
- [123] Baird, T.T., Waheed, A., Okuyama, T., Sly, W.S., Fierke, C.A.: Catalysis and Inhibition of Human Carbonic Anhydrase IV. *Biochemistry* **36**(9), 2669–2678 (1997). doi:10.1021/bi962663s
- [124] Hurt, J.D., Tu, C., Laipis, P.J., Silverman, D.N.: Catalytic Properties of Murine Carbonic Anhydrase IV. *Journal of Biological Chemistry* **272**(21), 13512–13518 (1997). doi:10.1074/jbc.272.21.13512
- [125] Earnhardt, J.N., Qian, M., Tu, C., Lakkis, M.M., Bergenheim, N.C.H., Laipis, P.J., Tashian, R.E., Silverman, D.N.: The Catalytic Properties of Murine Carbonic Anhydrase VII. *Biochemistry* **37**(30), 10837–10845 (1998). doi:10.1021/bi980046t
- [126] Wingo, T., Tu, C., Laipis, P.J., Silverman, D.N.: The Catalytic Properties of Human Carbonic Anhydrase IX. *Biochemical and Biophysical Research Communications* **288**(3), 666–669 (2001). doi:10.1006/bbrc.2001.5824

- [127] Ulmasov, B., Waheed, A., Shah, G.N., Grubb, J.H., Sly, W.S., Tu, C., Silverman, D.N.: Purification and kinetic analysis of recombinant CA XII, a membrane carbonic anhydrase overexpressed in certain cancers. *Proceedings of the National Academy of Sciences* **97**(26), 14212–14217 (2000). doi:10.1073/pnas.97.26.14212
- [128] Xie, D., Gulnik, S., Collins, L., Gustchina, E., Suvorov, L., Erickson, J.W.: Dissection of the pH Dependence of Inhibitor Binding Energetics for an Aspartic Protease: Direct Measurement of the Protonation States of the Catalytic Aspartic Acid Residues. *Biochemistry* **36**(51), 16166–16172 (1997). doi:10.1021/bi971550l
- [129] Parker, M.H., Lunney, E.A., Ortwine, D.F., Pavlovsky, A.G., Humblet, C., Brouillette, C.G.: Analysis of the Binding of Hydroxamic Acid and Carboxylic Acid Inhibitors to the Stromelysin-1 (Matrix Metalloproteinase-3) Catalytic Domain by Isothermal Titration Calorimetry. *Biochemistry* **38**(41), 13592–13601 (1999). doi:10.1021/bi991222g
- [130] Velazquez-Campoy, A., Luque, I., Todd, M.J., Milutinovich, M., Kiso, Y., Freire, E.: Thermodynamic dissection of the binding energetics of KNI-272, a potent HIV-1 protease inhibitor. *Protein Science* **9**(9), 1801–1809 (2000). doi:10.1110/ps.9.9.1801
- [131] Lindskog, S.: Effects of pH and Inhibitors on Some Properties Related to Metal Binding in Bovine Carbonic Anhydrase. *Journal of Biological Chemistry* **238**(3), 945–951 (1963)
- [132] Connelly, P.R., Ladbury, J.E.: *Structure-Based Drug Design: Thermodynamics, Modeling and Strategy*. Biotechnology intelligence unit. Springer, Berlin ; New York (1997)
- [133] Taylor, P.W., King, R.W., Burgen, A.S.V.: Influence of pH on the kinetics of complex formation between aromatic sulfonamides and human carbonic anhydrase. *Biochemistry* **9**(20), 3894–3902 (1970). doi:10.1021/bi00822a007
- [134] Petrauskas, V., Baranauskienė, L., Zubrienė, A., Matulis, D.: Isothermal Titration Calorimetry and Fluorescent Thermal and Pressure Shift Assays in Protein-Ligand Interactions. In: *Biocalorimetry*, pp. 261–280. CRC Press, ??? (2016). doi:10.1201/b20161-18
- [135] Zubrienė, A., Čapkauskaitė, E., Gylytė, J., Kišonaitė, M., Tumkevičius, S., Matulis, D.: Benzenesulfonamides with benzimidazole moieties as inhibitors of carbonic anhydrases I, II, VII, XII and XIII. *Journal of Enzyme Inhibition and Medicinal Chemistry* **29**(1), 124–131 (2014). doi:10.3109/14756366.2012.757223. 00000
- [136] Čapkauskaitė, E., Baranauskienė, L., Golovenko, D., Manakova, E., Gražulis, S., Tumkevičius, S., Matulis, D.: Indapamide-like benzenesulfonamides as inhibitors of carbonic anhydrases I, II, VII, and XIII. *Bioorganic & Medicinal Chemistry* **18**(21), 7357–7364 (2010). doi:10.1016/j.bmc.2010.09.016

- [137] Čapkauskaitė, E., Zubrienė, A., Baranauskienė, L., Tamulaitienė, G., Manakova, E., Kairys, V., Gražulis, S., Tumkevičius, S., Matulis, D.: Design of [(2-pyrimidinylthio)acetyl]benzenesulfonamides as inhibitors of human carbonic anhydrases. *European Journal of Medicinal Chemistry* **51**, 259–270 (2012). doi:10.1016/j.ejmech.2012.02.050. 00008
- [138] Dudutienė, V., Zubrienė, A., Smirnov, A., Gylytė, J., Timm, D., Manakova, E., Gražulis, S., Matulis, D.: 4-Substituted-2,3,5,6-tetrafluorobenzenesulfonamides as inhibitors of carbonic anhydrases I, II, VII, XII, and XIII. *Bioorganic & Medicinal Chemistry* **21**(7), 2093–2106 (2013). doi:10.1016/j.bmc.2013.01.008. 00010
- [139] Dudutienė, V., Matulienė, J., Smirnov, A., Timm, D.D., Zubrienė, A., Baranauskienė, L., Morkūnaitė, V., Smirnovienė, J., Michailovienė, V., Juozapaitienė, V., Mickevičiūtė, A., Kazokaitė, J., Bakšytė, S., Kasiliauskaitė, A., Jachno, J., Revuckienė, J., Kišonaitė, M., Pilipuitytė, V., Ivanauskaitė, E., Milinavičiūtė, G., Smirnovas, V., Petrikaitė, V., Kairys, V., Petrauskas, V., Norvaišas, P., Lingė, D., Gibieža, P., Čapkauskaitė, E., Audrius Zakšauskas, Kazlauskas, E., Manakova, E., Saulius Gražulis, Ladbury, J.E., Matulis, D.: Discovery and characterization of novel selective inhibitors of carbonic anhydrase IX. *J Med Chem* **57**, 9435–9446 (2014). doi:10.1021/jm501003k
- [140] Dudutienė, V., Zubrienė, A., Smirnov, A., Timm, D.D., Smirnovienė, J., Kazokaitė, J., Michailovienė, V., Zakšauskas, A., Manakova, E., Gražulis, S., Matulis, D.: Functionalization of Fluorinated Benzenesulfonamides and Their Inhibitory Properties toward Carbonic Anhydrases. *ChemMedChem* **10**(4), 662–687 (2015). doi:10.1002/cmdc.201402490. 00000
- [141] Khalifah, R.G., Zhang, F., Parr, J.S., Rowe, E.S.: Thermodynamics of binding of the carbon dioxide-competitive inhibitor imidazole and related compounds to human carbonic anhydrase I: An isothermal titration calorimetry approach to studying weak binding by displacement with strong inhibitors. *Biochemistry* **32**(12), 3058–3066 (1993). doi:10.1021/bi00063a017
- [142] Tanpure, R.P., Ren, B., Peat, T.S., Bornaghi, L.F., Vullo, D., Supuran, C.T., Poulsen, S.-A.: Carbonic Anhydrase Inhibitors with Dual-Tail Moieties To Match the Hydrophobic and Hydrophilic Halves of the Carbonic Anhydrase Active Site. *Journal of Medicinal Chemistry* **58**(3), 1494–1501 (2015). doi:10.1021/jm501798g



# Additional information

## 11 Manuscripts



Contents lists available at SciVerse ScienceDirect

## Bioorganic &amp; Medicinal Chemistry

journal homepage: [www.elsevier.com/locate/bmc](http://www.elsevier.com/locate/bmc)

## Characterization of human carbonic anhydrase XII stability and inhibitor binding

Vaida Jogaitė, Asta Zubrienė, Vilma Michailovienė, Joana Gylytė, Vaida Morkūnaitė, Daumantas Matulis\*

Department of Biothermodynamics and Drug Design, Vilnius University Institute of Biotechnology, Graičiūno 8, Vilnius LT-02241, Lithuania

### ARTICLE INFO

#### Article history:

Available online 27 October 2012

#### Keywords:

Carbonic anhydrase  
Isothermal titration calorimetry  
Thermal shift assay  
ThermoFluor®  
Intrinsic enthalpy of binding

### ABSTRACT

Human carbonic anhydrase isozyme XII is a transmembrane protein that is overexpressed in many human cancers. Therefore CA XII is an anticancer drug target. However, there are few compounds that specifically target CA XII. The design of specific inhibitors against CA XII relies on the detailed understanding of the thermodynamics of inhibitor binding and the structural features of the protein–inhibitor complex. To characterize the thermodynamic parameters of the binding of known sulfonamides, namely ethoxzolamide, acetazolamide and trifluoromethanesulfonamide, we used isothermal titration calorimetry and fluorescent thermal shift assay. The binding of these sulfonamides to CA XII was buffer and pH-dependent. Dissection of protonation–deprotonation reactions of both the water molecule bound to the CA XII active site and the sulfonamide group of the inhibitor yielded the intrinsic thermodynamic parameters of binding, such as binding enthalpy, entropy and Gibbs free energy. Thermal shift assay was also used to determine CA XII stabilities at various pH and in the presence of buffers and salts.

© 2012 Elsevier Ltd. All rights reserved.

### 1. Introduction

Carbonic anhydrases (CAs) are metalloenzymes that catalyze reversible CO<sub>2</sub> hydration reaction observed in all kingdoms—from bacteria to humans. Fifteen human CA isozymes belonging to alpha class have been identified. Twelve of them are catalytically active and widely differ in their cellular localization, distribution in organs and tissues, expression levels and enzymatic properties. CAs play an important function in such crucial physiological processes as maintaining an appropriate acid–base balance, respiration, transport of bicarbonate and CO<sub>2</sub>, electrolyte secretion in various tissues, biosynthetic reactions (such as gluconeogenesis, lipogenesis and ureagenesis), tumorigenicity, and many other processes. CA enzymes and inhibitors have been extensively reviewed.<sup>1–5</sup>

CA XII is a transmembrane protein that is overexpressed in human cancers, such as renal, breast, non-small lung, gastrointestinal, pancreatic, uterine, ovarian, and brain carcinomas.<sup>6–8</sup> In hypoxic tumor cells CA XII, together with other transmembrane protein CA IX, contribute to extracellular acidification and maintain intracellular pH more alkaline, thus promoting tumor cell survival in an acidic environment and low bicarbonate medium. The silencing of both CA IX and CA XII significantly reduces tumor xenograft cell growth.<sup>9</sup> In many types of cancers such as oral squamous cell car-

cinoma,<sup>10</sup> astrocytomas,<sup>11</sup> glioblastomas, the expression of CA XII is related with poor prognosis of patient's survival. Therefore CA XII is implicated as target for development of new specific anticancer drugs.<sup>12</sup> However, the application of CA XII inhibitors in treatment of cancer is likely to depend on the cancer cell type. High CA XII expression in cancer cells do not always correlate with patients' prognosis. Two studies demonstrate that a high CA XII tumor tissue expression is related to a better outcome in a large series of patients with non-small cell lung cancer<sup>13</sup> and breast cancer.<sup>14</sup>

The catalytic properties of recombinant form of wild type CA XII have been characterized.<sup>15</sup> The kinetic properties of this enzyme are very similar to that of another membrane-bound isozyme, CA IV and also similar to CA I. The value of  $k_{cat}$  for CA XII is 0.4 μs<sup>-1</sup>. The pH profile for the rate constant  $k_{cat}/K_m$  for hydration of CO<sub>2</sub> catalyzed by CA XII was determined by stopped flow spectrophotometry and showed the pK<sub>a</sub> of zinc bound water at 7.1. The same pK<sub>a</sub> was determined by measuring the hydrolysis of 4-nitrophenylacetate catalyzed by CA XII. The crystal structure of the extracellular catalytic domain of human CA XII at 1.55 Å resolution has been solved.<sup>16</sup> Two domains of CA XII form an isologous dimer. The active site clefts of each dimer are exposed on one face of the dimer and poised for catalysis.

Numerous inhibitors have been designed to inhibit various CAs. However, there are a limited number of sulfonamides that would exhibit high selectivity toward CA XII. Recently Supuran group demonstrated that 7,8-disubstituted coumarins having ethyl or propyl groups at 7 position and acetyl group at 8 position are CA XII-selective inhibitors with inhibition constants of 1 nM and of 0.98 nM, respectively.<sup>17</sup> A series of 2-thioxo-coumarin derivatives

Abbreviations: CA, carbonic anhydrase; CA XII, isozyme 12 of the human carbonic anhydrase protein family; ITC, isothermal titration calorimetry; TSA, thermal shift assay.

\* Corresponding author. Tel.: +370 5 269 1884; fax: +370 5 260 2116.

E-mail addresses: [matulis@bti.lt](mailto:matulis@bti.lt), [daumantas.matulis@bti.vu.lt](mailto:daumantas.matulis@bti.vu.lt) (D. Matulis).

were submicromolar inhibitors of CA XII and CA IX whereas CA II was not inhibited at all.<sup>18</sup> According to the proposed mechanism of action of this class inhibitors, CA catalyzes the hydrolysis of coumarins to *cis/trans*-2-hydroxycinnamic acid derivatives, which bind very differently to the CA active site than sulfonamides.<sup>19</sup>

The structure–activity relationship (SAR) of CA XII inhibitors is not fully understood because most inhibitors are only characterized by determining their enzyme inhibition constant ( $K_i$ ). In our opinion, it is also important to determine the intrinsic thermodynamic parameters of inhibitor binding to any protein in order to more deeply understand the SAR of a compound series that are being designed as drug leads.<sup>20</sup> Carbonic anhydrase inhibitor binding is linked to several reactions. Among them most important are linked protonation–deprotonation reactions of both the water molecule bound to the CA active site and the sulfonamide group of the inhibitor.<sup>2,21–24</sup> These linked reactions strongly affect the observed thermodynamic parameters of binding and often do not correlate with the intrinsic parameters. Only the intrinsic parameters should be used for compound SAR analysis.

Determination of the first compound intrinsic thermodynamic parameters requires numerous ITC experiments at various pH and in several buffers. However, consequent determinations could use the thermodynamic parameters of protonation determined for the first compound and would require only one ITC experiment at one pH in a defined buffer. The intrinsic parameters of binding then could be calculated by subtracting protonation contributions.

Here we determine the intrinsic parameters of three commonly used inhibitors, namely acetazolamide, ethoxzolamide, and trifluoromethanesulfonamide, binding to CA XII by combining two techniques. The observed binding enthalpies are determined by isothermal titration calorimetry (ITC) while Gibbs free energies (binding constants) are determined by ITC and fluorescent thermal shift assay (TSA). TSA is a rapid screening method used in pharmaceutical industry for the identification of binders and requires lower amounts of protein.<sup>25–30</sup> The TSA is not limited in the range of affinities while ITC has limitations.

The TSA technique was also used to determine CA XII stability in various buffers and salts. This is useful for protein purification, storage, and also fundamental understanding of factors determining protein stability. Interestingly, differently from some other CA isozymes, CA XII is significantly stabilized in high salt concentrations.

## 2. Results

### 2.1. Dissection of binding-linked protonation reactions

Aromatic and aliphatic sulfonamides, that are good inhibitors of carbonic anhydrase enzymes, undergo a protonation–deprotonation reactions dependent on the pH of the medium (Figure 1). The protonation  $pK_a$  is dependent on the electron-withdrawing capability of the adjacent functional groups. Fluorine atoms possess strong electron-withdrawing capacity and therefore trifluoromethanesulfonamide (TFMSA) has lowest  $pK_a$  of the three commonly studied inhibitors (Figure 1).

At pH 7.0, ethoxzolamide (EZA) will primarily be protonated, while TFMSA-deprotonated. However, only the deprotonated form of the inhibitor binds to the CA active site zinc atom. Therefore, EZA binding data at pH 7.0 would include a linked deprotonation reaction and thus influence the observed thermodynamic parameters. In order to study any structure–activity relationships of such inhibitors, it is important to study the intrinsic parameters that would not have contributions from other linked reactions.

Furthermore, in order for CA to bind sulfonamide inhibitor, the active site zinc-bound water molecule must be in its electrically

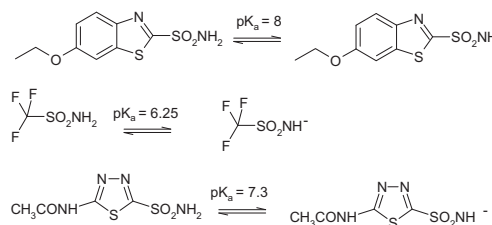


**Figure 1.** Chemical structures and deprotonation equilibria of commonly used CA inhibitors: ethoxzolamide (EZA), trifluoromethanesulfonamide (TFMSA), and acetazolamide (AZM).

neutral protonated form. Most CA isozymes have their  $pK_a$ s in the vicinity of 7. Therefore, their inhibitor binding capacity will also be pH-dependent. This binding-linked reaction must also be dissected from observed thermodynamics in order to obtain the intrinsic pH-independent parameters.

The intrinsic constant is related to the observed binding constant and the fractions of active binding species<sup>31</sup>:

$$K_b = K_{b,obs} / (f_{RSO_2NH} \cdot f_{CAZnH_2O}) \quad (1)$$

Where the fractions of deprotonated sulfonamide and protonated CA as a function of pH are:

$$f_{RSO_2NH} = \frac{10^{pH - pK_a - sulfonamide}}{1 + 10^{pH - pK_a - sulfonamide}} \quad (2)$$

$$f_{CAZnH_2O} = 1 - \frac{10^{pH - pK_3 - Zn - water}}{1 + 10^{pH - pK_3 - Zn - water}} \quad (3)$$

The intrinsic enthalpy of binding has contributions from the observed binding enthalpy ( $\Delta_b H_{obs}$ ), enthalpies of inhibitor ( $\Delta_{b,proton,inh}H$ ), CA ( $\Delta_{b,proton,CA}H$ ), and the buffer protonation ( $\Delta_{b,proton,buf}H$ ):

$$\Delta_b H = \Delta_b H_{obs} - n_{inh} \Delta_{b,proton,inh}H - n_{CA} \Delta_{b,proton,CA}H - n \Delta_{b,proton,buf}H, \quad (4)$$

where  $n_{inh} = f_{RSO_2NH} - 1$ ,  $n_{CA} = 1 - f_{CAZnH_2O}$ , and  $n = -(n_{inh} + n_{CA})$ .

Ethoxzolamide binding to the catalytic domain of CA XII was measured by ITC in two buffers with different protonation enthalpies—phosphate and TRIS. The enthalpies of binding were different indicating a linked protonation reaction(s) (Figure 2 and Table 1). Similarly, the binding ITC curve was strongly pH-dependent.

In addition to ITC measurements, the inhibitor binding reaction was studied by fluorescent thermal shift assay (TSA). The CA XII protein melting curves in the presence of varied inhibitor concentration and the dosing curves are shown in Figure 3. TSA has advantage over ITC in its higher speed and lower reagent consumption. TSA can also determine very tight subnanomolar binding reactions where ITC requires displacement experiments. However, the enthalpies and entropies of binding may be determined only by ITC. Therefore, both techniques are important and complementary for accurate determination of the intrinsic binding parameters.

Figure 4 shows the pH-dependencies of the observed inhibitor–CA binding Gibbs free energies and enthalpies as determined by TSA and ITC. The Gibbs free energies exhibit U-shape pH dependence that can be approximated by Eq. 1. The binding reaction appears strongest at near-neutral pH where the concentrations of the deprotonated sulfonamide and protonated CA are highest. The binding reaction weakens toward more acidic pH due to diminished concentration of deprotonated sulfonamide and toward alkaline pH due to diminished concentration of protonated CA. The

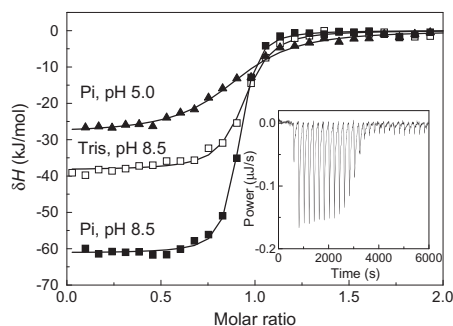


**Figure 2.** Ethoxzolamide binding to CA XII as determined by isothermal titration calorimetry. Integrated ITC curves in sodium phosphate buffer pH 5.0 ( $\blacktriangle$ ) and pH 8.5 ( $\blacksquare$ ), and TRIS chloride buffer ( $\square$ ), pH 8.5, all at 25 °C. The inset shows raw ITC curve at pH 7.5, TRIS chloride buffer, at 25 °C.

**Table 1**  
Observed thermodynamic parameters of EZA, TFMSA and AZM binding to CA XII in phosphate and TRIS buffers are listed as a function of pH, determined by ITC at 25 °C

Compound	pH	$K_{b, \text{obs}}$ ( $M^{-1}$ )	$\Delta\Delta G_{\text{obs}}$ (kJ/mol)	$\Delta\Delta H_{\text{obs}}$ (kJ/mol)	$T\Delta\Delta S_{\text{obs}}$ (kJ/mol)
<i>Phosphate buffer</i>					
EZA	5.0	$5.26 \times 10^6$	-38.4	-28.2	10.2
	6.0	$1.12 \times 10^7$	-40.2	-30.1	10.1
	7.0	$1.15 \times 10^8$	-46.0	-39.5	6.5
	8.0	$9.76 \times 10^7$	-45.6	-57.1	-11.5
	9.0	$2.28 \times 10^7$	-42.0	-67.4	-25.4
TFMSA	7.0	$4.84 \times 10^7$	-43.9	-35.5	8.3
AZM	7.0	$1.89 \times 10^7$	-41.5	-50.4	-8.8
<i>TRIS buffer</i>					
EZA	5.0	$1.20 \times 10^7$	-40.5	-62.2	-21.7
	6.0	$2.20 \times 10^7$	-41.9	-64.2	-22.3
	7.0	$6.00 \times 10^7$	-44.4	-55.7	-11.3
	8.0	$7.00 \times 10^7$	-44.8	-45.6	-0.8
	9.0	$2.80 \times 10^7$	-42.5	-38.2	4.3

intrinsic Gibbs free energy, shown by solid straight line, cannot be reached at any pH.

The observed enthalpies of EZA binding to CA XII exhibit even more complicated pH dependence (Figure 4c) due to large contributions of linked buffer protonation reactions. The lines in the Figure show approximation of the observed datapoints by applying Eq. 4. Dissection of linked reactions yielded the intrinsic thermodynamic parameters of sulfonamide inhibitor and CA protonation (Table 2) and the intrinsic parameters of all three studied inhibitor binding to CA XII (Table 3). The observed  $K_{b, \text{obs}}$  of EZA binding to CA XII reached  $1.15 \times 10^8 M^{-1}$  at pH 7.0, but the intrinsic  $K_b$  was  $2.3 \times 10^9 M^{-1}$ . This difference is significant and the difference would be even more significant if the  $pK_a$  of the inhibitor is greater.

In the case of TFMSA binding to CA XII, the observed and intrinsic parameters are quite similar. The observed binding constant  $K_{b, \text{obs}}$  of TFMSA binding to CA XII is  $4.8 \times 10^7 M^{-1}$  at pH 7.0, and the intrinsic  $K_b$  is  $7.0 \times 10^7 M^{-1}$ . This insignificant difference from the observed value is due to the low  $pK_a$  of TFMSA.

Intrinsic binding of AZM was tighter to CA XII than to CA XIII by about an order of magnitude while the binding of EZA and TFMSA to both isozymes was similar. The intrinsic enthalpies of EZA and AZM binding to CA XII were similar and equal to -50.6 and -50.9 kJ/mol, respectively. However, the intrinsic entropy of binding was positive for EZA and negative for AZM. Therefore, EZA exhibited the highest intrinsic affinity for CA XII of the three studied ligands.

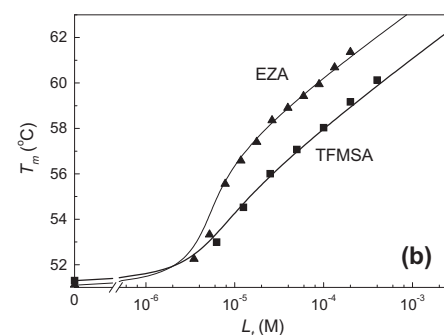
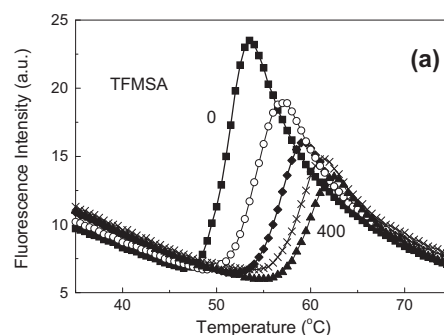


**Figure 3.** Thermal shift assay data of EZA and TFMSA binding to CA XII. (a) Thermal melting fluorescence curves of CA XII (concentration 10  $\mu\text{M}$ ), sodium phosphate buffer, pH 7.0, in the presence of various TFMSA concentrations, 0  $\mu\text{M}$  ( $\blacksquare$ ), 12  $\mu\text{M}$  ( $\circ$ ), 50  $\mu\text{M}$  ( $\blacklozenge$ ), 200  $\mu\text{M}$  ( $\times$ ) and 400  $\mu\text{M}$  ( $\blacktriangle$ ). Ligand addition shifted the protein melting temperatures upwards. (b) The melting temperatures ( $T_m$ ) from data in panel (a) plotted as a function of added EZA or TFMSA concentration. The lines are fitted according to Ref. 34.

It was also interesting that structurally simple TFMSA binds to CA XII with less favorable enthalpy but more favorable entropy than the other two ligands. Hakansson and Liljas had previously shown<sup>32</sup> that trifluoromethyl moiety of this ligand forms hydrophobic contacts with a hydrophobic pocket of CA II. Such contacts could explain the relatively higher entropic contribution to the Gibbs free energy of TFMSA binding to CA XII.

Thermodynamic parameters of CA hydroxide protonation were similar to previously determined parameters for CA XIII<sup>21</sup> as listed in Table 2. However, there is significant difference between the  $pK_a$ s of both enzymes. CA XII has  $pK_a$  7.0 while CA XIII has  $pK_a$  of 8.3. As seen from Table 2, this difference can be attributed primarily to entropic contribution. The enthalpies of protonation were essentially indistinguishable within the error of the experiments.

## 2.2. Characterization of CA XII stability by TSA

Fluorescent thermal shift assay is an efficient way to determine and compare protein stabilities at various pH values and in the presence of various substances, buffers, excipients, etc., among which may be an inhibitor. Figure 5 shows CA XII stability pH profiles in the presence of various concentrations of EZA or TFMSA inhibitors. The protein is most stable at pH 6.0 with an abrupt drop below about pH 5 and above pH 10. Similar stability profiles are in the presence of inhibitors despite significant stabilization of the protein by bound ligand. The equilibrium of bound ligand is

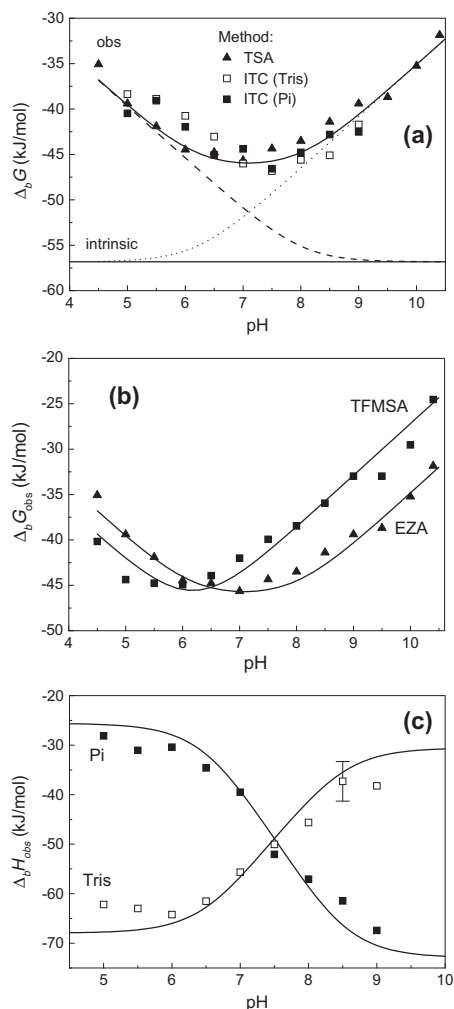


**Figure 4.** The observed Gibbs free energy of binding (binding constant) and observed enthalpy dependence on pH. (a) The observed and intrinsic Gibbs free energies of EZA binding to CA XII as a function of pH. Datapoints show  $\Delta_b G_{obs}$  obtained by ITC in phosphate (■) and TRIS (□) buffers and by TSA (▲). Solid bent line is the fit according to Eq. 1 recalculated to Gibbs free energies. Dashed and dotted lines show the contributions of the fractions of deprotonated EZA and protonated CA XII, respectively. Straight line shows the intrinsic Gibbs free energy of EZA binding, independent of pH. (b) Comparison of TFMSA (■) and EZA (▲) binding pH profiles. Curves show the fits according to Eq. 1 using parameters listed in Tables 1 and 2. Datapoints show  $\Delta_b G_{obs}$  obtained by TSA. (c) The observed enthalpies of EZA binding to CA XII in sodium phosphate (■) and TRIS chloride (□) buffer, at 25 °C, as a function of pH. Data points represent observed enthalpies obtained by ITC, while the curves are fit according to Eq. 4.

reversible and therefore the stabilizational effect is greater at greater inhibitor concentration. This is due to the entropy of mixing. However, the stabilizational effect is not identical at all pHs as predicted by weaker binding at low or high pH values. For example, CA XII stabilization by TFMSA at pH 10.0 or 10.5 is small compared to the effect at pH 6.0.

**Table 2**

Intrinsic thermodynamic parameters of protonation of the ionized inhibitor sulfonamide group or carbonic anhydrase-bound hydroxide anion to water molecule are listed as determined by ITC at 25 °C

Inhibitor/protein	p <i>K</i> <sub>a</sub>	$\Delta G_{prot}$ (kJ/mol)	$\Delta H_{prot}$ (kJ/mol)	$T\Delta S$ (kJ/mol)
EZA <sup>a</sup>	8.0	-45.7	-29.5	16.2
TFMSA <sup>b</sup>	6.3	-35.7	-22.4	13.3
AZM <sup>b</sup>	7.3	-41.7	-23.0	18.7
CA XII-Zn-H <sub>2</sub> O	7.0	-40.0	-28.0	12.0
CA XIII-Zn-H <sub>2</sub> O <sup>a</sup>	8.3	-47.1	-26.0	21.1

<sup>a</sup> Data taken from Ref. 21.

<sup>b</sup> Data taken from Ref. 24.

**Table 3**

Intrinsic thermodynamic parameters are listed for EZA, TFMSA, and AZM binding to CA XII, and XIII, determined by ITC at 25 °C

Inhibitor	$\Delta_b H_{intr}$ (kJ/mol)	$K_{b,intr}$ (M <sup>-1</sup> )	$\Delta_b G_{intr}$ (kJ/mol)	$T\Delta_b S_{intr}$ (kJ/mol)
<i>CA XII</i>				
EZA	-50.6	$2.3 \times 10^9$	-53.5	2.9
TFMSA	-28.9	$7.0 \times 10^7$	-44.8	15.9
AZM	-50.9	$1.2 \times 10^8$	-46.0	-4.9
<i>CA XIII</i>				
EZA <sup>a</sup>	-42.1	$1.8 \times 10^9$	-52.8	10.7
TFMSA <sup>a</sup>	-33.5	$4.6 \times 10^7$	-43.8	10.2
AZM <sup>a</sup>	-50.4	$1.9 \times 10^7$	-41.5	-8.9

<sup>a</sup> Data taken from Ref. 21.

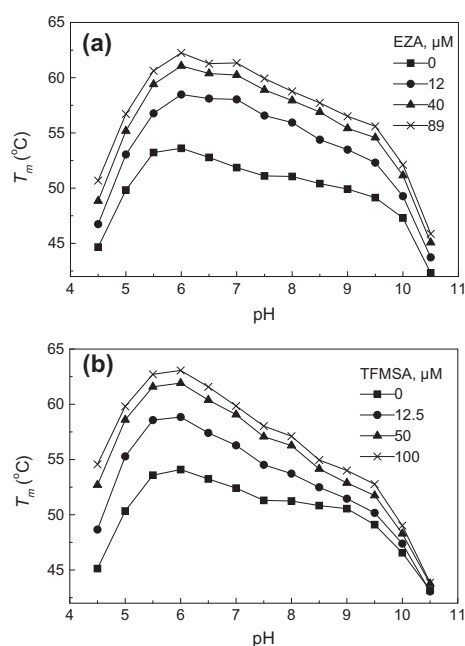


**Figure 5.** CA XII melting temperature ( $T_m$ ) dependence on pH at different concentrations of EZA (a) and TFMSA (b). The protein is most stable at pH 6.0 and becomes increasingly destabilized below pH 5.0 and above pH 10.0. The presence of increasing concentrations of EZA or TFMSA stabilized the protein, but to a different extent at various pH values. The decreased effect of the inhibitor is especially visible at high pH for both inhibitors.

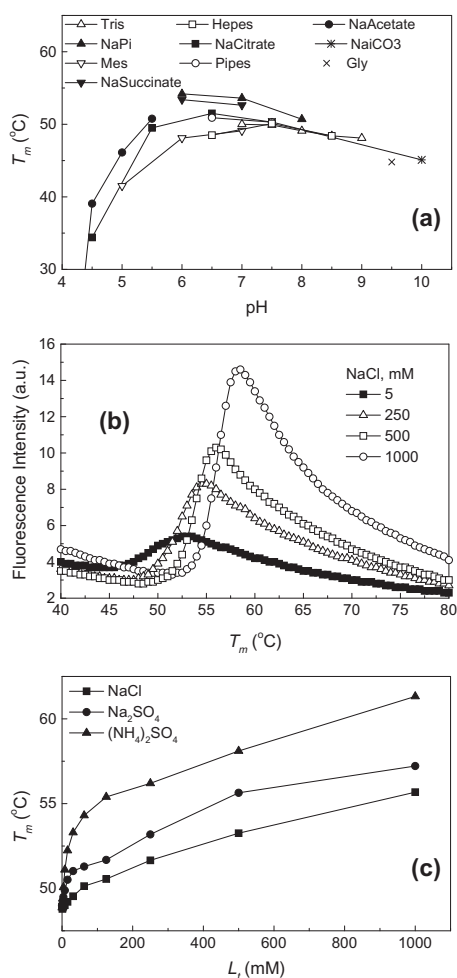


**Figure 6.** CA XII stability in various buffers, pH and salts. (a) CA XII melting temperature ( $T_m$ ) dependence on pH in various buffers (100 mM): sodium acetate (NaAcetate), sodium citrate (NaCitrate), sodium phosphate (NaPi), sodium succinate (NaSuccinate), sodium carbonate (NaHCO<sub>3</sub>), glycine (Gly), TRIS (Tris), MES (Mes), HEPES (Hepes) and PIPES (Pipes). (b) Thermal melting fluorescence curves of CA XII in 5 mM sodium phosphate buffer, pH 7.0, in the presence of various NaCl concentrations, 5 mM (■), 250 mM (□), 500 mM (○), 1000 mM (×). (c) CA XII melting temperature as a function of various salts concentrations: (NH<sub>4</sub>)<sub>2</sub>SO<sub>4</sub> (▲), Na<sub>2</sub>SO<sub>4</sub> (●), and NaCl (■).

CA XII stability is also highly affected by the pH, buffer, and the presence of various salts (Figure 6). For example, CA XII at pH 6.0 is significantly (by 5 °C) less stable in MES buffer than in sodium phosphate or sodium succinate buffer. Destabilization of CA XII by MES is observed at pH 5.0, 6.0, and 7.0. Similar effect is observed by HEPES. These buffers may have to be avoided in CA XII storage or production.

Regular salts such as sodium chloride, sodium sulfate, or ammonium sulfate exhibit strong stabilization effect on CA XII (Figure 6c).

Addition of 1 M ammonium sulfate stabilized CA XII by more than 10 °C. The effect of sodium chloride was significantly weaker, but still substantial. These results indicate that there are cation and anion-binding sites on CA surface that stabilize the protein molecule. Protein melting transition is more cooperative in high salt as seen in Panel (b). These results help practical aspects of choosing conditions for CA XII purification and storage.

### 3. Discussion

This study determined the intrinsic thermodynamic parameters of three inhibitors, namely, EZA, TFMSA, and AZM, binding to human CA XII. To obtain these parameters, it was necessary to dissect contributions of three linked protonation reactions—deprotonation of sulfonamide, protonation of the active site zinc hydroxide and protonation-deprotonation of buffer. Dissection yielded the thermodynamic parameters of Zn-bound water molecule protonation. The calculated intrinsic thermodynamic parameters were independent of the fractions of sulfonamide and CA XII in the active forms. To obtain these parameters, a large series of ITC experiments were necessary to be performed in several buffers and at various pH.

However, further studies with other inhibitors would not need to perform these large series of titrations at various conditions. It will be sufficient to perform two ITC and/or TSA experiments: a single well-controlled CA-inhibitor ITC titration in a buffer with known protonation enthalpy and at known pH and determine the  $pK_a$  and enthalpy of ionization of the sulfonamide inhibitor to be able to calculate the intrinsic Gibbs free energy and intrinsic enthalpy of the inhibitor binding to CA XII using Eqs. 1 and 4 and the parameters in Table 2.

Table 3 showed that there was no evident selectivity of the intrinsic binding of studied inhibitors to CA XII or CA XIII isozymes, despite the differences in the protein  $pK_{a,s}$ . Only AZM bound 10 times stronger to CA XII than to CA XIII. In order to build inhibitors that would bear significant difference in affinities between CA XII and XIII, one needs to have significantly larger functional groups than in AZM, TFMSA, or EZA.

The determined intrinsic parameters of inhibitor binding to CA XII should enable a more efficient determination of intrinsic binding parameters for other inhibitors. Most inhibition studies are so far usually limited to the determination of the observed thermodynamic parameters<sup>33</sup> that are primarily performed by stopped-flow inhibition assay of the CO<sub>2</sub> hydration activity by the CA. Such observed inhibition constants may not be correlated with structures because they are pH-dependent due to linked protonation reactions.

### 4. Conclusions

The binding affinity of EZA to CA XII is dependent on the buffer and pH. The pH dependence of the binding energetics is associated with linked inhibitor and protein deprotonation–protonation reactions. Dissection of binding-linked reactions yielded the intrinsic parameters of binding. The intrinsic enthalpy contributes the dominant fraction to the Gibbs free energy of binding of EZA, AZM and TFMSA to CA XII. The entropy of binding contributes favorably for EZA and TFMSA. The difference in the observed binding constants among the studied inhibitors is primarily due to the differences in sulfonamide  $pK_{a,s}$ .

Thermal shift assay showed that CA XII is most stable at pH 6 with significantly reduced stability below pH 5 and above pH 10. Regular salts such as sodium chloride, sodium sulfate, and ammonium sulfate stabilize CA XII.

## 5. Materials and methods

Ethoxzolamide (EZA) was purchased from Aldrich (Milwaukee, WI, USA), trifluoromethanesulfonamide (TFMSA) was purchased from Alfa Aesar, and acetazolamide was purchased from Sigma.

### 5.1. Construction, expression and purification of CA XII

Recombinant protein encoding CA XII from 30 to 291 amino acids was created according to Whittington.<sup>16</sup> DNA fragment of 810 bp was amplified by PCR from full CA XII gene cloned in pDNR-LIB-CA XII (RZPD) plasmid using forward primer with NdeI recognition site—5' AGTGCATATGTCCAAGTGGACTTATTTG 3' and reverse primer with BamHI recognition site—5' TAC-AGGATCCTTATTGGGAGAAGGAGGTG 3'. The PCR product was cloned into the bacterial expression vector pET21a (Novagen). The recombinant CA XII has catalytic domain and lacks the signal, transmembrane and cytoplasmic domains. Expression of the recombinant CA XII was done in *Escherichia coli* Rosetta (DE3) strain (Novagen). Transformed cells colony was transferred to LB medium, containing 100 µg/ml ampicillin, 34 µg/ml chloramphenicol and grown at 37 °C and 220 rpm for 16 h. Then the saturated culture was diluted (1:50) in fresh LB medium, containing 100 µg/ml ampicillin, 34 µg/ml chloramphenicol, 60 µM ZnSO<sub>4</sub> and grown to OD<sub>600</sub> ≈ 0.8. The expression of CA XII was induced with 1 mM isopropyl β-D-thiogalactoside (IPTG) and 0.5 mM ZnSO<sub>4</sub>. The culture was grown for 4 h at 30 °C and 220 rpm. The cells were harvested by centrifugation at 4000g for 20 min at 4 °C.

The pellet was suspended in lysis buffer (20 mM Hepes, 0.1% Triton X-100, 0.15 M NaCl, (pH 8.5) and 1 mM PMSF) containing protease inhibitor cocktail (Roche applied Science, Indianapolis, IN). The cells were incubated at 4 °C for 60 min and then disrupted by sonication. The supernatant, containing soluble proteins, was obtained after centrifugation at 30,000g for 25 min. The soluble protein was purified using a CA-affinity column containing *p*-aminomethylbenzene sulfonamide-agarose (Sigma-Life Science Aldrich). Eluted CA XII protein was dialyzed into a storage buffer containing 10 mM Hepes (pH 7.5), 50 mM NaCl, and stored at –80 °C.

The purity of the CA XII preparations was analyzed by SDS-PAGE. Protein concentrations were determined by UV–vis spectrophotometry using extinction coefficient  $\epsilon_{280} = 42922.5 \text{ M}^{-1} \text{ cm}^{-1}$  and confirmed by standard Bradford method.

### 5.2. Isothermal titration calorimetry (ITC)

ITC measurements were performed using a VP-ITC instrument (Microcal, Inc., GE-Healthcare, Northampton, MA, USA). Protein solution (6–8 µM in the cell, volume 1.4 ml) was titrated with compound solution in the syringe (60–80 µM, 250 µl). A typical experiment consisted of 25–30 injections, 10 µl each, with 3–4 min intervals between injections. Experiments were performed at 25 °C in 50 mM TRIS chloride or sodium phosphate buffers containing 100 mM NaCl and 0.5–2% DMSO concentration both in the cell and syringe. ITC data was integrated, fit and analyzed as previously described.<sup>34</sup>

### 5.3. Thermal shift assay (TSA)

TSA experiments were performed with Corbett Rotor-Gene 6000 (QIAGEN Rotor-Gene Q) instrument using the blue channel (excitation 365 ± 20, detection 460 ± 15 nm), applying the heating

rate of 1 °C/min. Usually, the samples contained 20 µl of 10 µM protein, 0–400 µM ligand, 50 µM 8-anilino-1-naphthalene sulfonate, 50 mM sodium phosphate at pH 7.0, 50 mM NaCl, and 2% DMSO. The pH dependence of the observed binding constant ( $K_b$ ) was determined in the buffer containing 50 mM sodium phosphate, 50 mM sodium acetate, and 25 mM sodium borate, pH 4.5–10.5. TSA data was fit and analyzed as previously described.<sup>34</sup>

### Acknowledgments

This research was funded by a grant (No. LIG-09/2012) from the Research Council of Lithuania. The authors also acknowledge FP7-REGPOT-2009-1 grant “MoBiLi”, Agreement No.: 245721, and the COST projects TD0905 and CM0804.

### References and notes

- Hassan, M. I.; Shajee, B.; Waheed, A.; Ahmad, F.; Sly, W. S. *Bioorg. Med. Chem.* **2012**. <http://dx.doi.org/10.1016/j.bmc.2012.04.044>.
- Krishnamurthy, V. M.; Kaufman, G. K.; Urbach, A. R.; Gitlin, I.; Gudiksen, K. L.; Weibel, D. B.; Whitesides, G. M. *Chem. Rev.* **2008**, *108*, 946.
- Sly, W. S.; Hu, P. Y. *Annu. Rev. Biochem.* **1995**, *64*, 375.
- Supuran, C. T. *Nat. Rev. Drug Disc.* **2008**, *7*, 168.
- Supuran, C. T. *Bioorg. Med. Chem. Lett.* **2010**, *20*, 3467.
- Hsieh, M.-J.; Chen, K.-S.; Chiou, H.-L.; Hsieh, Y.-S. *Eur. J. Cell Biol.* **2010**, *89*, 598.
- Hynninen, P.; Parkkila, S.; Huhtala, H.; Pastorekova, S.; Pastorek, J.; Waheed, A.; Sly, W. S.; Tomas, E. *APMIS* **2012**, *120*, 117.
- Pastorekova, S.; Zatovicova, M.; Pastorek, J. *Curr. Pharm. Des.* **2008**, *14*, 685.
- Chiche, J.; Ilc, K.; Laferriere, J.; Trottier, E.; Dayan, F.; Mazure, N. M.; Brahimi-Horn, M. C.; Pouyssegur, J. *Cancer Res.* **2009**, *69*, 358.
- Chien, M.-H.; Ying, T.-H.; Hsieh, Y.-H.; Lin, C.-H.; Shih, C.-H.; Wei, L.-H.; Yang, S.-F. *Oral Oncol.* **2011**, *48*, 417.
- Haapasalo, J.; Hilvo, M.; Nordfors, K.; Haapasalo, H.; Parkkila, S.; Hyrsyluoto, A.; Rantala, I.; Waheed, A.; Sly, W. S.; Pastorekova, S.; Pastorek, J.; Parkkila, A.-K. *Neuro Oncol.* **2008**, *10*, 131.
- Neri, D.; Supuran, C. T. *Nat. Rev. Drug Disc.* **2011**, *10*, 767.
- Ilie, M. I.; Hofman, V.; Ortholan, C.; Ammadi, R. E.; Bonnetaud, C.; Havet, K.; Venissac, N.; Mouroux, J.; Mazure, N. M.; Pouyssegur, J.; Hofman, P. *Int. J. Cancer* **2011**, *128*, 1614.
- Watson, P. H.; Chia, S. K.; Wykoff, C. C.; Han, C.; Leek, R. D.; Sly, W. S.; Gatter, K. C.; Ratcliffe, P.; Harris, A. L. *Br. J. Cancer* **2003**, *88*, 1065.
- Ulmasov, B.; Waheed, A.; Shah, G. N.; Grubb, J. H.; Sly, W. S.; Tu, C.; Silverman, D. N. *Proc. Natl. Acad. Sci. U.S.A.* **2000**, *97*, 14212.
- Whittington, D. A.; Waheed, A.; Ulmasov, B.; Shah, G. N.; Grubb, J. H.; Sly, W. S.; Christianson, D. W. *Proc. Natl. Acad. Sci. U.S.A.* **2001**, *98*, 9545.
- Maresca, A.; Scozzafava, A.; Supuran, C. T. *Bioorg. Med. Chem. Lett.* **2010**, *20*, 7255.
- Carta, F.; Maresca, A.; Scozzafava, A.; Supuran, C. T. *Bioorg. Med. Chem.* **2012**, *20*, 2266.
- Maresca, A.; Temperini, C.; Pochet, L.; Masereel, B.; Scozzafava, A.; Supuran, C. T. *J. Med. Chem.* **2010**, *53*, 335.
- Ladbury, J. E.; Klebe, G.; Freire, E. *Nat. Rev. Drug Disc.* **2010**, *9*, 23.
- Baranauskienė, L.; Matulis, D. *BMC Biophys.* **2012**, *5*, 12.
- Khalifah, R. G.; Zhang, F.; Parr, J. S.; Rowe, E. S. *Biochemistry* **1993**, *32*, 3058.
- Krishnamurthy, V. M.; Bohall, B. R.; Kim, C.-Y.; Moustakas, D. T.; Christianson, D. W.; Whitesides, G. M. *Chem. Asian J.* **2007**, *2*, 94.
- Matulis, D.; Todd, M. J. In *Thermodynamics—Structure Correlations of Sulfonamide Inhibitor Binding to Carbonic Anhydrase*; Ladbury, J. E., Doyle, M. L., Eds.; Wiley, 2004; pp 107–132.
- Cimpmperman, P.; Matulis, D. In *Protein Thermal Denaturation Measurements via A Fluorescent Dye*; Alberto Podjarny, A. D., Kieffer, B., Eds.; RSC Publishing, 2011; pp 247–274. Chapter 8.
- Kranz, J. K.; Schalk-Hihi, C. *Methods Enzymol.* **2011**, *493*, 277.
- Matulis, D.; Kranz, J. K.; Saleme, F. R.; Todd, M. J. *Biochemistry* **2005**, *44*, 5258.
- Mezzasalma, T. M.; Kranz, J. K.; Chan, W.; Struble, G. T.; Schalk-Hihi, C.; Deckman, I. C.; Springer, B. A.; Todd, M. J. *Biomol. Screen.* **2007**, *12*, 418.
- Zubriene, A.; Kazlauskas, E.; Baranauskienė, L.; Petrauskas, V.; Matulis, D. *Eur. Pharm. Rev.* **2011**, *16*, 56.
- Zubriene, A.; Matulienė, J.; Baranauskienė, L.; Jachno, J.; Torresan, J.; Michailoviene, V.; Cimpmperman, P.; Matulis, D. *Int. J. Mol. Sci.* **2009**, *10*, 2662.
- Baker, B. M.; Murphy, K. P. *Biophys. J.* **1996**, *71*(4), 2049.
- Hakansson, K.; Liljas, A. *FEBS Lett.* **1994**, *350*, 319.
- Alterio, V.; Fiore, A. D.; D'Ambrosio, K.; Supuran, C. T.; Simone, G. D. *Chem. Rev.* **2012**, *112*, 4421.
- Kazlauskas, E.; Petrikaitė, V.; Michailoviene, V.; Revuckiene, J.; Matulienė, J.; Grinius, L.; Matulis, D. *PLoS ONE* **2012**, *7*, e36899.

## Intrinsic thermodynamics of sulfonamide inhibitor binding to human carbonic anhydrases I and II

Vaida Morkūnaitė<sup>1</sup>, Joana Glytė<sup>1</sup>, Asta Zubrienė<sup>1</sup>, Lina Baranauskienė<sup>1</sup>, Miglė Kišonaitė<sup>1</sup>, Vilma Michailovienė<sup>1</sup>, Vaida Juozapaitienė<sup>1</sup>, Matthew J. Todd<sup>2</sup>, and Daumantas Matulis<sup>1</sup>

<sup>1</sup>Department of Biothermodynamics and Drug Design, Institute of Biotechnology, Vilnius University, Vilnius, Lithuania and  
<sup>2</sup>Janssen Pharmaceuticals, Johnson & Johnson, Inc., Welsh & Mc.Kean Rds., Springhouse, PA, USA

### Abstract

Human carbonic anhydrase (CA) I and II are cytosolic proteins, where their expression disorders can cause diseases such as glaucoma, edema, epilepsy or cancer. There are numerous inhibitors that target these isozymes, but it is difficult to design compounds that could bind to one of these proteins specifically. The binding of sulfonamide inhibitor to a CA is linked to several protonation reactions, namely, deprotonation of the sulfonamide group, protonation of the active site zinc hydroxide and the compensating protonation–deprotonation of buffer. By performing binding experiments at various pHs and buffers, all those contributions were dissected and the “intrinsic” binding parameters were calculated. Intrinsic thermodynamic binding parameters to CA I and II were determined for such widely studied drugs as acetazolamide, ethoxzolamide, methazolamide, trifluoromethanesulfonamide and dichlorophenamide. The assignment of all contributions should enhance our understanding of the underlying energetics and increase our capability to design more potent and specific CA inhibitors.

### Introduction

Carbonic anhydrases (CAs) are metalloenzymes that catalyze carbon dioxide and water conversion to bicarbonate ion and proton. This reaction occurs slowly at physiological pH [ $k_{\text{CO}_2} = 0.037 (\pm 0.002) \text{ s}^{-1}$ ], but CAs make it faster about  $10^6$  times<sup>1</sup>. Carbon dioxide is an essential metabolite in all living systems, therefore, five different CA classes have been identified in different kingdoms of living organisms:  $\alpha$ -,  $\beta$ -,  $\gamma$ -,  $\delta$ - and  $\zeta$ -CA<sup>2</sup>. They have little chain or structure similarities, but perform the same function<sup>3</sup>.  $\alpha$ -CA is the most investigated of all five classes, because it is most spread and is the only class that is found in human. There are 15 different CA isoforms in human body, only 12 of them are catalytically active<sup>4–6</sup>.

CA I and II are cytosolic CA isoforms, as are CA III, VII and XIII. Three-dimensional structural analysis shows a high degree of structural similarity between CA I and II isoforms<sup>7</sup>. High concentrations of CA I and II isozymes are found in erythrocytes. CA I is the most abundant non-hemoglobin protein in red blood cells and it is important for bone ossification process. However, its overexpression can cause retina and brain edema. CA II is the most spread isoform that has the highest catalytic activity. It is found in almost all organs and tissues but disorder of expression can be a reason of edema, epilepsy, glaucoma or several tumors, such as esophagus, kidney, pulmonary and others<sup>8</sup>. Therefore,

these CA isoforms are important targets for pharmaceutical research.

Numerous compounds have been designed as CA inhibitors. Best known are ligands that have primary sulfonamide group. About 30 of them are used as drugs. However, the main problem is to find an inhibitor that would be selective for one isoform. Design of such inhibitors requires detailed investigation of the structure–activity relationships (SARs) of the new compound. Most inhibitors are only characterized by determining their binding or inhibition constants. We think that it is important to determine the full thermodynamic profile, including the enthalpies and entropies of binding and estimate intrinsic parameters of protein–ligand binding. This would let us more deeply understand the SAR and allow the design of isoform-specific inhibitors<sup>4,9</sup>. Sulfonamide inhibitors bind CAs as anions, whereas they exist in solution at pH 7.0 as electrostatically neutral molecules<sup>10,11</sup>, thus exhibiting linked protonation events upon binding that should be subtracted.

Determination of intrinsic thermodynamic parameters of binding requires predetermination of Zn-bound hydroxy ion protonation parameters by performing numerous experiments by isothermal titration calorimetry (ITC) at various pHs in at least two different buffers. However, it is enough to perform this analysis only once for each CA isoform by using one model inhibitor. Intrinsic parameters of binding of other inhibitors can then be calculated by subtracting protonation contributions<sup>12,13</sup>.

Here, we determine the intrinsic parameters of well-known inhibitors, ethoxzolamide (EZA), trifluoromethanesulfonamide (TFS), acetazolamide (AZM), dichlorophenamide (DCP) and methazolamide (MZM) binding to CA I and CA II isoforms.

### Keywords

Carbonic anhydrase, enthalpy, fluorescent thermal shift assay, intrinsic parameters, isothermal titration calorimetry, ligand binding, thermal shift assay, ThermoFluor

### History

Received 29 January 2014  
Revised 21 March 2014  
Accepted 22 March 2014  
Published online 23 April 2014

Address for correspondence: Daumantas Matulis, Department of Biothermodynamics and Drug Design, Institute of Biotechnology, Vilnius University, Graičiūno 8, Vilnius LT-02241, Lithuania. Tel: +370-5-269-1884. Fax: +370-5-260-2116. E-mail: daumantas.matulis@bti.vu.lt, matulis@ibt.lt



Experiments were performed by ITC and fluorescent thermal shift assay (FTSA) methods.

ITC is the method that can determine the binding constant and binding enthalpy in a single experiment. However, there is a limit of binding constants that can be determined by ITC (about  $10^8 \text{ M}^{-1}$  depending on protein concentration). As some inhibitors bound stronger<sup>6</sup>, the binding constants of all inhibitors were also confirmed by FTSA (also called differential scanning fluorimetry and, in high-throughput format, ThermoFluor<sup>®</sup>). This method measures the increase in protein melting temperature in the presence of the inhibitor<sup>14–18</sup>. FTSA is a rapid screening method, that requires small amounts of proteins and can be applied to nearly all soluble protein–ligand systems<sup>16,17,19–22</sup>. A good agreement between the ITC and ThermoFluor<sup>®</sup> data confirmed the accuracy of binding constant determination by ITC.

## Materials and methods

### Proteins

CA isozymes I and II were purified as described in previous studies<sup>27,28</sup>. For comparison, we used CA isozyme I (from human erythrocytes, cat. # C4396) and II (from human erythrocytes, cat. # C6165) purchased from Sigma Chemical Co, St. Louis, MO. Concentration was determined by dry weight and spectrophotometrically (discrepancy between the methods did not exceed 15%). The observed thermodynamic parameters of inhibitor binding to CA I and II purchased from Sigma and the CAs purified from *Escherichia coli* cells in our laboratory were identical within the error margin of the experiment.

### Inhibitors

EZA was purchased from Aldrich, TFS was purchased from Alfa Aesar and Lancaster Synthesis, AZM, DCP and MZM were purchased from Sigma Chemical Co, St. Louis, MO. All inhibitors were used without further purification. Inhibitors, purchased from different suppliers, bound to the same enzymes with identical affinity.

### Isothermal titration calorimetry

ITC experiments were performed by using VP-ITC and ITC<sub>200</sub> instruments (Microcal, Inc., GE-Healthcare, Northampton, MA). Measurements of protein–ligand binding reactions were performed using 4–20  $\mu\text{M}$  protein solution in the cell and 40–200  $\mu\text{M}$  ligand solution in the syringe. A typical experiment consisted of 25 injections, 10  $\mu\text{L}$  each. Intervals between injections were 2 or 3 min. Experiments were performed at 25 °C in 50 mM sodium phosphate and Tris-chloride buffers, containing 100 mM NaCl and 2% DMSO, concentration equal in the syringe and the cell. For the determination of ligand binding at various pHs, the solution pH was carefully checked in the syringe and cell solution before and after the experiment. ITC data were integrated, fit and analyzed as described previously<sup>29</sup>.

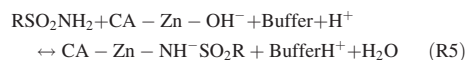
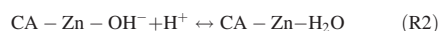
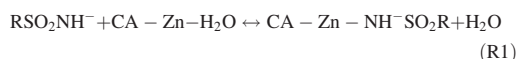
### Fluorescent thermal shift assay

FTSA experiments were performed with Corbett Rotor-Gene 6000 (QIAGEN Rotor-Gene Q, Hilden, Germany) instrument using the blue channel (excitation  $365 \pm 20$ , detection  $460 \pm 15 \text{ nm}$ ), applying the heating rate of 1 °C/min. The samples contained 20  $\mu\text{L}$  of 10  $\mu\text{M}$  protein, 0–400  $\mu\text{M}$  ligand, 50  $\mu\text{M}$  8-anilino-1-naphthalene sulfonate (ANS), 50 mM sodium phosphate at pH 7.0, 50 mM NaCl and 2% DMSO. The pH dependence of the observed binding constant ( $K_b$ ) was determined in the buffer containing 50 mM sodium phosphate, 50 mM sodium acetate and 25 mM sodium borate. The fluorescence and ligand dosing curves were fit as described previously<sup>17,27</sup>.

## Results

### Protonation reactions occurring upon binding

At least three protonation–deprotonation reactions (R2, R3 and R4) accompany the reaction of sulfonamide anion binding to CA (R1). First, the hydroxide ion that bound to zinc atom at the active site, must be protonated (R2). Second, amino group of the sulfonamide must become negatively charged – deprotonated (R3). Third, there will be a compensating protonation or deprotonation of the buffer (R4). Such reactions may be summarized as follows (R – inhibitor chemical groups other than sulfonamide):



Observed thermodynamic parameters represent the sum of all linked events (R5), whereas (R1) is the intrinsic binding reaction, free of protonation–deprotonation contributions representing a displacement of water molecule by a deprotonated inhibitor molecule.

### Observed thermodynamics of inhibitor binding to CA

Chemical structures of sulfonamide inhibitors used in this study are shown in Figure 1. These inhibitors exhibited the observed binding affinities spanning the range from  $10^6$  to  $10^8 \text{ M}^{-1}$  (Table 1). Figure 2 shows several typical FTSA data for inhibitor binding to CA. Figure 2(A) shows the CA II melting curves in the presence of EZA, whereas Figure 2(B) – in the presence of TFS. Figure 2(C) shows the dosing curves obtained from the data in panels A and B. Same concentration of EZA shifted the melting temperature of CA II more than TFS. Therefore, EZA is a stronger binder than TFS at pH 7.0. However, these are only the observed binding parameters.

Binding is highly dependent on buffer and pH. ITC experiments were carried out in buffers of different protonation enthalpy to determine the protonation reactions linked to the binding reaction. ITC curves in Figure 3 illustrate the binding dependence on buffer and its pH. If a net change in protonation occurs upon ligand binding, a corresponding change in buffer protonation should add to the observed enthalpy. We have performed the binding experiments in the sodium phosphate and Tris-chloride buffers at 25 °C. Deprotonation enthalpies of these buffers at this temperature are 5.10 kJ/mol and 47.5 kJ/mol, respectively.

The observed binding constants (observed Gibbs free energies), enthalpies and entropies are listed in Table 1 and in Figure 4. Both the observed binding constants and the observed enthalpies are dependent on pH and buffer. For example, EZA binding to CA I in phosphate buffer was about 10-fold weaker at pH 9.0 than at pH 7.0, but the enthalpy was much more exothermic at pH 9.0 (–75.60 kJ/mol) than at pH 7.0 (–29.07 kJ/mol). In Tris buffer, however, the enthalpy was more exothermic at pH 7.0 (–63.39 kJ/mol) than at pH 9.0 (–46.44 kJ/mol). The trend for CA II was generally similar but had significant differences discussed below.

Furthermore, binding of a given sulfonamide ligand to CA will be strongest at the pH when the ligand is deprotonated and the hydroxide ion bound to zinc is protonated. Therefore, optimal

Figure 1. Chemical structures and abbreviations of the CA inhibitors used in this study. Every inhibitor bears a sulfonamide group that binds to the zinc atom of the CA active site.

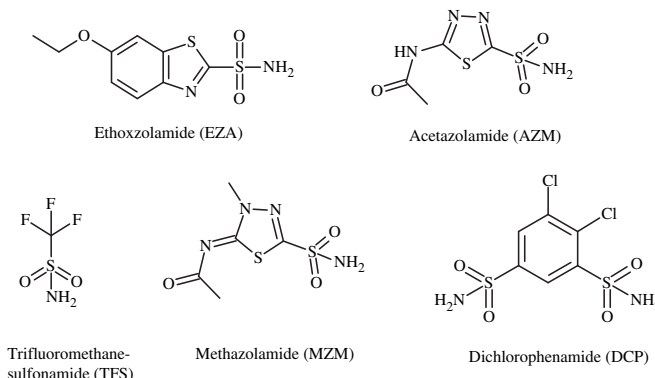


Table 1. The observed thermodynamic parameters of EZA, TFS and AZM binding to CA I and II in phosphate and Tris buffers at various pH, 25°C, determined by ITC.

Compound	pH	$K_{b-obs}$ , M <sup>-1</sup>	$\Delta_b G_{obs}$ , kJ/mol	$\Delta_b H_{obs}$ , kJ/mol	$T\Delta_b S_{obs}$ , kJ/mol
CA I, Phosphate buffer					
EZA	6.6	$3.59 \times 10^7$	-43.12	-27.42	15.70
	7.0	$2.55 \times 10^7$	-42.28	-29.07	13.21
	7.9	$1.68 \times 10^7$	-41.24	-44.10	-2.86
	9.0	$4.12 \times 10^6$	-37.76	-75.60	-37.84
TFS	7.0	$2.58 \times 10^7$	-42.31	-53.10	-10.79
AZM	7.0	$1.19 \times 10^6$	-34.68	-44.70	-10.02
MZM	7.0	$1.14 \times 10^7$	-40.29	-44.43	-4.14
DCP*	7.0	$1.85 \times 10^6$	-35.77	-32.34	3.43
CA I, Tris buffer					
EZA	6.6	$2.98 \times 10^7$	-42.66	-65.52	-22.86
	7.0	$5.31 \times 10^7$	-44.09	-63.39	-19.30
	7.9	$2.22 \times 10^7$	-41.93	-61.38	-19.45
	9.0	$1.74 \times 10^7$	-41.33	-46.44	-5.11
CA II, Phosphate buffer					
EZA	6.0	$2.59 \times 10^8$	-48.02	-49.29	-1.27
	7.0	$7.00 \times 10^7$	-44.76	-64.68	-19.92
	7.5	$1.94 \times 10^8$	-47.30	-70.79	-23.49
	7.9	$1.99 \times 10^8$	-47.37	-82.59	-35.22
TFS	7.0	$4.84 \times 10^7$	-43.86	-35.53	8.33
AZM	7.0	$5.91 \times 10^7$	-44.36	-53.35	-8.99
MZM	7.0	$2.89 \times 10^7$	-43.76	-52.05	-8.29
DCP*	7.0	$8.19 \times 10^7$	-45.17	-27.20	17.97
CA II, Tris buffer					
EZA	6.0	$1.45 \times 10^8$	-46.58	-87.11	-40.53
	6.9	$2.91 \times 10^8$	-48.31	-74.39	-26.08
	7.4	$5.30 \times 10^7$	-44.09	-70.96	-26.87
	7.9	$2.48 \times 10^8$	-47.92	-63.64	-15.72

\*Thermodynamic parameters of DCP binding to CA I and II from Sigma. Uncertainty of the  $\Delta_b G_{obs}$  is  $\pm 4$  kJ/mol,  $\Delta_b H_{obs}$  is  $\pm 4$  kJ/mol and  $T\Delta_b S_{obs}$  is  $\pm 6$  kJ/mol.

binding is in the pH region between the respective  $pK_a$ s when  $pK_a\text{-sulfonamide} < pK_a\text{-Zn-water}$ . When pH is below the  $pK_a\text{-sulfonamide}$  or above the  $pK_a\text{-Zn-water}$ , then the binding is weaker. The observed binding constant  $K_{b-obs}$  is equal to the intrinsic binding constant  $K_b$  multiplied by the available fractions of deprotonated inhibitor and protonated zinc hydroxy anion:

$$K_{b-obs} = K_b f_{RSO_2NH^-} f_{CAZnH_2O} \quad (1)$$

The Gibbs free energy in turn is:

$$\Delta_{b-obs} G = -RT \ln(K_b f_{RSO_2NH^-} f_{CAZnH_2O}) \quad (2)$$

Fraction of deprotonated sulfonamide can be calculated when the protonation  $pK_a$  is known:

$$f_{RSO_2NH^-} = \frac{10^{pH-pK_{a,sulfonamide}}}{1 + 10^{pH-pK_{a,sulfonamide}}} = 1 - \frac{10^{pK_{a,sulfonamide}-pH}}{1 + 10^{pK_{a,sulfonamide}-pH}} \quad (3)$$

Similarly, the fraction of enzyme molecules with protonated water molecules bound to the active site Zn atom can be calculated if respective protonation  $pK_a$  is known:

$$f_{CAZnH_2O} = 1 - \frac{10^{pH-pK_{a,Zn-water}}}{1 + 10^{pH-pK_{a,Zn-water}}} = \frac{10^{pK_{a,Zn-water}-pH}}{1 + 10^{pK_{a,Zn-water}-pH}} \quad (4)$$

Figure 5 shows the pH dependence of the observed binding constants obtained by using FTSA and ITC methods. Both methods yielded similar pH dependence as seen for TFS binding to CA I. However, due to high EZA affinity to CA II at pH range from 7.5 to 8.5, it was difficult to observe the binding constants by ITC because the Wiseman ( $c = K_b \times C$ , where  $C$  is protein molar concentration) factor falls out of the useful range of 5–500.

The binding constant does not depend on the chemical nature of the buffer provided that the buffer does not bind the ligand or the protein. There was essentially no difference between the binding Gibbs free energies obtained in phosphate and Tris buffers.

The intrinsic enthalpy of binding has contributions from the observed binding enthalpy ( $\Delta_b H_{obs}$ ), enthalpies of inhibitor ( $\Delta_{b\_proton\_inh}H$ ), CA ( $\Delta_{b\_proton\_CA}H$ ) and the buffer protonation ( $\Delta_{b\_proton\_buf}H$ ):

$$\Delta_b H = \Delta_b H_{obs} - n_{inh} \Delta_{b\_proton\_inh}H - n_{CA} \Delta_{b\_proton\_CA}H + n \Delta_{b\_proton\_buf}H$$

where:

$$\begin{aligned} n_{inh} &= f_{RSO_2NH^-} - 1 \\ n_{CA} &= 1 - f_{CAZnH_2O} \\ n &= n_{inh} + n_{CA} \end{aligned} \quad (6)$$

### Energetics of inhibitor protonation

Equation (R3) represents the deprotonation of the sulfonamide group. Only the deprotonated sulfonamide form is thought to bind to the CA<sup>23</sup>. The ionization form of inhibitor depends on the  $pK_a$  and pH of the solution. Most sulfonamide inhibitors are protonated at physiological pH and must undergo a linked deprotonation reaction upon binding to the protein.

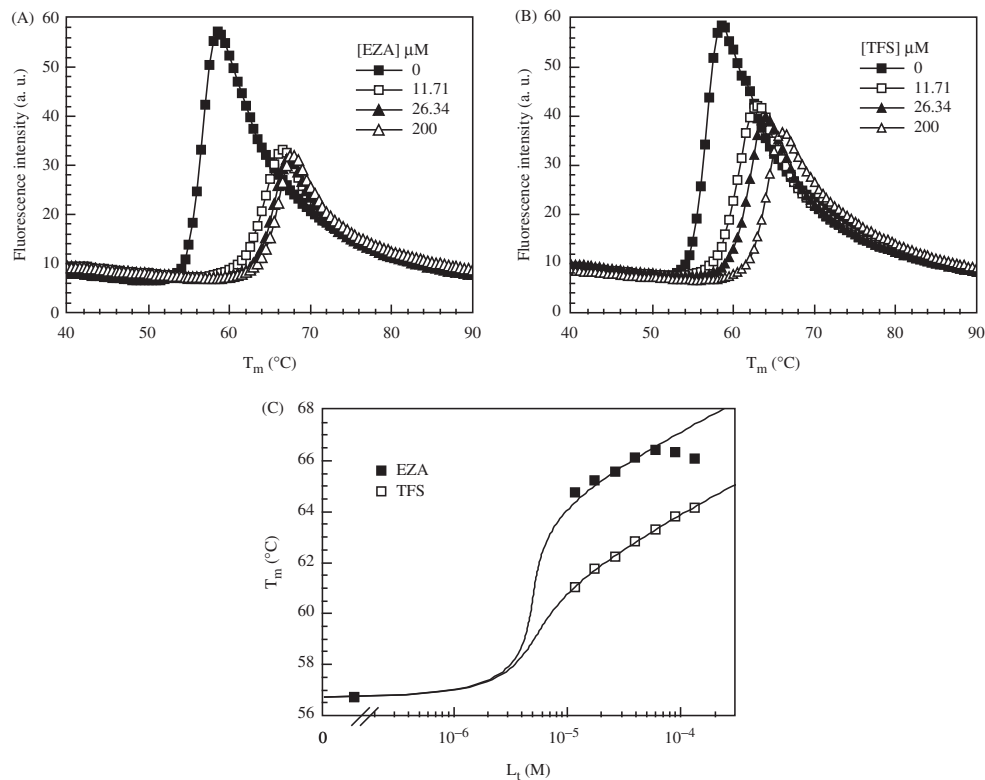


Figure 2. EZA and TFS binding to CA II observed by FTSA at pH 7.0. (A) and (B) show the protein melting fluorescence curves at several added concentrations of EZA and TFS, respectively. (C) Shows the dependence of the protein melting temperatures  $T_m$  on the added compound concentrations. Datapoints are the experimental values obtained from the upper graphs and the solid lines are simulated according to the model as described in the methods.

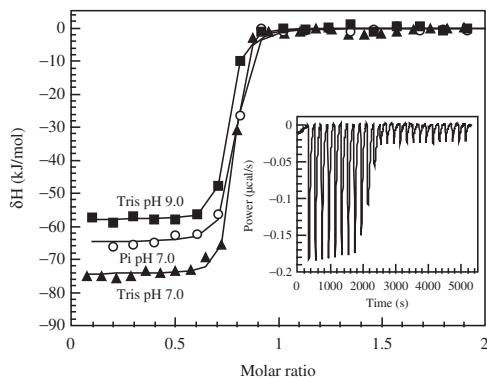


Figure 3. ITC data shows EZA binding to CA II dependence on buffer solution and pH value at the same temperature (25 °C). Integrated curves show observed data in Tris-chloride buffer at pH 7.0 (filled triangle) and pH 9.0 (filled square) and sodium phosphate buffer at pH 7.0 (open circle). The inset shows raw ITC curve in Tris-chloride buffer, pH 7.0, 25 °C.

The inhibitor protonation enthalpy is observed by titrating alkaline solution of the inhibitor (1.5 equivalent of base was added) with acid (Figure 6). The enthalpy of the second transition is equal to the enthalpy of inhibitor protonation. The first transition is due to neutralization of 0.5 equivalent of NaOH.

The same solutions and volumes as in the calorimetric experiments were used for potentiometric titration by using a pH-meter. A function describing two transitions was derived according to another study<sup>24</sup> and curves were simulated to match the experimental datapoints. Two representative titration curves are shown in Figure 6(C). The midpoint of the second transition matches the  $pK_a$  of the inhibitor.

The heat capacities of sulfonamide protonation were also determined by carrying out the ITC titration at different temperatures (Figure 6D). The slope of the enthalpy dependence on temperature is equal to the heat capacity of inhibitor protonation.

TFS has a  $pK_a$  of 6.25; therefore, at pH 7.0, almost all of the inhibitor exists in a negatively charged form (fraction = 0.91) and the affinity to CA is strong. The  $pK_a$  values of other measured inhibitors were  $>7$ . The enthalpies of inhibitor protonation (25 °C) were quite similar ( $-22.4$  to  $-29.5$  kJ/mol). Entropies of protonation were from 13.3 to 18.7 kJ/(mol  $\times$  K).

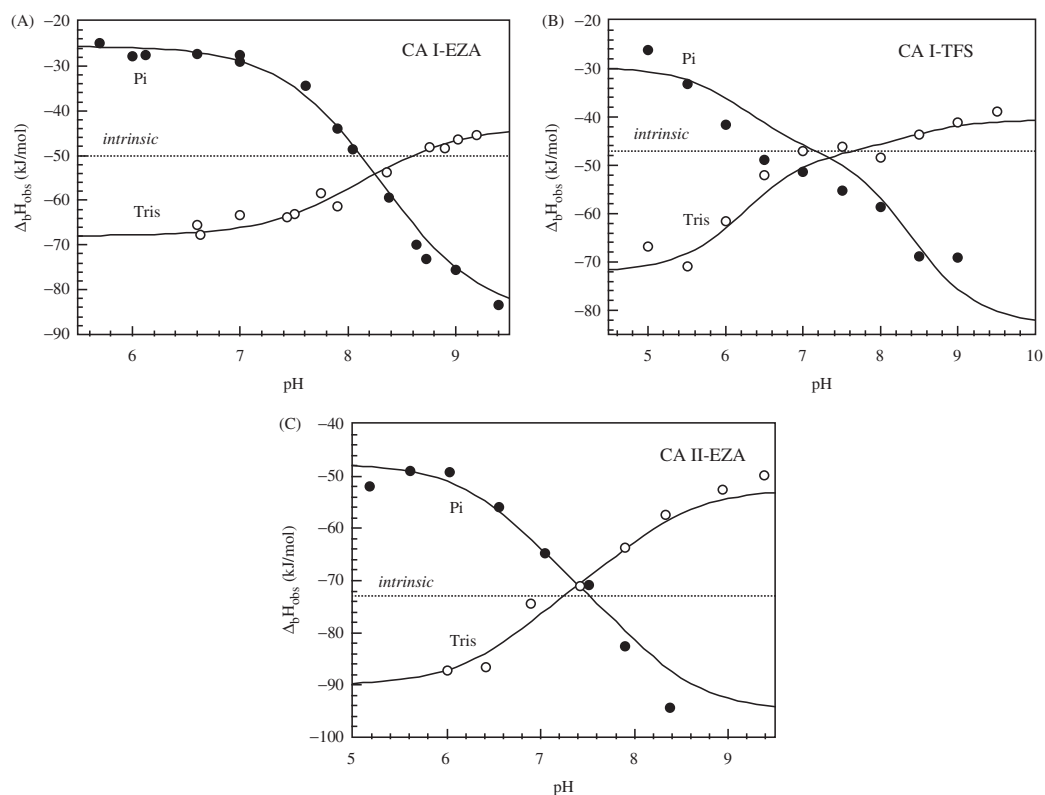


Figure 4. The observed enthalpies of binding are shown as a function of buffer pH. Panel A: CA I-EZA, Panel B: CA I-TFS and Panel C: CA II-EZA. Filled circles show the observed binding enthalpies in sodium phosphate buffer, open circles show binding enthalpies observed in Tris-chloride buffer. Experiments were performed by ITC at 25°C. Dotted line represents the intrinsic binding enthalpy. Curves are fit according to Equation (5).

The thermodynamic parameters of EZA and TFS protonation have been previously described<sup>12</sup>. Parameters for AZM, MZM have been described in other studies<sup>23,25</sup>, DCP also<sup>25</sup> and are consistent with these results.

#### Energetics of zinc hydroxy anion protonation

The hydroxy anion bound to the active site Zn must be protonated (electrostatically neutral) in order for the sulfonamide inhibitor binding reaction to occur. Equation (R2) shows this reaction. Table 2 lists the thermodynamic parameters of protonation of the hydroxide bound to Zn atom. The  $pK_a$  of CA II was found to be 7.1. However, the  $pK_a$  of CA I was significantly higher, = 8.4. Therefore, the Gibbs free energies of reaction (R2) for CA I and II differed by about 5 kJ/mol.

The enthalpies of (R2) for CA I and II were  $-41$  kJ/mol and  $-26$  kJ/mol, respectively. Thus, the enthalpy was slightly more exothermic for CA I than for CA II. The entropies were also contributing favorably to the protonation reaction. Comparison of observed parameters shows that the entropy contribution to the CA I protonation was greater than to CA II.

Comparing the thermodynamics of (R2) for CA I and II with other CAs (Table 2), it is clear that the  $pK_a$  of CA I is similar to the  $pK_a$  of CA XIII, whereas that of CA II to CA VII and XII. However, there is no clear  $pK_a$  correlation with the enthalpy and entropy of hydroxy anion protonation. The enthalpies varied from

$-26$  to  $-41$  kJ/mol, whereas the entropies varied from 5.3 to 21.1 kJ/mol. The process of protonation is primarily enthalpy-driven but also has smaller favorable entropy contribution.

#### Intrinsic thermodynamics of binding parameters

Table 3 lists the intrinsic thermodynamic parameters of inhibitor binding to CA I and II. These parameters are independent of pH, buffer and linked protonation events. Intrinsic binding constants of CA II are greater than the observed  $K_b$  values by about one order of magnitude except for EZA. However, the difference of intrinsic and observed binding constants for CA I is generally smaller than for CA II. Inhibitors bound tighter to CA II than to CA I by about an order of magnitude. This difference may be due to the different recognition of the surface of the binding pocket. The difference is not due to the linked protonation events and thus may be correlated to structure. In terms of Gibbs free energy, it is clear that TFS, MZM and DCP bind to CA I with nearly identical intrinsic affinity of  $-42.9$  to  $-43.9$  kJ/mol. The value for AZM is also quite similar ( $-37.8$  kJ/mol), but EZA bound significantly tighter ( $-51.4$  kJ/mol). Similar tendency is also observed for CA II. All these values differed significantly from the observed Gibbs free energies.

Inhibitor binding was enthalpy driven and had relatively negligible entropic contribution to binding except intrinsic thermodynamic parameters of DCP binding to CA II.

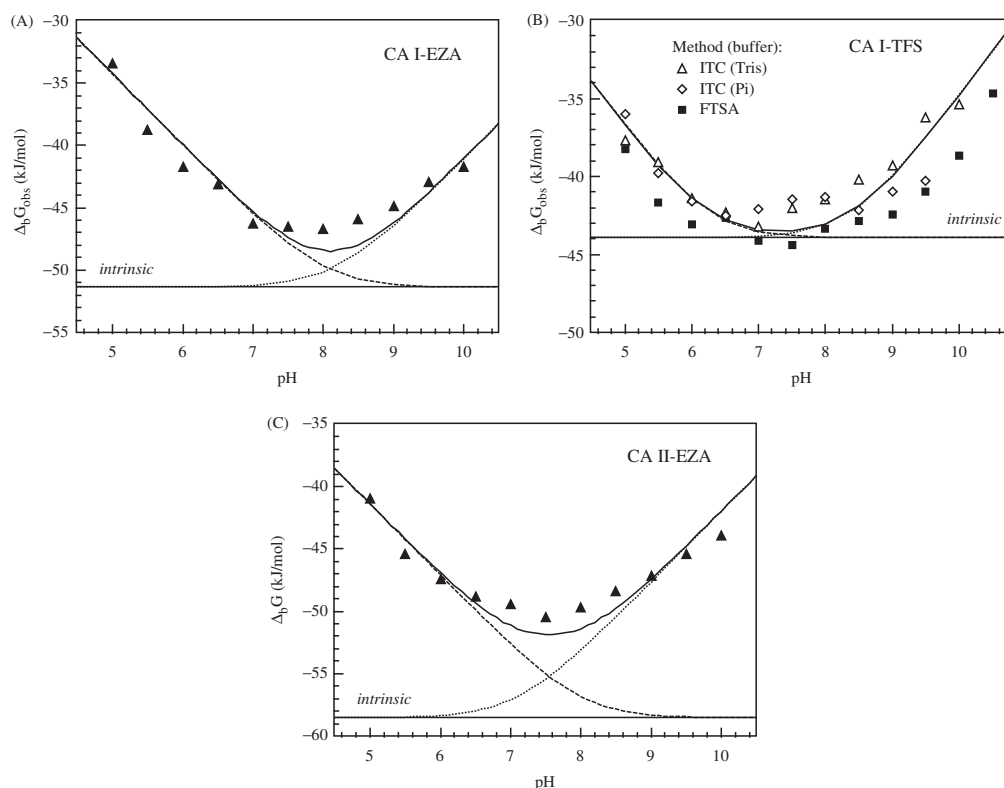


Figure 5. The observed Gibbs free energy ( $\Delta_p G_{obs}$ ) of EZA (Panel A) and TFS (Panel B) binding to CA I, and EZA binding to CA II (Panel C) at various pH. TFS binding to CA I was determined by ITC in Tris-chloride (open triangle, Panel B) and sodium phosphate (open diamond) buffers and by FTSA (filled square). EZA binding to CA I and CA II was performed by FTSA (Panels A and C). Solid line shows the fit according to Equation (2) using parameters listed in tables. Dashed and dotted lines show the contributions of deprotonated ligand and protonated CA, respectively. Straight line shows the intrinsic Gibbs free energy of binding.

## Discussion

Structure–activity relationships in drug design are usually limited to the analysis of enzyme inhibition constants or inhibitor binding constants. However, other thermodynamic parameters describing protein–inhibitor interaction, such as enthalpy, entropy, heat capacity and volume add significant information for inhibitor improvement and may lead to the design of drugs with better properties of target binding<sup>9,26</sup>.

Thermodynamic parameters of ligand–protein binding are often thought to be determinable by a single titration calorimetry experiment. Unfortunately, most such determinations cannot be understood in terms of structural features of protein–ligand interface. Instead, a detailed study is needed to be able to correlate binding parameters with structure. First, it is necessary to perform experiments in various buffers to show that there are no linked protonation–deprotonation reactions. Only if there are no linked reactions one can relate such parameters to structure. In reality, even the simplest reactions of one inhibitor molecule binding to a specific site on a protein is usually linked to a series of complicated protonation–deprotonation and other reactions such as conformational changes or other ion binding.

CA–sulfonamide inhibitor binding is linked to at least three protonation reactions. Their impact on observed thermodynamic parameters is very significant. Without the dissection of the linked

reactions, the structural reason for the observed parameters cannot be understood. The enthalpy of hydroxide or amino group protonation ( $-40$  to  $-50$  kJ/mol) is comparable with the enthalpy of binding.

The contributing linked reactions of MZM binding to CA I were determined earlier<sup>23</sup>. Their obtained enthalpy of MZM binding to CA I ( $-56.5$  kJ/mol) is close to our intrinsic enthalpy ( $-56.9$  kJ/mol) (Table 3). The  $pK_a$  of zinc hydroxide protonation was assumed to be the same as that of the CA I containing cobalt atom in the active site. The presence of cobalt enabled  $pK_a$  determination by spectral methods. The Co hydroxide protonation  $pK_a$  was equal to  $7.41 \pm 0.04$ . Our determined zinc hydroxide  $pK_a$  in CA I was  $= 8.4$ . Therefore, an assumption that Co and Zn enzymes will have the same  $pK_a$  is not correct. Furthermore, our results show that CA I and CA II zinc hydroxide  $pK_a$ s differ significantly (it is  $= 7.1$  for CA II).

Interestingly, DCP-bound CA I with the negative entropy ( $T\Delta_p S_{int} = -11.7$  kJ/mol) while CA II with the positive entropy ( $16.2$  kJ/mol). Furthermore, DCP bound stronger to CA II than to CA I, but the enthalpy was more exothermic for the binding to CA I. There is no clear reason for such behavior, but there is enthalpy–entropy compensation effect.

Thermodynamic dissection of contributing linked reactions should improve the design of CA inhibitors. The major contributor to the binding weakness of some of the studied inhibitors is a

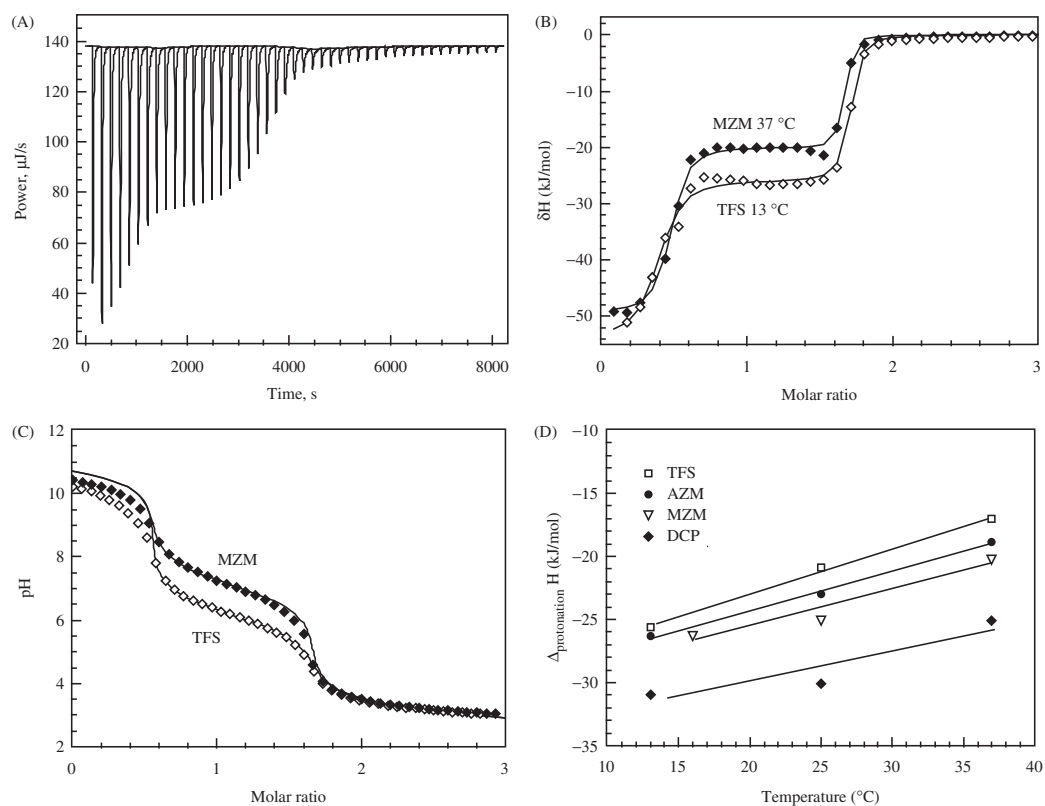


Figure 6. Panel A – representative raw ITC data of alkaline inhibitor (MZM) protonation with HCl at 25°C. About 1.5 equivalents of NaOH were added to the neutral inhibitor solution. Concentrations and volumes used for ITC experiments were identical to pH titration experiments shown in Panel C. First portion of the titration curve represents the reaction between  $H^+$  and excess  $OH^-$ . The second portion of the titration curve having the stoichiometry of 1.0 represents the inhibitor protonation. Solid line is the baseline. Panel B – integrated ITC curves of TFS (open diamond) at 13°C and MZM (filled diamond) at 37°C titration with HCl. The enthalpy of the first portion of the titration (stoichiometry  $\sim 0.5$ ,  $\Delta H \sim -54$  kJ/mol) is a value close to the expected value for the reaction of  $H^+ + OH^- = H_2O$ . The enthalpy of the second portion of the titration curve (stoichiometry  $\sim 1.0$ ) represents the enthalpy of sulfonamide protonation. Panel C – the pH titration curves for MZM (filled diamond) and TFS (open diamond), determined potentiometrically at 24°C. Concentrations and volumes were identical to ITC experiments (panels A and B). Two transitions are seen: 0.5 equivalent of  $H^+$  reaction with  $OH^-$ , and one equivalent of sulfonamide protonation. The  $pK_a$  is approximately equal to the pH at the midpoint of the second stage of the titration. Datapoints are experimental pH values and the line is fit according to another study<sup>24</sup>. Panel D – the temperature dependence of inhibitor sulfonamide group protonation (reaction R3 in reverse) enthalpy as determined by ITC. Datapoints are experimentally determined integral enthalpies for, TFS (open square), AZM (filled circle), MZM (inverted open triangle), and DCP (filled diamond). Lines are linear fits of the experimental data. Slopes of the lines are positive and equal to the heat capacities of about  $190\text{--}290$   $J \times mol^{-1} K^{-1}$ .

Table 2. Thermodynamic parameters of inhibitor sulfonamide groups and also CA I and CA II Zn-bound hydroxide anion protonation at 25°C.

Inhibitor/protein	$pK_a$	$\Delta G_{prot}$ , kJ/mol	$\Delta H_{prot}$ , kJ/mol	$T\Delta S$ , kJ/mol
EZA*	8.0	-45.7	-29.5	16.2
TFS†	6.25	-35.7	-22.4	13.3
AZM‡	7.3	-41.7	-23.0	18.7
MZM‡	7.1	-40.5	-25.1	15.4
DCP‡	8.2	-46.8	-29.3	17.5
CA I-Zn-H <sub>2</sub> O	8.4	-46.3	-41.0	5.3
CA II-Zn-H <sub>2</sub> O	7.1	-40.5	-26.0	14.5
CA VII-Zn-H <sub>2</sub> O‡	7.0	-40.0	-33.0	7.0
CA XII-Zn-H <sub>2</sub> O¶	7.0	-40.0	-28.0	12.0
CA XIII-Zn-H <sub>2</sub> O*	8.3	-47.1	-26.0	21.1

\*Data taken from Reference<sup>12</sup>.

†Data taken from Reference<sup>25</sup>.

‡Data taken from Reference<sup>30</sup>.

¶Data taken from Reference<sup>13</sup>.

large  $pK_a$  of inhibitor deprotonation. It should be advantageous to design inhibitors with  $pK_a$ s < 8. This may be achieved by introducing electron withdrawing groups on the inhibitor molecule.

Specificity and selectivity of the studied inhibitors is limited. There is about  $10 \times$  preference to bind CA II over CA I. Apparently, large differences in chemical structures of ligands such as TFS and MZM actually lead to very small differences in intrinsic binding constants. Instead, most of the difference lies in the deprotonation of sulfonamide group necessary for the binding to occur. In order to be more specific, inhibitors need to bear larger structural differences.

## Conclusions

Dissection of all contributing reactions to the observed thermodynamics of inhibitor binding to a protein is necessary in order to

Table 3. Intrinsic thermodynamic parameters of deprotonated inhibitor binding to CA I and CA II containing the protonated Zn-bound water molecule at 25°C.

Inhibitor	$\Delta_p H_{intr}$ kJ/mol	$K_{b\ intr}$ M <sup>-1</sup>	$\Delta_p G_{intr}$ kJ/mol	$T\Delta_p S_{intr}$ kJ/mol
CA I				
EZA	-50.0	$1.0 \times 10^9$	-51.4	1.4
TFS	-47.0	$5.0 \times 10^7$	-43.9	-3.1
TFS*	-49.0	$4.0 \times 10^7$	-43.4	-5.6
AZM*	-48.1	$4.2 \times 10^6$	-37.8	-10.3
MZM*	-56.9	$3.3 \times 10^7$	-42.9	-14.0
DCP*	-54.8	$3.5 \times 10^7$	-43.1	-11.7
CA II				
EZA	-73.0	$1.8 \times 10^{10}$	-58.5	-14.5
TFS	-36.7	$1.0 \times 10^8$	-45.7	9.0
TFS*	-36.8	$2.0 \times 10^8$	-47.4	10.6
AZM	-56.0	$3.5 \times 10^8$	-48.8	-7.2
AZM*	-59.8	$4.8 \times 10^8$	-49.5	-10.3
MZM	-47.8	$1.3 \times 10^8$	-46.4	-1.4
MZM*	-53.6	$2.2 \times 10^8$	-47.6	-6.0
DCP*	-38.5	$3.8 \times 10^9$	-54.7	16.2

\*Thermodynamic parameters of inhibitor binding to CA purchased from Sigma.

correlate the thermodynamic parameters with the structure of the protein–ligand complex. Sulfonamide inhibitors bound stronger to CA II isozyme than to CA I. An especially large difference of about two orders of magnitude was observed for AZM. The smallest difference among the two isozymes was observed for TFS binding. The major difference in affinities of the inhibitors lay within the differences of sulfonamide group p*K*<sub>s</sub>. For all ligands, the binding was enthalpy driven.

#### Declaration of interest

The authors report no conflict of interest. This research was funded by the European Social Fund under the Global Grant measure (no. VP1-3.1.-SMM-07-K-02-009). Authors thank FP7-REGPOT-2009-1 grant 'MoBiLi' agreement No.: 245721 and the COST projects TD0905 and CM0804.

#### References

- Khalifah RG. The carbon dioxide hydration activity of carbonic anhydrase. i. stop-flow kinetic studies on the native human isoenzymes b and c. *J Biol Chem* 1976;246:2561–73.
- Xu Y, Feng L, Jeffrey PD, et al. Structure and metal exchange in the cadmium carbonic anhydrase of marine diatoms. *Nature* 2008;452:56–61.
- Supuran CT. Carbonic anhydrase inhibitors. *Bioorg Med Chem Lett* 2010;20:3467–74.
- Krishnamurthy VM, Kaufman GK, Urbach AR, et al. Carbonic anhydrase as a model for biophysical and physical-organic studies of proteins and protein-ligand binding. *Chem Rev* 2008;108:946–1051.
- Sly WS, Hu PY. Human carbonic anhydrases and carbonic anhydrase deficiencies. *Annu Rev Biochem* 1995;64:375–401.
- Supuran CT. Carbonic anhydrases: novel therapeutic applications for inhibitors and activators. *Nat Rev Drug Discov* 2008;7:168–81.
- Hassan I, Shajee B, Waheed A, et al. Structure, function and applications of carbonic anhydrase isozymes. *Bioorg Med Chem* 2013;21:1570–82.
- Alterio V, Di Fiore A, D'Ambrosio K, et al. Multiple binding modes of inhibitors to carbonic anhydrases: how to design specific drugs targeting 15 different isoforms? *Chem Rev* 2012;112:4421–68.
- Ladbury JE, Klebe G, Freire E. Adding calorimetric data to decision making in lead discovery: a hot tip. *Nat Rev Drug Discov* 2010;9:23–7.
- King RW, Burgen AS. Kinetic aspects of structure-activity relations: the binding of sulphonamides by carbonic anhydrase. *Proc R Soc Lond B Biol Sci* 1976;193:107–25.
- Kumar K, King RW, Carey PR. Carbonic anhydrase-aromatic sulfonamide complexes, a resonance raman study. *FEBS Lett* 1974;48:283–87.
- Baranauskienė L, Matulis D. Intrinsic thermodynamics of ethoxzolamide inhibitor binding to human carbonic anhydrase XIII. *BMC Biophys* 2012;5:12.
- Jogaite V, Zubriene A, Michailoviene V, et al. Characterization of human carbonic anhydrase XII stability and inhibitor binding. *Bioorg Med Chem* 2013;21:1431–6.
- Pantoliano MW, Petrella EC, Kwasnoski JD, et al. High-density miniaturized thermal shift assays as a general strategy for drug discovery. *J Biomol Screen* 2001;6:429–40.
- Todd MJ, Salemme FR. Direct binding assays for pharma screening. *Genetic Eng News* 2003;23:28–9.
- Kranz JK, Schalk-Hihi C. Protein thermal shifts to identify low molecular weight fragments. *Methods Enzymol* 2011;493:277–98.
- Cimpmperman P, Matulis D. Protein thermal denaturation measurements via a fluorescent dye. Cambridge, UK: RSC Publishing; 2011, Ch. 8, pp. 247–74.
- Niesen FH, Berglund H, Vedadi M. The use of differential scanning fluorimetry to detect ligand interactions that promote protein stability. *Nat Protoc* 2007;2:2212–21.
- Zubriene A, Matulienė J, Baranauskienė L, et al. Measurement of nanomolar dissociation constants by titration calorimetry and thermal shift assay – radicicol binding to Hsp90 and ethoxzolamide binding to CA II. *Int J Mol Sci* 2009;10:2662–80.
- Matulis D, Kranz JK, Salemme FR, Todd MJ. Thermodynamic stability of carbonic anhydrase: measurements of binding affinity and stoichiometry using thermofluor. *Biochemistry* 2005;44:5258–66.
- Mezzasalma TM, Kranz JK, Chan W, et al. Enhancing recombinant protein quality and yield by protein stability profiling. *J Biomol Screen* 2007;12:418–28.
- Zubriene A, Kazlauskas E, Baranauskienė L, et al. Isothermal titration calorimetry and thermal shift assay in drug design. *Eur Pharmaceut Rev* 2011;16:56–9.
- Khalifah RG, Zhang F, Parr JS, Rowe E. Thermodynamics of binding of the CO<sub>2</sub>-competitive inhibitor imidazole and related compounds to human carbonic anhydrase I: an isothermal titration calorimetry approach to studying weak binding by displacement with strong inhibitors. *Biochemistry* 1993;32:3058–66.
- Butler JN, Cogley DR. Ionic equilibrium. Solubility and pH calculations. New-York: John Wiley and Sons Inc.; 1998.
- Matulis D, Todd MJ. Thermodynamics-structure correlations of sulfonamide inhibitor binding to carbonic anhydrase. Chichester, England: John Wiley & Sons; 2004, Ch. 6, pp. 107–32.
- Ladbury JE. Calorimetry as a tool for understanding biomolecular interactions and an aid to drug design. *Biochem Soc Trans* 2010;38:888–93.
- Baranauskienė L, Hilvo M, Matulienė J, et al. Inhibition and binding studies of carbonic anhydrase isozymes I, II, and IX with benzimidazo[1,2-c][1,2,3]thiadiazole-7-sulphonamides. *J Enzyme Inhib Med Chem* 2010;25:863–70.
- Cimpmperman P, Baranauskienė L, Jachimovičiūtė S, et al. A quantitative model of thermal stabilization and destabilization of proteins by ligands. *Biophys J* 2008;95:3222–31.
- Kazlauskas E, Petrikaite V, Michailoviene V, et al. Thermodynamics of aryl-dihydroxyphenyl-thiadiazole binding to human Hsp90. *PLoS One* 2012;7:e36899.
- Pilipuityte V, Matulis D. Intrinsic thermodynamics of trifluoromethanesulfonamide and ethoxzolamide binding to human carbonic anhydrase VII. Submitted.



Contents lists available at ScienceDirect

Biochimica et Biophysica Acta

journal homepage: [www.elsevier.com/locate/bbagen](http://www.elsevier.com/locate/bbagen)

## Intrinsic thermodynamics of inhibitor binding to human carbonic anhydrase IX



Vaida Linkuvienė, Jurgita Matulienė, Vaida Juozapaitienė, Vilma Michailovienė, Jelena Jachno, Daumantas Matulis\*

Department of Biothermodynamics and Drug Design, Institute of Biotechnology, Vilnius University, Graičiūno 8, Vilnius LT-02241, Lithuania

### ARTICLE INFO

#### Article history:

Received 11 November 2015  
Received in revised form 30 December 2015  
Accepted 12 January 2016  
Available online 18 January 2016

#### Keywords:

Intrinsic thermodynamics of protein–ligand binding  
Carbonic anhydrase  
Benzenesulfonamide inhibitors  
Fluorescent thermal shift assay  
Isothermal titration calorimetry  
Drug design

### ABSTRACT

**Background:** Human carbonic anhydrase 9th isoform (CA IX) is an important marker of numerous cancers and is increasingly interesting as a potential anticancer drug target. Various synthetic aromatic sulfonamide-bearing compounds are being designed as potent inhibitors of CA IX. However, sulfonamide compound binding to CA IX is linked to several reactions, the deprotonation of the sulfonamide amino group and the protonation of the CA active site Zn(II)-bound hydroxide. These linked reactions significantly affect the affinities and other thermodynamic parameters such as enthalpies and entropies of binding.

**Methods:** The observed and intrinsic affinities of compound binding to CA IX were determined by the fluorescent thermal shift assay. The enthalpies and entropies of binding were determined by the isothermal titration calorimetry.

**Results:** The  $pK_a$  of CA IX was determined to be 6.8 and the enthalpy of CA IX–Zn(II)-bound hydroxide protonation was  $-24$  kJ/mol. These values enabled the analysis of intrinsic thermodynamics of a library of compounds binding to CA IX. The most strongly binding compounds exhibited the intrinsic affinity of 0.01 nM and the observed affinity of 2 nM.

**Conclusions:** The intrinsic thermodynamic parameters of compound binding to CA IX helped to draw the compound structure to thermodynamics relationship.

**General significance:** It is important to distinguish the intrinsic from observed parameters of any disease target protein interaction with its inhibitors as drug candidates when drawing detailed compound structure to thermodynamics correlations.

© 2016 Elsevier B.V. All rights reserved.

### 1. Introduction

The measurements of the affinity of protein–ligand interaction are an important phase of target-based rational drug design. Compound hits from the high-throughput screening are often ranked according to their affinities towards the disease targets. However, often there are various binding-linked reactions, primarily protonation reactions, that affect the observed affinity. Therefore it is important to distinguish the ‘intrinsic’ affinity from the ‘observed’ affinity. Furthermore, it is important to select the lead binders not only according to their affinities but also according to other thermodynamic parameters of binding, primarily enthalpy and entropy [1]. Here we determine the intrinsic binding enthalpies, entropies and Gibbs energies (affinities) of a series of substituted benzenesulfonamides to carbonic anhydrase IX (CA IX) and characterize this anticancer target protein.

CA IX is a zinc-containing metalloenzyme that reversibly converts carbon dioxide to bicarbonate ion and acid protons. It is one of the 12 catalytically active CA isoforms present in the human body. The protein is composed of several domains: the signaling sequence, the proteoglycan (PG) domain, the catalytic domain, transmembrane helix and an intracellular domain. The PG domain is required for focal adhesion of tumor cells [2]. The catalytic activity of CA IX is similar to or slightly exceeds that of CA II [3–8]. The expression of CA IX occurs only in few normal human tissues, the gastrointestinal tract epithelium [9–11], ovarian coelomic epithelium, pancreatic ductal cells, cells of the hair follicles and fetal rete testis [12,13]. In most cases, CA IX expression is strongly associated with tumors [9,14]. Increased CA IX expression has been shown to participate in the acidification of the extracellular environment [15] and help tumor cells survive, migrate and invade [2].

The most common CA inhibitors are various sulfonamides, many of them are clinically used to treat diseases related to unbalanced expression of CAs [16]. Novel CA inhibitors were often designed by attaching a tail to the pharmacophoric benzenesulfonamide headgroup [17–19]. Benzenesulfonamide makes hydrogen bonds with the zinc ion and

\* Corresponding author.

E-mail addresses: [daumantas.matulis@bti.vu.lt](mailto:daumantas.matulis@bti.vu.lt), [matulis@ibt.lt](mailto:matulis@ibt.lt) (D. Matulis).



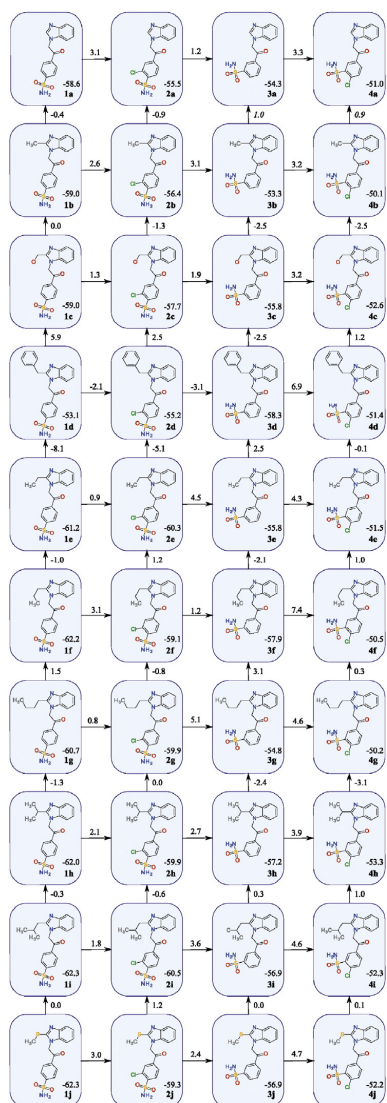


**Fig. 1.** Correlation map of the inhibitor chemical structures with their intrinsic binding affinities ( $\Delta_b G_{intr}$ ) to CA IX. Numbers within compound boxes show the  $\Delta_b G_{intr}$  calculated from FTSA data, while the numbers next to the arrows show the differences between closely structurally related compounds.

Thr199 [20] while different substituents interact with other residues and solvent molecules in the CA active site [19,18,21].

CA IX has become an attractive therapeutic target since the first report showing that the inhibition of this enzyme reduces the growth of cancer cells [22]. Numerous compounds exhibit high affinity towards CA IX, but also strongly bind to undesired off-target CAs showing side effects. Several partially selective CA IX inhibitors have been synthesized and their binding and inhibition constants to CA IX were measured [23–25]. However, only the ‘observed’ parameters were determined that depend on experimental conditions such as the buffer and its *pH*. Here we emphasize the importance of the ‘intrinsic’ binding parameters

that were determined by subtracting the linked protonation events from the observed reactions [26].

Thermodynamic parameters provide an insight into the energetic reasons of the binding reaction. Gibbs energy ( $\Delta G$ ) shows the overall affinity of the interaction while the changes in enthalpy ( $\Delta H$ ) and entropy ( $\Delta S$ ) upon binding provide additional molecular information about the process. The  $\Delta H$  shows the heat evolved during complex formation (at constant temperature and pressure). It is related to the strength and number of formed and broken bonds [1]. The entropy indicates an increase and decrease of the degrees of freedom of the free and bound ligand, protein and water. The decrease of enthalpy and increase of entropy contributes favorably to the binding process. These parameters of binding may also provide insight into the structure of water at the binding interface [27].

Isothermal titration calorimetry (ITC) provides all these three parameters in a single experiment. ITC directly measures the heat evolved ( $\Delta H$ ) while the  $K_b$  can be estimated from the slope of ITC curve and  $\Delta G$  can be calculated using the equation:

$$\Delta G = -RT \ln K_b \quad (1)$$

where  $R$  is the universal gas constant and  $T$  is the absolute temperature. Entropy can be estimated by subtraction:

$$T\Delta S = \Delta H - \Delta G. \quad (2)$$

ITC experiments determine the *observed* thermodynamic parameters that may depend on various factors such as *pH*, buffer, salt, temperature, etc. However, it is important to determine the *intrinsic* thermodynamic parameters of binding that would be observed in the hypothetical absence of any linked reactions. For example, if a protein should bind a proton in order to be able to bind the ligand, the observed energy would be lower by the amount necessary to protonate the protein. This energy would be *pH*-dependent and increased 10-fold upon increasing the *pH* of the medium by one unit (when  $pH > pK_a$ ).

Fluorescent thermal shift assay (FTSA, also called Thermofluor, differential scanning fluorimetry, DSF) can be conveniently used to characterize protein stabilities in various buffers [28,29] and determine the ligand binding affinities based on a shift in protein melting temperature ( $T_m$ ) [30–33]. The  $T_m$  is observed when the fluorescence of a solvatochromic dye changes upon heat-induced protein unfolding [34,35,31,36–38].

During sulfonamide inhibitor binding to CAs, there are two linked protonation reactions, the protonation of the protein and deprotonation of the ligand. Such reactions may reduce the affinity thousands of times. Determination of the intrinsic thermodynamic parameters ( $K_{b, intr}$ ,  $\Delta G_{intr}$ ,  $\Delta H_{intr}$ ,  $\Delta S_{intr}$ ) requires multiple measurements in several buffers at various *pH*s. Upon protonation, the protons are picked up from or released to the buffer and the effect should be subtracted to determine the actual binding reaction [27,39–45].

## 2. Materials and methods

### 2.1. Proteins

The cDNA of human carbonic anhydrase IX (CA IX) was purchased from RZPD Deutsches Ressourcenzentrum für Genomforschung GmbH (Germany). To prevent the dimerization of CA IX monomers, the site-directed mutagenesis of cysteine (41) to serine was performed using the sense (5′-TCGCCCTCAGCCCGCCCTG-3′) and antisense (5′-CAGGGCCGGGCTGAAGCGGCGA-3′) mutagenic primers according to the procedure described in QuikChange Site-Directed Mutagenesis instruction manual (Stratagene).

Expression of CA IX and CA IX mutant (CAIX<sup>C41S</sup>) proteins was carried out using pCEP4ds [46] or pCEP4S vectors designed for the secretion of recombinant mammalian proteins. The pCEP4S vector was made from the pCEP4 vector (purchased from Invitrogen) by introducing a secretion

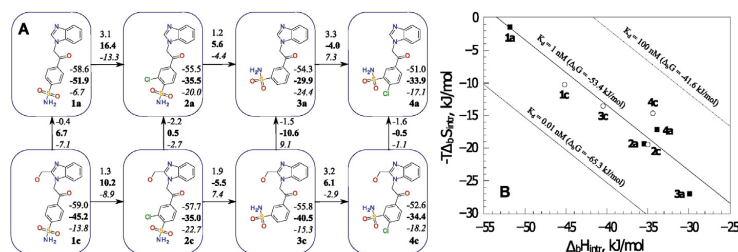


**Fig. 2.** Correlation map of the inhibitor chemical structures with their intrinsic thermodynamics of binding to CA IX. Panel A. The map includes the  $\Delta G_{bind}$  (top number),  $\Delta H_{bind}$  (bold number) and  $-T\Delta S_{bind}$  (bottom number in italic) of binding. Panel B. The enthalpy–entropy compensation graph. Open circles represent compounds 1–4(a), filled rectangles – 1–4(c). Diagonal lines represent protein–ligand binding affinity.

signal into a multiple cloning site. Two complementary single stranded oligonucleotides, containing the secretion signal from the V-J2-C region of murine Ig kappa chain were chemically synthesized and annealed. The resultant double stranded oligonucleotide was digested at the 5' and 3' ends with KpnI and HindIII, respectively, and ligated into the vector cut with the same enzymes.

For the construction of CA IX expression plasmids, the DNA fragments, corresponding to the catalytic domain of CA IX (amino acids 138 to 390) and the mutated CA IX catalytic domain (amino acids 138 to 390, containing the Cys41Ser mutation) were inserted into the multicloning site of pCEP4dS or pCEP4S vector. Due to the linker located between the secretion signal and the coding sequences of CA IX, both CA IX and CAIX<sup>C41S</sup> recombinant proteins have additional 5 amino acids (DAAHM) at the N terminus.

Expression of the pCEP4dS–CA IX and pCEP4dS–CA IX<sup>C41S</sup> plasmids in mammalian cells was performed using FreeStyle Max 293 expression system (Invitrogen) according to the procedure described in Dudutiene et al. [23]. However, the pCEP4S–CA IX and pCEP4S–CA IX<sup>C41S</sup> plasmids were expressed according to a modified protocol as explained below. FreeStyle 293-F suspension cell culture was maintained in Erlenmeyer flasks containing FreeStyle medium in a 37 °C incubator with a humidified atmosphere of 8% CO<sub>2</sub>, on an orbital shaker platform rotating at 135 rpm. 20–30 mL of FreeStyle 293-F cell suspension was transfected with the purified pCEP4S–CA IX or pCEP4S–CA IX<sup>C41S</sup> plasmids according to the manufacturer's recommendations. After two days, the culture was transferred to a 50 mL tube and kept for 1–2 min to sediment the cell clumps. Two thirds of the culture was aspirated from the top and transferred to a new flask, containing fresh FreeStyle medium (one third of the culture volume). Hygromycin B was added to the culture (100 µg/mL) to select for a hygromycin-resistant transfected cells.

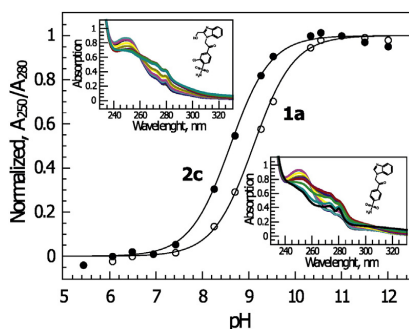


**Fig. 3.** Spectrophotometric determination of the  $pK_a$  of the compound sulfonamide group. The compound absorbance spectra were taken in various buffers as a function of  $pH$  for compounds 1a and 2c at 25 °C. (insets). The normalized absorbance ratio ( $A_{250}/A_{280}$ ) was plotted as a function of  $pH$  and fit to the model Eq. (5).

After two days of culturing, the cells were counted and diluted ~3 times with hygromycin B-containing FreeStyle medium to the cell density of  $\sim 7 \times 10^5$ /mL and cultured further for three days until the final ~3 times dilution to  $\sim 7 \times 10^5$ /mL density. Three days later, the culture was centrifuged at 6000g for 20 min and the secreted recombinant proteins were purified from the supernatant using a CA-affinity column containing p-aminomethylbenzene sulfonamide-agarose (Sigma-Life Science Aldrich). The eluted CA IX and CA IX<sup>C41S</sup> proteins were dialyzed into a storage buffer containing 20 mM HEPES,  $pH$  7.5 and 50 mM NaCl. All purified proteins were stored at  $-80$  °C.

## 2.2. Compounds

Ethoxzolamide (**EZA**) was purchased from Aldrich. Compound synthesis has been previously described: 1–3(a–j) were described by Zubrienė et al. [47], 4(a–j) were described by Čapkauskaitė et al. [48]. Instant JChem (Instant JChem 6.1.3, 2013, ChemAxon, <http://www.chemaxon.com>) was used for structure database management, search and prediction.

## 2.3. Fluorescent thermal shift assay (FTSA)

FTSA is a rapid screening method used for the identification of compounds that bind to target proteins. FTSA experiments were performed in Corbett Rotor-Gene 6000 (QIAGEN Rotor-Gene Q) instrument using the blue channel (excitation  $365 \pm 20$ , detection  $460 \pm 15$  nm). Protein samples containing various compound concentrations were heated from 25 to 99 °C at a rate of 1 °C/min while observing the fluorescence yield. The samples contained constant concentration of protein, varied concentrations of a compound and were prepared in 50 mM phosphate buffer ( $pH$  7.0) containing 50 µM ANS (8-anilino-1-naphthalene sulfonate), 100 mM NaCl and up to 2% DMSO. The protein melting temperatures were determined at each inhibitor concentration. Data analysis was performed as previously described [7,35].

## 2.4. Isothermal titration calorimetry (ITC)

Compound binding to proteins was also determined by ITC, the experiments were performed by using VP-ITC instrument (Microcal, Inc., part of Malvern, Northampton, MA, USA).

For the binding reactions of 1–4(a,c) to CA IX<sup>C41S</sup>, the calorimeter cell contained 4 µM protein, 2% DMSO, 50 mM sodium phosphate buffer ( $pH$  7.0) and 100 mM sodium chloride. Syringe contained 40 µM ligand, 2% DMSO, 50 mM phosphate buffer ( $pH$  7.0) and 100 mM sodium chloride. Experiments consisted of 25 injections, volume of the first injection was 5 µL, while others were 10 µL, added at 200 s intervals, at 25 °C.

The experiments of **EZA** binding at various  $pH$ s were performed using 4 µM of protein, 2% DMSO, 50 mM sodium phosphate or TRIS buffer containing 100 mM sodium chloride in the cell and 40 µM of **EZA**, 2%

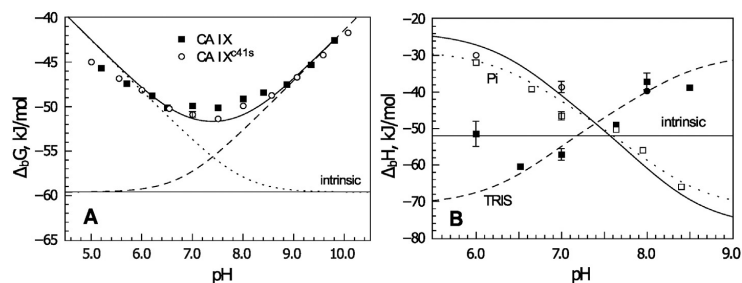


**Fig. 4.** The thermodynamics of **EZA** binding to CA IX at various *pH*s. Panel A shows the  $\Delta_b G_{obs}$  dependence on *pH* and the  $\Delta_b G_{intr}$  that is independent of *pH* (solid straight line). The observed binding constants of **EZA** binding to CA IX (nonmutated, filled rectangles) and CA IX<sup>415</sup> were determined by FTSA. The solid U-shape line is the fit according to the Eq. (4). The dashed line shows the contribution of the protonated CA and the dotted line shows the contribution of the deprotonated ligand. Panel B shows the observed binding enthalpy ( $\Delta_b H_{obs}$ ) dependence on *pH* while the intrinsic enthalpy ( $\Delta_b H_{intr}$ ) is independent of *pH* (solid straight line). ITC titrations were performed in sodium phosphate (open symbols) or TRIS chloride (filled symbols) at 25 °C. The observed enthalpies formed an X-shape dependence on *pH*. Rectangles represent titrations to CA IX while the circles – CA IX<sup>415</sup>. Dashed (in TRIS) and dotted (in Pi) lines were fit according to Eq. (7). Solid curve represents the fit of a situation if the buffer had zero enthalpy of protonation.

DMSO and phosphate or TRIS buffer containing 100 mM sodium chloride in the syringe. Buffer solution was the same in the syringe and in the cell and *pH* values were checked before and after the experiment. Experiments consisted of 25 injections, volume of the first injection was 5  $\mu$ L, while others were 10  $\mu$ L, added at 200 s intervals, at 25 °C.

The enthalpy of inhibitor protonation was measured by titrating with 5 mM HNO<sub>3</sub> the cell solution containing the inhibitor (0.25 mM) and 1.5 equivalent (0.375 mM) of NaOH. The experiment consisted of 56 injections. The volume of each injection was 5  $\mu$ L, added at 200 s intervals. DMSO concentrations in the syringe and the sample cell were equal (2.5%). Experiments were performed at 25 °C. ITC data was integrated, fit and analyzed as previously described [49].

### 2.5. Measurements of *pK<sub>a</sub>* of the compound's sulfonamide group

The *pK<sub>a</sub>* values of the sulfonamide group of the compounds were measured with the spectrophotometer Agilent 89090A as previously described by Snyder et al. [34]. Ultraviolet spectra in the wavelength range from 200 to 380 nm were collected at each half *pH* unit between 5.0 and 12.0. Samples contained 30–50  $\mu$ M compound, 1% DMSO, 50 mM NaCl and the universal buffer (containing 50 mM sodium acetate, 50 mM sodium phosphate and 25 mM sodium borate). The normalized ratio of absorbances at two wavelengths (above and below the isosbestic point) was plotted as a function of *pH*. The *pK<sub>a</sub>* value was determined as the midpoint of the fitted curve.

### 2.6. Calculation of intrinsic thermodynamic parameters

The CA can bind a compound when the zinc-bound hydroxide anion is protonated (water molecule) and the sulfonamide compound is in the

deprotonated form. However, at the physiological *pH* the CA mostly contains the hydroxide anion and the compound sulfonamide is mostly protonated. Thus, the observed enthalpy of the CA-sulfonamide binding highly depends on the *pH*.

The intrinsic binding constant  $K_{b, intr}$  is equal to the observed binding constant divided by the fractions of binding-active species:

$$K_{b, intr} = \frac{K_{b, obs}}{f_{RSO_2NH^-} - f_{CAZn(II)H_2O}} \quad (3)$$

The Gibbs energy in turn is:

$$\Delta_b G_{intr} = -RT \ln(K_{b, intr}) \quad (4)$$

where  $f_{RSO_2NH^-}$  is the fraction of the deprotonated sulfonamide compound and  $f_{CAZn(II)H_2O}$  is the fraction of the protonated hydroxide molecule (H<sub>2</sub>O) bound to the zinc cation in the active site of CA.  $f_{RSO_2NH^-}$  and  $f_{CAZn(II)H_2O}$  can be calculated when the *pK<sub>a</sub>*s of both the sulfonamide and the Zn(II)-bound water molecule are known:

$$f_{RSO_2NH^-} = \frac{[RSO_2NH^-]}{[RSO_2NH^-] + [RSO_2NH_2]} = \frac{10^{pH - pK_{a, RSO_2NH^-}}}{1 + 10^{pH - pK_{a, RSO_2NH^-}}} \quad (5)$$

$$f_{CAZn(II)H_2O} = \frac{[CAZn(II)H_2O]}{[CAZn(II)H_2O] + [CAZn(II)OH^-]} = \frac{10^{pK_{a, CAZn(II)H_2O} - pH}}{1 + 10^{pK_{a, CAZn(II)H_2O} - pH}} \quad (6)$$

To calculate the intrinsic enthalpy ( $\Delta_b H_{intr}$ ), the protonation/deprotonation of the buffer, the deprotonation of sulfonamide and the

**Table 1**

The intrinsic thermodynamics of compound binding to CA IX at 25 °C. The  $K_d, intr$  and the  $\Delta_b G_{intr}$  were calculated from the values determined by FTSA of compound binding to CA IX. The  $\Delta_b H_{intr}$  and the  $-T\Delta_b S_{intr}$  were calculated from the values obtained by ITC of compound binding to CA IX<sup>415</sup> except for **EZA** where ITC was performed with non-mutated CA IX.

Compound	$K_d, intr$ , nM	$\Delta_b G_{intr}$ , kJ/mol	$\Delta_b H_{intr}$ , kJ/mol	$-T\Delta_b S_{intr}$ , kJ/mol
<b>1a</b>	0.462	-53.3	-51.9	-1.4
<b>2a</b>	0.249	-54.8	-35.5	-19.3
<b>3a</b>	0.110	-56.9	-29.9	-27.0
<b>4a</b>	1.16	-51.0	-33.9	-17.1
<b>1c</b>	0.196	-55.4	-45.2	-10.2
<b>2c</b>	0.293	-54.4	-35.0	-19.4
<b>3c</b>	0.345	-54.0	-40.5	-13.5
<b>4c</b>	2.61	-49.0	-34.4	-14.6
<b>EZA</b>	0.0357	-59.6	-53.0	-6.6

**Table 2**

Thermodynamics of compound protonation at 25 °C. The *pK<sub>a</sub>*, *K<sub>a</sub>* and  $\Delta_b prot, inh G$  were determined spectrophotometrically, the  $\Delta_b prot, inh H$  was determined by ITC and the  $-T\Delta_b prot, inh S$  was determined by the subtraction.

Compound	<i>pK<sub>a</sub></i>	<i>K<sub>a</sub></i> , nM	$\Delta_b prot, inh G$ , kJ/mol	$\Delta_b prot, inh H$ , kJ/mol	$-T\Delta_b prot, inh S$ , kJ/mol
<b>1a</b>	9.1	0.79	-51.9	-36.8	-15.1
<b>2a</b>	8.6	2.5	-49.1	-31.8	-17.3
<b>3a</b>	9.4	0.40	-53.7	-37.2	-16.5
<b>4a</b>	9.0	1.0	-51.4	-30.5	-20.9
<b>1c</b>	9.1	0.79	-51.9	-36.4	-15.5
<b>2c</b>	8.6	2.5	-49.1	-32.2	-16.9
<b>3c</b>	9.5	0.32	-54.2	-38.5	-15.7
<b>4c</b>	9.0	1.0	-51.4	-31.8	-19.6
<b>EZA<sup>a</sup></b>	8.0	10	-45.7	-29.5	-16.2

<sup>a</sup> Data taken from [44].

**Table 3**

Thermodynamics of protonation of Zn(II)-bound hydroxide in the active site of several CA isoforms at 25 °C. The  $pK_a$  and  $\Delta_b \text{prot}_{CA}G$  were determined by a combined fit of the FTSA and ITC U-shape and X-shape data as shown in Fig. 4.

Protein	$pK_a$	$\Delta_b \text{prot}_{CA}G$ , kJ/mol	$\Delta_b \text{prot}_{CA}H$ , kJ/mol	$-T\Delta_b \text{prot}_{CA}S$ , kJ/mol
CA I-Zn(II)-H <sub>2</sub> O <sup>a</sup>	8.4	-47.9	-41.0	-6.9
CA II-Zn(II)-H <sub>2</sub> O <sup>a</sup>	7.1	-40.5	-26.0	-14.5
CA VB-Zn(II)-H <sub>2</sub> O <sup>b</sup>	7.2	-41.1	-30.0	-11.1
CA VI-Zn(II)-H <sub>2</sub> O <sup>c</sup>	6.2	-35.4	-32.0	-3.4
CA VII-Zn(II)-H <sub>2</sub> O <sup>d</sup>	7.0	-40.0	-33.0	-7.0
CA IX-Zn(II)-H <sub>2</sub> O	6.8	-38.8	-24.0	-14.8
CA XII-Zn(II)-H <sub>2</sub> O <sup>e</sup>	7.0	-40.0	-28.0	-12.0
CA XIII-Zn(II)-H <sub>2</sub> O <sup>f</sup>	8.3	-47.4	-44.0	-3.4

<sup>a</sup> Data taken from [40].

<sup>b</sup> Data taken from [45].

<sup>c</sup> Data taken from [41].

<sup>d</sup> Data taken from [42].

<sup>e</sup> Data taken from [43].

<sup>f</sup> Data taken from [26].

protonation of the Zn(II)-bound hydroxide anion in the active site should be subtracted from the observed enthalpy ( $\Delta_b H_{obs}$ ) value:

$$\Delta_b H_{intr} = \Delta_b H_{obs} - n_{inh} \Delta_b \text{prot}_{inh} H - n_{CA} \Delta_b \text{prot}_{CA} H + n_{buf} \Delta_b \text{prot}_{buf} H \quad (7)$$

**Table 4**

Thermodynamics of compound binding to CA IX at 25 °C. The  $K_{d,obs}$  and  $\Delta_b G_{obs}$  were determined by FTSA with standard error from two independent repeats. Experiments were performed in phosphate buffer at pH 7.0. The  $K_{d,intr}$  and  $\Delta_b G_{intr}$  were calculated from the  $K_{d,obs}$  values except EZA where intrinsic energies were obtained from the U-shape data in Fig. 4.

Compound	$K_{d,intr}$ , nM	$\Delta_b G_{intr}$ , kJ/mol	$K_{d,obs}$ , nM	$\Delta_b G_{obs}$ , kJ/mol
1a E79	0.054	-58.6	17.5	-44.3 ± 1.4
2a E11-36	0.190	-55.5	20.0	-43.9 ± 0.7
3a E11-37	0.307	-54.3	200	-38.2 ± 1.0
4a E2	1.16	-51.0	303	-37.2 ± 0.6
1b E80	0.047	-59.0	15.4	-44.6 ± 1.6
2b E11-38	0.130	-56.4	11.0	-45.4 ± 2.4
3b E11-39	0.465	-53.3	303	-37.2 ± 1.1
4b E3	1.67	-50.1	435	-36.3 ± 0.6
1c E86	0.046	-59.0	14.9	-44.7 ± 0.3
2c E11-50	0.079	-57.7	8.30	-46.1 ± 0.7
3c E11-51	0.167	-55.8	137	-39.2 ± 0.8
4c E6	0.618	-52.6	161	-38.8 ± 0.8
1d E87	0.508	-53.1	167	-38.7 ± 1.3
2d E11-52	0.211	-55.2	22.2	-43.7 ± 0.9
3d E11-53	0.061	-58.3	40.0	-42.2 ± 0.8
4d E7	0.982	-51.4	256	-37.6 ± 0.7
1e E81	0.019	-61.2	6.2	-46.8 ± 2.1
2e E11-40	0.027	-60.3	2.9	-48.8 ± 0.6
3e E11-41	0.170	-55.8	111	-39.7 ± 0.8
4e E12	0.958	-51.5	250	-37.7 ± 0.5
1f E85	0.013	-62.2	4.2	-47.8 ± 2.3
2f E11-42	0.045	-59.1	4.8	-47.5 ± 0.7
3f E11-43	0.073	-57.9	47.6	-41.8 ± 0.5
4f E18	1.42	-50.5	370	-36.7 ± 0.9
1g E93	0.024	-60.7	7.7	-46.3 ± 0.8
2g E11-44	0.033	-59.9	3.5	-48.3 ± 0.8
3g E11-45	0.256	-54.8	167	-38.7 ± 0.9
4g E14	1.60	-50.2	417	-36.4 ± 0.7
1h E82	0.014	-62.0	4.6	-47.6 ± 2.3
2h E11-46	0.032	-59.9	3.3	-48.4 ± 0.5
3h E11-47	0.096	-57.2	62.5	-41.1 ± 0.9
4h E13	0.451	-53.3	118	-39.6 ± 0.9
1i E83	0.012	-62.3	4.0	-47.9 ± 2.4
2i E11-48	0.026	-60.5	2.7	-48.9 ± 0.5
3i E11-49	0.107	-56.9	55.6	-41.4 ± 0.8
4i E19	0.696	-52.3	182	-38.5 ± 0.7
1j E84	0.012	-62.3	4.0	-47.9 ± 0.7
2j E11-54	0.041	-59.3	4.4	-47.7 ± 0.6
3j E11-55	0.110	-56.9	71.4	-40.8 ± 0.7
4j E22	0.723	-52.2	189	-38.4 ± 1.0
EZA	0.0357	-59.6	2.11	-49.5 ± 0.6

where  $\Delta_b H_{obs}$  is the observed binding enthalpy,  $n_{inh}$  is the number of protons released during the deprotonation of the sulfonamide and equal to  $n_{inh} = f_{R_{SO_2NH}} - 1$ ,  $\Delta_b \text{prot}_{inh} H$  is the enthalpy of inhibitor protonation,  $n_{CA}$  is the number of protonated hydroxide ions bound to the active site Zn(II) and can be calculated according to equation  $n_{CA} = 1 - f_{CAZn(II)H_2O}$ ,  $\Delta_b \text{prot}_{CA} H$  is the enthalpy of CA protonation,  $n_{buf}$  is the number of protons taken or released by the buffer and equal  $n_{buf} = n_{inh} + n_{CA}$ ,  $\Delta_b \text{prot}_{buf} H$  is the buffer protonation enthalpy [50].

### 3. Results

#### 3.1. Intrinsic thermodynamic parameters of compound binding to CA IX

The intrinsic Gibbs energies ( $\Delta_b G_{intr}$ ) of 40 sulfonamide compound binding to the catalytic domain of CA IX were determined. Compounds are benzenesulfonamides with benzimidazole moiety divided into four groups: the *para*-substituted benzenesulfonamides without chlorine in *meta*-position (1(a-j)) and bearing chlorine atom (2(a-j)) and the *meta*-substituted benzenesulfonamides without chlorine atom in *para*-position (3(a-j)) and with the Cl (4(a-j)). The  $\Delta_b G_{intr}$  of each compound binding to CA IX are listed next to the compound structure (Fig. 1) while the differences ( $\Delta \Delta_b G_{intr}$ ) are shown on the arrows connecting the compound structures. The horizontal arrows show the differences between four head-groups with the same tail moiety, while the vertical arrows compare the compounds with different tails, but the same benzenesulfonamide head-group moieties. These values help us to determine different functional group contributions to the intrinsic binding affinity.

The *para*-substituted benzenesulfonamides (1 and 2) exhibited stronger binding affinity than the *meta*-substituted compounds. There

**Table 5**

Thermodynamics of selected compound binding to CA IX<sup>641s</sup> as determined by ITC at 25 °C. The  $K_{d,obs}$  and  $\Delta_b G_{obs}$  were obtained from the ITC data and significantly differs from the data in Table 4. ITC underestimated the affinity in reactions where the Wiseman parameter  $c$  is near or above the limit of 500 and thus the FTSA data in Table 4 are more accurate than the ITC data, shown in this table only for the comparison of two methods. ITC data are in singlicate except for EZA. ITC experiments were performed in sodium phosphate buffer at pH 7.0.

Compound	$K_{d,obs}$ , nM	$\Delta_b G_{obs}$ , kJ/mol	$\Delta_b H_{obs}$ , kJ/mol
1a	152	-38.9	-32.0
2a	26.3	-43.3	-21.0
3a	71.4	-40.8	-9.5
4a	714	-35.1	-20.3
1c	64.4	-41.0	-25.7
2c	31.0	-42.9	-20.2
3c	283	-37.4	-18.8
4c	680	-35.2	-19.6
EZA	3.46	-47.4	-46.5

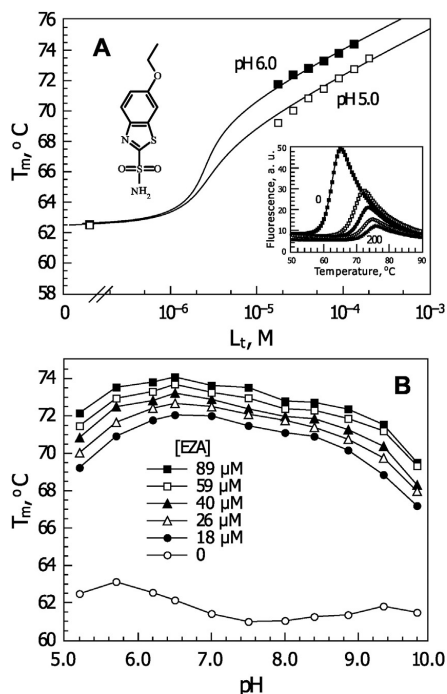


**Fig. 5.** FTSA data of EZA binding to CA IX as a function of pH. Panel A shows the protein melting temperature dependence on ligand concentration at pH 5.0 and pH 6.0. The  $K_{d,obs}$  values were equal to  $1.0 \times 10^8$  M and  $3.5 \times 10^8$  M, respectively. The inset shows the raw curves of unfolding of the CA IX as a function of temperature. The shift of the  $T_m$  depends on ligand concentration: '0' marks the protein in the absence of the ligand and '200' labels the protein with 200  $\mu$ M added ligand concentration. Panel B. Protein  $T_m$  dependence on pH at various added EZA concentrations, at 25 °C.

was an exception where **2d** and **3d** were stronger binders than **1d** and **4d**. In most cases, the *para*-substituted benzenesulfonamides bearing chlorine atom in the *meta*-position were stronger binders to CA IX than compounds without the chlorine. However, when sulfonamide group was in the *meta*-position, the benzenesulfonamides bound

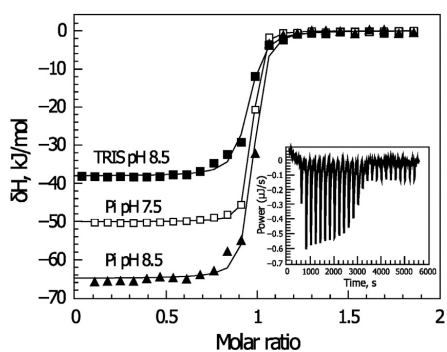


**Fig. 6.** ITC titrations of EZA binding to CA IX in various buffers and at various pH. The inset shows the raw ITC data of EZA binding to CA IX in Pi buffer at pH 7.5. The filled squares represent the ITC data in TRIS chloride buffer at pH 8.5, filled triangles – in Pi buffer at pH 8.5 and open squares – in Pi buffer at pH 7.5. The experiments were performed at 25 °C.

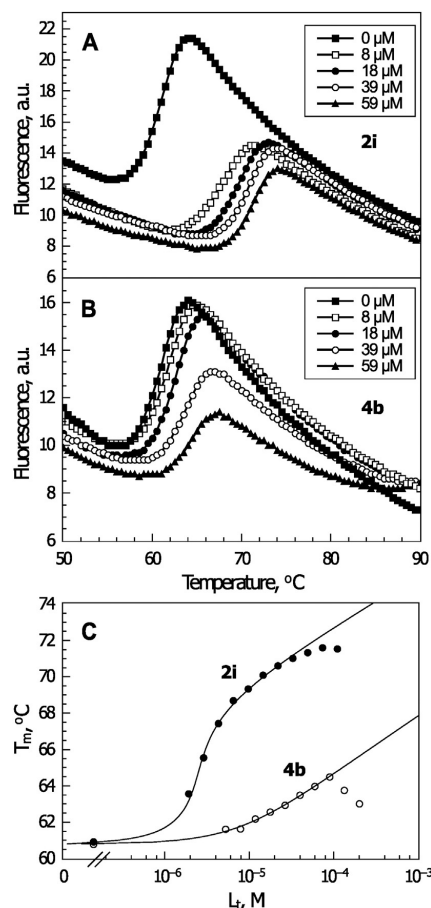


**Fig. 7.** FTSA data of **2i** and **4b** binding to CA IX at 25 °C. Panel A. ANS fluorescence curves of CA IX (5  $\mu$ M) thermal melting in the presence of various concentrations of **2i** and **4b** (Panel B). Panel C. The dose response curves as a function of added concentration of **2i** (filled circles) and **4b** (open circles). Datapoints are experimental data while the lines represent the fit as explained in the methods section. Partial inconsistency of the modeled and experimental  $T_m$  at higher compound concentrations are due to the limited aqueous solubility of the compounds.

stronger to CA IX when the compounds did not possess the chlorine atom on the benzene ring.

The  $\Delta_b G_{intr}$  for **1–2(a–j)** was in the range from  $-53.1$  kJ/mol to  $-62.3$  kJ/mol, while the  $\Delta_b G_{intr}$  of **3–4(a–j)** was in the range from  $-50.1$  kJ/mol to  $-58.3$  kJ/mol. The highest binding affinity to CA IX was exhibited by the compounds **1i**, **1j**, **1f** and **1h** ( $\Delta_b G_{intr} \approx -62.0$  kJ/mol) and the weakest were **4b**, **4g** and **4f**.

The intrinsic enthalpies ( $\Delta_b H_{intr}$ ) and entropies ( $-T\Delta_b S_{intr}$ ) of compound binding to CA IX were determined by ITC for 8 compounds (from series a and c). All three intrinsic thermodynamic parameters of binding for these 8 ligands are shown in Fig. 2 (Panel A) ( $\Delta_b H_{intr}$  is in bold,  $-T\Delta_b S_{intr}$  is in italic). The differences between compounds are listed next to the arrows. The  $\Delta_b G_{intr}$  were calculated from the FTSA data. The intrinsic enthalpy–entropy compensation graph is shown in Panel B of Fig. 2. The enthalpies and entropies spanned a wide range, while dissociation constants were distributed in a relatively narrow range. All compound binding reactions were primarily enthalpically driven with a relatively minor favorable entropy contribution (at

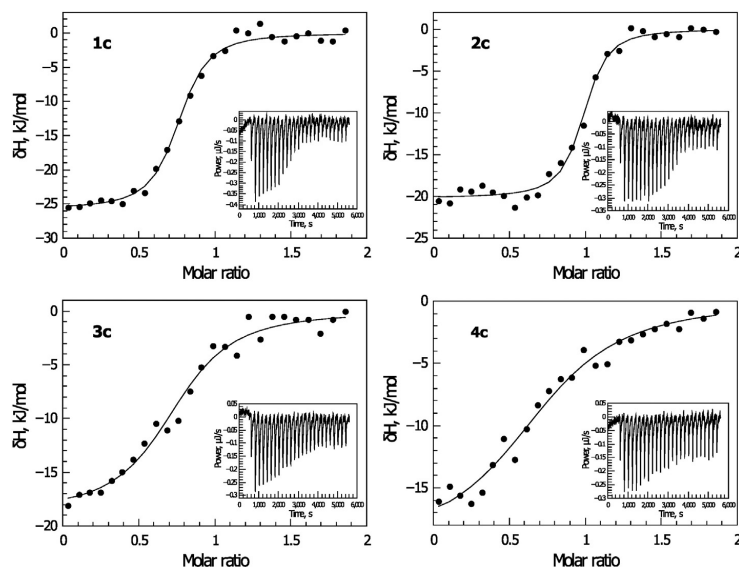


Fig. 8. ITC data of 1–4(c) binding to CA IX<sup>445</sup>. Integrated ITC binding curves were observed in sodium phosphate buffer at pH 7.0. Insets show the raw ITC curves.

25 °C). Only for compound **3a** the enthalpy and entropy contributions were nearly identical.

### 3.2. Thermodynamics of the compound protonation

In order to determine the intrinsic binding parameters it is necessary to know the protonation state of the compound sulfonamide group. The compound at physiological pH exists primarily in the protonated form while it binds to a CA in the deprotonated form whose fraction depends on solution pH and the  $pK_a$  of the compound. The  $pK_a$ s of compounds were measured spectrophotometrically as previously described [51, 52]. The ratio of absorbances at two wavelengths where the pH effect is large was normalized and plotted as a function of pH yielding the  $pK_a$  of the sulfonamide head-group (Fig. 3). Due to limited solubility of compounds, the ionization constants were determined only for 12 ligands. For compounds **1(a–c)** the  $pK_a$  values were equal to 9.1. For **2(a–c)** the  $pK_a$  values were equal to 8.6 ( $\pm 0.1$ ). For **3c**, **3d**, **3i** the  $pK_a$ s were 9.5, 9.4 and 9.3, respectively. For **4a**, **4c** and **4d** the  $pK_a$ s were 9.0.

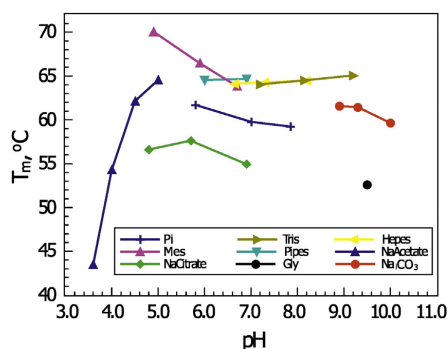


Fig. 9. Thermal stability of CA IX in various buffers as a function of pH. The melting temperature of CA IX (5  $\mu$ M) was determined by FTSA in various buffers (100 mM). The protein is strongly destabilized by citrate and to a lesser extent – by the Pi buffer.

These values show that the four head-groups of 40 compounds have different ionization constants, but the tails have minor effect: the  $pK_a$  of *para*-substituted benzenesulfonamides is 9.1, for *para*-substituted benzenesulfonamides bearing chlorine atom is 8.6, for *meta*-substituted benzenesulfonamides  $pK_a$  is 9.4 and for *meta*-substituted benzenesulfonamides with chlorine atom is 9.0. The chlorine atom lowered the ionization constant of a compound. The lowest  $pK_a$ s were measured for the *para*-substituted benzenesulfonamides bearing chlorine atom and the highest  $pK_a$  for the *meta*-substituted benzenesulfonamides without the Cl.

The enthalpies of protonation ( $\Delta_{b,proL,inh}H$ ) were measured for 8 compounds (**1–4(a,c)**) using ITC as previously described in [40], [26], [53] by titrating the deprotonated compound (containing excess base) with acid. The enthalpies of protonation together with other protonation thermodynamic parameters are listed in Table 2. Compounds containing electron-withdrawing Cl atoms exhibited slightly reduced  $pK_a$ s and slightly less exothermic enthalpies than the compounds that did not bear the Cl atoms.

Since the compound  $pK_a$  is around 9.0, most of the compound at physiological pH exists in the protonated form. Significant energy is required to remove the proton in order for the compound to bind the CA. This energy will reduce the affinity and therefore the intrinsic affinities of such compounds are significantly larger than the observed affinities.

### 3.3. Thermodynamics of the Zn(II)-bound hydroxide anion protonation

The zinc cation is bound in the active site of all 12 catalytically active human CA isoforms through three histidines and has the fourth coordination bond exposed towards the solvent. This bond is occupied by a hydroxide anion or a water molecule. Only the water molecule can be displaced by the negatively charged sulfonamide inhibitor amino group. The hydroxide group must be protonated into a water molecule in order to be displaced. The  $pK_a$ s of CAs are usually between 6 and 8 and their protonation state varies depending on the pH and the buffer. If the  $pK_a$  is low, around 6, then at pH 7.0 the CA should undergo the protonation reaction upon inhibitor binding and this binding-linked protonation reaction will reduce the inhibitor binding affinity.

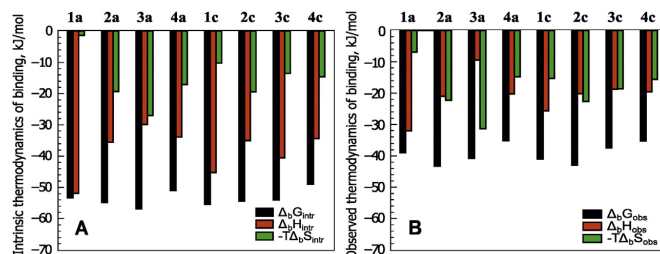


**Fig. 10.** Comparison between the intrinsic (Panel A) and the observed (Panel B) parameters of compound binding to CA IX<sup>c41s</sup> at 25 °C. The black bars represent Gibbs energy, red bars – enthalpy and green bars – entropy. There is a large difference between the intrinsic and the observed parameters. Only the intrinsic parameters are meaningful for structure-thermodynamics correlation analysis while the observed parameters represent a snapshot of a situation at the particular given conditions, pH 7.0 and sodium phosphate buffer.

The  $pK_a$  value of CA IX was determined by both FTSA and ITC methods (Fig. 4). Ethoxzolamide (EZA) was chosen for the determination of the  $pK_a$  of CA IX. The ligand binding affinity as determined by FTSA as a function of pH is shown in Fig. 4A. The affinity has a U-shape dependence on pH. There was essentially no difference observed between the native and the Cys mutant CA IX catalytic domain. The solid U-shape line is a fit of experimental data to the model [54,52,44] and the intrinsic Gibbs energy of binding (solid straight line) was determined ( $\Delta_b G_{intr} = -59.6$  kJ/mol, Table 1). The  $pK_a$  that best fit the U-shape line for both the native and mutated CA IX was equal to  $6.8 \pm 0.1$  (Table 3).

To determine the protonation enthalpy of the CA-bound hydroxide anion and the intrinsic enthalpy of EZA binding to CA IX, the ITC titrations were performed in TRIS and sodium phosphate (Pi) buffers (that have different protonation enthalpies) at a series of pHs (Fig. 4B). Several experiments were performed also with CA IX<sup>c41s</sup> yielding essentially same results as nonmutated CA IX. The pH dependence of the observed enthalpy ( $\Delta_b H_{obs}$ ) of EZA binding to CA IX exhibited an X-shape when performed in TRIS and Pi buffers. The solid sigmoidal line shows the observed enthalpy that would be observed if the buffers had zero enthalpy of protonation. Only the protonation contributions from the ligand and protein would be observed. The horizontal solid line shows the intrinsic enthalpy ( $\Delta_b H_{intr}$ ) that was obtained from this analysis of the ITC data. The dashed and dotted lines represent the fits of experimental data in TRIS and Pi buffers, respectively. These fits confirmed that the  $pK_a$  of CA IX is 6.8 (Table 3) and the intrinsic enthalpy of EZA binding to CA IX was determined to be ( $\Delta_b H_{intr} = -53.0$  kJ/mol, Table 1).

#### 3.4. Observed thermodynamic parameters of compound binding to CA IX

Fig. 5 shows FTSA results of EZA binding to CA IX. Addition of the compound to the solution of CA IX shifts the protein melting temperature upwards (inset in Panel A). The  $T_m$ s plotted as a function of added ligand (Panel A) exhibit a continuously increasing behavior. The binding is stronger at pH 6.0 than at pH 5.0 because the upshift is greater. Panel B shows the shifts at various added EZA concentrations as a function of pH. This results in a U-shape dependence of affinities on pH (Fig. 4A).

Fig. 6 shows ITC data at various pHs indicating that the pH influences not only the binding constants but also the enthalpies. Furthermore, the observed enthalpies are strongly dependent on buffer, while the observed Gibbs energies are not.

When measuring the affinities of the 40 compounds shown in Fig. 1 by using FTSA, direct observation yields the observed affinities ( $\Delta_b G_{obs}$ ). Application of the protonation model yields the intrinsic affinities ( $\Delta_b G_{intr}$ ). Intrinsic and observed affinities of the 40 compounds are compared in Table 4. It can be seen that the intrinsic affinities are significantly greater than the observed affinities. It is important to note that the binding affinities at physiological pH of 7.0 would be equal to the observed values. Compound potency as a drug should be equal to the observed values. However, intrinsic values become important when we compare numerous compounds and make attempts to correlate which

chemical structures would cause particular increments in the energetics of binding. Then it is important to use the intrinsic values of the interaction.

The tendency of the observed binding is similar to the intrinsic parameters (the *para*-substituted benzenesulfonamides have a higher binding affinity than the *meta*-substituted compounds, except (1–4)d group and 2d and 3d are better binders than 1d and 4d). The  $\Delta_b G_{obs}$  of 1–2(a–j) derivatives are in the range from  $-38.7$  kJ/mol to  $-48.9$  kJ/mol, while  $\Delta G$  of 3–4(a–j) differs from  $-36.3$  kJ/mol to  $-42.2$  kJ/mol. The highest affinity of binding to CA IX is exhibited by compounds 2i, 2e, 2h and 2g ( $\Delta_b G_{obs} < -48.0$  kJ/mol) and the smallest – by 4b and 4g. The FTSA curves of 4b and 2i binding to CA IX are shown in Fig. 7. Several data points at higher concentrations of the compound are below the model line due to the limited solubility of the ligands. ITC data of four compound (1–4(c)) binding to CA IX<sup>c41s</sup> is shown in Fig. 8. Experimentally measured by ITC, the observed thermodynamic parameters of 8 compound binding to CA IX<sup>c41s</sup> are listed in Table 5.

#### 3.5. Stability profile of CA IX

FTSA is useful to determine the stability of a protein at various conditions such as pH, salt concentration, buffer and other. The stability profile of CA IX in sodium phosphate buffer at various pHs can be seen in Fig. 5C. The highest stability of the protein (without a ligand) is at the lowest pH values and from pH 7.0 to 10.0 stability remains almost the same. However, various buffers significantly affect the protein stability. The CA IX  $T_m$  dependence as a function of pH is shown in Fig. 9. The CA IX is most stable in MES buffer at pH 5.0 while at higher pHs the  $T_m$  is lower. The effect of sodium acetate buffer shows the limit of CA IX stability in acidic buffers. Significant reduction in stability is observed below the pH 4.0. CA IX is quite stable between pH 5 and 9 in MES, TRIS, PIPES, HEPES and acetate buffers, but significantly destabilized by the sodium citrate buffer and to a lesser extent – by sodium phosphate. This information could be useful for the purification of CA IX when it is important to use conditions that do not destabilize the protein.

## 4. Discussion

In the studies of protein-ligand binding thermodynamics it is important to determine whether the protein or the ligand undergoes a binding-linked reaction that could influence the measurements. The most common binding-linked reaction is the protonation (or deprotonation) of the ligand or protein. Sulfonamide ligand binding to carbonic anhydrases at nearly all conditions involves binding-linked protonation of the Zn(II)-bound hydroxide and deprotonation of the compound sulfonamide group [54]. Only a small fraction of the ligand and the protein exists in solution at pH 7.0 in the binding-ready ionization form. The linked reactions affect the observed parameters variably.

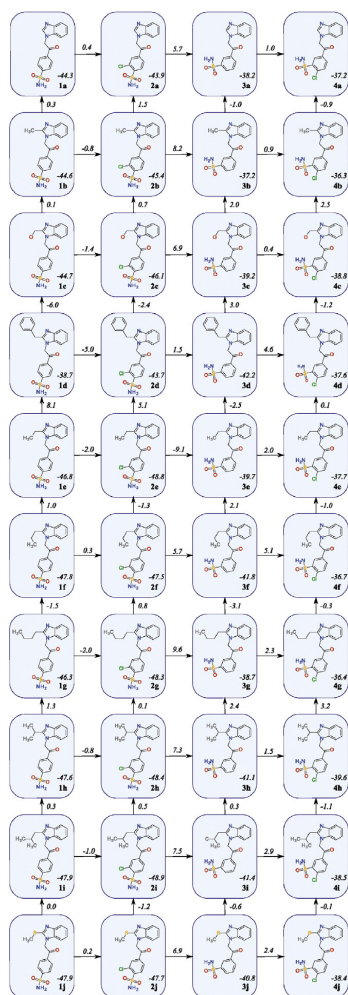


**Fig. 11.** The correlation map of the inhibitor chemical structures with their observed binding affinities ( $\Delta_b G_{obs}$ ) to the CA IX at pH 7.0 and at 25 °C. The numbers within the compound boxes show the  $\Delta_b G_{obs}$  calculated from the FTSA data, while the numbers next to the arrows show the differences between the closely structurally related compounds. This map is useful to see the functional group contributions observed at physiologically relevant pH 7.0 and could be compared to Fig. 1.

The intrinsic and observed thermodynamic parameters of compound binding to CA IX are shown in Fig. 10. Panel A shows the intrinsic parameters while panel B — the parameters observed at pH 7.0 in sodium phosphate buffer (Fig. 11). First, the intrinsic affinities are significantly greater than the observed ones. Second, the intrinsic enthalpies are also significantly more exothermic than the observed ones. The entropies are not experimentally measured. Instead, they are obtained by subtraction and thus may lead towards an artificial compensation if not carefully measured and analyzed [55]. The error analysis of our intrinsic parameters indicate that the standard deviations for  $\Delta_b G_{intr}$  did not exceed about 2 kJ/mol, for  $\Delta_b H_{intr}$  — about 4 kJ/mol and for  $-T\Delta_b S_{intr}$  — about 5 kJ/mol. Such relatively small errors should not significantly affect the compound enthalpy–entropy contribution. All 8 compound

binding was both enthalpy and entropy-driven, always dominated by the enthalpy at 25 °C.

Unfortunately, most researchers do not determine the intrinsic binding thermodynamics. Usually only the observed affinities or inhibition constants are determined at particular conditions (usually at pH 7.0). Such determinations are valid and desirable to directly observe the potency of each compound at physiologically relevant conditions. Unfortunately, the observed parameters could mislead us when comparing compounds with significantly different  $pK_a$ s. In such cases, the structure — thermodynamics correlations may lead to incorrectly understood physical reasons for an increased or decreased affinity. Furthermore, the importance of intrinsic parameters are not limited to protonation. For example, if a protein should undergo a conformational change upon ligand binding, the observed energy would be lower by the amount necessary for the conformational change. Thus, the observed affinity would be lower than the intrinsic affinity. Since we are interested only in the binding process, it would be important to subtract the energy required for the conformational change.

On the other hand, determination of the intrinsic binding parameters may not always be straightforward and practical. It is often sufficient in medicinal chemistry compound screening to determine only the observed parameters and select the best binding leads. However, caution should be used when attempting to assign particular functional groups of the compound to an increased or decreased affinity. Furthermore, such affinity ranking would be valid only for the tested conditions and should not be extrapolated to significantly different conditions.

Here we determined the  $pK_a$  of the hydroxide anion bound to the Zn(II) located in the active site of CA IX and found it to be equal to 6.8. Values of the  $pK_a$  of the full length and the catalytic domain of the CA IX were previously determined to be 6.49 and 7.01, respectively [6] and 6.3 [8]. Our determined value reasonably confirms previous determinations. The mutation of the cysteine that participates in the dimerization of CA IX did not affect the  $pK_a$ .

However, the value of the protonation enthalpy  $\Delta_b \text{prot}_{CAH}$  of the CA IX-bound hydroxide has been determined by ITC here for the first time. The thermodynamics of the protonation of CA IX was determined to be quite similar to CA II. This correlates with the high affinity of EZA to these two CA isoforms.

Our most potent and most selective inhibitors towards CA IX isoform have been previously described [23]. None of the 40 compounds described in this study exhibited extremely high observed affinity nor extreme selectivity towards isoform CA IX. However, previous publications described only the observed and did not describe the intrinsic parameters of binding. As discussed above, the present analysis is necessary for the proper structure–thermodynamics analysis of the compounds.

This study of the intrinsic thermodynamics of sulfonamide inhibitor binding to CA IX will enable other researchers to determine the intrinsic binding parameters of other compounds. The researchers will be able to calculate the  $K_{d,intr}$  and the  $\Delta_b G_{intr}$  of any compound binding to CA IX if the  $pK_a$  of the newly-synthesized compound is determined experimentally or estimated computationally. Furthermore, if the observed enthalpy of binding ( $\Delta_b H_{obs}$ ) of the newly-synthesized compounds is determined by ITC, then the researcher will be able to calculate the intrinsic enthalpy and entropy of the compound binding to CA IX. This should be useful in the future design of anticancer CA IX inhibitors.

#### Competing interests

The authors declare that they have no competing interests.

#### Author's contributions

VL made all thermodynamic measurements and analysis, wrote the manuscript. JM, VJ and JJ cloned and expressed the proteins from mammalian cells. VM purified the protein. DM supervised the project and wrote the manuscript.



## Transparency document

The [Transparency document](#) associated with this article can be found, in online version.

## Acknowledgments

This research was funded by a grant (no. SEN-04/2015) from the Research Council of Lithuania.

## References

- [1] J.E. Ladbury, G. Klebe, E. Freire, Adding calorimetric data to decision making in lead discovery: a hot tip, *Nat. Rev. Drug Discov.* 9 (1) (2010) 23–27, <http://dx.doi.org/10.1038/nrd3054>.
- [2] J. Pastorek, S. Pastorekova, Hypoxia-induced carbonic anhydrase ix as a target for cancer therapy: from biology to clinical use, *Semin. Cancer Biol.* 31 (2015) 52–64, <http://dx.doi.org/10.1016/j.semcancer.2014.08.002>.
- [3] C.T. Supuran, Carbonic anhydrases: novel therapeutic applications for inhibitors and activators, *Nat. Rev. Drug Discov.* 7 (2) (2008) 168–181, <http://dx.doi.org/10.1038/nrd2467>.
- [4] C.T. Supuran, A. Scozzafava, Carbonic anhydrases as targets for medicinal chemistry, *Bioorg. Med. Chem.* 15 (13) (2007) 4336–4350, <http://dx.doi.org/10.1016/j.bmc.2007.04.020>.
- [5] M. Hilvo, L. Baranauskienė, A.M. Salzano, A. Scaloni, D. Matulis, A. Innocenti, A. Scozzafava, S.M. Monti, A. Di Fiore, G. De Simone, M. Lindfors, J. Janis, J. Valjakka, S. Pastorekova, J. Pastorek, M.S. Kulomaa, H.R. Nordlund, C.T. Supuran, S. Parkkila, Biochemical characterization of CA IX, one of the most active carbonic anhydrase isozymes, *J. Biol. Chem.* 283 (41) (2008) 27799–27809, <http://dx.doi.org/10.1074/jbc.M800938200>.
- [6] A. Innocenti, S. Pastorekova, J. Pastorek, A. Scozzafava, G. De Simone, C.T. Supuran, The proteoglycan region of the tumor-associated carbonic anhydrase isoform ix acts as an intrinsic buffer optimizing CO<sub>2</sub> hydration at acidic pH values characteristic of solid tumors, *Bioorg. Med. Chem. Lett.* 19 (20) (2009) 5825–5828, <http://dx.doi.org/10.1016/j.bmcl.2009.08.088>.
- [7] L. Baranauskienė, M. Hilvo, J. Matulienė, D. Golovenko, E. Manakova, V. Dudutienė, V. Michailovienė, J. Torresan, J. Jachno, S. Parkkila, A. Maresca, C.T. Supuran, S. Gražulis, D. Matulis, Inhibition and binding studies of carbonic anhydrase isozymes I, II and IX with benzimidazo[1,2-c][1,2,3]thiadiazole-7-sulphonamides, *J. Enzyme Inhib. Med. Chem.* 25 (6) (2010) 863–870, <http://dx.doi.org/10.3109/14756360903571685>.
- [8] T. Wingo, C. Tu, P.J. Lajpits, D.N. Silverman, The catalytic properties of human carbonic anhydrase IX, *Biochem. Biophys. Res. Commun.* 288 (3) (2001) 666–669 (URL [http://www.ncbi.nlm.nih.gov/entrez/query.fcgi?cmd=Retrieve&db=PubMed&dopt=Citation&list\\_uids=11676494](http://www.ncbi.nlm.nih.gov/entrez/query.fcgi?cmd=Retrieve&db=PubMed&dopt=Citation&list_uids=11676494)).
- [9] P.C. McDonald, J.Y. Winum, C.T. Supuran, S. Dedhar, Recent developments in targeting carbonic anhydrase IX for cancer therapeutics, *Oncotarget* 3 (1) (2012) 84–97.
- [10] S.Y. Liao, C. Brewer, J. Zavada, J. Pastorek, S. Pastorekova, A. Manetta, M.L. Berman, P.J. DiSaia, E.J. Stanbridge, Identification of the mn antigen as a diagnostic biomarker of cervical intraepithelial squamous and glandular neoplasia and cervical carcinomas, *Am. J. Pathol.* 145 (3) (1994) 598–609.
- [11] S. Pastorekova, S. Parkkila, A.K. Parkkila, R. Opavský, V. Zelnik, J. Saarnio, J. Pastorek, Carbonic anhydrase IX, MN/CA IX: analysis of stomach complementary DNA sequence and expression in human and rat alimentary tracts, *Gastroenterology* 112 (2) (1997) 398–408.
- [12] B.C. Leibovich, Y. Sheinin, C.M. Lohse, R.H. Thompson, J.C. Cheville, J. Zavada, E.D. Kwon, Carbonic anhydrase IX is not an independent predictor of outcome for patients with clear cell renal cell carcinoma, *J. Clin. Oncol.* 25 (30) (2007) 4757–4764, <http://dx.doi.org/10.1200/JCO.2007.12.1087>.
- [13] S. Ivanov, S.Y. Liao, A. Ivanova, A. Danilkovitch-Miagkova, N. Tarasova, G. Weirich, M.J. Merrill, M.A. Proescholdt, E.H. Oldfield, J. Lee, J. Zavada, A. Waheed, W. Sly, M.I. Lerman, E.J. Stanbridge, Expression of hypoxia-inducible cell-surface transmembrane carbonic anhydrases in human cancer, *Am. J. Pathol.* 158 (3) (2001) 905–919, [http://dx.doi.org/10.1016/S0002-9440\(10\)64038-2](http://dx.doi.org/10.1016/S0002-9440(10)64038-2).
- [14] Y. Li, H. Wang, E. Oosterwijk, C. Tu, K.T. Shiverick, D.N. Silverman, S.C. Frost, Expression and activity of carbonic anhydrase IX is associated with metabolic dysfunction in MDA-MB-231 breast cancer cells, *Cancer Invest.* 27 (6) (2009) 613–623, <http://dx.doi.org/10.1080/07357900802653464>.
- [15] P. Swietach, R.D. Vaughan-Jones, A.L. Harris, Regulation of tumor pH and the role of carbonic anhydrase 9, *Cancer Metastasis Rev.* 26 (2) (2007) 299–310, <http://dx.doi.org/10.1007/s10555-007-9064-0>.
- [16] C.T. Supuran, A. Scozzafava, A. Casini, Carbonic anhydrase inhibitors, *Med. Res. Rev.* 23 (2) (2003) 146–189.
- [17] L.E. Riafrecha, O. M. Rodríguez, D. Vullo, C. T. Supuran, P. A. Colinas, Attachment of carbohydrates to methoxyaryl moieties leads to highly selective inhibitors of the cancer associated carbonic anhydrase isoforms IX and XII, *Bioorg. Med. Chem.* <http://dx.doi.org/10.1016/j.bmc.2014.07.052>.
- [18] V. Alterio, A. Di Fiore, K. D'Ambrosio, C.T. Supuran, G. De Simone, Multiple binding modes of inhibitors to carbonic anhydrases: how to design specific drugs targeting 15 different isoforms? *Chem. Rev.* 112 (8) (2012) 4421–4468, <http://dx.doi.org/10.1021/cr200176r>.
- [19] C.T. Supuran, A. Scozzafava, J. Conway, Carbonic Anhydrase – Its Inhibitors and Activators, CRC Press, Boca Raton, FL, USA, 2004.
- [20] A.D. Scott, C. Phillips, A. Alex, M. Flocco, A. Bent, A. Randall, R. O'Brien, L. Damian, L.H. Jones, Thermodynamic optimisation in drug discovery: a case study using carbonic anhydrase inhibitors, *ChemMedChem* 4 (12) (2009) 1985–1989, <http://dx.doi.org/10.1002/cmdc.200900386>.
- [21] B.P. Mahon, M.A. Pinard, R. McKenna, Targeting carbonic anhydrase IX activity and expression, *Molecules* 20 (2) (2015) 2323–2348, <http://dx.doi.org/10.3390/molecules20022323>.
- [22] W.R. Chegwidan, I.M. Spencer, Sulphonamide inhibitors of carbonic anhydrase inhibit the growth of human lymphoma cells in culture, *InflammoPharmacology* 3 (1995) 231–239.
- [23] V. Dudutienė, J. Matulienė, A. Smirnov, D.D. Timm, A. Zubrienė, L. Baranauskienė, V. Morkūnaitė, J. Smirnovienė, V. Michailovienė, V. Juozapaitienė, A. Mickevičiūtė, J. Kazokaitė, S. Bakšytė, A. Kasiliauskaitė, J. Jachno, J. Revuckienė, M. Kišonaitė, V. Piliupitytė, E. Ivanauskaitė, G. Milinavičiūtė, V. Smirnovas, V. Petrikaitė, V. Kairys, V. Petrauskas, P. Norvaišas, D. Lingė, P. Gibieža, E. Čapkauskaitė, A. Zakšauskas, E. Kazlauskas, E. Manakova, S. Gražulis, J.E. Ladbury, D. Matulis, Discovery and characterization of novel selective inhibitors of carbonic anhydrase IX, *J. Med. Chem.* 57 (22) (2014) 9435–9446, <http://dx.doi.org/10.1021/jm501003k>.
- [24] A. Sharma, M. Tiwari, C.T. Supuran, Novel coumarins and benzocoumarins acting as isoform-selective inhibitors against the tumor-associated carbonic anhydrase IX, *J. Enzyme Inhib. Med. Chem.* 29 (2) (2014) 292–296, <http://dx.doi.org/10.3109/14756366.2013.777334>.
- [25] T. Rogez-Florent, S. Meignan, C. Foulon, P. Six, A. Gros, C. Bal-Mahieu, C.T. Supuran, A. Scozzafava, R. Frédérick, B. Masereel, P. Depreux, A. Lansiaux, J.-F. Goossens, S. Gluszk, L. Goossens, New selective carbonic anhydrase IX inhibitors: synthesis and pharmacological evaluation of diarylpyrazole-benzenesulfonamides, *Bioorg. Med. Chem.* 21 (6) (2013) 1451–1464, <http://dx.doi.org/10.1016/j.bmc.2012.10.029>.
- [26] M. Kišonaitė, A. Zubrienė, E. Čapkauskaitė, S. Alexey, S. Joana, V. Kairys, V. Michailovienė, E. Manakova, S. Gražulis, D. Matulis, Intrinsic thermodynamics and structure correlation of benzenesulfonamides with a pyrimidine moiety binding to carbonic anhydrases I, II, VII, XII, and XIII, *PLoS One* 9 (12) (2014), e114106 <http://dx.doi.org/10.1371/journal.pone.0114106>.
- [27] G. Klebe, Applying thermodynamic profiling in lead finding and optimization, *Nat. Rev. Drug Discov.* 14 (2) (2015) 95–110, <http://dx.doi.org/10.1038/nrd4486>.
- [28] T.E. Carver, B. Bordeau, M.D. Cummings, E.C. Petrella, M.J. Pucci, L.E. Zawadzke, B.A. Dougherty, J.A. Tredup, J.W. Bryson, J. Yanchunas, M.L. Doyle, M.R. Witmer, M.I. Nelen, R.L. Desjarlais, E.P. Jaeger, H. Devine, E.D. Asel, B.A. Springer, R. Bone, F.R. Salemme, M.J. Todd, Decrypting the biochemical function of an essential gene from streptococcus pneumoniae using thermofluor technology, *J. Biol. Chem.* 280 (12) (2005) 11704–11712, <http://dx.doi.org/10.1074/jbc.M413278200>.
- [29] T.M. Mezzasalma, J.K. Kranz, W. Chan, G.T. Struble, C. Schalk-Hihi, I.C. Deckman, B.A. Springer, M.J. Todd, Enhancing recombinant protein quality and yield by protein stability profiling, *J. Biomol. Screen.* 12 (3) (2007) 418–428, <http://dx.doi.org/10.1177/1087057106297984>.
- [30] M. Todd, F.R. Salemme, Direct binding assays for pharma screening, *Genetic Eng. News* 23 (3) (2003) 28–29.
- [31] D. Matulis, J.K. Kranz, F.R. Salemme, M.J. Todd, Thermodynamic stability of carbonic anhydrase: measurements of binding affinity and stoichiometry using thermofluor, *Biochemistry* 44 (13) (2005) 5258–5266, <http://dx.doi.org/10.1021/bi048135v>.
- [32] J. Kervinen, H. Ma, S. Bayoumy, C. Schubert, C. Milligan, F. Lewandowski, K. Moriarty, R.L. Desjarlais, K. Ramachandren, H. Wang, C.A. Harris, B. Grasberger, M. Todd, B.A. Springer, I. Deckman, Effect of construct design on mapkap kinase-2 activity, thermodynamic stability and ligand-binding affinity, *Arch. Biochem. Biophys.* 449 (1–2) (2006) 47–56, <http://dx.doi.org/10.1016/j.abb.2006.03.018>.
- [33] A. Zubrienė, E. Kazlauskas, L. Baranauskienė, V. Petrauskas, D. Matulis, Isothermal titration calorimetry and thermal shift assay in drug design, *Eur. Pharm. Rev.* 16 (2011) 56–59.
- [34] J.K. Kranz, C. Schalk-Hihi, Protein thermal shifts to identify low molecular weight fragments, *Methods Enzymol.* 493 (2011) 277–298, <http://dx.doi.org/10.1016/B978-0-12-381274-2.00011-X>.
- [35] P. Cimmperman, D. Matulis, Protein Thermal Denaturation Measurements via a Fluorescent Dye, RSC Publishing, 2011 247–274 (Ch. 8).
- [36] J. Slavik, Anilnonaphthalene sulfonate as a probe of membrane composition and function, *Biochim. Biophys. Acta* 694 (1) (1982) 1–25 (URL [http://www.ncbi.nlm.nih.gov/entrez/query.fcgi?cmd=Retrieve&db=PubMed&dopt=Citation&list\\_uids=6751394](http://www.ncbi.nlm.nih.gov/entrez/query.fcgi?cmd=Retrieve&db=PubMed&dopt=Citation&list_uids=6751394)).
- [37] D. Matulis, R. Lovrien, 1-anilino-8-naphthalene sulfonate anion-protein binding depends primarily on ion pair formation, *Biophys. J.* 74 (1) (1998) 422–429.
- [38] D. Matulis, C.G. Baumann, V.A. Bloomfield, R.E. Lovrien, 1-anilino-8-naphthalene sulfonate as a protein conformational tightening agent, *Biopolymers* 49 (6) (1999) 451–458.
- [39] B.M. Baker, K.P. Murphy, Evaluation of linked protonation effects in protein binding reactions using isothermal titration calorimetry, *Biophys. J.* 71 (4) (1996) 2049–2055.
- [40] V. Morkūnaitė, J. Gyltė, A. Zubrienė, L. Baranauskienė, M. Kišonaitė, V. Michailovienė, V. Juozapaitienė, M. J. Todd, D. Matulis, Intrinsic thermodynamics of sulfonamide inhibitor binding to human carbonic anhydrases I and II, *J. Enzyme Inhib. Med. Chem.* <http://dx.doi.org/10.3109/14756366.2014.908291>.
- [41] J. Kazokaitė, G. Milinavičiūtė, J. Smirnovienė, J. Matulienė, D. Matulis, Intrinsic binding of 4-substituted-2,3,5,6-tetrafluorobenzenesulfonamides to native and recombinant human carbonic anhydrase vi, *FEBS J.* 282 (5) (2015) 972–983, <http://dx.doi.org/10.1111/febs.13196>.
- [42] V. Piliupitytė, D. Matulis, Intrinsic thermodynamics of trifluoromethanesulfonamide and ethoxzolamide binding to human carbonic anhydrase VII, *J. Mol. Recognit.* 28 (3) (2015) 166–172, <http://dx.doi.org/10.1002/jmr.2404>.

- [43] V. Jogaitė, A. Zubrienė, V. Michailovienė, J. Gylytė, V. Morkūnaitė, D. Matulis, Characterization of human carbonic anhydrase XII stability and inhibitor binding, *Bioorg. Med. Chem.* 21 (6) (2013) 1431–1436, <http://dx.doi.org/10.1016/j.bmc.2012.10.016>.
- [44] L. Baranauskienė, D. Matulis, Intrinsic thermodynamics of ethoxzolamide inhibitor binding to human carbonic anhydrase XIII, *BMC Biophys.* 5 (12) (2012) <http://dx.doi.org/10.1186/2046-1682-5-12>.
- [45] A. Kasiliauskaitė, V. Časaitė, V. Juozapaitienė, A. Zubrienė, V. Michailovienė, J. Revuckienė, L. Baranauskienė, R. Meškys, D. Matulis, Thermodynamic characterization of human carbonic anhydrase VB stability and intrinsic binding of compounds, *J. Therm. Anal. Calorim.* <http://dx.doi.org/10.1007/s10973-015-5073-3>.
- [46] D. Dekaminavičiute, R. Lasickiene, S. Parkkila, V. Jogaitė, J. Matuliene, D. Matulis, A. Zvirbliene, Development and characterization of new monoclonal antibodies against human recombinant ca XII, *Biomed. Res. Int.* 2014 (2014) 309307, <http://dx.doi.org/10.1155/2014/309307>.
- [47] A. Zubrienė, E. Čapkauskaitė, J. Gylytė, M. Kišonaitė, S. Tumkevičius, D. Matulis, Benzenesulfonamides with benzimidazole moieties as inhibitors of carbonic anhydrases I, II, VII, XII and XIII, *J. Enzyme Inhib. Med. Chem.* 29 (1) (2014) 124–131, <http://dx.doi.org/10.3109/14756366.2012.757223>.
- [48] E. Čapkauskaitė, L. Baranauskienė, D. Golovenko, E. Manakova, S. Gražulis, S. Tumkevičius, D. Matulis, Indapamide-like benzenesulfonamides as inhibitors of carbonic anhydrases I, II, VII, and XIII, *Bioorg. Med. Chem.* 18 (21) (2010) 7357–7364, <http://dx.doi.org/10.1016/j.bmc.2010.09.016>.
- [49] E. Kazlauskas, V. Petrikaitė, V. Michailovienė, J. Revuckienė, J. Matulienė, L. Grinius, D. Matulis, Thermodynamics of aryl-dihydroxyphenyl-thiadiazole binding to human hsp90, *PLoS ONE* 7 (5) (2012), e36899 <http://dx.doi.org/10.1371/journal.pone.0036899>.
- [50] A. Zubrienė, M. Gutkowska, J. Matulienė, R. Chaleckis, V. Michailovienė, A. Voroncova, V. Venclovas, A. Zylicz, M. Zylicz, D. Matulis, Thermodynamics of radicicol binding to human hsp90 alpha and beta isoforms, *Biophys. Chem.* 152 (1–3) (2010) 153–163, <http://dx.doi.org/10.1016/j.bpc.2010.09.003>.
- [51] V.M. Krishnamurthy, B.R. Bohall, C.-Y. Kim, D.T. Moustakas, D.W. Christianson, G.M. Whitesides, Thermodynamic parameters for the association of fluorinated benzenesulfonamides with bovine carbonic anhydrase II, *Chem. Asian. J.* 2 (2007) 94–105.
- [52] V.M. Krishnamurthy, G.K. Kaufman, A.R. Urbach, I. Gitlin, K.L. Gudiksen, D.B. Weibel, G.M. Whitesides, Carbonic anhydrase as a model for biophysical and physical-organic studies of proteins and protein-ligand binding, *Chem. Rev.* 108 (3) (2008) 946–1051, <http://dx.doi.org/10.1021/cr050262p>.
- [53] A. Zubrienė, J. Smirmovienė, A. Smirnov, V. Morkūnaitė, V. Michailovienė, J. Jachno, V. Juozapaitienė, P. Norvaišas, E. Manakova, S. Gražulis, D. Matulis, Intrinsic thermodynamics of 4-substituted-2,3,5,6-tetrafluorobenzenesulfonamide binding to carbonic anhydrases by isothermal titration calorimetry, *Biophys. Chem.* 205 (2015) 51–65, <http://dx.doi.org/10.1016/j.bpc.2015.05.009>.
- [54] R.W. King, A.S. Burgen, Kinetic aspects of structure-activity relations: the binding of sulphonamides by carbonic anhydrase, *Proc. R. Soc. Lond. B Biol. Sci.* 193 (1111) (1976) 107–125.
- [55] S.G. Krimmer, G. Klebe, Thermodynamics of protein-ligand interactions as a reference for computational analysis: how to assess accuracy, reliability and relevance of experimental data, *J. Comput. Aided Mol. Des.* <http://dx.doi.org/10.1007/s10822-015-9867-y>.

## Kinetically Selective Inhibitors of Human Carbonic Anhydrase Isozymes I, II, VII, IX, XII, and XIII

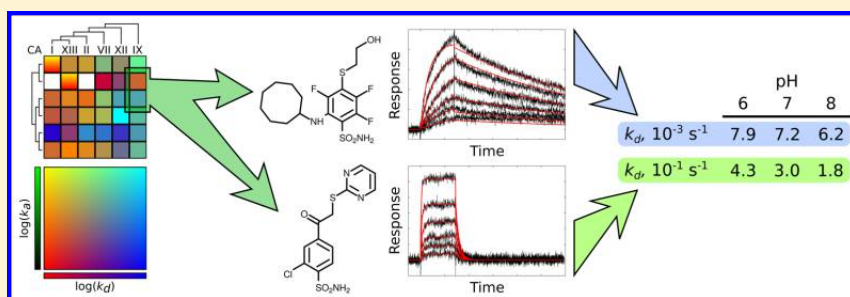
Vladimir O. Talibov,<sup>†</sup> Vaida Linkuvienė,<sup>‡</sup> Daumantas Matulis,<sup>‡</sup> and U. Helena Danielson<sup>\*,†,§</sup>

<sup>†</sup>Department of Chemistry – BMC, Uppsala University, Box 576, Uppsala SE-751 23, Sweden

<sup>‡</sup>Department of Biothermodynamics and Drug Design, Institute of Biotechnology, Vilnius University, V.A. Graičiūno 8, Vilnius LT-02241, Lithuania

<sup>§</sup>Science for Life Laboratory, Uppsala University, Uppsala SE-751 23, Sweden

**S** Supporting Information



**ABSTRACT:** To get a better understanding of the possibility of developing selective carbonic anhydrase (CA) inhibitors, interactions between 17 benzenesulphonamide ligands and 6 human CAs (full-length CA I, II, VII, and XIII and catalytic domains of CA IX and XII) were characterized using surface plasmon resonance and fluorescent-based thermal shift assays. Kinetics revealed that the strongest binders had subnanomolar affinities with low dissociation rates (i.e.,  $k_d$  values around  $1 \times 10^{-3} \text{ s}^{-1}$ ) or were essentially irreversible. Chemodynamic analysis of the interactions highlighted an intrinsic mechanism of the CA–sulphonamide interaction kinetics and showed that slow dissociation rates were mediated by large hydrophobic contacts. The studied inhibitors demonstrated a high cross-reactivity within the protein family. However, according to chemical phylogenetic analysis developed for kinetic data, several ligands were found to be selective against certain CA isozymes, indicating that it should be possible to develop selective CA inhibitors suitable for clinical use.

### INTRODUCTION

Carbonic anhydrases (CAs) catalyze the reversible conversion of carbon dioxide and water into hydrocarbonate and a proton (or a hydronium cation).<sup>1</sup> Enzymes of this family, being involved in a basic homeostasis reaction, are present in all biological species.<sup>2,3</sup> A prominent class within the family is represented by the  $\alpha$ -carbonic anhydrases. They are found predominantly in mammals, and at least 15 homologous variants are expressed in humans.<sup>4</sup> The cellular localization of the isozymes varies and includes cytosolic (CA I, II, III, VII, and XIII), membrane bound (CA IV, IX, XII, and XIV), secreted (CA VI), and mitochondrial (CA VA and VB) forms.<sup>5</sup> The  $\alpha$ -carbonic anhydrase domain is usually formed by 10  $\beta$ -strands and 7 right-handed  $\alpha$ -helices.<sup>6</sup> The active site cleft is cone-shaped and consists of hydrophobic and hydrophilic walls, with the  $\text{Zn}^{2+}$  ion at the bottom. The zinc cation is a prosthetic cofactor, tetragonally coordinated by three histidine residues and a water molecule or a hydroxide anion.

A variety of cellular functions are mediated by CAs,<sup>7</sup> and the tissue-dependent expression of these isozymes makes them a

target for the treatment of different diseases. CA inhibitors serve as diuretic agents and are used for glaucoma, epilepsy, and osteoporosis therapy. Today, approximately 30 CA inhibitors are used in clinical practice.<sup>8</sup> The majority of these compounds are sulphonamides or isosteres thereof. Although other groups exist, the sulphonamide functional group serves as the most efficient pharmacophore in CA inhibitors. It provides tight binding to the active site and inhibits activity by substitution of the water molecule within the zinc coordination sphere, which is crucial for catalysis.<sup>9</sup>

Of particular interest to us is that recent studies have shown the importance of certain CA isozymes in tumorigenesis. For example, the membrane-bound isozyme CA IX is a low-abundance protein in healthy tissues but is overexpressed in several types of cancer.<sup>10</sup> CA XII, another membrane-bound isozyme, is also a tumor-associated protein.<sup>11</sup> Development of

Received: November 5, 2015

Published: January 25, 2016

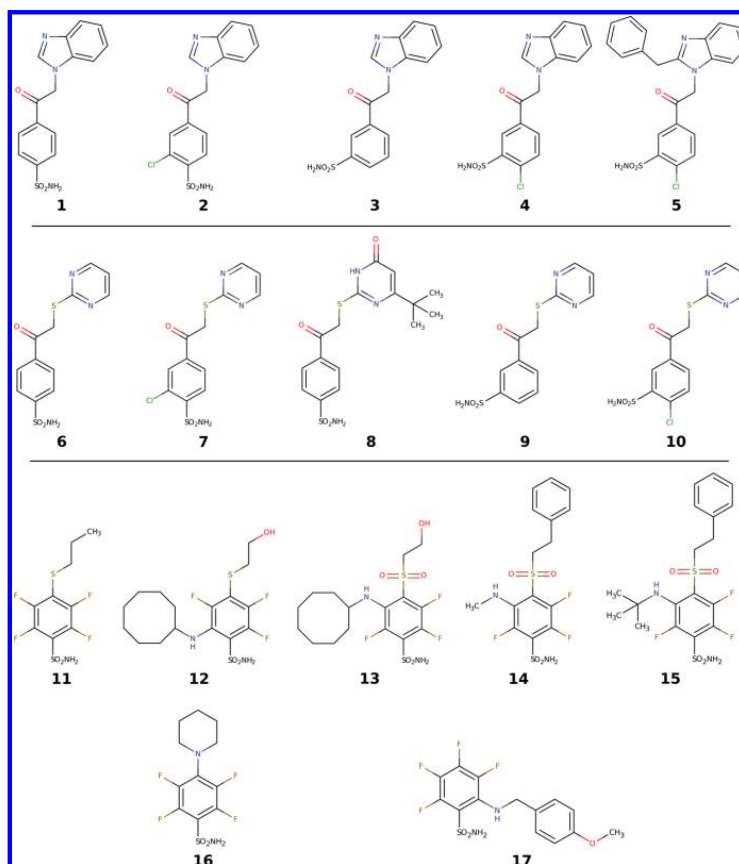


**Figure 1.** Structures of the studied benzenesulphonamides: N-alkylated benzimidazole derivatives 1–3,<sup>20</sup> 4, and 5;<sup>23</sup> S-alkylated 2-thiopyrimidine derivatives 6, 8, 10,<sup>24</sup> 7, and 9;<sup>21</sup> and fluorine-substituted benzenesulphonamides 11, 16,<sup>25</sup> 12, 13,<sup>22,26</sup> 14, 15, and 17.<sup>26</sup>

specific CA inhibitors is, therefore, a possible route to novel chemotherapeutic agents.<sup>12</sup>

A major challenge is the diffuse distribution of different isozymes across all tissue types, which is linked to potential adverse effects of CA inhibitor medication. The high structural similarity of the active site of all isoforms in the protein family makes selective inhibition of certain isozymes difficult.<sup>5</sup> A detailed biophysical characterization is expected to be important in order to better understand how efficient, potentially selective drugs can be designed. Kinetic parameters, simplified to association and dissociation rate constants ( $k_a$  and  $k_d$ , respectively), and the residence time are useful for ranking and optimization of leads.<sup>13,14</sup> Among kinetic methods, surface plasmon resonance (SPR) biosensor technology remains the state-of-the-art technique for characterization of the dynamic properties of interactions.

In contrast to previous studies that have used CA as a model system for SPR application development<sup>15–18</sup> and that typically involve human CA II or its bovine orthologue,<sup>19</sup> the present research is focused on studying interactions with CAs with relevance as drug targets. In addition, a library of inhibitors was kinetically characterized against different species of the CA protein family in order to better understand isozyme selectivity. The compounds designed as leads have previously been

characterized with respect to binding thermodynamics to various CA isoforms,<sup>20–22</sup> but their interaction kinetics had not been studied previously.

Here, we report the interaction between 17 benzenesulphonamide-based inhibitors (Figure 1) and 6 recombinant human carbonic anhydrases, namely, CA I, II, VII, and XIII and the catalytic domains of CA IX and XII. The equilibrium interaction parameters were determined using a fluorescence-based thermal shift assay (FTSA), and the kinetics of the interactions were determined using SPR biosensor assays.

## RESULTS

**Interaction Kinetic Analysis. Preparation of Sensor Surfaces.** In order to evaluate the kinetics of the interactions of the benzenesulphonamide-based inhibitors with different isozymes of the human CA family, SPR biosensor analysis was employed. Full-length CA I, II, VII, and XIII and the catalytic domains of CA IX and XII (CA IX<sub>cd</sub> and XII<sub>cd</sub>) were immobilized to the dextran matrix of standard sensor chips. Despite the high similarity among the structures of the selected proteins, it was impossible to use the same conditions for the immobilization of all enzyme variants. Thus, both protein concentration and coupling buffer pH were adjusted for each isozyme. The level of immobilization ranged from 4000

resonance units (RU) for CA IX<sub>cd</sub> to 12 000 RU for CA XII<sub>cd</sub>, whereas CA I, II, VII, and XIII were immobilized at approximately the same level, 6000 RU.

In general, the generated sensor surfaces were stable enough under the developed assay conditions to be used for a couple of days. An exception was the sensor surface for CA IX<sub>cd</sub>, which demonstrated a reduction of the baseline level during the assay cycles, approaching half of the initial immobilization level. However, the surface decay was slow and did not influence the  $R_{\max}$  value within a concentration series.

CA XII<sub>cd</sub> tended to precipitate on the surface when 10 mM acetate buffer was used for the immobilization, resulting in unexpectedly high immobilization levels. This effect was observed not only for the activated carboxymethyl-dextran matrix but also for the intact or activated/deactivated surface. Uncovalently bound enzyme could be removed by 10 mM phosphate buffer in the presence of 1 M NaCl, indicating the electrostatic nature of the aggregation.

**Kinetic Experiments.** Time-resolved interaction curves (sensorgrams) were collected for the interactions between 6 human CA isozymes and 17 ligands. The sensor surfaces had a high enough sensitivity to detect all of the interactions and to provide sufficient levels of signal for the kinetic analysis despite the low molecular weight of the studied compounds (300–400 Da; exemplified in Figure 2 by CA VII and compound 14).

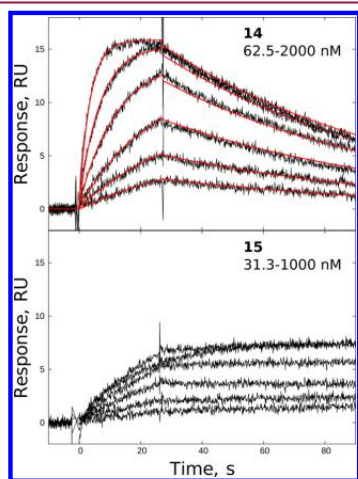


**Figure 2.** Sensorgrams for the interactions between CA VII and two structurally related ligands, 14 and 15. For compound 14, a reversible one-step model was fitted to the processed experimental data (red line).

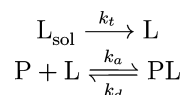
The kinetic analysis was severely restricted by the high stability of the formed complexes. Several interactions (for example, between CA VII and compound 15; Figure 2) did not have any observable dissociation. A variety of common regeneration strategies were explored, such as forced complex dissociation using elevated or decreased pH values, chaotropic agents, and high detergent concentrations. These approaches were unsuccessful or resulted in irreversible protein denaturation. An alternative strategy involved displacement of the tight binder by an injection of an excess of a low-affinity binder. This methodology allowed the kinetics of the majority of the potent binders to be analyzed, but it did not work for the tightest

complexes, i.e., those with subnano- or picomolar affinities, as estimated by FTSA.

Obtaining replicate data for the majority of the interactions became a practical limitation because a proper replicate experiment requires not only the preparation of fresh ligand but also the generation of a new surface. In the present study, the number and diversity of the proteins used for the immobilization resulted in the experiments being time-consuming and expensive. Therefore, only experiments with the most interesting interaction pairs, for example, the interactions of benzenesulphonamides with CA IX<sub>cd</sub>, were repeated in duplicates and triplicates.

**Data Analysis.** To extract the kinetic parameters for the interactions, the processed sensorgrams were analyzed using nonlinear regression. A reversible one-step model with mass-transport limitations (Scheme 1) was the simplest model that

**Scheme 1. Reversible One-Step Interaction with Mass Transport for the Interaction between Protein and Ligand<sup>a</sup>**



<sup>a</sup>P, protein;  $L_{\text{sol}}$ , ligand in the flow phase; L, ligand within the surface layer.  $k_a$  and  $k_d$  are the association and dissociation rate constants, respectively, and  $k_t$  is the diffusion rate constant.

provided satisfactory fits for the majority of the interactions. Mass-transport effects for the given interactions could be considered negligible since the diffusion rate constants were a few orders of magnitude higher than the association rate constants and satisfied the empirical criterion proposed by Karlsson<sup>27</sup> ( $k_a \times R_{\max}/k_t < 5$ ). This model is in agreement with the current model of sulphonamide binding to the active site of CAs.<sup>28</sup> The extracted kinetic parameters are listed in Table 1.

A one-step binding model with variable  $R_{\max}$  between the different cycles for a concentration series was used to analyze the tight interactions that resulted in surfaces that could not be regenerated or that could be partially regenerated. For such surfaces, the  $R_{\max}$  decreased with increasing analyte concentration, indicating irreversible blocking of the protein binding sites (reduction of the surface-specific binding capacity). The approximate values for the kinetic parameters were used, therefore, only for a qualitative description of the kinetics.

The affinities for the interactions determined by SPR ( $K_D^{\text{SPR}}$ ) were similar to the affinities obtained using FTSA ( $K_D^{\text{FTSA}}$ ), as shown in Figure 3. The largest mismatches were observed for the interactions with slow dissociation rates (Table 1). Essentially irreversible interactions identified by SPR analysis had subnanomolar  $K_D^{\text{FTSA}}$  values.

Structure–kinetic relationships were identified through the kinetic analysis. To visualize the kinetics and analyze the difference between the interactions of the isozymes and the ligands, the data was graphed in interaction kinetic plots as  $\log_{10}(k_d)$  vs  $\log_{10}(k_a)$  (Figure 4). In general, *p*-substituted acetylated heterocyclic derivatives of the studied benzenesulphonamides showed higher affinities than *m*-substituted derivatives. With some exceptions, the benzimidazole heterocyclic moiety within the benzenesulphonamide structure was more favorable than the pyrimidine. The highest affinities were found among the fluorine-substituted derivatives (Table 1 and Figure 4). Within the first and second compound groups

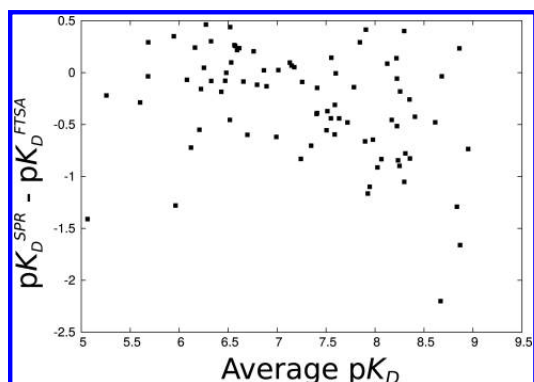
Table 1. Kinetic Parameters and Equilibrium Dissociation Constants for the Interactions between Benzenesulphonamides and Recombinant Human CA Isoforms I, II, VII, IX, XII, and XIII<sup>4†</sup>

compound	CA I			CA II			CA VII		
	$k_p$ , M <sup>-1</sup> s <sup>-1</sup>	$k_d$ , s <sup>-1</sup>	$K_D^{SPR}$ , M	$k_p$ , M <sup>-1</sup> s <sup>-1</sup>	$k_d$ , s <sup>-1</sup>	$K_D^{FTSA}$ , M	$k_p$ , M <sup>-1</sup> s <sup>-1</sup>	$k_d$ , s <sup>-1</sup>	$K_D^{FTSA}$ , M
1	$2 \times 10^5$	$7.9 \times 10^{-3}$	$3.7 \times 10^{-8}$	n/d	n/d	$1.5 \times 10^{-9}$	$8.1 \times 10^5$	$5.5 \times 10^{-3}$	$6.8 \times 10^{-9}$
2	$3.3 \times 10^5$	$7.5 \times 10^{-3}$	$2.2 \times 10^{-8}$	$7.7 \times 10^5$	$4.6 \times 10^{-3}$	$3.3 \times 10^{-9}$	$9.8 \times 10^5$	$1.7 \times 10^{-2}$	$1.7 \times 10^{-8}$
3	$1.8 \times 10^4$	$7.9 \times 10^{-1}$	$4.4 \times 10^{-5}$	$8.2 \times 10^5$	$6.2 \times 10^{-1}$	$1.7 \times 10^{-6}$	$4.4 \times 10^5$	$6.5 \times 10^{-1}$	$1.5 \times 10^{-6}$
4	n/d	n/d	n/d	$2.8 \times 10^5$	$1.5 \times 10^{-1}$	$5.3 \times 10^{-7}$	$1.6 \times 10^5$	$2.7 \times 10^{-1}$	$1.7 \times 10^{-6}$
5	n/d	n/d	n/d	$3.8 \times 10^5$	$1.3 \times 10^{-1}$	$3.3 \times 10^{-7}$	$6.7 \times 10^{-7}$	$6.1 \times 10^{-2}$	$3.1 \times 10^{-7}$
6	$2.0 \times 10^5$	$1.2 \times 10^{-2}$	$6.3 \times 10^{-8}$	$1.6 \times 10^6$	$8.0 \times 10^{-3}$	$7.1 \times 10^{-9}$	$2.9 \times 10^6$	$2.2 \times 10^{-2}$	$2.0 \times 10^{-8}$
7	$3.1 \times 10^5$	$8.4 \times 10^{-3}$	$2.7 \times 10^{-8}$	$3.9 \times 10^5$	$4.2 \times 10^{-3}$	$3.3 \times 10^{-9}$	$3.7 \times 10^6$	$4.4 \times 10^{-2}$	$1.2 \times 10^{-8}$
8	$6.3 \times 10^5$	$1.7 \times 10^{-3}$	$2.6 \times 10^{-9}$	$6.4 \times 10^5$	$3.0 \times 10^{-2}$	$4.7 \times 10^{-8}$	$4.9 \times 10^5$	$2.5 \times 10^{-2}$	$5.1 \times 10^{-8}$
9	$1.8 \times 10^5$	$2.1 \times 10^{-1}$	$1.2 \times 10^{-6}$	$3.4 \times 10^5$	$1.8 \times 10^{-1}$	$4.3 \times 10^{-7}$	$6.4 \times 10^5$	1.4	$2.2 \times 10^{-6}$
10	$1.2 \times 10^5$	$4.3 \times 10^{-1}$	$3.5 \times 10^{-6}$	$5.5 \times 10^5$	$7.3 \times 10^{-2}$	$1.3 \times 10^{-7}$	$4.1 \times 10^5$	$1.5 \times 10^{-1}$	$3.7 \times 10^{-7}$
11	s/d	s/d	s/d	$3.3 \times 10^{-11}$	s/d	s/d	$9.1 \times 10^{-10}$	$3.3 \times 10^{-2}$	$6.5 \times 10^{-9}$
12	n/d	n/d	n/d	$9.1 \times 10^{-6}$	n/d	n/d	$4.5 \times 10^{-7}$	$1.0 \times 10^{-2}$	$5.1 \times 10^{-7}$
13	n/d	n/d	n/d	$3.3 \times 10^{-7}$	$8.7 \times 10^{-3}$	$1.0 \times 10^{-7}$	$2.0 \times 10^4$	$2 \times 10^{-3}$	$4.0 \times 10^{-8}$
14	$3.9 \times 10^5$	$1.0 \times 10^{-2}$	$2.5 \times 10^{-8}$	$1.3 \times 10^6$	$8.2 \times 10^{-3}$	$6.4 \times 10^{-9}$	$2.9 \times 10^5$	$1.3 \times 10^{-2}$	$4.5 \times 10^{-8}$
15	n/d	n/d	n/d	$2.2 \times 10^{-7}$	s/d	s/d	$5.9 \times 10^{-10}$	s/d	s/d
16	s/d	s/d	s/d	$1.4 \times 10^6$	$9.3 \times 10^{-3}$	$6.8 \times 10^{-9}$	$4.5 \times 10^{-9}$	$7.1 \times 10^{-2}$	$2.7 \times 10^{-8}$
17	$1.1 \times 10^5$	$6.6 \times 10^{-3}$	$6.1 \times 10^{-8}$	$3.9 \times 10^5$	$2.6 \times 10^{-2}$	$6.6 \times 10^{-8}$	$3.0 \times 10^4$	$1.4 \times 10^{-1}$	$4.8 \times 10^{-6}$

compound	CA IX <sub>cat</sub>			CA XII <sub>cat</sub>			CA XIII		
	$k_p$ , M <sup>-1</sup> s <sup>-1</sup>	$k_d$ , s <sup>-1</sup>	$K_D^{SPR}$ , M	$k_p$ , M <sup>-1</sup> s <sup>-1</sup>	$k_d$ , s <sup>-1</sup>	$K_D^{FTSA}$ , M	$k_p$ , M <sup>-1</sup> s <sup>-1</sup>	$k_d$ , s <sup>-1</sup>	$K_D^{FTSA}$ , M
1	$1.6 \times 10^6$	$5.9 \times 10^{-2}$	$3.7 \times 10^{-8}$	$2.8 \times 10^5$	$5.1 \times 10^{-2}$	$1.9 \times 10^{-7}$	$2.3 \times 10^5$	$5.7 \times 10^{-3}$	$2.4 \times 10^{-8}$
2	$3.1 \times 10^6$	$1.4 \times 10^{-1}$	$4.7 \times 10^{-8}$	$3.8 \times 10^5$	$1.7 \times 10^{-1}$	$4.5 \times 10^{-7}$	$6.3 \times 10^5$	$2.0 \times 10^{-3}$	$3.2 \times 10^{-8}$
3	$1.3 \times 10^6$	$3.1 \times 10^{-1}$	$2.4 \times 10^{-7}$	$7.2 \times 10^4$	$5.12 \times 10^{-1}$	$7.1 \times 10^{-6}$	$9.3 \times 10^4$	$4.9 \times 10^{-2}$	$5.2 \times 10^{-7}$
4	$1.8 \times 10^6$	$8.4 \times 10^{-1}$	$4.6 \times 10^{-7}$	$1.6 \times 10^5$	$1.4 \times 10^{-1}$	$9.0 \times 10^{-7}$	n/d	n/d	n/d
5	n/d	n/d	n/d	$1.0 \times 10^5$	$2.0 \times 10^{-2}$	$2.0 \times 10^{-7}$	$8.3 \times 10^4$	$4.3 \times 10^{-2}$	$5.1 \times 10^{-7}$
6	$3.2 \times 10^6$	$2.1 \times 10^{-1}$	$6.6 \times 10^{-8}$	$2 \times 10^7$	2.7	$1.4 \times 10^{-7}$	$2.8 \times 10^5$	$1.7 \times 10^{-2}$	$6.1 \times 10^{-8}$
7	$1.8 \times 10^6$	$2.6 \times 10^{-1}$	$1.5 \times 10^{-7}$	$1.6 \times 10^6$	$3.2 \times 10^{-1}$	$2.0 \times 10^{-7}$	$7.2 \times 10^5$	$4.6 \times 10^{-3}$	$6.4 \times 10^{-9}$
8	$2.5 \times 10^6$	$8.4 \times 10^{-2}$	$3.3 \times 10^{-8}$	$4.0 \times 10^5$	$2.5 \times 10^{-2}$	$6.3 \times 10^{-8}$	$2.4 \times 10^6$	$1.0 \times 10^{-2}$	$4.2 \times 10^{-9}$
9	$1.2 \times 10^6$	$3.1 \times 10^{-1}$	$2.6 \times 10^{-7}$	n/d	n/d	n/d	$7.1 \times 10^4$	$5.1 \times 10^{-2}$	$7.1 \times 10^{-7}$
10	$2.0 \times 10^6$	$4.0 \times 10^{-1}$	$2.0 \times 10^{-7}$	$8.8 \times 10^5$	$1.6 \times 10^{-1}$	$1.8 \times 10^{-7}$	$5.0 \times 10^{-7}$	$2.2 \times 10^{-2}$	$1.8 \times 10^{-7}$
11	$9.2 \times 10^6$	$1.1 \times 10^{-1}$	$1.1 \times 10^{-8}$	$1.3 \times 10^6$	$2.5 \times 10^{-2}$	$1.9 \times 10^{-8}$	$1.4 \times 10^{-8}$	s/d	s/d
12	$2.9 \times 10^5$	$7.7 \times 10^{-3}$	$2.7 \times 10^{-8}$	$1.3 \times 10^5$	$5.0 \times 10^{-2}$	$4.0 \times 10^{-7}$	s/d	s/d	s/d
13	s/d	s/d	s/d	$6.7 \times 10^{-12}$	s/d	s/d	$1.1 \times 10^{-9}$	$7.9 \times 10^{-3}$	$1.5 \times 10^{-8}$
14	$6.5 \times 10^6$	$1.0 \times 10^{-1}$	$1.6 \times 10^{-8}$	$1.5 \times 10^6$	$1.4 \times 10^{-1}$	$9.5 \times 10^{-8}$	$1.0 \times 10^{-7}$	s/d	s/d
15	$7.0 \times 10^5$	$6.4 \times 10^{-3}$	$9.2 \times 10^{-9}$	$1.8 \times 10^5$	$1.1 \times 10^{-2}$	$5.9 \times 10^{-8}$	$1.7 \times 10^{-8}$	s/d	s/d
16	$1.5 \times 10^7$	$1.5 \times 10^{-1}$	$1.0 \times 10^{-8}$	$8.8 \times 10^5$	$4.1 \times 10^{-2}$	$4.6 \times 10^{-8}$	$3.3 \times 10^{-8}$	$1.1 \times 10^{-2}$	$1.1 \times 10^{-8}$
17	$1.8 \times 10^6$	$2.6 \times 10^{-1}$	$1.5 \times 10^{-7}$	n/d	n/d	n/d	$1.0 \times 10^5$	$2.2 \times 10^{-2}$	$2.1 \times 10^{-7}$

<sup>a</sup>n/d, no data; s/d, slow dissociation rate. The SPR-estimated dissociation constants ( $K_D^{SPR}$ ) were determined from the kinetic parameters according to eq 4 and measured independently using FTSA ( $K_D^{FTSA}$ ). SPR and FTSA analyses were performed at 25°C.



**Figure 3.** Agreement between equilibrium dissociation constants determined by SPR and FTSA, shown as a Bland–Altman correlation plot (data from Table 1).

(Figure 4A,B), the *ortho*-chlorine substituent reduced the  $K_D$  for binding to all isozymes except CA IX<sub>cd</sub>. Ligands with a bulky hydrophobic functional group, such as a *t*-butyl (Figure 2; compound 15), phenyl, or cyclooctyl, demonstrated the lowest dissociation rate constants for the interaction.

**Selectivity Analysis.** The generated data was used to analyze the selectivity of the studied compounds. Although all compounds involved in the experiments interacted with  $K_D$  values equal to or less than  $10^{-6}$  M, it was possible to identify compounds with a higher affinity toward particular isozymes. In addition, compounds with affinities within a few orders of magnitude for the different protein variants demonstrated a clear difference in the interaction kinetics. This is exemplified

for the interactions between compound 8 and all six studied proteins in Figure 5. The affinity was highest for CA I and XIII and resulted in the formation of a stable complex. The rest of the isozymes had lower affinities, primarily as a result of faster dissociation rates. Thus, we consider compound 8 to be an example of a kinetically selective inhibitor. Likewise, compounds 12 and 13 are selective for the catalytic domain of CA IX, as justified by the interaction kinetics.

Comparison of the common trends for interactions between a set of compounds and multiple isozymes, considering the diversity of ligands and proteins, is difficult for a large data set. Thus, we performed a chemical phylogenetic analysis for the interaction kinetics of 6 human CAs and 17 benzenesulphonamides (Figure 6). Bidirectional hierarchical clustering was performed in a manner similar to that proposed by Bradner et al.,<sup>29</sup> but the interactions were weighted by their kinetic parameters ( $k_a$  and  $k_d$ ). It revealed that compounds interacted with CA IX<sub>cd</sub> and, to some extent, CA XII<sub>cd</sub> with faster association and dissociation rates than with other isozymes.

**pH Profiling of Interaction Kinetics.** The catalytic domains of CA IX and XII were chosen for pH-dependent interaction profiling. Ligands were chosen to be structurally related (compounds 6–8) or selective against CA IX (12), an enzyme isoform that may physiologically be influenced by varying pH.<sup>11,30</sup>

The kinetic analysis of the interactions at different pH values showed a clear pH dependence (Figure 7 and Table 2). Higher pH values of the reaction medium resulted in lower equilibrium dissociation constants and more rapid association kinetics. For the pyrimidine derivatives (6–8), an effect of pH was observed for both the apparent association and dissociation rate constants. Interestingly, the unhalogenated derivative 6 had

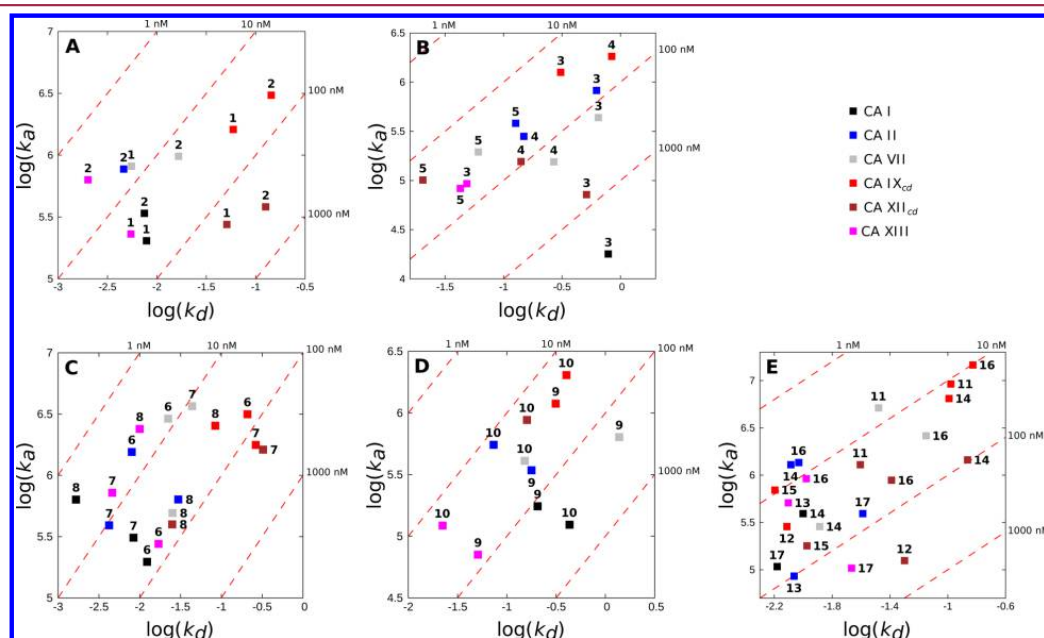


**Figure 4.** Interaction kinetic profiles for the benzenesulphonamides: (A) *p*- and (B) *m*-substituted benzimidazole analogues, (C) *p*- and (D) *m*-substituted thiopyrimidine analogues, and (E) fluorine-substituted analogues.

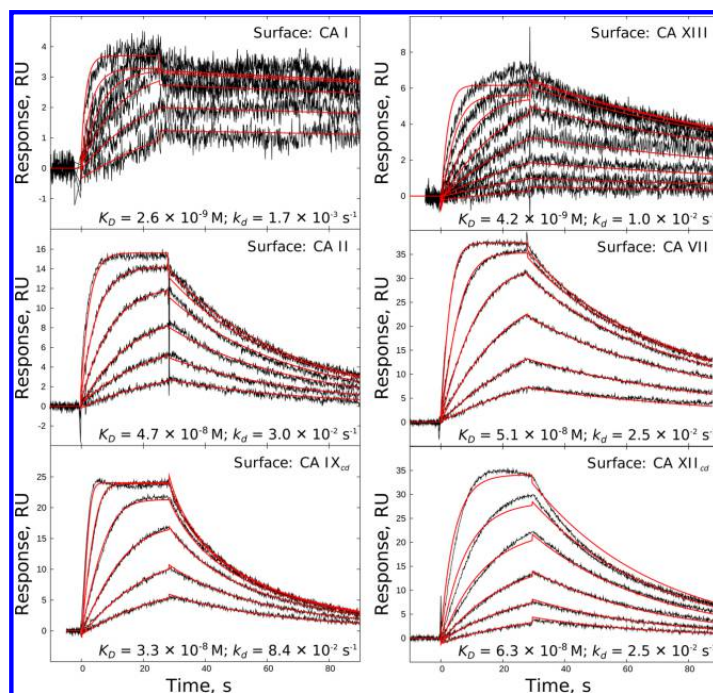


**Figure 5.** Selectivity analysis for compound **8** and six different CA isoforms. A reversible one-step model was fitted to the processed experimental data (red line).

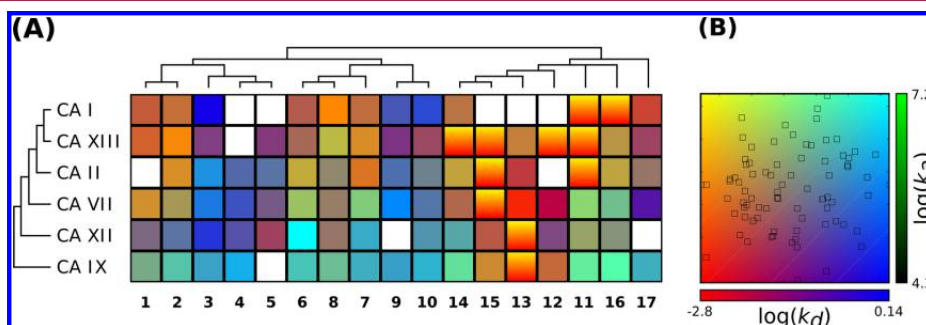


**Figure 6.** Chemical phylogenetic analysis of the interaction kinetics between studied benzenesulphonamides and six CA isoforms. Each entry in the rectangular array (A) corresponds to the individual set of association and dissociation rate constants from SPR analysis, distributed and scaled as shown in panel B. Protein and ligands are grouped according to structural similarity. Yellow-to-red gradient filling represents essentially irreversible interactions; white color corresponds to the absence of SPR data.

faster association rates than its halogenated analogue **7**, whereas larger compounds (e.g., **8**) had slower interactions.

The observed pH dependence should correlate with the  $pK_a$  of the sulphonamide group as it can be attributed to the protonation state of the amide. It needs to be deprotonated in order to establish a stable interaction with the  $Zn^{2+}$  cation in the active site. Moreover, the hydroxide anion within the metal coordination sphere should be protonated prior to the substitution by the deprotonated  $SA^{\ominus}$  (Scheme 2).

As a means to interpret the pH-dependencies of the rate constants, the effects of the protonation of the active site and the inhibitor were analyzed. By expressing the fractions of protonated enzyme and deprotonated inhibitor as

$$f_p = \frac{[(His)_3Zn-OH_2]^{2+}}{[(His)_3Zn-OH_2]^{2+} + [(His)_3Zn-OH]^{-}} \quad (1)$$

$$f_L = \frac{[RSO_2NH^{-}]}{[RSO_2NH^{-}] + [RSO_2NH_2]} \quad (2)$$

the second-order rate equation for complex formation (Scheme 1 with no mass transport) can, in the simplest case, be derived in the following way

$$\frac{d[PL]}{dt} = k_a^{int} f_p [P] f_L [L] - k_d^{int} [PL] \quad (3)$$



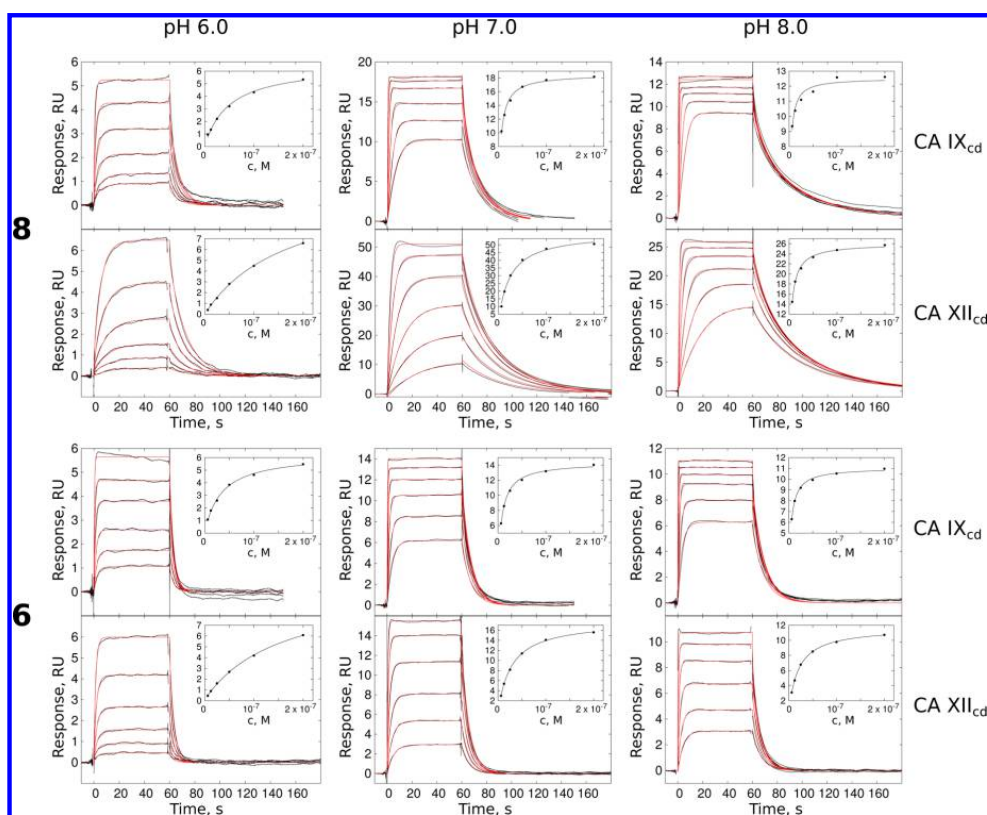


**Figure 7.** pH-dependent interaction profiling for CA IX<sub>cd</sub>, CA XII<sub>cd</sub>, and compounds **8** and **6** at pH 6.0, 7.0, and 8.0. Insets correspond to the binding isotherms. Estimated kinetic and equilibrium parameters are presented in Table 2.

**Table 2.** pH Dependence of the Interactions between the Catalytic Domains of CA IX and XII and Structurally Related Inhibitors 6–8 and CA IX-Selective Inhibitor 12<sup>a</sup>

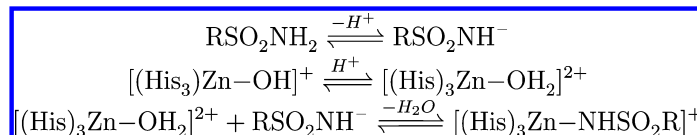
compound	parameter	pH 6.0		pH 7.0		pH 8.0	
		CA IX <sub>cd</sub>	CA XII <sub>cd</sub>	CA IX <sub>cd</sub>	CA XII <sub>cd</sub>	CA IX <sub>cd</sub>	CA XII <sub>cd</sub>
6	$k_{on}$ , M <sup>-1</sup> s <sup>-1</sup>	$(9.2 \pm 2.8) \times 10^5$	$(2.5 \pm 0.8) \times 10^5$	$(2.3 \pm 0.8) \times 10^6$	$(6.1 \pm 1.5) \times 10^5$	$(3.3 \pm 0.3) \times 10^6$	$(1.3 \pm 3) \times 10^6$
	$k_{off}$ , s <sup>-1</sup>	$(2.9 \pm 0.1) \times 10^{-1}$	$(2.5 \pm 0.5) \times 10^{-1}$	$(1.4 \pm 0.5) \times 10^{-1}$	$(1.6 \pm 0.5) \times 10^{-1}$	$(1.2 \pm 0.5) \times 10^{-1}$	$(1.2 \pm 0.4) \times 10^{-1}$
	$K_D^{kin}$ , M	$(3.3 \pm 0.9) \times 10^{-7}$	$(1.1 \pm 0.6) \times 10^{-6}$	$(6.2 \pm 0.6) \times 10^{-8}$	$(2.6 \pm 0.3) \times 10^{-7}$	$(3.8 \pm 1.3) \times 10^{-8}$	$(9.0 \pm 1.1) \times 10^{-8}$
	$K_D^S$ , M	$(3.3 \pm 0.1) \times 10^{-7}$	$(1.1 \pm 0.7) \times 10^{-6}$	$(8.0 \pm 1.7) \times 10^{-8}$	$(3.3 \pm 0.7) \times 10^{-7}$	$(1.1 \pm 0.8) \times 10^{-7}$	$(1.4 \pm 0.6) \times 10^{-7}$
7	$k_{on}$ , M <sup>-1</sup> s <sup>-1</sup>	$(4.4 \pm 2.0) \times 10^5$	$(3.6 \pm 0.5) \times 10^5$	$(1.8 \pm 0.8) \times 10^6$	$(8.6 \pm 0.9) \times 10^5$	$(1.7 \pm 0.2) \times 10^6$	$(1.8 \pm 1.0) \times 10^6$
	$k_{off}$ , s <sup>-1</sup>	$(4.3 \pm 0.3) \times 10^{-1}$	$(3.1 \pm 0.2) \times 10^{-1}$	$(3.0 \pm 1.5) \times 10^{-1}$	$(1.8 \pm 0.3) \times 10^{-1}$	$(1.8 \pm 0.1) \times 10^{-1}$	$(2.0 \pm 1.1) \times 10^{-1}$
	$K_D^{kin}$ , M	$(1.1 \pm 0.6) \times 10^{-6}$	$(8.6 \pm 1.8) \times 10^{-7}$	$(1.6 \pm 0.2) \times 10^{-7}$	$(2.1 \pm 0.2) \times 10^{-7}$	$(1.0 \pm 0.1) \times 10^{-7}$	$(1.2 \pm 0.1) \times 10^{-7}$
	$K_D^S$ , M	$(9.4 \pm 2.5) \times 10^{-7}$	$(1.1 \pm 0.2) \times 10^{-6}$	$(2.6 \pm 1.0) \times 10^{-7}$	$(2.7 \pm 0.5) \times 10^{-7}$	$(1.9 \pm 0.6) \times 10^{-7}$	$(1.9 \pm 0.8) \times 10^{-7}$
8	$k_{on}$ , M <sup>-1</sup> s <sup>-1</sup>	$(4.0 \pm 0.1) \times 10^5$	$(5.7 \pm 1.1) \times 10^4$	$(3.1 \pm 0.3) \times 10^6$	$(2.5 \pm 0.3) \times 10^5$	$(3.3 \pm 1.0) \times 10^6$	$(1.1 \pm 0.1) \times 10^6$
	$k_{off}$ , s <sup>-1</sup>	$(1.5 \pm 0.1) \times 10^{-1}$	$(7.1 \pm 0.9) \times 10^{-2}$	$(1.4 \pm 0.3) \times 10^{-1}$	$(5.6 \pm 0.5) \times 10^{-2}$	$(4.0 \pm 1.3) \times 10^{-2}$	$(4.9 \pm 0.8) \times 10^{-2}$
	$K_D^{kin}$ , M	$(3.6 \pm 0.1) \times 10^{-7}$	$(1.3 \pm 0.4) \times 10^{-6}$	$(4.6 \pm 0.5) \times 10^{-8}$	$(2.3 \pm 0.2) \times 10^{-7}$	$(1.3 \pm 0.2) \times 10^{-8}$	$(4.4 \pm 0.3) \times 10^{-8}$
	$K_D^S$ , M	$(4.4 \pm 0.7) \times 10^{-7}$	$(1.4 \pm 0.5) \times 10^{-6}$	$(5.6 \pm 1.7) \times 10^{-8}$	$(2.6 \pm 0.4) \times 10^{-7}$	$(2.0 \pm 0.3) \times 10^{-8}$	$(8.2 \pm 4.3) \times 10^{-8}$
12	$k_{on}$ , M <sup>-1</sup> s <sup>-1</sup>	$(5.8 \pm 0.1) \times 10^4$	n/d	$(1.6 \pm 0.4) \times 10^5$	n/d	$(3.3 \pm 0.3) \times 10^5$	n/d
	$k_{off}$ , s <sup>-1</sup>	$(7.9 \pm 0.8) \times 10^{-3}$	n/d	$(7.2 \pm 0.5) \times 10^{-3}$	n/d	$(6.2 \pm 1.0) \times 10^{-3}$	n/d
	$K_D^{kin}$ , M	$(1.4 \pm 1.1) \times 10^{-7}$	n/d	$(4.6 \pm 1.0) \times 10^{-8}$	n/d	$(1.9 \pm 0.5) \times 10^{-8}$	n/d
	$K_D^S$ , M	n/d	$(2.6 \pm 2.0) \times 10^{-6}$	n/d	$(8.4 \pm 1.9) \times 10^{-7}$	n/d	$(3.9 \pm 2.1) \times 10^{-7}$

<sup>a</sup>Kinetic assays were performed in 50 mM sodium phosphate, 150 mM NaCl at pH 6.0, 7.0, and 8.0;  $K_D^{kin}$ , dissociation constant calculated from the kinetic parameters;  $K_D^S$ , dissociation constant calculated from the saturation signals using eq 5. Data is given as an average from triplicates with a corresponding standard deviation.

where  $k_a^{int}$  and  $k_d^{int}$  in eq 3 correspond to intrinsic rate constants and concentrations are total reactant concentrations equal to

the sum of protonated/deprotonated forms. The apparent  $k_a$  values should be pH-dependent. However, this is not case for

Scheme 2. Sulphonamide Interaction with Carbonic Anhydrase Active Site and Linked Protonation/Deprotonation Reactions



apparent  $k_d$  values, as  $k_d = k_d^{\text{int}}$ . As expected, the present data showed a pH dependence of the  $k_a$  values as well as an unexpected pH dependence of  $k_d$  values. This indicates that the interaction with inhibitors 6–8 has a more complex intrinsic mechanism of dissociation than that described by eq 3. Curiously, the  $k_d$  values for compound 12 were not strongly influenced by pH.

The  $\text{p}K_a$  values for compound 6 and 8 are similar; however, the *t*-butyl substituent considerably decreased the dissociation rate.

## DISCUSSION

The designed SPR assay proved to be a powerful method for characterizing the interactions between sulphonamide inhibitors and the closely related CA isoforms. The main restriction was that the kinetic parameters could not be quantified for some interactions due to the high stability of the formed complexes. We have reported this problem earlier,<sup>31,32</sup> and no universal solution has yet been found. Instead, a qualitative analysis was used to discriminate the kinetic profiles for the tight binding ligands.

A low surface density was achieved for CA IX<sub>cd</sub>, which is most likely a result of the presence of only two lysine residues in the primary structure of the domain, namely, Lys133 and Lys354. This explains the low immobilization level of the isoform when standard amine coupling was employed. The observed decay of the baseline level is in accordance with the fact that CA IX exists as a cystine-linked covalent dimer, which is also the case in the truncated form containing the catalytic domain alone.<sup>33,34</sup> Surface stabilization by the injection of reducing reagent (e.g.,  $\beta$ -mercaptoethanol or dithiothreitol) was considered but not employed as such reagents were avoided due to the presence of a conservative intramolecular disulfide bridge.<sup>33</sup>

As can be seen from the structures of human CA currently deposited in the PDB, the active site is highly conserved within the whole  $\alpha$ -CA family and is formed by almost the same amino acid residues.<sup>35</sup> Still, there is a difference in the topology of the active site and variations in the accessibility of the prosthetic Zn<sup>2+</sup> cation. However, any sulphonamide-containing compound is a potential binder to the catalytic site of a carbonic anhydrase. Thus, the simplest approach in the design of CA inhibitors is the introduction of a sulphonamide functional group as a warhead that can provide the majority of the binding energy. Our data suggest that compounds with such a strong pharmacophore cross-reacts with all isoforms in the CA family. Therefore, an approach in the design of isoform-selective inhibitors is to search for compounds that fit into the active site while being structurally unfavorable (i.e., due to steric hindrance) for paralogous proteins. It has been reported earlier that fluorine-substituted benzenesulphonamides with a bulky hydrophobic moiety, such as a cyclooctyl-substituted secondary amine (compounds 12 and 13), have higher free binding energy for CA IX<sub>cd</sub> than for other isoforms.<sup>22</sup> Current interaction kinetic analysis confirmed this observation.

A clear pH dependence of the affinity for interactions between several CA isoforms and sulphonamides has previously been determined by numerous techniques.<sup>28,36–41</sup> Our interest was to investigate the pH dependence of the interaction kinetics, as we have done for several enzymes previously, including BACE-1,<sup>42</sup> HIV-1 protease,<sup>43</sup> and HCV polymerase.<sup>44</sup> The present study revealed an unexpectedly complex dissociation mechanism for the studied sulphonamides that was detected via an observed pH dependence of the dissociation rates. We suggest that the reverse reaction is linked to protonation/deprotonation events in a similar manner as association. This can be attributed to a water molecule (or hydroxide anion) involved in the dissociation reaction, keeping Zn<sup>2+</sup> in a favorable tetragonal coordination, and/or the protonation of sulphonamides within the Zn coordination sphere prior the initiation of dissociation. Following this logic, the minor influence of pH on the apparent  $k_d$  of compound 12 is interesting. It is likely that this compound (and 13, which is similar) efficiently blocks the active site of the enzyme, making the prosthetic group inaccessible and changing the rate-limiting step for the dissociation reaction. Inhibitors targeting membrane-bound forms of CA have to be charged to avoid membrane permeability and thus the risk of cross-targeting intracellular forms of CA. They should also be potent under acidified conditions, considering the role of membrane-bound isoforms in tumor acidosis. From this consideration, polyfluorinated benzenesulphonamides with bulky hydrophobic moieties serve as promising scaffolds for membrane-bound CA inhibitors.

The  $\text{p}K_a$  values for compounds 6 and 8 are similar; however, the *t*-butyl substituent of 8 considerably decreased the dissociation rate of this compound. We suggest that the formation of large hydrophobic contacts is essential for the design of ligands whose complexes demonstrate an extended half-life. This observation is even more evident considering the dissociation rates for the interactions between the studied isoforms and compounds with cycloalkyl substituents, e.g., CA IX<sub>cd</sub> and compound 12, or interactions between CA VII and inhibitors 14 and 15 (Figure 2). Such interactions are often stable enough to be essentially irreversible in the SPR experimental setup (Figure 6).

Affinities determined by SPR were close to those determined by FTSA. The advantage of SPR was the ability to dissect thermodynamic equilibrium information into kinetics in terms of association and dissociation rates. However, for tight interactions, such as compound 13 binding to CA IX, the dissociation rates were too slow for the unambiguous determination of kinetic rate constants and affinity parameters via SPR. In such cases, FTSA is a useful method capable of quantifying even picomolar affinities.

## CONCLUSIONS

Development of isoform-selective ligands (e.g., isoform-selective inhibitors) requires use of biophysical methods that reveal the details of the actual molecular recognition

mechanism. SPR-based biosensor analysis allows the study of interactions under different conditions, resolving the interaction into its individual components. Also, the binding kinetics reveal the dynamics of the interaction. However, orthogonal assays for interaction analysis are required to exclude the misidentification of leads and to extend the biophysical space for ligand characterization. A combination of SPR-based analysis with thermodynamic methods, like the fluorescent thermal shift assay and isothermal titration calorimetry, is therefore necessary for the design and development of efficient drug candidates.

Enzymes of the CA family are important not only as targets for chemotherapy but also as good models for ligand selectivity studies. Similar logic can be applied to other protein families that are important as drug targets or functionally significant for fundamental research. Taking into account the existence of structurally similar proteins will result in reduced cross-reactivity of a potential drug lead and in the development of highly selective chemical probes.

## ■ EXPERIMENTAL SECTION

**Enzymes and Ligands.** CA isozymes were expressed and purified according to the following previously published protocols: CA I by Baranauskienė et al.,<sup>45</sup> CA II by Cimmperman et al.,<sup>46</sup> CA VII and XIII by Sūdžius et al.,<sup>47</sup> CA IX by Dudutienė et al.,<sup>22</sup> and CA XII by Jogaitė et al.<sup>38</sup>

Compounds were synthesized according to the following previous publications: 1–3 in Zubrienė et al.,<sup>20</sup> compounds 4 and 5 in Čapkauskaitė et al.,<sup>23</sup> compounds 6, 8, and 10 in Čapkauskaitė et al.,<sup>24</sup> compounds 7 and 9 in Čapkauskaitė et al.,<sup>21</sup> compounds 11 and 16 in Dudutienė et al.,<sup>25</sup> compounds 12 and 13 in Dudutienė et al.,<sup>22,26</sup> and compounds 14, 15, and 17 in Dudutienė et al.<sup>26</sup>

The purity of the synthetic ligands was verified by HPLC to be >95% using an Agilent 1290 Infinity instrument with a Poroshell 120 SB-C18 (2.1 mm × 100 mm, 2.1 μm) reversed-phase column. Analytes were eluted using a linear gradient of water/methanol (20 mM ammonium formate in both phases) from 60:40 to 30:70 over 7 min, from 30:70 to 20:80 over 1 min, and then 20:80 over 5 min at a flow rate of 0.2 mL min<sup>-1</sup>. UV detection was at 254 nm.

Marvin v15.11.2.0 (ChemAxon, <http://www.chemaxon.com>) was used for drawing, displaying, and characterizing (including properties prediction) chemical structures.

**Fluorescence-Based Thermal Shift Assay.** Fluorescent thermal shift assay (FTSA, also termed ThermoFluor and differential scanning fluorimetry) experiments were performed using a Corbett Rotor-Gene 6000 (QIAGEN Rotor-Gene Q) instrument. The blue channel was used for measurements, with excitation at 365 ± 20 and detection at 460 ± 15 nm. Samples contained 5 or 10 μM protein, 0–200 μM ligand, 50 μM solvatochromic dye ANS (8-anilino-1-naphthalenesulfonate), 100 mM NaCl, 50 mM phosphate buffer at pH 7.0, and a final DMSO concentration of 2%. The samples were heated from 25 to 99 °C at a rate of 1 °C min<sup>-1</sup> while recording the ANS fluorescence. The melting temperature was determined for each isozyme at every inhibitor concentration. Data was analyzed as described previously.<sup>48</sup>

**Interaction Kinetic Studies.** *General.* Interaction kinetic assays were performed using the following SPR biosensor instruments: BIAcore 2000, BIAcore S51, and BIAcore T200 (GE Healthcare, Uppsala, Sweden). For protein immobilization, research-grade CMS and Series S CMS sensorchips were used (GE Healthcare, Uppsala, Sweden). Protein samples dissolved in buffers with primary amines (e.g., Tris-HCl) before experiments were buffer-exchanged into the required coupling buffer using spin desalting columns with a molecular weight cutoff of 7 kDa (Thermo Scientific, Rockford, IL, USA) following the supplied instructions.

*Immobilization of Isozymes.* Isozymes were immobilized using amine coupling chemistry at 25 °C. For all six isozymes, the running buffer used for immobilization consisted of 10 mM Na<sub>2</sub>HPO<sub>4</sub>, 1.8 mM KH<sub>2</sub>PO<sub>4</sub>, 137 mM NaCl, and 2.7 mM KCl, pH 7.4 (PBS),

supplemented with 0.05% Tween-20 (PBST). The surface was activated by a 10 min injection of 0.4 M 1-ethyl-3-(3-(dimethylamino)propyl)-carbodiimide (EDC) and 0.1 M *N*-hydroxysuccinimide (NHS) at a flow rate of 20 μL min<sup>-1</sup>, followed by a 7 min injection (flow rate 5 μL min<sup>-1</sup>) of a protein dissolved in the appropriate coupling buffer (described below). Unreacted activated groups of the dextran matrix were deactivated by a 10 min injection of 1 ethanolamine, pH 8.5, at a flow rate of 20 μL min<sup>-1</sup>.

The protein concentration and the pH of the coupling buffer (10 mM sodium acetate buffer) were adjusted to suit each isozyme: 75 μg mL<sup>-1</sup> at pH 5 for CA I, 100 μg mL<sup>-1</sup> at pH 5 for CA II, 25 μg mL<sup>-1</sup> at pH 5 for CA VII, 100 μg mL<sup>-1</sup> at pH 4.5 for CA IX, 25 μg mL<sup>-1</sup> at pH 5 for CA XII, and 75 μg mL<sup>-1</sup> at pH 5 for CA XIII. The CA XII-modified surface was washed by a 30 s pulse injection of 10 mM sodium phosphate, 1 M NaCl, pH 7.4, after the immobilization.

*Interaction Kinetic Assay.* All assays were performed at 25 °C using buffer consisting of PBST supplemented with 2% (v/v) dimethyl sulfoxide (DMSO), pH 7.4. All ligands were stored in 10 mM, 100 μM, 50 μM, or 25 μM aliquots in 100% DMSO as stock solutions. Ligands were prepared as concentration series in 2-fold dilutions ranging from 15.6 to 2000 nM and injected over the surface at a flow rate of 30 or 90 μL min<sup>-1</sup>. Association was monitored for 30 s, and dissociation, for 180 s. For ligands with a slow dissociation rate, a regeneration step was included in the assay cycle. Regeneration was performed by a 60 s injection of 200 μM sulphanimide dissolved in the running buffer. At the end of each cycle, the flow system except for the flow cell itself was washed with 25% DMSO to avoid carry-over effects.

*pH-Dependence Studies.* To evaluate the pH dependence of the interaction kinetics, kinetic analysis was performed for CA IX<sub>cd</sub>, CA XII<sub>cd</sub>, and selected ligands. Surfaces were prepared as described above except that for the reference surfaces proteins were immobilized and denatured by sequential 3 min injections of 50 mM NaOH, 6 M guanidinium chloride, and 0.5 M ethylenediaminetetraacetic acid (EDTA). A set of 50 mM sodium phosphate, 150 mM NaCl buffers with pH values of 6.0, 7.0, and 8.0 was prepared by mixing the calculated amounts of 0.2 M Na<sub>2</sub>HPO<sub>4</sub> and NaH<sub>2</sub>PO<sub>4</sub>, according to the Henderson–Hasselbach equation, additionally titrated to adjust the required pH values with 0.1 M H<sub>3</sub>PO<sub>4</sub> or NaOH and supplemented with 0.05% Tween-20 and 2% DMSO.

Ligands were prepared as 2-fold concentration series ranging from 62.5 to 2000 nM (compounds 6–8) or from 31.3 to 1000 nM (compound 12) at different pH values and were further injected over the surface for 60 s followed by dissociation from 90 to 360 s.

All assays were performed in triplicates with a new surface for each replicate.

*SPR Data Analysis.* Data was analyzed using BIAcore T200 evaluation software v.1.0 and BIAevaluation software v.3.0 (GE Healthcare, Uppsala, Sweden). Sensorgrams were solvent-corrected and double-referenced by subtracting the signals from a reference surface and average signals from two blank injections for each concentration series. The sensorgrams were fitted in the software according to 1:1 Langmuir binding model with mass-transport limitation to extract values of the association and dissociation constants ( $k_a$  and  $k_d$ ). The equilibrium dissociation constant was calculated from the kinetic parameters using eq 4.

$$K_D = \frac{k_d}{k_a} \quad (4)$$

For pH-dependent interaction studies,  $K_D$  values were also determined using the steady-state approximation (eq 5)

$$R = \frac{R_{\max} \times [L]}{[L] + K_D^{ss}} \quad (5)$$

where  $R_{\max}$  is the maximal theoretical signal,  $[L]$  is the concentration of a ligand injected over a surface, and  $R$  is the saturation signal level for the given concentration of a ligand (corresponds to average from three points within 10 s before the end of the injection).

**Chemical Phylogenetic Analysis.** All sequence manipulations were done using Jalview v2.9.0b2 software.<sup>49</sup> Amino acid sequences for the protein variants were obtained from UniProtKB database: CA I accession number (a/n) P00915 aa2–261, CA II a/n P00918 aa2–260, CA VII a/n P43166, CA IX<sub>cd</sub> a/n Q16790 aa113–414, CA XII<sub>cd</sub> a/n O43570 aa25–301, and CA XIII a/n Q8N1Q1. Alignment of multiple protein sequences was performed using MUSCLE<sup>50</sup> with the Protein Alignment server preset. The PAM250 scoring matrix was used for calculating the phylogenetic tree. JKlustor was used for structure-based hierarchical clustering of synthetic ligands, JChem v15.11.2.0 (ChemAxon, <http://www.chemaxon.com>).

## ■ ASSOCIATED CONTENT

### Supporting Information

The Supporting Information is available free of charge on the ACS Publications website at DOI: 10.1021/acs.jmedchem.5b01723.

SMILES strings for compounds 1–17 and association and dissociation rate constants with human CAs (CSV)

## ■ AUTHOR INFORMATION

### Corresponding Author

\*E-mail: [helena.danielson@kemi.uu.se](mailto:helena.danielson@kemi.uu.se). Phone: +46 18 4714545.

### Author Contributions

All authors contributed intellectually as the project unfolded. U.H.D. and D.M. supervised the research. V.O.T. designed and performed SPR experiments and analyzed the kinetic data. V.L. performed and analyzed FTSA experiments. D.M. delivered compounds. V.O.T. wrote the manuscript. All the authors contributed to editing the manuscript.

### Notes

The authors declare no competing financial interest.

## ■ ACKNOWLEDGMENTS

This project was supported by the Swedish Research Council (VR) (no. D0571301) (U.H.D.) and by the European Social Fund under the Global Grant measure (no. VP1-3.1.-SMM-07-K-02-009) (D.M.). The authors thank Dr. Helena Nordström (SciLifeLab, Uppsala University) for providing access to the BIAcore T200 instrument.

## ■ ABBREVIATIONS USED

ANS, 8-anilino-1-naphthalenesulfonate; CA, carbonic anhydrase; EDC, 1-ethyl-3-(3-(dimethylamino)propyl)-carbodiimide; FTSA, fluorescence-based thermal shift assay; NHS, N-hydroxysuccinimide; RU, resonance units; SA, sulphonamide; SPR, surface plasmon resonance

## ■ REFERENCES

- (1) Lindskog, S. Structure and mechanism of carbonic anhydrase. *Pharmacol. Ther.* **1997**, *74*, 1–20.
- (2) Smith, K. S.; Jakubzick, C.; Whittam, T. S.; Ferry, J. G. Carbonic anhydrase is an ancient enzyme widespread in prokaryotes. *Proc. Natl. Acad. Sci. U. S. A.* **1999**, *96*, 15184–15189.
- (3) Maren, T. H. Carbonic anhydrase: chemistry, physiology, and inhibition. *Physiol. Rev.* **1967**, *47*, 595–781.
- (4) Aggarwal, M.; Boone, C. D.; Kondeti, B.; McKenna, R. Structural annotation of human carbonic anhydrases. *J. Enzyme Inhib. Med. Chem.* **2013**, *28*, 267–277.
- (5) Alterio, V.; Di Fiore, A.; D'Ambrosio, K.; Supuran, C. T.; De Simone, G. Multiple binding modes of inhibitors to carbonic anhydrases: how to design specific drugs targeting 15 different isoforms? *Chem. Rev.* **2012**, *112*, 4421–4468.

(6) Eriksson, A. E.; Jones, T. A.; Liljas, A. Refined structure of human carbonic anhydrase II at 2.0 Å resolution. *Proteins: Struct., Funct., Genet.* **1988**, *4*, 274–282.

(7) Henry, R. P. Multiple roles of carbonic anhydrase in cellular transport and metabolism. *Annu. Rev. Physiol.* **1996**, *58*, 523–538.

(8) Supuran, C. T. Carbonic anhydrase inhibitors. *Bioorg. Med. Chem. Lett.* **2010**, *20*, 3467–3474.

(9) Kanamori, K.; Roberts, J. D. Nitrogen-15 nuclear magnetic resonance study of benzenesulfonamide and cyanate binding to carbonic anhydrase. *Biochemistry* **1983**, *22*, 2658–2664.

(10) Pastorekova, S.; Zavada, J. Carbonic anhydrase IX (CA IX) as a potential target for cancer therapy. *Cancer Ther* **2004**, *2*, 245–262.

(11) Chiche, J.; Ilc, K.; Laferrière, J.; Trottier, E.; Dayan, F.; Mazure, N. M.; Brahim-Horn, M. C.; Pouyssegur, J. Hypoxia-inducible carbonic anhydrase IX and XII promote tumor cell growth by counteracting acidosis through the regulation of the intracellular pH. *Cancer Res.* **2009**, *69*, 358–368.

(12) Lou, Y.; McDonald, P. C.; Oloumi, A.; Chia, S.; Ostlund, C.; Ahmadi, A.; Kyle, A.; Auf dem Keller, U.; Leung, S.; Huntsman, D.; Clarke, B.; Sutherland, B. W.; Waterhouse, D.; Bally, M.; Roskelley, C.; Overall, C. M.; Minchinton, A.; Pacchiano, F.; Carta, F.; Scozzafava, A.; Touisni, N.; Winum, J.-Y.; Supuran, C. T.; Dedhar, S. Targeting tumor hypoxia: suppression of breast tumor growth and metastasis by novel carbonic anhydrase IX inhibitors. *Cancer Res.* **2011**, *71*, 3364–3376.

(13) Lu, H.; Tonge, P. J. Drug-target residence time: critical information for lead optimization. *Curr. Opin. Chem. Biol.* **2010**, *14*, 467–474.

(14) Swinney, D. C. Biochemical mechanisms of New Molecular Entities (NMEs) approved by United States FDA during 2001–2004: mechanisms leading to optimal efficacy and safety. *Curr. Top. Med. Chem.* **2006**, *6*, 461–478.

(15) Navratilova, I.; Hopkins, A. L. Fragment screening by surface plasmon resonance. *ACS Med. Chem. Lett.* **2010**, *1*, 44–48.

(16) Myszka, D. G. Analysis of small-molecule interactions using Biacore S51 technology. *Anal. Biochem.* **2004**, *329*, 316–323.

(17) Papalia, G. A.; Leavitt, S.; Bynum, M. A.; Katsamba, P. S.; Wilton, R.; Qiu, H.; Steukers, M.; Wang, S.; Bindu, L.; Phogat, S.; Giannetti, A. M.; Ryan, T. E.; Pudlak, V. A.; Matusiewicz, K.; Michelson, K. M.; Nowakowski, A.; Pham-Baginski, A.; Brooks, J.; Tieman, B. C.; Bruce, B. D.; Vaughn, M.; Baksh, M.; Cho, Y. H.; Wit, M. D.; Smets, A.; Vandersmissen, J.; Michiels, L.; Myszka, D. G. Comparative analysis of 10 small molecules binding to carbonic anhydrase II by different investigators using Biacore technology. *Anal. Biochem.* **2006**, *359*, 94–105.

(18) Nordström, H.; Gossas, T.; Hämäläinen, M.; Källblad, P.; Nyström, S.; Wallberg, H.; Danielson, U. H. Identification of MMP-12 inhibitors by using biosensor-based screening of a fragment library. *J. Med. Chem.* **2008**, *51*, 3449–3459.

(19) Rogez-Florent, T.; Duhamel, L.; Goossens, L.; Six, P.; Drucbert, A.-S.; Depreux, P.; Danzé, P.-M.; Landy, D.; Goossens, J.-F.; Foulon, C. Label-free characterization of carbonic anhydrase-novel inhibitor interactions using surface plasmon resonance, isothermal titration calorimetry and fluorescence-based thermal shift assays. *J. Mol. Recognit.* **2014**, *27*, 46–56.

(20) Zubrienė, A.; Čapkauskaitė, E.; Glytė, J.; Kišonaitė, M.; Tumkevičius, S.; Matulis, D. Benzenesulfonamides with benzimidazole moieties as inhibitors of carbonic anhydrases I, II, VII, XII and XIII. *J. Enzyme Inhib. Med. Chem.* **2014**, *29*, 124–131.

(21) Čapkauskaitė, E.; Baranauskienė, L.; Golovenko, D.; Manakova, E.; Gražulis, S.; Tumkevičius, S.; Matulis, D. Indapamide-like benzenesulfonamides as inhibitors of carbonic anhydrases I, II, VII, and XIII. *Bioorg. Med. Chem.* **2010**, *18*, 7357–7364.

(22) Dudutienė, V.; Matulienė, J.; Smirnov, A.; Timm, D. D.; Zubrienė, A.; Baranauskienė, L.; Morkūnaitė, V.; Smirnovienė, J.; Michailovienė, V.; Juozapaitienė, V.; Mickevičiūtė, A.; Kazokaitė, J.; Bakšytė, S.; Kasiliauskaitė, A.; Jachno, J.; Revuckienė, J.; Kišonaitė, M.; Pilipuitytė, V.; Ivanauskaitė, E.; Milinavičiūtė, G.; Smirnovas, V.; Petrikaitė, V.; Kairys, V.; Petrauskas, V.; Norvaišas, P.; Lingė, D.

- Gibieža, P.; Capkauskaitė, E.; Zakšauskas, A.; Kazlauskas, E.; Manakova, E.; Gražulis, S.; Ladbury, J. E.; Matulis, D. Discovery and characterization of novel selective inhibitors of carbonic anhydrase IX. *J. Med. Chem.* **2014**, *57*, 9435–9446.
- (23) Čapkauskaitė, E.; Baranauskienė, L.; Golovenko, D.; Manakova, E.; Gražulis, S.; Tumkevičius, S.; Matulis, D. Indapamide-like benzenesulfonamides as inhibitors of carbonic anhydrases I, II, VII, and XIII. *Bioorg. Med. Chem.* **2010**, *18*, 7357–7364.
- (24) Čapkauskaitė, E.; Zubrienė, A.; Baranauskienė, L.; Tamulaitienė, G.; Manakova, E.; Kairys, V.; Gražulis, S.; Tumkevičius, S.; Matulis, D. Design of [(2-pyrimidinylthio) acetyl] benzenesulfonamides as inhibitors of human carbonic anhydrases. *Eur. J. Med. Chem.* **2012**, *51*, 259–270.
- (25) Dudutienė, V.; Zubrienė, A.; Smirnov, A.; Gylytė, J.; Timm, D.; Manakova, E.; Gražulis, S.; Matulis, D. 4-Substituted-2,3,5,6-tetrafluorobenzenesulfonamides as inhibitors of carbonic anhydrases I, II, VII, XII, and XIII. *Bioorg. Med. Chem.* **2013**, *21*, 2093–2106.
- (26) Dudutienė, V.; Zubrienė, A.; Smirnov, A.; Timm, D. D.; Smirnovienė, J.; Kazokaitė, J.; Michailovienė, V.; Zakšauskas, A.; Manakova, E.; Gražulis, S.; Matulis, D. Functionalization of Fluorinated Benzenesulfonamides and Their Inhibitory Properties toward Carbonic Anhydrases. *ChemMedChem* **2015**, *10*, 662–687.
- (27) Karlsson, R. Affinity analysis of non-steady-state data obtained under mass transport limited conditions using BIAcore technology. *J. Mol. Recognit.* **1999**, *12*, 285–292.
- (28) Krishnamurthy, V. M.; Kaufman, G. K.; Urbach, A. R.; Gitlin, I.; Gudiksen, K. L.; Weibel, D. B.; Whitesides, G. M. Carbonic anhydrase as a model for biophysical and physical-organic studies of proteins and protein-ligand binding. *Chem. Rev.* **2008**, *108*, 946–1051.
- (29) Bradner, J. E.; West, N.; Grachan, M. L.; Greenberg, E. F.; Haggarty, S. J.; Warnow, T.; Mazitschek, R. Chemical phylogenetics of histone deacetylases. *Nat. Chem. Biol.* **2010**, *6*, 238–243.
- (30) Swietach, P.; Vaughan-Jones, R. D.; Harris, A. L. Regulation of tumor pH and the role of carbonic anhydrase 9. *Cancer Metastasis Rev.* **2007**, *26*, 299–310.
- (31) Elinder, M.; Selhorst, P.; Vanham, G.; Öberg, B.; Vrang, L.; Danielson, U. H. Inhibition of HIV-1 by non-nucleoside reverse transcriptase inhibitors via an induced fit mechanism-Importance of slow dissociation and relaxation rates for antiviral efficacy. *Biochem. Pharmacol.* **2010**, *80*, 1133–1140.
- (32) Gossas, T.; Nordström, H.; Xu, M.-H.; Sun, Z.-H.; Lin, G.-Q.; Wallberg, H.; Danielson, U. H. The advantage of biosensor analysis over enzyme inhibition studies for slow dissociating inhibitors-characterization of hydroxamate-based matrix metalloproteinase-12 inhibitors. *MedChemComm* **2013**, *4*, 432–442.
- (33) Hilvo, M.; Baranauskienė, L.; Salzano, A. M.; Scaloni, A.; Matulis, D.; Innocenti, A.; Scozzafava, A.; Monti, S. M.; Di Fiore, A.; De Simone, G.; Lindfors, M.; Jänis, J.; Valjakka, J.; Pastoreková, S.; Pastorek, J.; Kulomaa, M. S.; Nordlund, H. R.; Supuran, C. T.; Parkkila, S. Biochemical characterization of CA IX, one of the most active carbonic anhydrase isozymes. *J. Biol. Chem.* **2008**, *283*, 27799–27809.
- (34) Alterio, V.; Hilvo, M.; Di Fiore, A.; Supuran, C. T.; Pan, P.; Parkkila, S.; Scaloni, A.; Pastorek, J.; Pastorekova, S.; Pedone, C.; Scozzafava, A.; Monti, S. M.; De Simone, G. Crystal structure of the catalytic domain of the tumor-associated human carbonic anhydrase IX. *Proc. Natl. Acad. Sci. U. S. A.* **2009**, *106*, 16233–16238.
- (35) Imtaiyaz Hassan, M.; Shajee, B.; Waheed, A.; Ahmad, F.; Sly, W. S. Structure, function and applications of carbonic anhydrase isozymes. *Bioorg. Med. Chem.* **2013**, *21*, 1570–1582.
- (36) King, R. W.; Burgen, A. S. Kinetic aspects of structure-activity relations: the binding of sulphonamides by carbonic anhydrase. *Proc. R. Soc. London, Ser. B* **1976**, *193*, 107–125.
- (37) Baranauskienė, L.; Matulis, D. Intrinsic thermodynamics of ethoxzolamide inhibitor binding to human carbonic anhydrase XIII. *BMC Biophys.* **2012**, *5*, 12.
- (38) Jogaitė, V.; Zubrienė, A.; Michailovienė, V.; Gylytė, J.; Morkūnaitė, V.; Matulis, D. Characterization of human carbonic anhydrase XII stability and inhibitor binding. *Bioorg. Med. Chem.* **2013**, *21*, 1431–1436.
- (39) Morkūnaitė, V.; Gylytė, J.; Zubrienė, A.; Baranauskienė, L.; Kišonaitė, M.; Michailovienė, V.; Juozapaitienė, V.; Todd, M. J.; Matulis, D. Intrinsic thermodynamics of sulfonamide inhibitor binding to human carbonic anhydrases I and II. *J. Enzyme Inhib. Med. Chem.* **2015**, *30*, 204–211.
- (40) Pilipuitytė, V.; Matulis, D. Intrinsic thermodynamics of trifluoromethanesulfonamide and ethoxzolamide binding to human carbonic anhydrase VII. *J. Mol. Recognit.* **2015**, *28*, 166–172.
- (41) Kazokaitė, J.; Milinavičiūtė, G.; Smirnovienė, J.; Matulienė, J.; Matulis, D. Intrinsic binding of 4-substituted-2,3,5,6-tetrafluorobenzenesulfonamides to native and recombinant human carbonic anhydrase VI. *FEBS J.* **2015**, *282*, 972–983.
- (42) Christopheit, T.; Stenberg, G.; Gossas, T.; Nyström, S.; Baraznenok, V.; Lindström, E.; Danielson, U. H. A surface plasmon resonance-based biosensor with full-length BACE1 in a reconstituted membrane. *Anal. Biochem.* **2011**, *414*, 14–22.
- (43) Gossas, T.; Danielson, U. H. Analysis of the pH-dependencies of the association and dissociation kinetics of HIV-1 protease inhibitors. *J. Mol. Recognit.* **2003**, *16*, 203–212.
- (44) Winquist, J.; Abdurakhmanov, E.; Baraznenok, V.; Henderson, L.; Vrang, L.; Danielson, U. H. Resolution of the interaction mechanisms and characteristics of non-nucleoside inhibitors of hepatitis C virus polymerase. *Antiviral Res.* **2013**, *97*, 356–368.
- (45) Baranauskienė, L.; Hilvo, M.; Matulienė, J.; Golovenko, D.; Manakova, E.; Dudutienė, V.; Michailovienė, V.; Torresan, J.; Jachno, J.; Parkkila, S.; Maresca, A.; Supuran, C. T.; Gražulis, S.; Matulis, D. Inhibition and binding studies of carbonic anhydrase isozymes I, II and IX with benzimidazo[1,2-c][1,2,3]thiadiazole-7-sulphonamides. *J. Enzyme Inhib. Med. Chem.* **2010**, *25*, 863–870.
- (46) Cimmerman, P.; Baranauskienė, L.; Jachimovičiūtė, S.; Jachno, J.; Torresan, J.; Michailovienė, V.; Matulienė, J.; Sereikaitė, J.; Bumelis, V.; Matulis, D. A quantitative model of thermal stabilization and destabilization of proteins by ligands. *Biophys. J.* **2008**, *95*, 3222–3231.
- (47) Šūdžiū, J.; Baranauskienė, L.; Golovenko, D.; Matulienė, J.; Michailovienė, V.; Torresan, J.; Jachno, J.; Sukackaitė, R.; Manakova, E.; Gražulis, S.; Tumkevičius, S.; Matulis, D. 4-[N-(substituted 4-pyrimidinyl)amino]benzenesulfonamides as inhibitors of carbonic anhydrase isozymes I, II, VII, and XIII. *Bioorg. Med. Chem.* **2010**, *18*, 7413–7421.
- (48) Kazlauskas, E.; Petrikaitė, V.; Michailovienė, V.; Revuckienė, J.; Matulienė, J.; Grinius, L.; Matulis, D. Thermodynamics of aryl-dihydroxyphenyl-thiadiazole binding to human Hsp90. *PLoS One* **2012**, *7*, e36899.
- (49) Waterhouse, A. M.; Procter, J. B.; Martin, D. M.; Clamp, M.; Barton, G. J. Jalview Version 2-a multiple sequence alignment editor and analysis workbench. *Bioinformatics* **2009**, *25*, 1189–1191.
- (50) Edgar, R. C. MUSCLE: multiple sequence alignment with high accuracy and high throughput. *Nucleic Acids Res.* **2004**, *32*, 1792–1797.

## **12 Permissions**

From: "Permissions Helpdesk" <permissionshelpdesk@elsevier.com>  
Subject: RE: Permission to use the articles in the thesis  
Date: Wed, August 23, 2017 4:32 pm  
To: "Vaida Linkuvienė" <morkunaite@ibt.lt>

---

Dear Ms. Linkuvienė:

As an Elsevier journal author, you retain the right to Include the article in a thesis or dissertation (provided that this is not to be published commercially) whether in full or in part, subject to proper acknowledgment; see <https://www.elsevier.com/about/our-business/policies/copyright/personal-use> for more information. As this is a retained right, no written permission from Elsevier is necessary.

If I may be of further assistance, please let me know.

Best of luck with your PhD thesis and best regards,  
Hop

Hop Wechsler  
Permissions Helpdesk Manager  
ELSEVIER | Global E-Operations Books  
+1 215-239-3520 office  
[h.wechsler@elsevier.com](mailto:h.wechsler@elsevier.com)<<mailto:h.wechsler@elsevier.com>>

Contact the Permissions Helpdesk  
+1 800-523-4069 x3808 |  
[permissionshelpdesk@elsevier.com](mailto:permissionshelpdesk@elsevier.com)<<mailto:permissionshelpdesk@elsevier.com>>

-----Original Message-----

From: "Vaida Linkuvienė" [<mailto:morkunaite@ibt.lt>]  
Sent: Wednesday, August 23, 2017 9:31 AM  
To: Permissions Helpdesk  
Subject: Permission to use the articles in the thesis

\*\*\* External email: use caution \*\*\*

Dear Editor,

I have published an article in the Elsevier journals Bioorganic and Medicinal Chemistry and Biochimica et Biophysica Acta:

Jogaitė, V., Zubrienė, A., Michailovienė, V., Gyltė, J., Morkūnaitė, V., Matulis, D. Characterization of human carbonic anhydrases XII stability and inhibitor

binding. Bioorg. Med. Chem. 21(6) (2013) 1431-1436.

Linkuvienė, V., Matulienė, J., Juozapaitienė, V., Michailovienė, V., Jachno, J., Matulis, D. Intrinsic thermodynamics of inhibitor binding to human carbonic anhydrase IX. Biochim.Biophys.Acta, Gen.Subj. 1860 (2016) 708-718.

I would like to ask the permission to include the whole article in my PhD thesis.

Sincerely,

Vaida Linkuvienė (Morkunaite)

---

**Attachments:**

<b>untitled-[2].html</b>	
Size:	10 k
Type:	text/html

---





Taylor & Francis  
Taylor & Francis Group

Our Ref: JB/IENZ/P17/1397

11<sup>th</sup> September 2017

Dear Vaida Linkuvienė

Thank you for your correspondence requesting permission to reproduce the following article published in our journal in your printed thesis and to be posted in your university's repository.

**MATERIAL REQUESTED: 'Intrinsic thermodynamics of sulfonamide inhibitor binding to human carbonic anhydrases I and II' by Vaida Morkūnaitė, Joana Gylytė, Asta Zubrienė, Lina Baranauskienė, Miglė Kišonaitė, Vilma Michailovienė, Vaida Juozapaitienė, Matthew J. Todd & Daumantas Matulis *Journal of Enzyme Inhibition and Medicinal Chemistry* Vol 30:2 pp. 204-211 (2015).**

We will be pleased to grant permission on the sole condition that you acknowledge the original source of publication and insert a reference to the article on the Journals website:

This is the authors accepted manuscript of an article published as the version of record in *Journal of Enzyme Inhibition and Medicinal Chemistry* on 23<sup>rd</sup> April 2014.

<http://www.tandfonline.com/> <http://dx.doi.org/10.3109/14756366.2014.908291>

Please note that this license does not allow you to post our content on any third-party websites or repositories.

Thank you for your interest in our Journal.

Yours sincerely

**Jo Bateman** – Permissions Administrator, Journals  
Taylor & Francis Group  
3 Park Square, Milton Park, Abingdon, Oxon, OX14 4RN, UK.  
Tel: +44 (0)20 7017 7617  
Fax: +44 (0)20 7017 6336  
Web: [www.tandfonline.com](http://www.tandfonline.com)  
e-mail: [joanne.bateman@tandf.co.uk](mailto:joanne.bateman@tandf.co.uk)

2&4 Park Square, Milton Park, Abingdon, Oxfordshire OX14 4RN  
Tel: +44 (0) 20 7017 6000; Fax: +44 (0) 20 7017 6336

[www.tandf.co.uk](http://www.tandf.co.uk)

Registered in England and Wales. Registered Number: 1072954  
Registered Office: 5 Howick Place, London, SW10 1WG

an informa business

From: jmc@jmedchem.acs.org  
Subject: RE: Permission  
Date: Mon, June 19, 2017 3:30 pm  
To: Vaida Linkuvienė <morkunaite@ibt.lt>

---

Dear Vaida Linkuvienė:

Please see the below for information taken from the FAQ section in the Copyright Learning Module: What Chemists Need to Know about Copyright ([http://pubs.acs.org/page/copyright/learning\\_module/module.html](http://pubs.acs.org/page/copyright/learning_module/module.html)) ([http://pubs.acs.org/page/copyright/learning\\_module/module.html](http://pubs.acs.org/page/copyright/learning_module/module.html))).

You have the permission of the Journal of Medicinal Chemistry to reproduction the information within the guidelines provided by the ACS.

I am a student writing my thesis. May I use papers I have authored in ACS journals, or material from them, in my thesis without obtaining explicit permission?

You may reuse all or part of the Submitted, Accepted, or Published versions of your ACS papers in your thesis or dissertation. Such reuse is permitted subject to the ACS' Ethical Guidelines to Publication of Chemical Research (<http://pubs.acs.org/page/policy/ethics/index.html>) and you should secure written confirmation from the respective ACS journal editor(s) to avoid potential conflicts with journal prior publication policies (<http://pubs.acs.org/page/policy/prior/index.html>) (<http://pubs.acs.org/page/policy/prior/index.html%3E>). The ACS copyright credit line should be noted on the appropriate pages and appropriate citation of any Published versions. If the thesis or dissertation to be published is in electronic format, a direct link to the Published Work must be included using the ACS Articles on Request <http://pubs.acs.org/page/policy/articlesonrequest/index.html> link.

Although ACS grants students automatic permission to use their ACS articles in theses, it is highly likely that the graduate school requires a statement of written permission. Students should use Rightslink (<http://pubs.acs.org/page/copyright/permissions.html>) to obtain permission, and provide their graduate school with the written document provided by Rightslink.

You may also wish to view the ACS Thesis Policy ([http://pubs.acs.org/page/copyright/permissions\\_journals.html](http://pubs.acs.org/page/copyright/permissions_journals.html)) [PDF].

Sincerely,

Sandy K. Dewing  
Journal Administrator  
Journal of Medicinal Chemistry  
Phone: 612-624-6184  
Fax: 202-513-8609  
Email: [jmc@jmedchem.acs.org](mailto:jmc@jmedchem.acs.org)

-----Original Message-----

From: "Vaida Linkuvienė" <[morkunaite@ibt.lt](mailto:morkunaite@ibt.lt)>  
Sent: Friday, June 16, 2017 6:54am  
To: [georg-office@jmedchem.acs.org](mailto:georg-office@jmedchem.acs.org)  
Subject: Permission

Dear Editor,

I have published an article in the Journal of Medicinal Chemistry:

Talibov, V. O., Linkuvienė, V., Matulis, D., Danielson U. H. Kinetically Selective Inhibitors of Human Carbonic Anhydrase Isozymes I, II, VII, IX, XII, and XIII. J.Med.Chem. 59 (2016) 2083-2093.

<http://pubs.acs.org/doi/abs/10.1021/acs.jmedchem.5b01723>

I would like to ask your permission to include the whole article in my PhD thesis.

Sincerely,  
Vaida Linkuvienė

---

**Attachments:**

<b>untitled-[2].html</b>
Size: 6.5 k
Type: text/html

---

## **13 Curriculum Vitae**

# VAIDA LINKUVIENĖ

## Curriculum Vitae

### Personal information

Previous surname: Morkūnaitė  
Date of birth: 27 August 1988  
Place of birth: Panevėžys, Lithuania  
E-mail: morkunaite@ibt.lt  
Mob. no: +370 689 87303

### Work address

Department of Biothermodynamics and Drug Design  
Institute of Biotechnology, Vilnius University  
Life Sciences Center, Saulėtekio 7  
LT-10257, Vilnius, Lithuania

## ACADEMIC EDUCATION

---

**PhD student in Biophysics, Vilnius University, Lithuania** 2013 - 2017

- Supervisor: Prof. Daumantas Matulis
- Degree thesis: Observed and intrinsic thermodynamic and kinetic parameters of sulfonamide derivative binding to carbonic anhydrases

**M.Sc. in Biophysics, Vilnius University, Lithuania** 2011 - 2013

- Supervisor: Prof. Daumantas Matulis
- Degree thesis: Inhibitors search and determination of intrinsic binding parameters to carbonic anhydrases I, II, VII, XII and XIII

**B.Sc. in Biophysics, Vilnius University, Lithuania** 2007 - 2011

- Supervisor: Prof. Osvaldas Rukšėnas
- Degree thesis: Gender effects on odor discrimination

## ACADEMIC AFFILIATIONS

---

**Institute of Biotechnology, Vilnius University** October 2014 - Present

- Position: Junior researcher
- Department: Biothermodynamics and Drug Design
- Group: Biophysics

**Institute of Biotechnology, Vilnius University** October 2011 - 2014

- Position: Bioengineer
- Department: Biothermodynamics and Drug Design
- Group: Biophysics

## INTERNSHIPS

---

**Uppsala University, Sweden** October 2016 - November 2016  
*Erasmus practice*

- Advisor: prof. U. Helena Danielsson
- Kinetics of carbonic anhydrase-ligand binding

- “Jožef Stefan” institute, Slovenia** February 2016 - March 2015  
*Erasmus practice*
- Advisor: prof. Janez Štrancar
  - Fluorescent detection of carbonic anhydrase inhibition in cancer cells
- Sygnature Discovery, United Kingdom** January 2015 - February 2015  
*Trainee*
- Advisor: Martin Redhead
  - Kinetic analysis of protein-ligand binding using SPR
- Institute de Chemie de Nice, France** June 2012 - September 2012  
*Erasmus practice*
- Advisor: Dr. Nadine Martinet
  - Analysis of compounds using HPLC and fluorescence methods
- TA Instruments Division of Waters, Sollentuna, Sweden** November 2011  
*Trainee*
- Advisor: Peter Vikegard
  - Measurements of protein-ligand binding by using TAM III calorimeter
- Linkoping University, Linkoping, Sweden** November 2011  
*Trainee*
- Advisor: Per Hammarstrom
  - Measurements of protein-ligand binding by using Wilburn-Anderson method

## MEMBERSHIPS

---

- Member of the American Biophysical Society** 2013, 2017  
*www.biophysics.org*
- Member of the Lithuanian Biophysical Society** Since 2014  
*www.lbfd.lt*
- Member of the Lithuanian Biochemical Society** 2016  
*www.biochemistry.lt*

## PATENT APPLICATION

---

Selected inhibitors of Carbonic Anhydrase. PCT/IB2015/056626. 2015-09-01. Čapkauskaitė, E., Zakšauskas, A., Linkuvienė, V., Matulis, D.

## **PROJECTS**

---

Lithuanian–Latvian–Chinese (Taiwanese) Tripartite Cooperation Programme, Project No. TAP LLT-1/2015 „Design of Anticancer Pharmaceutical Compounds Using Structure and Energetics of Lead – Target Interaction”. 2016 – 2018.

VP1-3.1-ŠMM-07-K-009 „Support to Research Activities of Scientists and Other Researcher (Global Grant)“. “Design of selective carbonic anhydrase, Hsp90, and Hsp70 inhibitors and investigation of their anticancer properties”. 2012 09 02 – 2015 10 01.